A Solution Adaptive Grid (SAG) for incompressible flows simulations an attempt towards enhancing SAG algorithm for Large Eddy Simulation (LES)

Kaennakham, Sayan

Award date:
2010

Awarding institution:
Coventry University

Solution Adaptive Grid (SAG) for Incompressible Flows Simulations: An Attempt Towards Enhancing SAG Algorithm for Large Eddy Simulation (LES)

Sayan Kaennakham

A Thesis Submitted in Partial Fulfillment of the Requirements of
Coventry University for the Degree of Doctor of Philosophy

The programme of research was carried out at the Energy & Environmental Technology Applied Research Group, Faculty of Engineering and Computing, Coventry University, United Kingdom.

April 2010

Dedicated To

His Majesty King Bhumibol Adulyadej, Our Beloved King of Thailand

May You Live Forever

Acknowledgements

First and foremost, I would like to thank my family; my mum, dad, brother and sister who have been there for me during every up and every down over the past few years. Without their support I very much doubt I would have come this far.

I would also like to express the deepest appreciation to those who have been involved academically in this thesis. Firstly, I would like to truly acknowledge my primary supervisor, Professor Arne Erik Holdø for his guidance as well as his patience and ultimately for giving me the opportunity to work on this interesting subject. Secondly, a big thank also goes to Dr. Caroline Lambert and Dr. Humberto Medina who have jumped in to pick things up in the time of crisis, without them both this PhD would not have come to fruition.

Several of my dear friends; Dr. G. Polanco, Dr. K. Chow and Dr. M. Virk, and D. Blundred also deserve my deep appreciation for their help and support, as well as the many fun times we have had together. A big thank from the bottom of my heart also for Dr. D. McCluskey and Tara Baskerville who have been helping and looking after me, their unconditional and everlasting generosity has truly fascinated me.

I would like to show my gratitude to the government of Thailand for giving me the opportunity to study for a PhD in the first place, and for their continued financial support throughout my studies. This means the world for people who come from certain background of Thai society and would like to have proper education like myself.

Last but not least, I would also like to take this opportunity to say a special thank you to Kanitha, your unfaltering love, support, patience and understanding has been invaluable along the way.

Sayan Kaennakham

May 2010

Abstract

A study of the use of solution adaptive grid (SAG) method for simulations of incompressible flows is carried out in this work. Both laminar and turbulent types of flows are chosen.

Investigation on laminar flow simulation starts with mesh adaptation criteria that are based on strong changes of some selected flow parameters; pressure and velocity components. Three most common laminar types of flows are studied; flow in a circular pipe, flow in a channel with sudden expansion and flow in a cavity with a moving lid. It is found that with the use of SAG, a reduction in both computational grid nodes and CPU time can be obtained when compared to those of fixed grid while satisfactory solutions are also achievable. Nevertheless, the refinement criteria setup procedure reveals inconveniences and requirement for several judgments that have to be defined *'ad hoc'*. This hence, makes the refinement criteria dubious for real engineering applications.

For the study of turbulent flows with large eddy simulation (LES) and implicit filtering, examination of literature reveals that the lack of connections between the filter width and a physical scale has made LES somewhat unclosed, i.e. in a physical sense. In addition, it is known that numerical and modelling errors are always combined and it is difficult to study each of them separately making the total error magnitude difficult to control. Since both error types are characterised by the grid size, LES users very often find cases where a finer mesh no longer provides better accuracy.

An attempt to address this 'physical' enclosure property of LES and its complication to implement/setup in FLUENT begins with the construction of a new refinement variable as a function of the Taylor scale. Then a new SAG algorithm is formed. The requirement to satisfy a condition of the selected subgrid scale (SAG) model, the Smagorinsky model, is taken into consideration to minimize the modeling error. The construction of a new refinement algorithm is also aimed to be the key to studying the interaction between the two types of error and could lead to the means of controlling their total magnitude.

The validation in terms of its effectiveness, efficiency and reliability of the algorithm are made based on several criteria corresponding to suitability for practical applications. This includes the simplicity to setup/employ, computational affordability, and the accuracy level. For this, two different turbulent flow types that represent different commonly found turbulent phenomena are chosen; plane free jet and the flow over a circular cylinder. The simulations of the two cases were carried out in two dimensions.

It is found that there are two key factors that strongly determine the success of the algorithm. The first factor is the Taylor scale definition, with literature only available for the turbulent plane jet study, for which good level of accuracy is expected. Unfortunately, this is not true for the flow over a circular cylinder, indicating a need for further analytical work. The second encountered difficulty results from limited access to software codes, which makes it impossible to implement the proposed scheme. As a result, the algorithm formulation needs be modified with carful judgment.

Nevertheless, overall results are in reasonably good agreement with their corresponding experimental data.

CONTENTS

LIST OF FIGURES

LIST OF TABLES

NOMENCLATURE

C_s	The Smagorinsky constant
C_D	Drag coefficient
C_L	Lift coefficient
$\overline{C_p}$	Mean drag coefficient
$\overline{C}_{P_{back}}$	Back-pressure coefficient
E	Turbulent kinetic energy per unit mass
K_c	The Kolmogorov constant
L	Turbulent integral length scale
L_r/D	Normalized recirculation length
L_t	Turbulent integral time scale
N_p	Number of grid points
$N_{p\lambda}$	Number of grid points based on Taylor space scale
$N_{t\lambda}$	Number of time steps based on the Taylor time scale
N_t	Number of time steps
Re, Re_x	Reynolds number, local Reynolds number
Re_L	Turbulence Reynolds number
Re_{crt}	Critical Reynolds number where laminar becomes turbulent
R	Autocorrelation coefficient
St	Strouhal number
$\bar{S}_{ij}$	The strain rate tensor
u_i	Velocity component in the i-direction
u'	Fluctuation component of a velocity u
k	Kinetic energy

φ	Flow parameter
p	Fluid pressure
ρ	Fluid density
$\overline{\emptyset}$	Filtered component in LES
$\Delta x, \Delta y$	Grid cell spacing in x-direction, y-direction
e_1, e_2	First, second gradient
∇f	Euclidean morn
$\nabla^2 f$	Laplacian operation
Δt	Time difference
A_{cell}	Cell area
$R^{\emptyset}$,	Residual sum
U_{max}	Maximum velocity
U_{avg}, U_{mean}	Mean velocity
C^*	Refinement constant
U_{dt}, Ucl	Dominant velocity magnitude
$^{j}\overline{\emptyset}$	Mean, surface-averaged value of a flow parameter $\emptyset$
$\overline{U}_{cl}$	Mean centreline velocity (for a plane jet)
U_0	Inlet velocity (for a plane jet)
D	Nozzle diameter for plane jet, Circular cylinder diameter
l	Subgrid length scale
A_i	Constants
l	Length scale
E	Turbulent kinetic energy
E_l	Local refinement variable
$Y_{(\frac{1}{2})}$	Jet half-width

K_1	Jet spreading rate
K_2	Centreline velocity decay rate
$u'v'$	Reynolds shear stress
$u'u', v'v'$	Reynolds stress
$Urms, Vrms$	Root-mean-square value of velocity u, v

GREEK SYMBOLS

η	Kolmogorov length scale
η_t	Kolmogorov time scale
T_{ij}	Reynolds stresses ($= -\rho\langle u_i' u_j' \rangle$)
κ	Von Karman's constant
λ	Taylor micro scale
μ_t	Turbulent or eddy viscosity
ν_t	Subgrid scale turbulent viscosity
ε	Turbulent kinetic energy dissipation rate
υ	Kinematic viscosity
θ_S	Mean separation angle
Δ	Filter width
Δ_{mesh}	Grid spacing
τ_{ij}	Subgrid scale stress tensor
$\varepsilon_1^*, \varepsilon_2^*$	Refinement thresholds
ω	Weight function
δ_x	Local turbulence characteristic length scale
δ_j^*	Finite difference operator.
$\emptyset_f$	Face value

SUBSCRIPTS

i	In the x-direction
j	In the y-direction
k	In the z-direction
x, l	Locally defined
crit	Critical value
t	Related to turbulence
t	Related to time
f	Related to face of cell volume

ABBREVIATIONS

CFD	Computational Fluid Dynamics
SAG	Solution Adaptive Grid
DGA	Dynamic Grid Adaptation
AMG	Algebraic multigrid
MMPDE	Mesh moving partial differential equation
DNS	Direct Numerical Simulation
LES	Large Eddy Simulation
RANS	Reynolds-Average Navier-Stoke
SGS	Subgrid scale
PDE's	Partial Differential Equations
FD	Finite Difference
FE	Finite Element
FV	Finite Volume
QUICK	Quadratic Upwind Differencing Scheme

CFL	Courant-Friedrich-Lewy
SIMPLE	Semi-Implicit method for pressure-linked equation
VLES	Vary large eddy simulation
MFEM	Moving Finite Element method

CHAPTER 1 INTRODUCTION

1.1 MOTIVATION

One serious disadvantage of using fixed grids for solving complex Computational Fluid Dynamics (CFD) problems is that the grid points are generated and distributed in the domain before any details on the nature of the solution are known. As a result, time and computational cost are normally required to ensure mesh independence. Moreover, the task of distributing the mesh normally requires knowledge of the flow problem at hand. In other words, a proper design of the mesh requires a good understanding of the fluid dynamics being investigated. One of the main objectives of developing Solution Adaptive Grid (SAG), also known as Dynamic Grid Adaptation (DGA), method is to alleviate this problem.

When adaptation is performed properly, the resulting mesh is optimal for the flow solution because the solution is used to determine where more cells are added, i.e. computational resources are not wasted by the inclusion of unnecessary cells. Therefore, another primary goal of SAG will be to efficiently reduce the numerical error in the digital solution, with minimal numerical cost. This is particularly crucial when the use of well-defined fixed uniform mesh becomes computationally prohibitive.

The two most commonly used refinement strategies are mesh moving or r-refinement and h-refinement. The former is based on the idea of fixing the number of grid points and allowing the grid points to move accordingly to some pre-defined '*mesh driving*' function in order to capture the main flow feature while the calculation is progressing. h-refinement, on the other hand, allows the number of grid points to vary. Nodes are added in to regions of interest, normally those with high gradient of flow parameters and/or taken from where high mesh density is no longer needed.

Unfortunately it is not possible to state, with certainty, which refinement strategy is superior. This is due to the fact that the choice is highly determined by several factors;

grid topology, means of region of interest identification, numerical method or solver and the physics of the flow at hand.

For r-refinement type, a wide range of choices in defining a proper mechanism to drive the mesh has existed for several decades; moving finite element method (MFEM) (Miller & Miller 1981), mesh moving partial differential equation (MMPDE) (Huang *et al*. 1994, Huang & Russell 1999), mesh moving based on deformation mappings (Bochev *et al.* 1996), moving based on the variational approach (Cao *et al.* 1999, Cao *et al.* 1999) in which its users' input monitor functions study are Winslow's function (Winslow 1967, Brackbill 1993, Tang *et al.* 2003) and those based on harmonic maps (Dvinsky 1991, Li *et al.* 2001). Despite a number of choices available in r-refinement family, the necessity of solving additional mesh driving functions which introduces extra requirement of computational memory storage together with the lack of reliability and high requirement for users' input robust monitor or weight function for broader range of flow problems have effectively made this mesh refinement strategy relatively less attractive. For this reason in this work the main attention is focused on the h-refinement type instead.

In CFD study, while there is a large number of studies of mesh adaptation applied to compressible and Euler flows (Ait-Ali-Yahia *et al.* Dompierre *et al.* 2002, Frey & Alauzet 2005), it is interesting to see such a relatively small number of works done in the area of incompressible flows (Kaennakham & Holdø 2008), particularly flows with high Reynolds number (With & Holdø 2005). The rapid growth of sophisticated computers capability in the past decades has effectively made simulations of flows with low Reynolds number more affordable, as far as computational time is concerned. From an engineering point of view however, using fixed mesh still relies on mesh refinement to achieve mesh independent solutions. In addition, another important aspect that has great role to play is also the knowledge of the flow at hand required when the mesh is first generated/distributed and this makes the process of mesh generation time consuming. Therefore, it is of interest to expand range of studies to cover a wider range of refinement variables as well as flow problems that are close to engineering applications. This is to investigate how the use of solution adaptive grid can be beneficial for flows at low Reynolds numbers. This comes as the first task of this thesis.

In the numerical study of flow with high Reynolds number or turbulence, while the standard RANS model is known not to be capable of effectively reproducing time dependence nature and while direct numerical simulation (DNS) is computationally prohibitive for flows with high Reynolds number, the most favorable choice remains the Large Eddy Simulation (LES). This is where the complications and difficulties of utilizing the methodology of mesh adaptation come in.

Resulting from the principal concept of LES in which turbulence scales are decomposed by the filtering process, the filtered governing equations contain extra terms and require subgrid scale (SGS) model to close the equation system. Consequently, the quality assessment of LES is then determined by two main sources of error; numerical error and modelling error (assuming that the third type of errors, computation program/round-off is controlled). For the Smagorinsky subgrid scale model as used in this study, it occurs that its potential modelling error is also determined by the grid spacing. It then implies that determining the size of the grid used has direct effect on characterizing the magnitude of both numerical and modelling error. A question then comes into mind regarding this point: how should the grid size be prepared in order to maximize the final result quality, i.e. minimize the magnitudes of both error types. This suggests that means to take control of their total contribution to the final solution of a simulation of turbulence would be significantly useful.

Examination of literature reveals that most LES work existing nowadays determines the smallest scales to be explicitly calculated by the mesh based predominately on the computational capability available. In this regard, the effect of the SGS, due to the mesh and corresponding to the fundamental concept of SGS used and its assumption, is not being taken into consideration. The lack of connections between the filter width and a physical scale has made LES somewhat unclosed, i.e. in a physical sense, when it comes to defining the grid size.

Studied by many authors (Ghosal 1996, Kravchenko & Moin 1997), for implicit filtering LES (as is the case in this work), refining the mesh and hence increasing the grid resolution results in more small scales to be resolved and thus is further decreasing the effect of the SGS. This phenomenon remains until the mesh size is comparable to the

smallest turbulence scale namely Kolmogorov scales and the LES process then loses its identity and becomes DNS. From this point, one might have a preconception that an improvement in solutions should always be attained when the mesh is further refined. Unfortunately, under the context of LES with implicit filtering this is not always the case. The existance of the SGS can unexpectedly cause a high level of error and eventually contaminate the final result.

Looking at the modelling side of LES, the most widely used SGS model especially in industrial applications is the Smagorinsky model. Here the effect of the filtered out scales is accounted for via an additional viscous term. With this model, it is necessary that the smallest filter width (or grid size in this study) is lying in the inertial area of turbulence spectrum where the balance of kinetic energy production and dissipation is assumed. From the study of turbulence scale point of view where only three types are known and are possible to be estimated, the one called Taylor scale seems to fit this requirement. It then is of great interest to bridge together the grid size and the real turbulence physical scale in order to close the LES system as well as to have more control in dealing with the two error types mentioned earlier and their interaction. To this end, since the Taylor scale is a function of position, the methodology of local mesh adaptation or SAG then has an important role to play. From this investigation stems the main focus of this work – towards the capability of SAG for simulations of turbulent flows.

Furthermore, evidence demonstrated from the previous study on laminar flows shows that the chosen h-refinement strategy has also shown undesired aspects and deserved more attention. Key ingredients of that strategy should encompass a proper match of refinement variables and the region of interest, a normalization of mean parameters to prevent the algorithm from generating large changes of raw values, and a method to stop the algorithm producing redundant cells. The latter of these if satisfied either, by specifying a level of refinement, or generating the smallest grid size allowable. However, it occurs then that h-refinement strategy is not much superior to the mesh moving or r-refinement strategy after all.

As a consequence, alongside with the main aim of this work, which is to fix the un-closure nature of a LES system, an equally important target of the work is also to

simultaneously alleviate the drawbacks normally encountered when it comes to using h-refinement strategy.

Geometries of the two dimensional models studied in this work and their meshing process were carried out using a commercial software called GAMBIT version 2.2.30 and the calculation and post-processing process were done using FLUENT.

1.2 OBJECTIVES AND AIM OF STUDY

Despite the wide variety of choices of SAG extensively studied nowadays and the entire benefits one can expect to achieve for some certain types of problems, each of these approaches has their own difficulties and undesired aspects. The complication of having to setup a number of components for a refinement criterion has brought some doubts. Together with complications when applied with large eddy simulation (LES), the existing SAG methodologies have shown uncertainties and this is the main reason why grid adaptation algorithm is still not trusted, particularly when it comes to industrial applications. All these undesired features of SAG for LES applications encourage modern researchers to come up with new alternatives of mesh refinement algorithm targeting to alleviate the undesired aspects.

With this in mind, it is the aim of this study that a new SAG algorithm can be constructed and proposed. This new algorithm is to be designed specifically to enhance the efficiency of SAG methodology in terms of simplicity in defining, less user's judgment and interference, designed especially for standard Smagorinsky LES and computational affordability. This algorithm is also aimed to close the LES system in a physical sense in which a bridge between the numerical and physical aspect of LES has been built via the turbulence Taylor scale.

This has led to the main objectives of the work;

- To demonstrate the benefits of solution adaptive grid (SAG) achievable for simulations of incompressible laminar flows. This is to also investigate effects of refinement variable choices and components for different kinds of laminar flows.

- To provide an overall feature of SAG in general applications in PDE's based problems. This includes also pointing out what should be the main key of ideal SAG algorithms, as well as weak points of the method will finally be unlighted.
- To propose a new h-refinement algorithm designed aiming specifically to alleviate the difficulties and uncertainties caused by both undesired aspects of SAG and its application to large eddy simulation (LES). This is carried out by taking into consideration the intrinsic properties of the Smagorinsky subgrid model, and by studying the corresponding linkage between the smallest grid size and a Taylor scale. By doing this, it also means that the fundamental drawback of LES is overcome as an explicit link between the filter widths and a real physical turbulence scale is made.
- To gain a further insight into the limitations as well as capabilities of the proposed algorithm for turbulent flows with different phenomena and geometries in order to further develop the methodology of SAG.

1.3 THESIS OUTLINE

The investigation carried out in this work begins with providing the fundamental background of all the important components involved including computational fluid dynamics (CFD), turbulence and its modelling and the methodology of solution adaptive grid (SAG) and all these elements are developed in Chapter 2.

Chapter 3 gives demonstrations of SAG application for flows with low Reynolds number. Here the same simple SAG algorithm was applied to three selected laminar cases; flow in a circular pipe, flow in a confined jet and lid-driven cavity flow. It will be seen that SAG can be a very useful and effective tool for laminar flow simulations.

Before simulations of turbulent flows can be tackled, some developments and modifications on the fundamental of the ingredients involved, have to be made and this is contained in Chapter 4. Here a SAG algorithm is constructed with taking into consideration the essential features concerning real turbulence applications (towards

engineering prospects), overall computational affordability requirement and the concept of ideal SAG algorithm.

The new SAG algorithm is then tested in Chapter 5, by application to two distinct turbulent flows: a free plane jet and the flow over a circular cylinder. The first flow exhibits the specificity of a nearly zero velocity region, while in the latter case the presence of a wall constitutes an additional feature

The general results produced by both of the cases together with those previously obtained from the laminar cases are then discussed in Chapter 6 before the main conclusions of the entire investigation are drawn, together with recommendations for further work, and presented in Chapter 7.

CHAPTER 2 THEORETICAL BACKGROUND AND LITERATURE REVIEW

The study of applications of the methodology of solution adaptive grid (SAG) for simulations of incompressible flows as the main focus in this work involves several important components. This includes the art of numerically study of fluid flows with the means of mathematics as known as computational fluid dynamic (CFD), the method in using CFD to tackle problem of turbulence, i.e. turbulence modelling and principal and general idea of solution adaptive grid for CFD. In this chapter, each of which mentioned above is respectively provided in details.

2.1 COMPUTATIONAL FLUID DYNAMICS (CFD)

Over decades a number of mathematical formulae have been constructed and developed to represent different kinds of phenomena found in nature including the motion of liquids and gases. Most of these formulae are in non-linear Partial Differential Equation (PDE) forms which makes it very difficult to solve analytically except for only a very few specific cases. It is however still possible to obtain approximate computer-based solutions of PDE problems and this is known as numerical method. The use of this method with fluid flow problems is called Computational Fluid Dynamics (CFD). CFD consists of 3 main components;

- **Mathematical modelling**: Partial Differential Equations (PDE's).
- **Numerical Methods**: discretisation and solution techniques.
- **Computer Solvers**: software for pre- and post-processing.

2.1.1 Governing equations

The equations that govern the fluid mechanics phenomena are based on the three fundamental physical principal of mechanics: conservation of mass, momentum and

energy. In this study however only the first two will be provided here since the main work is concerning isothermal state of fluids, i.e. no heat transfers involved.

Conservation of mass: The unsteady, compressible and three-dimensional mass conservation or continuity equation is expressed as.

$$\frac{\partial \rho}{\partial t} + \frac{\partial (\rho u)}{\partial x} + \frac{\partial (\rho v)}{\partial y} + \frac{\partial (\rho w)}{\partial z} = 0 \qquad (2.1)$$

Where for incompressible fluids the first term disappears.

Conservation of momentum: Newton's second law states that the rate of change of momentum of a fluid particle equals the sum of the forces on the particle. From this the well-known Navier-Stokes equations can be derived for a viscous Newtonian fluid with a constant density, ρ, and regardless all the body forces, as follows.

$$\frac{\partial u_i}{\partial t} + \frac{\partial u_i u_j}{\partial x_j} = -\frac{1}{\rho}\frac{\partial p}{\partial x_i} + \frac{1}{\rho}\left[\mu \frac{\partial}{\partial x_j}\left(\frac{\partial u_i}{\partial x_j} + \frac{\partial u_j}{\partial x_i}\right)\right] \qquad (2.2)$$

Where u_i , p , μ , denote the velocity components in each direction, pressure and viscosity respectively. The second term on the left hand side is convective which is non-linear while the second one on the right hand side is diffusive.

2.1.2 Numerical solution to the governing equations

With the non-linear nature of the governing equations above together with the complexity of boundary conditions as well as geometry of the domain, analytical solution for most fluid problems are still impossible to achieve. As a consequence, the governing equations (2.1), (2.2), and/or additional transport equations of other scalars/species when appropriate, have to be solved numerically instead. To do this, the methods of discretisation are introduced where the continuous governing equations are replaced by a large discrete number of elements in space and time. This results in a system of algebraic equations and with some proper initial and boundary conditions, the system can be numerically calculated. Along the line however, the whole process is not an easy task. A good understanding of both numerical method/algorithm and physical feature of the flow

calculated at hand has great influence on the outcome results accuracy. In brief, numerical solution method components and properties are (Ferziger & Peric 2002);

- **Mathematical Model:** could be incompressible, inviscid, turbulent; two- or three-dimensional, etc. and it normally is in non-linear partial differential form together with boundary conditions.
- **Discretisation Methods:** are a method of approximating the differential equations by a system of algebraic equations for the variables at some set of discrete locations in space and time. Three well-known methods are finite difference (FD), finite element (FE) and finite volume (FV).
- **Numerical Grid:** is used to divides the solutions domain into a finite number of sub-domains; elements, control volumes etc.
- **Finite Approximations:** are selected to be used in the discretisation process which varies from method to method of discretisation..
- **Solution Method:** is used to solve the non-linear algebraic equations generated by the discretisation step and since they are non-linear, to solve them an iteration scheme is very often required.
- **Convergence Criteria:** is needed to decide when to stop the iterative process.

Next section will give clearer figure of how to calculate flow problem numerically.

2.1.3 Finite Volume Method (FV)

Finite Volume method is one of the most widely used methods adopted to convert the governing equations to algebraic equations which make them numerically solvable. Here the integral forms of governing equations are considered. The technique consists of dividing the physical space into a number of discrete control volumes and integrating the governing equations over each control volume resulting in a surface integral form. This ensures the conservation of each quantity on a control volume. For instance, consider the integral form of a pure steady convective-diffusive equation of a scalar φ show in equation (2.3).

$$\oint_s \boldsymbol{n} \cdot (\rho\varphi\boldsymbol{u})ds = \oint_s \boldsymbol{n} \cdot (\Gamma\, grad\, \varphi)ds \qquad (2.3)$$

Where $\boldsymbol{n}$, Γ denote the normal vector to each surface and the diffusive coefficient respectively. As can be seen, the integral forms are then approximated by the sum of the fluxes crossing the individual faces of the control volume. Generally, it is quite effective to use the well-known central differencing method for the diffusion term on the right hand side of equation (2.3). The convective terms, on the other hand, need some extra cares in order to avoid the so-called 'wiggles' due to the fact that convection spreads influence only in the flow direction. This makes the use of the central differencing method dependant on the relative strengths of convection and diffusion. Some popular alternative choices are the upwind differencing scheme, the hybrid differencing scheme, the power-law scheme and the Quadratic Upwind Differencing Scheme (QUICK).

So far, the above argument is only for steady convection-diffusion problem. In most cases, however, fluid flow problems normally have transient behaviour and pressure forces are also present. The appearance of these two terms introduces complications into the calculation process and some additional numerical aspects will have to be taken into consideration.

Time integration: There are normally two ways of dealing with the transient term, the first term in equation (2.2); implicit and explicit. In the explicit formulation, the current solutions are calculated straightaway from the existing solutions obtained from the previous time step. The implicit method on the other hand involves both the solutions from the time step previously solved and those from the current new time step. It is unfortunate not to be able to say which one of these is better than the other. This is because each of them has its own advantages and disadvantages. The explicit method is straightforward and fast but it is only conditionally stable. This forces the possible time step size to be very small. In the implicit method however, a relatively bigger time step size can be allowed and the method is theoretically unconditionally stable. Nevertheless, more computational efforts are required to complete one time step calculation as it involves iterative process.

Pressure-velocity coupling: The problem of coupling velocity and pressure occurs when the pressure source term appears in the momentum equations but there is no transport equation accounting for it. This is always the case particularly for incompressible flows. A proper coupling method introduces a constraint on the solution of the flow field i.e. if the correct pressure field can be obtained and applied to the momentum equations, the velocity field should satisfy continuity (Ferziger & Peric 2002). Some well known algorithms used to remedy this problem are the Semi-Implicit method for pressure-linked equation (SIMPLE), the SIMPLER algorithm and the PISO algorithm.

2.2 TURBULENCE AND ITS MODELLING

It remains as the most challenging problem in studying fluid mechanics to study turbulence. The necessity of better understanding in turbulence still persists due to the fact that fluids form most encountered in daily life is turbulent. The primary attempts to studying turbulent flows are mostly experimental and the numerical part has been growing as more sophisticated computers become available. General parameters such as time-averaged drag or heat transfer are possible to measure by engineering devices. There are however some types of measurements, for more complex flows, for example the fluctuating pressure within a flow are almost impossible to make. As a result, numerical methods have an important role to play. In attempts to investigate the complex chaotic phenomena of a flow numerically, the so-called turbulence models are needed due to the limited capability of today's computer software to resolve all the length and time scales. The idea of turbulence models normally bases on statistical approaches where the governing equations are averaged in either time or space which can be classified in Table 2-1. Also note that apart from those shown in the table, there is one other way to numerically study turbulent problems called the Direct Numerical Simulation (DNS) where all the turbulence scales are represented by the grid.

Table 2-1 Some most widely used and well-known turbulence models

Based on time-averaged Reynolds equations	Based on space-filtered equations
• zero equation model (mixing length model) • two-equation model ($k-\varepsilon$ model) • Reynolds stress equation model • algebraic stress model	• Large eddy simulation (LES)

2.2.1 Characteristics of turbulence

The measure for the relation between the convective and the viscous terms in the Navier-Stoke equations, equation (2.2) is given by the non-dimensional parameter called the Reynolds number, defined as equation (2.4);

$$Re_L = \frac{UL}{\upsilon} \tag{2.4}$$

Where U and L are characteristic velocity and length scales of the largest motion and υ is the kinematic viscosity of the fluid. The transition from laminar to turbulence occurs at a certain Reynolds number called critical Reynolds number (Re_{crt}). The range of the critical Reynolds number varies from flow to flow depending on conditions involved. With an increase of the Reynolds number, the flow becomes unstable and large flow structures break up in smaller and smaller eddies until these are diffused into heat by viscous effects.

The word 'turbulence' is regarded to describe many different physical phenomena, which exhibit the common characteristics of disorder and complexity. There is no universal definition of turbulence. Rather, another way to describe turbulence is by listing its characteristic features (Ferziger & Peric 2002);

- **Irregularity** : Turbulence consists of a spectrum of different scales (eddy sizes) where the largest eddies are of the order of the flow geometry i.e. boundary layer thickness, jet width, etc. and the smallest eddies with the size proportional to power $(-3 / 4)$ of the Reynolds number of the flow. Even though it is seen as chaotic, it is deterministic and is still governed by the Navier-Stoke equations just like laminar flows.
- **Diffusivity** : As a flow becomes turbulent, the spreading rate of boundary layers, jets etc. increases. The turbulence increases the exchange of momentum in e.g. boundary layers and reduces or delays thereby separation at bluff bodies such as cylinders, aerofoil and cars. The increased diffusivity also increases the resistance (wall friction) in internal flows such as in channels and pipes.
- **Dissipation :** At the smallest eddies there is a transformation of the kinetic energy passed down from the larger once into internal energy by the viscous effect. The process of transferring energy from the larger to smaller eddies is known as the *energy cascade*.
- **High Reynolds number and three dimensional :** Turbulence normally occurs at relatively high Reynolds number and is three dimensional by nature. In fact the mechanism that drives the process of energy cascade is the vortex stretching which is three dimensional by nature. However, for the sake of simplicity of study and restricted by the computational availability, in some special cases two dimensional turbulence is still widely acceptable.
- **Continuum** : Even though we have small turbulence scales in a flow, they are much larger than the molecular scale and we can treat the flow as continuum.

2.2.2 Turbulence scales and Taylor scale

In the study of turbulence there are three most commonly referred to scales of eddies: the integral length scale (L), the Taylor scale (λ), and the Kolmogorov scale (η). The first two can be defined using the autocorrelation function, also known as the autocorrelation coefficient (R) (Tenneckes & Lumley 1972; Pope 2000), expressed as;

$$R_{u'u'}(r) = \frac{\langle u'(x)u'(x+r)\rangle}{\langle u'(x)u'(x)\rangle} \tag{2.5}$$

Where the $\langle \quad \rangle$ represents time averaged values, $u'(x)$ is the velocity fluctuation at point x and with r being a distance away from that point. Integrating equation (2.5) over the entire distance gives the definition of the integral length scales, equation (2.6).

$$L = \int_0^\infty R_{u'u'}(r)dr \tag{2.6}$$

The integral time scale can also be defined in the same manner. Next, the second derivative of the autocorrelation function at the origin can be used to define the Taylor scale:

$$\left.\frac{\partial^2 R}{\partial r^2}\right|_{r=0} = -\frac{2}{\lambda^2} \tag{2.7}$$

Following the first Kolmogorov hypothesis which states that for flows at finite Reynolds numbers, the statics of the small scale motions have a universal form that depends only on dissipation rate (ε) and the kinematic viscosity (υ), and with using dimensional analysis, the Kolmogorov length and time scale can now be written respectively as;

$$\eta = \left(\frac{\upsilon^3}{\varepsilon}\right)^{1/4} \quad , \quad \tau = \left(\frac{\upsilon}{\varepsilon}\right)^{1/2} \tag{2.8}$$

In the framework of isotropic and homogenous turbulence studies, it is common to define the Taylor scale and assume the dissipation rate as a function of the Taylor scale, shown as follow.

$$\lambda^2 = \frac{\langle u'^2\rangle}{\langle\left(\frac{\partial u'}{\partial x_1}\right)^2\rangle} \quad , \quad \varepsilon = 2\upsilon\langle\left(\frac{\partial u'}{\partial x_1}\right)^2\rangle = 2\upsilon\frac{\langle u'^2\rangle}{\lambda^2} \tag{2.9}$$

Assuming that the production and dissipation of the kinetic energy are equal, the energy dissipation rate (ε) at the smallest scales can be estimated using the large scale parameters, U and L as;

$$\varepsilon \equiv \frac{U^3}{L} \tag{2.10}$$

Following the definition of the Reynolds number characterizing the largest scale of turbulent motion, equation (2.4), together with the relations in equation (2.8), (2.9) and (2.10), and since it is isotropic, we can write $\langle u'^2 \rangle = U^2$, the relations between the three turbulence scales can now be related as follows.

$$\frac{\eta}{L} \approx A_1 (Re_L^{-\frac{3}{4}}) \tag{2.11}$$

$$\frac{\lambda}{L} \approx A_2 (Re_L^{-\frac{1}{2}}) \tag{2.12}$$

$$\frac{\eta}{\lambda} \approx A_3 (Re_L^{-\frac{1}{4}}) \tag{2.13}$$

Where A_i are constants. The time scales can also be related in the same way. It can be seen now that the Taylor scale lies somewhere in between the other two, $\eta \ll \lambda \ll L$.

2.2.3 Energy cascade and energy spectrum

The concept of energy cascade in turbulence begins with the largest eddies receiving the kinetic energy from the mean flow. The kinetic energy is then passed on to smaller and smaller eddies, generated when the larger ones are broken down due to vortex stretching and this process carries on until the energy reaches the smallest eddies. Here is where the viscosity effect becomes greater and eventually dominant, high enough to stop the process of generating any smaller scales. Instead, the effect is responsible for dissipating the largest percent of kinetic energy passed down to heat. It has also to be mentioned that some amount of this energy is also transferred back to larger eddies and

this is called *backscatter*. The concept of energy cascade can be illustrated as a figure using the energy spectrum shown in Figure 2-1.

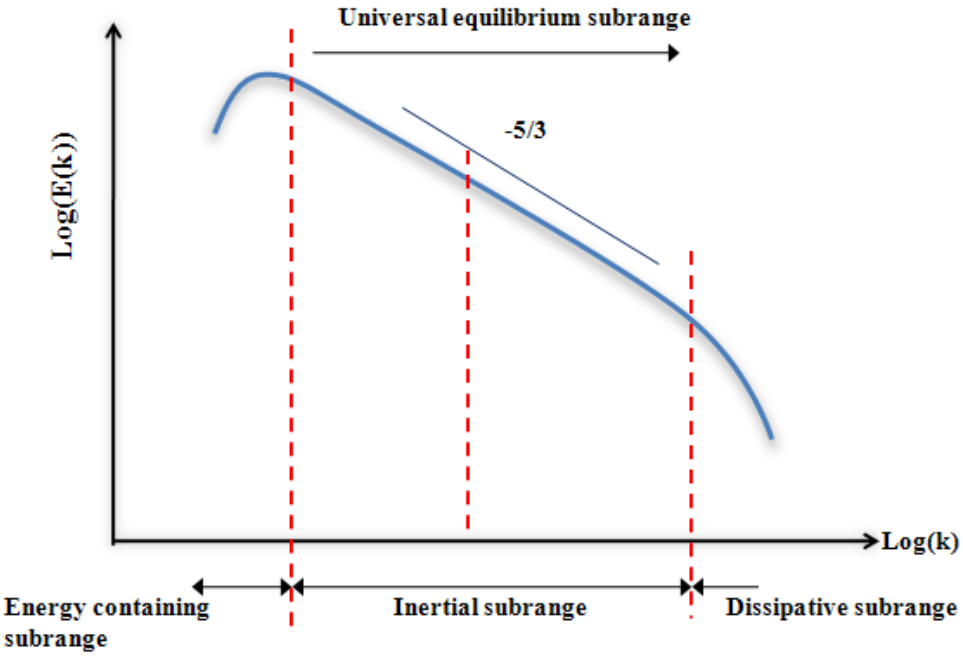

Figure 2-1 Turbulent kinetic energy spectrum.

The spectrum shows how the kinetic energy ($k = \frac{1}{2}\langle u_i' u_i' \rangle$) is distributed over the wave number range and illustrates three regions which correspond to;

- The region where most kinetic energy is contained and this is where the integral length scale L resides.
- The region where the kinetic energy is passed on to smaller and smaller scales. Regarding the second Kolmogorov hypothesis which states that for turbulent flows at sufficiently high Reynolds numbers there exists a range of scales that depends only on dissipation (ε) and a length scale ($l \approx \frac{1}{k}$), independent of kinematic viscosity (υ) and since the energy is transferred from the larger scales without loss together with the use of dimensional analysis, the relation for the turbulent kinetic energy per unit mass (E) shown below holds;

$$E(k) = K_c \varepsilon^{\frac{2}{3}} k^{-\frac{5}{3}} \tag{2.14}$$

Where K_c is the Kolmogorov constant and equation (2.14) is known as the Kolmogorov spectrum law or the $-5/3$ law. It is this range of the spectrum that expands proportionally to the increase of the Reynolds number.

- The most of kinetic energy is dissipated by the viscous forces and this takes place at the smallest turbulence scale known as the Kolmogorov scales (η).

2.2.4 Reynolds-Average Navier-Stoke (RANS) equation

It is known as the simplest way to mathematically handle turbulence to time average the governing equations. The process begins with decomposing the instantaneous value of a flow parameter (φ) into a summation of its mean value ($\langle\varphi\rangle$) and its fluctuation component (φ'), see Figure 2-2, and expressed as:

$$\varphi = \langle\varphi\rangle + \varphi' \tag{2.15}$$

Applying this to the governing equations and together with some properties of their combinations, derivatives and integrals, the time-averaged continuity and Navier-Stoke equations for incompressible flow can be written respectively in their new form as:

$$\frac{\partial\langle u\rangle}{\partial x} + \frac{\partial\langle v\rangle}{\partial y} + \frac{\partial\langle w\rangle}{\partial z} = 0 \tag{2.16}$$

$$\frac{\partial\rho\langle u_i\rangle}{\partial t} + \frac{\partial\rho\langle u_i\rangle\langle u_j\rangle}{\partial x_j} = -\frac{\partial\langle p\rangle}{\partial x_i} + \frac{\partial}{\partial x_j}\left[\mu\left(\frac{\partial\langle u_i\rangle}{\partial x_j}\right) - \rho\langle u_i' u_j'\rangle\right] \tag{2.17}$$

The resulting second averaged equations, equation (2.17), looks pretty much like the original form apart from the appearance of the terms, $T_{ij} = -\rho\langle u_i' u_j'\rangle$. These terms are called the Reynolds stress tensor and the equations themselves are called the **Reynolds-Average Navier-Stoke** (RANS) equations. The tensor is symmetric ($T_{ij} = T_{ji}$) and as a result, there are in total ten unknowns, six Reynolds stresses, one mean pressure and three mean velocity components. The number of equations is however only four and this leads

to a mathematically closure problem and this is where the concept of turbulence modelling comes in. To close this equation system, it is the fundamental problem of turbulence modelling to somehow relate all the Reynolds stresses to the mean flow quantities, $\langle u \rangle$ and $\langle p \rangle$. In 1877, Boussinesq proposed an assumption that Reynolds stresses could be linked to mean rates of deformation, as shown below.

$$\mathrm{T}_{ij} = -\rho\langle u_i' u_j' \rangle . = \mu_t \left(\frac{\partial \langle u_i \rangle}{\partial x_j} + \frac{\partial \langle u_j \rangle}{\partial x_i} \right) \tag{2.18}$$

Here, μ_t represents the turbulent or eddy viscosity. Ever since, it has remained the main task for time-averaged turbulence models to determine μ_t. Many assumptions have been proposed for this matter and some well-known models are provided in Table 2-1.

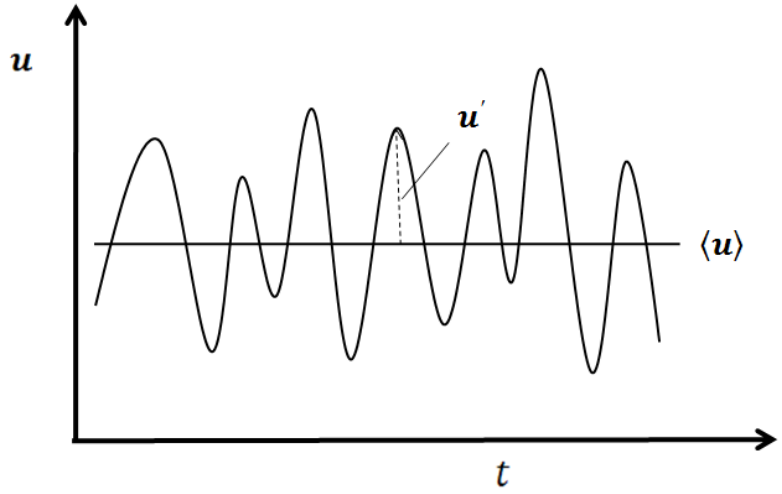

Figure 2-2 Velocity instantaneous value (u) of a stationary turbulence and its decomposition form with its time averaged value (⟨u⟩) and the fluctuation part (u′).

2.2.5 Direct Numerical Simulation (DNS)

In Direct Numerical Simulation (DNS), all scales of turbulence, from the largest to the smallest in both time and space, are explicitly resolved by the computational mesh. This requires no turbulence models since there is no need for approximating or averaging the governing equations. This simply means that for the discretisation in space, the numerical grid must be no larger than the smallest scale, the Kolmogorov length scales

(η). It is known as the most accurate method to predict turbulence. Nevertheless, considering the fact that all scales will have to be represented by the mesh, the number of grid points (N_p) needed in DNS can be estimated for three dimensional domain as;

$$N_p \approx \left(\frac{L}{\eta}\right)^3 \approx Re_L^{\frac{9}{4}} \tag{2.19}$$

By calculating the number of time steps (N_t) in the similar manner to above based on the same fact that the allowed time step size must also no larger than the Kolmogorov time scales (η_t), it is obtained that $N_t \approx Re_L^{\frac{3}{4}}$. Combining both together, the cost for DNS is proportional to Re_L^3 which is practically impossible in most of engineering problems due to the currently available super-computer capacities limitations. DNS as a result, is restricted only to flows with low and moderate Reynolds numbers. When applicable however, DNS has proven to play an important role as a very useful tool in CFD community.

2.3 LARGE EDDY SIMULATION (LES)

2.3.1 Filtering

Lying between DNS and RANS is Large Eddy Simulation (LES). Unlike DNS where one has to resolve down to the smallest scales resulting in a requirement of a very fine grid and unlike RANS where all scales of turbulence are modelled, LES uses a relatively coarser grid to resolve only the large scales by the computational grid and model only the smaller ones. From a physical point of view, this is because the larger scales are much more problem-dependent and more affected by the flow geometry and conditions involved as well as they carry most of the kinetic energy. Therefore this part requires high accuracy and needs to be resolved by the grid whereas the smaller ones are, on the other hand, more isotropic and easier to model.

The process of decomposing the eddies, the large scales from the smaller ones, is done by using a filter operator. A filtering process can be carried out in Fourier (wave-number) space or physical space. A filtered flow parameter, ϕ, is defined as:

$$\bar{\phi}(x) = \int_{-\infty}^{\infty} G(x - x', \Delta)\phi(x')dx' \tag{2.20}$$

Where $G(x - x_i, \Delta)$ is called a filter kernel with a characteristic length, or filter width, of Δ. There are different kinds of filter kernel and the most used ones are Gaussian filter, box or top-hat filter and cut-off filter (Sagaut 1998). In this study, however, the finite-volume discretisation itself implicitly provides the box-like filtering operation, i.e. the filtering is the same as the discretisation, expressed as.

$$G(x - x', \Delta) = \begin{cases} 1/\Delta & |x - x'| \leq \Delta/2 \\ 0 & otherwise \end{cases} \tag{2.21}$$

Where the filter width, Δ, is the computational cell volume. This means that the eddies whose scales are smaller than the filter width are effectively filtered out and it is the larger ones only being resolved by the computational grid. The effects of the unresolved filtered out small scales on the larger ones are instead accounted for via the use of a subgrid scale (SGS) model.

2.3.2 The filtered governing equations

The filtering process has decomposed a flow parameter, $\emptyset$, into a summation of its filtered (which is to be resolved directly from the grid) and residual component, $\emptyset = \overline{\emptyset} + \emptyset'$. This decomposition is known as the Leonard decomposition. One important feature about LES which is different from RANS is that in LES the flow parameters are spatial averaged rather than time. This gives some crucial properties in derivation of the new filtered governing equation; $\overline{\emptyset}' \neq 0$ and $\overline{\overline{\emptyset}} \neq \overline{\emptyset}$. The filtering operation is then applied to the governing equations resulting in the filtered governing equation expressed as.

$$\frac{\partial \overline{u_\iota}}{\partial x_i} = 0 \tag{2.22}$$

$$\frac{\partial \rho \overline{u_\iota}}{\partial t} + \frac{\partial \rho \overline{u_\iota u_J}}{\partial x_j} = -\frac{\partial \bar{p}}{\partial x_i} + \frac{\partial}{\partial x_j}\left(\mu \frac{\partial \overline{u_\iota}}{\partial x_j}\right) \tag{2.23}$$

The filtered non-linear term of equation (2.23), second on the left, requires some special treatment as it quantifies the interaction between the resolved scales and the residual or unresolved scales. It can be expanded in the following from.

$$\overline{u_i u_j} = \overline{(\bar{u}_i + u_i')(\bar{u}_j + u_j')} = \overline{\bar{u}_i \bar{u}_j} + \overline{u_i \bar{u}_j} + \overline{\bar{u}_i u_j} + \overline{u_i' u_j'} \tag{2.24}$$

As mentioned previously that a double filtering does not reproduce a single filtering value, equation (2.24) can be re-written as.

$$\overline{u_i u_j} - \bar{u}_i \bar{u}_j = \left(\overline{\bar{u}_i \bar{u}_j} - \bar{u}_i \bar{u}_j\right) + \left(\overline{u_i \bar{u}_j} + \overline{\bar{u}_i u_j}\right) + \overline{u_i' u_j'} \tag{2.25}$$

Each group shown on the right hand side is referred to as the Leonard stress, cross stresses and Reynolds stresses respectively and each of these terms has different physical interpretation. The Leonard term is responsible for the non-linear interaction between eddies within the resolved components. The cross term represents advection of the resolved field by the unresolved one where the interaction among the subgrid scales is represented by the Reynolds term. Since each of them represent different physical phenomena, it might be sensible for each of which to be treated separately. It is common in using LES however, to handle them all together and this process introduces the subgrid scale stress tensor, $\tau_{ij} = \overline{u_i u_j} - \bar{u}_i \bar{u}_j$. This stress is unknown and needs to be modelled using a proper pre-chosen "subgrid scale (SGS) model.

2.3.3 Subgrid scale models

Substituting the subgrid scale stress back to equation (2.24) , a new form is below.

$$\frac{\partial \rho \bar{u}_i}{\partial t} + \frac{\partial \bar{u}_i \bar{u}_j}{\partial x_j} = -\frac{1}{\rho}\frac{\partial \bar{p}}{\partial x_i} + \frac{\partial}{\partial x_j}\left(\nu \frac{\partial \bar{u}_i}{\partial x_j} - \tau_{ij}\right) \tag{2.26}$$

The last term needs to be modelled in order to close the equation system and this is where the subgrid scale models come in. The idea of modelling this term starts from adopting the Boussinesq hypothesis where the assumption of relating the stress tensor and the resolved strain rate tensor is made, shown as.

$$\tau_{ij} - \frac{1}{3}\tau_{kk}\delta_{ij} = -2\nu_t \bar{S}_{ij} \tag{2.27}$$

Where ν_t is the subgrid scale turbulent viscosity, δ_{ij} is the Kronecker delta function, the isotropic part τ_{kk} is not to be modelled but rather added to the filtered static pressure term. The last term is the resolved rate of strain tensor defined by.

$$\bar{S}_{ij} = \frac{1}{2}\left(\frac{\partial \overline{u_i}}{\partial x_j} + \frac{\partial \overline{u_j}}{\partial x_i}\right) \tag{2.28}$$

The main task remained now is to model the subgrid scale turbulent viscosity ν_t and over decades several models have been proposed.

Smagorinsky-Lilly model : The most well known and widely used model is the Smagorinsky model (Smagorinsky 1963). The idea starts with the second hypothesis of Kolmogorov with the use of the dimensional analysis, the subgrid scale viscosity can be expressed as a function of the energy dissipation rate and the length scale as below.

$$\nu_t = (C_s\Delta)^{4/3}\varepsilon^{1/3} \tag{2.29}$$

Assuming the balance of production and dissipation in the initial subrange on the energy spectrum, Figure 2-1, and since the scales in that region are isotropic, an estimation of the energy dissipation is obtained.

$$\varepsilon = 2\nu_t \bar{S}_{ij}\bar{S}_{ij} \tag{2.30}$$

By substituting this back to the previous equation, the final form of Smagorinsky-Lilly model is;

$$\nu_t = (C_s\Delta)^2|\bar{S}| \tag{2.31}$$

Where $\bar{S} = (2\bar{S}_{ij}\bar{S}_{ij})^{\frac{1}{2}}$ and the Smagorinsky constant C_s is found to be problem-dependent.

Two drawbacks about this model are concerned with the two parameters appearing in the form; the constant and the filter width. Firstly, it is important to note that this model is valid only if the scales of size on the order of the primary filter with Δ are lying within the inertial subrange which is larger than the actual dissipation scales. This results in the model not being capable of representing the 'backscatter' phenomena of energy since this feature takes place on scales smaller than those represented by the model. Secondly, the constant C_s. This constant should be adaptive based on the flow regimes, should be zero for those with laminar flow behaviour, for instance. To remedy this, the method of locally calculating this value is needed and this is done in the dynamic Smagorinsky model (Piomelli *et al*. 1991, Elhami *et al*. 2005).

2.4 SOLUTION ADAPTIVE GRID (SAG)

2.4.1 General ideas of SAG

Solution procedures for Partial Differential Equations based on numerical methods utilizes fixed spatial grids where results are obtained at grid points. Valid solutions, for most conventional numerical methods can be achieved from this approach when the grid is well defined. However, problems arise when dealing with simulations of fluid flows which include more complex physical phenomena as the grid distribution may no longer provide reliable results. This is due to the fact that the grid is constructed and distributed in the domain before details of the solution are known. Consequently, the influence mesh distribution and density have on the flow field calculated is not known either. Ideally, more refined grids are needed for those regions with high variation in variables which requires 'a priori' knowledge of the flow features. The issues seem to become even more serious for multi-dimensional, time-dependent and high Reynolds flows. The first attempt to handle this situation is to adapt the mesh based on the information/solution obtained from the initial mesh calculation. This requires the user to periodically stop the calculation, in order to modify the mesh and restart the calculation again. Adapting the mesh in this way can be thought of as 'Static Grid Adaptation (SGA)' which is considered time consuming and a priori knowledge of the flow field is still needed. Therefore, the study of grids that are capable of adapting themselves accordingly to the flow in order to

accurately capture the main flow phenomena has attracted attention in Computational Fluid dynamics (CFD) community. This idea forms an approach known as 'Dynamic Grid Adaptation (DGA)' or mesh refinement approach. As most of existing DGA are based on solution previously calculated on the initial mesh, it is also known as 'Solution Adaptive Grid (SAG)' method.

It is expected that the numerical solution, using SAG, given the desired accuracy, should be attained with the least number of degree of freedom without the needs of time consuming in grid testing. When adaptation is performed properly, the resulting mesh is optimal for the flow solution because the solution is used to determine where more cells are added. In other words, computational resources are not wasted by the inclusion of unnecessary cells. Therefore, the primary goal of SAG will be to efficiently reduce the numerical error in the digital solution, with minimal numerical cost.

In the past decade, the methodology of DGA has been extensively used in a wide range of science and engineering applications. This is ranging from fluid dynamics concerning shock waves and boundary layers, hydraulics, combustion, heat transfer and material science. This includes application to particle-in-cell simulations of plasmas and beams (Vay *et al.* 2004), radiation diffusion (Howell & Greenough 2003), Hamilto-Jacobi (H-J) equations which is concerning with differential games, front propagation and image enhancement (Tang *et al.* 2003), water flow and chemical transport (Mansell *et al.* 2002), atmospheric modelling including front-agenesis problem (Dietachmayer & Droegemeier 1992), the evolution of a buoyant thermal (Fiedler & Trapp 1993) as well as the anelastic equations (Prusa & Smolarkiewicz 2003). In this work nevertheless, the main focus is paid on the field of CFD.

In order to achieve a successful application of SAG for CFD study, there are generally four major questions need to be answered;

- When should the grid be adapted?
- How is the grid adaptation process carried out?
- Where in the domain should the grid adaptation take place?
- How often should the adaptation take place?

The answer for the first question is quite straightforward as the process can take place depending on the time-dependent nature of the problem at hand. For steady flow problems, it can be set to perform at every fixed number of iterations, while for time-dependent problems it can be carried out at every fixed number of either/both iteration or/and of time-steps. Figure 2-3 illustrates a simple algorithm for typical SAG algorithms coupled with a PDEs based problem calculation procedure.

The answer to how the grid adaptation process is carried out can be achieved by taking a look at different refinement strategies. The study of area of interest identification will provide the answer to where the mesh should be adapted. For the last question, nevertheless, there is no by far universal criterion and hence the choices are arbitrary.

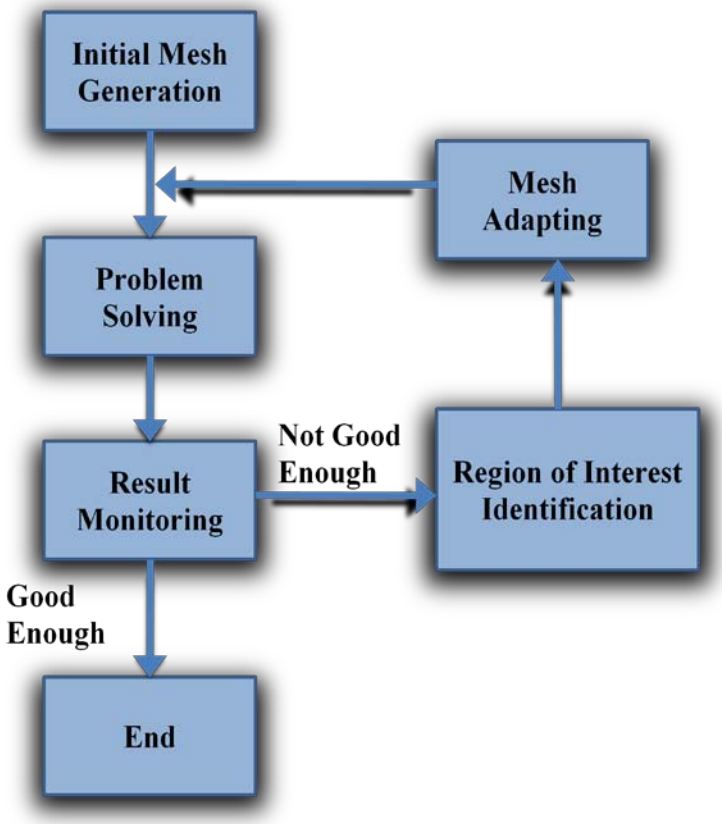

Figure 2-3 An example of a numerical calculation procedure coupled with SAG algorithm.

2.4.2 Refinement strategies

There are four, or other combinations of, main techniques to adapt the mesh widely adopted in SAG applications for CFD which are h-refinement, r-refinement, p-refinement and m-refinement strategy.

- **h-Refinement**

This method adds more grid to the regions where needed and/or removing grid points from those regions where fine grid points are no longer necessary during the computing process. Developments of this scheme generally concentrate on both the process of inserting more grid points and the strategy of taking grid points out. This is important because even though it does make sense that finer grids tends to give more accurate results, successive refinements may lead to an excessive amount number of volumes in regions of the flow filed where those volumes are no longer needed. This is particularly true for time-dependent problems where target locations change with time. Figure 2-4 depicts an example of mesh distribution from using h-refinement strategy.

Figure 2-4 Sample feature of h-refinement; before (above) and after (below) adaptation applied to a simulation of flow in a confined jet at Re = 80. Source Kennakham & Holdø (2008).

Potential advantages

1. The method allows easy error analysis and normally provides satisfactory solution. It is also conceptually easy to apply and usually reliable.
2. There is no need for introduction of additional equation to the physical equation like those needed for r-refinement

3. For the case consisting of several number of wave fronts or interesting flow feature, the method is capable of capturing it all.
4. The method seems to be well suited to vector and parallel processors.
5. The effect of conservation can be negligible.

Potential disadvantages

1. Adding or removing points to achieve a desired level of accuracy normally requires a complicated data structures and technical complex methods to communicate information amongst different levels, as well as the same level of refinements. Level of refinement is shown in Figure 2-5. This makes the programming of the method difficult to implement.
2. The requirement of expensive computational cost will be needed when dealing with the locations of variations, shock waves and contact surfaces as these normally change in time. This problem can be even more serious in the case of 3D with complex geometries.
3. In most of the cases, interpolation/extrapolation is required to define the solution on the fine/coarse mesh which can introduce undesired numerical diffusion. In the finite difference context, extra care must be taken to stably discretise the system.

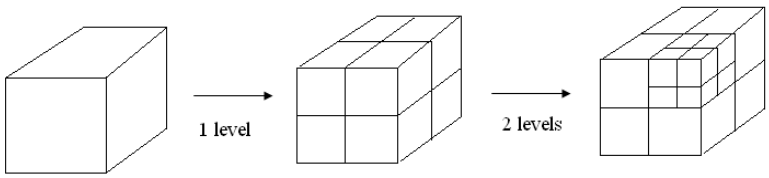

Figure 2-5 General feature of different levels of refinement for h-refinement approach.

- **r-Refinement strategy**

Unlike the h-refinement method, r-refinement or mesh movement or redistribution method, keeps the number of nodes fixed. During the calculation the nodes are relocated or moved around the domain depending on appropriate refinement criteria, Figure 2-6.

Clustering around regions where more nodes are needed, normally those with high-gradient of some flow parameters while coarsening them at low-gradient regions, would considerably improve the numerical solution of problems that involve shocks, boundary layers and vortices.

Figure 2-6 A sample figure of r-mesh distribution showing; above) adapted 121×91 grid and below) density contours for supersonic laminar viscous flow in a channel, source: Scott (2000).

Most of existing r-refinement methods have a process consisting of three main parts;

1. Selecting a criterion to detect the regions where important solution features occur. This is associated with defining appropriate weight or monitor function representing those regions.
2. The process of redistributing the grid points. Extra care is required for maintaining grid quality, as measured by orthogonality, cell aspect ratio, and smoothness as well as the geometric fidelity of solid boundary.

3. Modifying/redistributing the solution or re-evaluating the flow variables on the relocated nodes.

This mesh adaptation method has received little attention from scientists and engineers despite the fact that it has been known for many decades. One of the reasons for this is the difficulty in developing a general and robust moving mesh method in higher dimension (Weiming *et al.* 2001). Nevertheless, for structured grid topologies, it is by far the simplest to implement and most widely utilized grid adaptation strategy (Soni *et al.* 2000).

Potential advantages

1. There is no need to introduce complicated tree data structures in terms of coding. It can easily be incorporating with existing code based on fixed grids. In other words, as the data structure is simple, it is easy to implement.
2. The interpolation between the same as well as the different levels of mesh refinement, which can cause numerical dissipation, is not required.
3. The simplicity in principle of computing the mesh using continuous time integration.
4. The method can, when applied properly, allow significantly larger time steps without introducing instability problems and it also requires considerably fewer mesh points then the alternative h-refinement.

Potential disadvantages

1. It appears to be a problem for higher dimension computations to develop a general and robust moving mesh method as the process may introduce ‘mesh tangling’.
2. Some of existing moving mesh methods mixes the mesh-redistribution algorithm and the solution algorithm. As a consequence, any change of the governing PDEs may require the whole code to be re-modified.
3. As some additional conditions, as well as boundary conditions, are added to the physical equations and they all need to be calculated simultaneously, the calculation process as a result can be costly.

4. Since the number of grid points is fixed for the whole process, problems can arise when there are several important flow features simultaneously need finer grid points.
5. Even though the applications in case of structured mesh are largely successful, there are still limitations for unstructured mesh.

- **p-refinement**

In this method a principally fixed grid is used, but an adaptive solution is obtained by locally varying the order of spatial discretisation. Methods which do accomplish the addition of higher-order shape functions are the conventional polynomials (Gui & Babuska 1986) hierarchical shape functions (Zienkiewicz & Zhu 1987) or spectral element functions (Mavriplis 1990). For problems with exhibit a high degree of smoothness, particularly for elliptic or parabolic partial differential type this method is considered a viable one while in situations with discontinuities care must be taken to handle the oscillations, particularly when higher order of space discretisation is used. The approach has been widely-used in the finite element context and often used in conjunction with h-refinement (Devloo *et al.* 1988, Demkowicz *et al.* 1991, Lohner 1995).

- **m-refinement**

This method aims to completely rebuild the computational mesh regarding to error indicator introduced from discretisation step. The process of re-meshing is taking place either locally or globally in order to improve the goodness of the discretisation (Lohner 1988, Lohner 1989). The method has proven to provide the possibility of stretching elements when adapting features that are of lower dimensionality than the problem at hand as well as the ability to accommodate in a straightforward manner problems with moving bodies or free surfaces (Hetu & Pelletier 1992). However, this method normally requires high computing time.

- **Combinations**

Developments in solution adaptive grid have combined conventional refinement strategies in order to obtain improved results. For instance, it has become clear that the full potential of anisotropic grids can be unleashed only by combining grid

refinement/coarsening strategies with an improved mesh movement scheme (Oden *et al.* 1986, Habashi *et al.* 2000). Another well-known combined method is the so called hp-refinement. The method is focusing on refinement/coarsening and increasing the degree of the piecewise polynomials. An algorithm proposed by Li *et al.* (2001) has provided a benefit from combining the advantages of h-refinement, the two parts; a solution algorithm and a mesh selection algorithm are independent of each other and r-refinement, the number of nodes is fixed. The simplicity and reliability were demonstrated by a number of numerical examples in two dimensional problems (Devloo *et al.* 1988, Demkowicz *et al.* 1991, Li *et al.* 2002, Khawaja *et al.* 2000). There is also another widely studied area of combination or h- and r-refinement (often referred as hr-refinement) mainly in anisotropic way (Fortin *et al.* 1994, Castro-Diaz *et al.* 1997, Habashi *et al.* 1997). For instance, Peraire *et al.* (1987) have suggested a directional approach in constructing anisotropic grid with resolution along rapidly changing error estimate directions. The method was applied in conjunction with a two-dimensional hr-refinement to inviscid steady state flows of triangular meshes. Recent applications of combination of r- and h-refinement for 2D and 3D problem can also be found in Habashi *et al.* (2000), Ait-Ali-Yahia *et al.* (2002); Dompierre *et al.* (2002), Anderson *et al.* (2005), Lin *et al.* (2006).

2.4.3 Regions of interest identification

To reach the ultimate goal of applying SAG, it is important to know where more / less number of grid points is needed. It is expected that these types of regions should ideally be provided by a method of error measurements. However, the nonlinearity of the governing Navier-Stokes equations, together with transport equations for turbulence modelling quantities make this task not easy to handle. There are two widely-used strategies which are; indicators based on flow gradients and the use of error estimators.

- **Indicator based on flow gradients :** is quite straightforward to implement since the indicators can be computed as gradients of a variable characteristic involved in the flow field. The grid will be refined in those regions with large variations of these key variables, referred later as ***'refinement variables'***, which are readily available. Lohner (1995) has made a list of some most often used forms of this type of error

measurement; jump in refinement variable, interpolation method, comparison of derivatives and energy of spatial modes.

- **The use of error estimators :** The concept begins with an attempt to measure the precision of a solution obtained by a given mesh with respect to the unknown exact one and it can be done in advance, *a-priori*, or determined as a result of a solution on the current mesh, *a-posteriori*. Most used forms are derived from two fundamental ideas which are Richardson extrapolation-based error estimators (Ilinca *et al.* 2000) and Interpolation-based error estimators (Zienkiewicz & Zhu 1987).

General downside of adopting grid adaptation algorithm involving error estimator is that it relies on the smoothness of the differential equation, singularity in case of discontinuous flows. This is known to be remediable by grid smoothing procedure and as a result, the grid adaptation near discontinuities is readily driven by the grid smoothing procedure rather than the error estimator itself (Yamaleev 2001, Yamaleev & Carpenter 2002). Alternatively to this, the use of error indicators, generally based on large flow gradients, also receives attentions from recent grid adaptation researches. Even though this indicator is straightforward and simple to implement, it must be noted that continuous local refinement based on local dominant flow feature does not always reduce certain measures of the global error (Lohner 1987, Warren *et al.* 1991, Baker 1997). This indicates that difficulties can arise in selecting a robust match between error indicator formulation and its accordingly chosen flow parameters, referred to as refinement variables.

The error indicators/estimators obtained from the above procedures may then be analyzed to decide where in the domain the SAG should be carried out. Most of the analysis required for this task is normally based on the maximum values, the mean values or a norm of the indicators/estimators. This is the areas with indicators/estimators greater or lower than a specified threshold which will be submitted to the grid adaptive process. For example, given two non-zero and positive thresholds ε_1^* and ε_2^* where $\varepsilon_1^* < \varepsilon_2^*$ a judgment for mesh adaptation can be defined, for an indicator E_i of any element i, as.

- need coarser mesh where: $E_1 < \varepsilon_1^*$
- to be remained untouched where : $\varepsilon_1^* < E_i < \varepsilon_2^*$

- finer mesh is required where : $\varepsilon_2^* < E_i$

2.5 POTENTIAL DRAWBACKS OF SAG METHODOLOGY

2.5.1 Ideal SAG algorithms

Before giving any details in what remains an issue that prevents the use of solution adaptive grid from being recognized as an ultimate and reliable tool for CFD community, it is worth providing the properties that an ideal mesh refinement algorithm is expected to preserve (Lohner & Baum 1992, Darke & Manoranjan 1996, Drake & Manoranjan 1996, Scott 2000). The method should;

I. be conservative. A mesh change should not result in the production or loss of mass, momentum or energy.

II. be reducing spatial discretisation error.

III. result in quantifiable solution accuracy improvement.

IV. introduce a minimum amount of additional error.

V. be automatic. In other words, the process can perform without users' intervention.

VI. be as independent of solver and mesh topology as possible so that it can be more easily applicable to broader range of problems.

VII. have the algorithm that generates and maintains the new mesh with good quality.

VIII. be simple enough with significant speed up and be applicable to a large number of problems.

With all these in mind, it can be conceived that to have an algorithm that satisfies all above can be challenging. Each of them is generally the case under some certain combination of a number factors such as the solver used, fluid mechanics, mesh topology etc. With wide varieties in options of each of the factors available nowadays, it is then practically impossible for an algorithm to cover every aspect from **I** to **VIII**. To enhance an algorithm's capabilities as a result, it is then more practical to start with a choice of refinement strategy being made (in which the commercial software utilized remains the main key). Then a survey for shortcomings normally encountered for that particular type

of refinement strategy is conducted before each of which is addressed and attempts to enhance it can then be made.

The two mostly used refinement strategies; r- and h- are looked at in the next two sections. Concerns and undesired features are stated and this will lead to the answer to the question why the methodology of mesh refinement still remains skeptical and causes high level of hesitation of users.

2.5.2 r-Refinement or mesh moving method

Since most of these grid generation techniques have been developed using an original idea of the 'Equidistribution principle' (Boor 1974), defined as equation (2.32), in which the point distribution is set based on a product of a suitable positive weight function ω and grid cell spacing Δx, it then remains selecting appropriate weight functions for a problem at hand which is an important task for successful grid adaptation

$$\omega \Delta x = constant \tag{2.32}$$

Initially, this was designed to deal with one-dimensional problems, a number of ideas to extend this in to higher dimensions have been put forward (Soni & Yang 1992, Ribault *et al.* 1999, Anderson 1983). Well-known drawbacks were the non-linearity of the coupling between the solution and mesh equation that requires high computational cost Newton iteration for each time step. In addition, the convergence of the iteration is very sensitive to the dense clustering of mesh points near discontinuities. Dwer *et al.* (1980), and Catherall (1991) found that poor quality grid in terms of smoothness, skewness and orthogonality was also suffered from. Alternatively, Miller & Miller (1981) proposed the so-called moving finite element method where the residual of the original equations is minimized and the method uses the gradient-weighted finite element method to adapt current mesh. The problems uncounted were the difficulty in selecting user's input parameters due to the sensitivity and complexity of the method and the singularity of the mesh matrix requires a certain and modulation penalty function and, moreover, mesh tangling could also be a big issue.

Cao *et al.* (1999) studied the mesh moving based on the variational approach where the adaptation is done by minimizing the map between the physical domain and the computational domain. It also often involves important properties; mesh concentration in areas where greater resolutions are needed, mesh alignment as well as the preservation of mesh smoothness and orthogonality, and employs a monitor function to control mesh concentration. The difficulty is then the choice of choosing proper monitor functions. Following this line are those known as Winslow's function (Winslow 1967, Brackbill 1993, Tang *et al.* 2003) and those based on harmonic maps (Dvinsky 1991, Li *et al.* 2001). Huang *et al.* (1994) and Huang & Russell (1999) developed the so-called mesh moving partial differential equation (MMPDE) where a system of parabolic equations were solved to determine the movement of the mesh. Despite some successful applications, the method suffers from the coupling of the system which is hard to solve. Furthermore, mesh distribution smoothness is required to remedy the interpolation error and therefore well chosen monitor function is crucial (Li & Petzold 1997, Ceniceros & Hou 2001). Lying amongst those mentioned above is the mesh moving based on deformation mappings developed by Bochev *et al.* (1996). Once again, users' input such as weight functions have important role to play and some choices can be found in Semper & Liao (1995), Liu *et al.* (1998) and Liao *et al.* (2000).

The necessity of solving additional mesh driving functions which introduces extra requirement of computational memory storage together with the lack of reliable and high requirement for users' input robust monitor or weight function for broader range of flow problems have accordingly made this mesh refinement strategy relatively less attractive.

2.5.3 h-Refinement

Unlike the mesh moving method, no extra mesh driving equations required in this mesh refinement strategy. Instead, studies pay attention to development of means to insert(refining) and remove(coarsening) grid points. Kallinderis & Vijavan (1993) and Speares & Berzing (1997) studied the method known as the hierarchical techniques which is based on edge, face, and element subdivision with help from the data hierarchy construction. Although one can benefit from the bounded element quality degradation, a shortcoming is the requirement of good quality initial mesh in computational domain and

therefore users' knowledge in mesh quality is needed. The longest-side bisection technique, widely studied by Kim *et al.* (1991), Nambiar *et al.* (1993) also Delaunay algorithms by Delaunay (1934) and Bova & Carey (1992) were designed to handle the triangulation refinement problem often encountered in finite element context. Downside of this approach is that child meshes are sometimes over refined resulting in redundant cells and addition of extra computational memory storage and consequently some users' bounding criteria is needed.

In addition, without any additional function to drive the mesh as in r-refinement, the means in identifying the regions of interest for performing mesh adaptation are crucial. Ideally, these regions should be provided by a method of error measurements. However, the nonlinearity of the governing Navier-Stokes equations, together with additional transport equations makes this task not easy to handle. Many researcher have made use of error estimators, available from Richardson extrapolation-based (Ilinca *et al.* 2000) to interpolation-based (Zienkiewicz & Zhu 1987). Developing mesh adaptation algorithm in conjunction with error estimation can be a success as in the work of Habashi *et al*. (2000), Ait-Ali-Yahia *et al.*(2002) and Dompierre *et al.*(2002). General downside of adopting grid adaptation algorithm involving error estimator is that it relies on the smoothness of the differential equation, singularity in case of discontinuous flows. This is known to be remediable by grid smoothing procedure and as a result, the grid adaptation near discontinuities is readily driven by the grid smoothing procedure rather than the error estimator itself (Yamaleev 2001, Yamaleev & Carpenter 2002).

An alternative is the attempt to control the variation of the chosen region of interest identification mean over the domain and is generally done by adopting a normalization method and once again, a well-defined one is important to efficiently represent local error compared to the global one. Apart from this, in order to prevent the algorithm from producing too small elements, and therefore redundant cells, a users' judgment in controlling the size of the smallest elements generated is also required. With *et al.* (2003) adopted the same refinement criteria but different upper/lower thresholds to model flow around a circular cylinder. They found that the choices not only affect the final number of elements but also the quality of flow prediction particularly with flows

involving variety of scales such as turbulent flows where flow phenomena is sensitively affected by the mesh density and distribution.

From this, it can be conceived that successful applications of SAG approach in CFD are strongly dependent on several important factors such as appropriate error indicators, grid adaptive strategies, refinement variables, refinement bounds and frequency etc. Sophisticated and complex algorithms may provide impressive results but at the same time involve some undesired feature such as high computational demand to deal with extra terms and users' interfere and judgments. As a consequence, defining a proper refinement algorithm or criteria is very often a compromise between the three features; the computational demand, convenience and simplicity to use and the level of accuracy acceptable. An attempt to construct a reasonably cheap computational calculating algorithm in which comparatively requires users interfere and capable of producing desired results remains an important target of this study.

2.6 SUMMARY

In this chapter we have provided all the components that are involved in the main investigation of this work. The concept of studying fluid behaviour by means of mathematical model or CFD has been given with a wide range of alternative choices in methods as well as the conditions involved. Approaches available to address turbulence problems ranging from time to space averaged have also been detailed. Towards the end of the chapter, the chapter has also given a brief introduction to the methodology of automatic mesh adaptation or solution adaptive grid. Its general fundamentals, advantages, disadvantages as well as their roles to play in CFD community have also been provided.

In the next chapter, investigations of SAG application and its capability as well as limitations begin. This starts with simulation of flows with low Reynolds number before moving on to a much more challenging case of turbulence. Aspects concerning its performance and effectiveness will then be discussed for each flow case selected.

CHAPTER 3 SOLUTION ADAPTIVE GRID (SAG) WITH LAMINAR FLOWS

As the first step of this work, this chapter gives demonstrations of the use of Solution Adaptive Grid (SAG) with selected common-studied incompressible laminar flow problems. Alongside with providing some perception of using SAG for CFD, this chapter is also dedicated to investigating the effect of refinement variables on the flow simulations. This gives some ideas on how to select proper flow variables to be good candidates for refinement variables when performing SAG with laminar flow simulations.

In addition, the process of setting up the algorithm for this study of laminar flows is also to demonstrate what is normally required for a typical h-refinement strategy. It will be shown that the choices of refinement variables, proper regions of interest identification, normalization means, user's judgment in normalisation value thresholds as well as level of refinement are essential. This all will then prompt a motivation to constructing a new SAG algorithm for turbulence study that is still based on h-refinement strategy but with alleviated level of requirement for those mentioned.

Results are presented for three steady benchmarking incompressible iso-thermal flows; flow in a pipe, flow in channel with a sudden expansion and flow in a lid-driven cavity. To validate the final solution quality from this application, the exact solution is adopted for the first case study, the experimental works of Fearn *et al.* (1990) and Oliveira (2003) and of Ghia & Shin (1982) are referred to for the comparison in the case of sudden expansion flow and lid-driven cavity respectively.

All the two dimensions models studied as well as their meshing process were constructed using GAMBIT 2.2.30. Each model was then exported to FLUENT 6.2.16 for the processing as well as post-processing process.

3.1 GENERAL SETUP

3.1.1 Refinement criteria and its implementation in FLUENT

A major issue under grid refinement study is to define the criteria of grid refinement. Generally, as previously discussed in Section 2.4.3, this could be answered by considering the error indicators and/or error estimators of the flow field computation. Unfortunately, direct error estimation for point-insertion adaptation schemes, h-refinement, is not easily accomplished because of the complexity of accurately estimating and modelling the error in the adapted grids. In fact, no comprehensive mathematically rigorous theory for error estimation and convergence is available yet for CFD simulations (Fluent 2003). Therefore, in this work, the refinement criteria were defined by considering the error indicator of the flow field instead.

Figure 3-1 shows the **Gradient Adaptation** panel in FLUENT which can be accessed directly from the main FLUENT console window. The figure shows an example of gradient of x-velocity component as the refinement variable, with the **Scale** type of normalization means with 0.3 and 0.7 being the lower and upper bound respectively. Assuming the greatest error occurs in high-gradient regions, the readily available physical features of the evolving flow field may be used to drive the grid adaptation process. Amongst different schemes of error indications, the present study considers two methods derivative comparison as error indicators; (i) the first gradient e_1 and (ii) the second gradient (curvature) e_2 of a selected field variable f, respectively defined as follows.

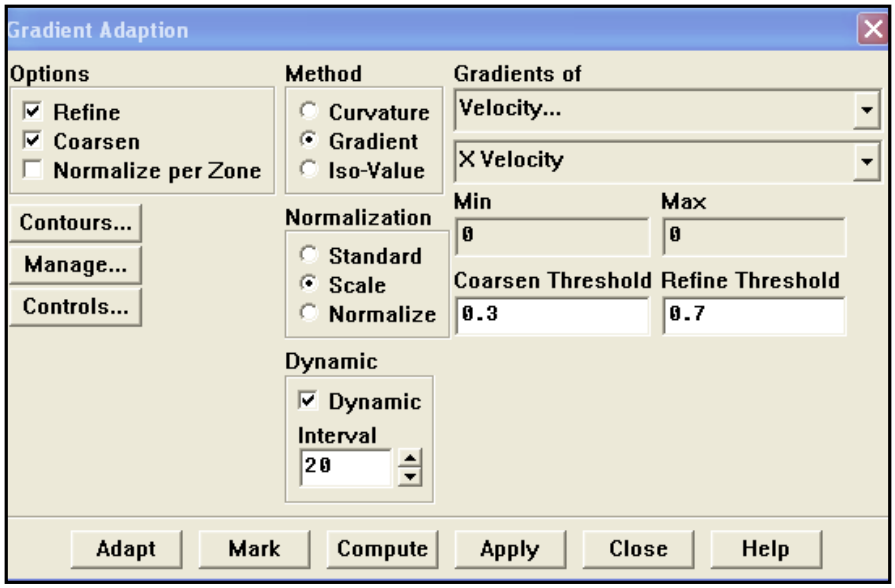

Figure 3-1 The Gradient Adaptation panel in FLUENT.

$$e_1 = (A_{cell})^{\frac{1}{2}} |\nabla f| \tag{3.1}$$

$$e_2 = (A_{cell})^{\frac{1}{2}} |\nabla^2 f| \tag{3.2}$$

Where A_{cell} is the cell area (in 2D), ∇f and $\nabla^2 f$ are the Euclidean norm of the gradient and the undivided Laplacian of the desired field variable f respectively.

These two gradients will be considered carefully combining with physical flow variable in order to determine the suitable refinement variables. However, it is necessary to mention ***the normalisation of the error indicator.*** This is because performing dynamic grid adaptation would probably produce a strong change of the raw values during the computation, which would also necessitate a readjustment of the coarsen and refine thresholds. In this case, a scale gradient, defined as below is used.

$$\frac{|e_i|}{avg|e_i|} \tag{3.3}$$

Here $avg|e_i|$ refers to its average value. The ***lower and upper threshold*** recommended by Fluent (2003) of 0.3 and 0.7 respectively are to be used.

All the simulations are initiated on uniform rectangular grids. In the adaptation process, the mesh for the whole domain is refined or coarsen with respect to the error indicator. The refinement process proceeds after a specific number of iterations; 100, 300 and 200 for flow in a pipe, flow in channel with sudden expansion and lid-driven cavity flow respectively. The refinement frequency can be set in **Interval** section in the **Gradient Adaption** panel as shown in Figure 3-1. It is important to note here that the grid that is coarsen than the grid generated as the initial mesh cannot be created. In order to avoid excessive refinement that can cause redundant mesh, the level of refinement to be 2 [n ***level of refinement*** , Figure 2-5, can increase the number of cells by the factor of 2^{2n} in 2D domain] for both the case of flow in a pipe and in sudden expansion flow, and 3 for lid-driven cavity case were used. The level of refinement can be set in the **Max Level of Refine** section in the **Grid Adaptation Control** panel as shown in Figure 3-2, accessible via. the **Control** section in the **Gradient Adaptation** panel.

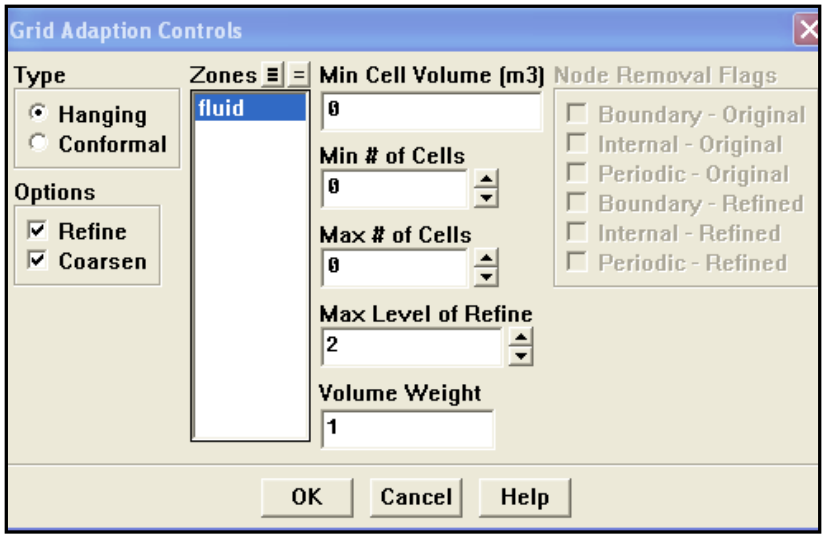

Figure 3-2 The Grid Adaptation Controls panel in FLUENT.

To maintain accuracy, neighbouring cells are not allowed to differ by more than one level of refinement. This prevents the adaptation from producing excessive cell volume variations and ensures that the positions of the original and refined cell centroids are similar which reduces errors in the flux evaluations. Additional restriction and simulation results corresponding to each case will be discussed for more detail afterwards.

3.1.2 Numerical setup

Under a carefully selected Reynolds number for each model, flow applications selected here are supposed to be steady, laminar and able to be simulated in two dimensions. The governing equations for all the cases are those shown as follows, with constant density.

$$\frac{\partial u_i}{\partial x_i} = 0 \tag{3.4}$$

$$\frac{\partial \rho u_i u_j}{\partial x_j} = -\frac{\partial p}{\partial x_i} + \frac{\partial}{\partial x_j}\left[\mu\left(\frac{\partial u_i}{\partial x_j} + \frac{\partial u_j}{\partial x_i}\right)\right] \tag{3.5}$$

Where u_i represents the $\boldsymbol{i}$ the Cartesian component of velocity, p is the pressure, ρ and μ is the constant fluid density and viscosity respectively.

The governing equations are discretised by the finite volume method and yields non-linear (discrete) governing equations which will be linearised in order to produce a system of equations for the dependent variables in every computational cell. The second-order upwind scheme is used to discretise both the viscous and convection terms. In the linearization process, each discrete equation will be linearized implicitly with respect to that equation's dependent variable. This will result in a system of linear equations with one equation for each cell in the domain. A point implicit (Gauss-Seidel) linear equation solver is used in conjunction with an algebraic multigrid (AMG) method to solve the resultant scalar system of equations for the dependent variable in each cell (Fluent, 2003). To avoid checker-boarding of pressure, a procedure similar to that outlined by Rhie & Chow (1983) is employed, the scheme interpolates the pressure values at the face using momentum equation coefficients. Pressure-velocity coupling is achieved by using a semi-implicit method for pressure linked equations (SIMPLE) algorithm.

All the simulations for all three cases are judged for the convergence purpose by monitoring the residual sum, $R^{\emptyset}$, for each of the conserved variables, $\emptyset$, over all the computational cells, P , which is defined as below.

$$R^{\emptyset} = \frac{\sum_{cell\ P}\left|\sum_{nb} a_{nb}\emptyset_{nb} + b - a_p\emptyset_P\right|}{\sum_{cell\ P}|a_P\emptyset_P|} \tag{3.6}$$

Here, a_P is the centre coefficient, a_{ab} are the influence coefficients for the neighbouring cells, b is the contribution of the constant part of the source term and of the boundary conditions. The numerical processes for the first, second and third case are carried out until the residual, defined above for all monitored variables reached approximately 10e-4, 10e-6 and 10e-5 respectively. Nevertheless, it must be noted that the whole process for a simulation is stopped when there is no significant change in the residual trends during three successive adaptive procedures observed.

3.2 CIRCULAR PIPE FLOW

3.2.1 Introduction

To give more clear idea about the approach of SAG, flow in a circular pipe was first selected. This kind of flows is involved in many practical engineering applications. It is therefore important to accurately predict the flow behaviour inside. A flow enters a pipe, Figure 3-3, and the growth of the boundary layer along the pipe is expected which, provided that the pipe is long enough, eventually evolved and completely merge each other. This causes the flow to become fully-developed with parabolic velocity profile, the parabolic Hagen-Poisenuille profile, with no variation in the axial direction, x. The profile is well known to be one of the few exact solutions of the Navier-Stokes equations. For a circular pipe a parabolic velocity profile, $U(r)$ can be written as;

$$U(r) = \frac{R^2}{4\mu}\left(-\frac{\partial p}{\partial x}\right)\left[1 - \left(\frac{r}{R}\right)^2\right] \tag{3.7}$$

The maximum velocity, U_{max} in the pipe is the centreline, $r = 0$, then the above equation yields.

$$U_{max} = \frac{R^2}{4\mu}\left(-\frac{\partial p}{\partial x}\right) \tag{3.8}$$

And also it is easily shown that $U_{max} = 2U_{avg}$

The Reynolds number of 200, based on diameter of the pipe $(D = 2R)$ and average velocity U_{avg} is chosen and the numerical results will be compared directly to the analytical solution.

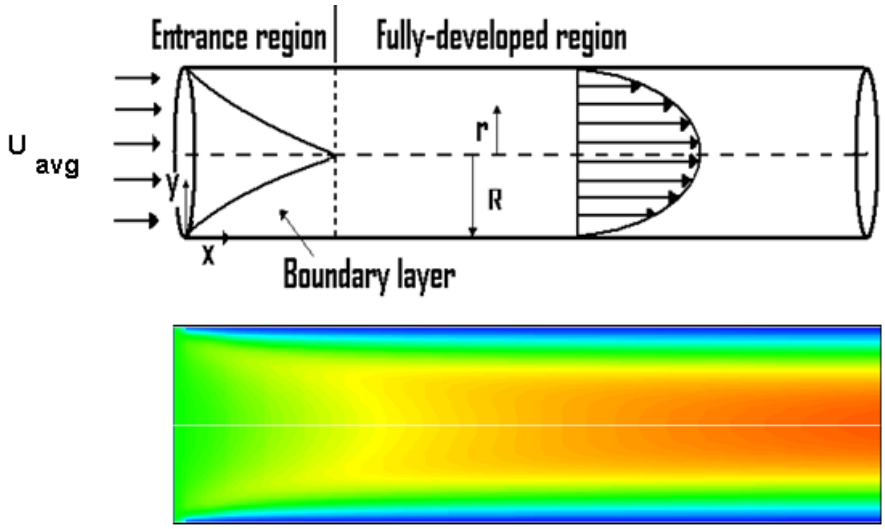

Figure 3-3 Above) Geometry of flow in a circular pipe with fully-developed velocity profile, Below) Velocity magnitude contour with red being high and blue being low, Figure modified from Fox *et al.* (2008).

3.2.2 Model setup and results

The investigation for this case began with introducing a flow into an 8 m long pipe with a diameter D of 0.2 meter. The Reynolds number of the study was 200. Therefore, according to the exact solution for axial velocity at a distance r from the centre-line for the area with fully-developed flow and below is the exact solution for this case.

$$U(r) = 4\left[1 - \left(\frac{r}{R}\right)^2\right] \tag{3.9}$$

The mesh shown in Figure 3-4(a) is adopted to be the initial mesh for the calculation. The variables selected to be the testing refinement variables here are the first and second (curvature) gradient of axial velocity since their behaviour are well-known from the exact solution. As can be seen in Figure 3-4(b) in case of gradient adaptation, the

distribution mostly occurs in those regions close to the wall due to high velocity gradient and less mesh refinement around the centre-line as predicted. From the inlet to approximately $x = 1.5$ m where the flow is expected to be growing there is also no any significant refinement. For curvature adaptation, beyond the entrance region far to the outflow, due to the parabolic profile the flow is supposed to give constant second gradient of velocity. Figure 3-4(c) shows the mesh distribution of this case. Figure 3-5 displays the results compared with the analytic solutions of axial velocity profile on the centre-line together with the velocity profile development in the entrance region. Two meshes with approximately 10 and 100 times higher in grid density than the initial mesh were carried out for grid convergence test and the resulting solutions are also shown in Figure 3-5.

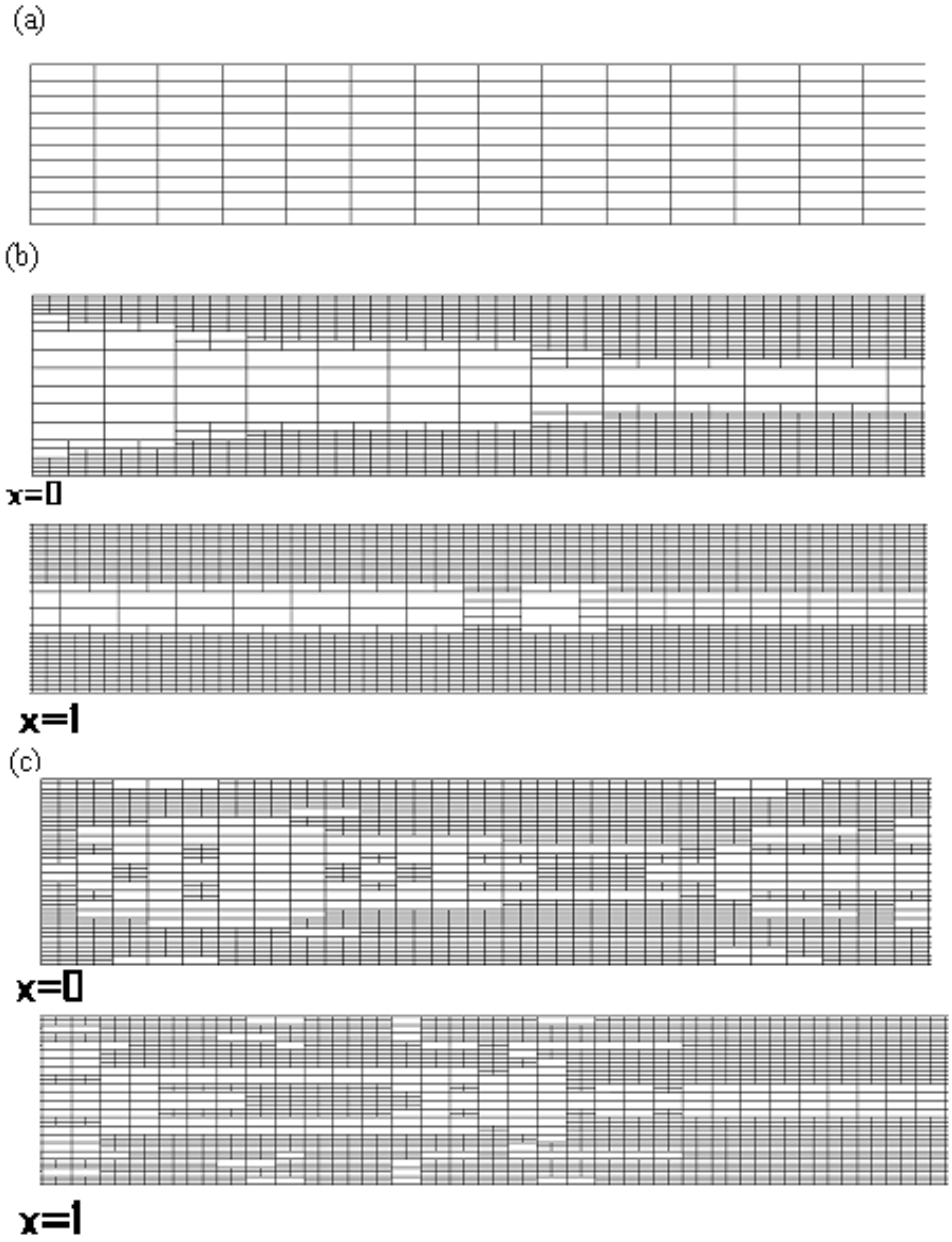

Figure 3-4 Grid distribution for the case of (a) Initial mesh, (b) Axial velocity gradient adaptation and (c) Axial velocity curvature adaptation.

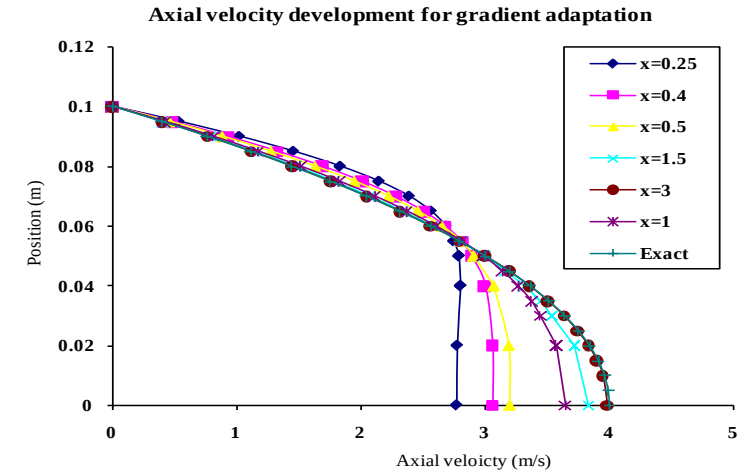

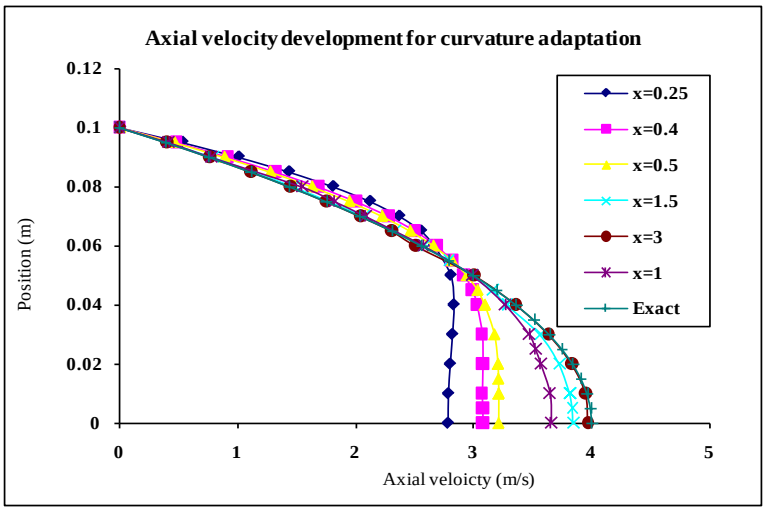

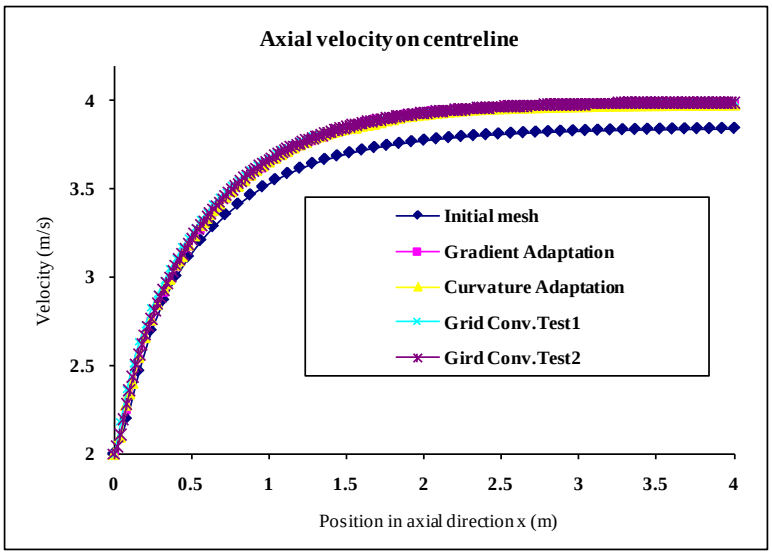

Figure 3-5 Velocity profiles comparisons for differing refinement methods and axial locations.

3.3 SUDDEN EXPANSION FLOW

3.3.1 Introduction

Flows through expansion (also known as confined jet), Figure 3-6, have important applications in science and engineering. Some examples are extrusions, free jets, refrigeration and manufacturing processes. In recent years, there are many significant studies, both in numerical and experimental conducted to investigate, calculate and measure fluid behaviour, with both Newtonian and non-Newtonian fluids, of this kind of flows and have explored much information. It is well-known that steady laminar inflows in two-dimensional channels with symmetric expansion can reveal either non-symmetric or symmetric solution, depending on the value of the Reynolds number or, in other words; it exhibits a transition phenomenon from symmetric to asymmetric equilibrium states. It is concluded by many experimental investigations (Sobey (1984), Durst *et al.* (1974), Fearn *et al.* (1990)) that with low Reynolds number,($< \mathrm{Re}_{\mathrm{crit}}$),the flow is observed to remain steady two-dimensional and symmetric with two separation zones near the expansion corners. When the Reynolds number is increased, however, the flow stays steady two-dimensional but becomes asymmetric with separation zones of different length which can occur either attaching to the lower or upper wall of the channel. If the Reynolds number is further increased, the flow may become three-dimensional, time dependent and finally turbulent. Fearn *et al.* (1990) have demonstrated that this experimental behaviour can be found as a result of a pitchfork symmetry-breaking bifurcation point, when solving Navier-Stoke equations, where the symmetric state loses its stability and evolves into asymmetric state when the Reynolds number reaches the critical one ($> \mathrm{Re}_{\mathrm{crit}}$). Table 3-1 shows the critical Reynolds number, gathered from both numerical and experimental work, varying from author to author.

In 1997, numerical linear stability studies were conducted by Battaglia *et al.* (1997) to investigate the effect of channel expansion ratio on the asymmetric states performance. The main conclusion is that the critical Reynolds number at which the transition to asymmetric states occurs decreases with increasing channel expansion ratio.

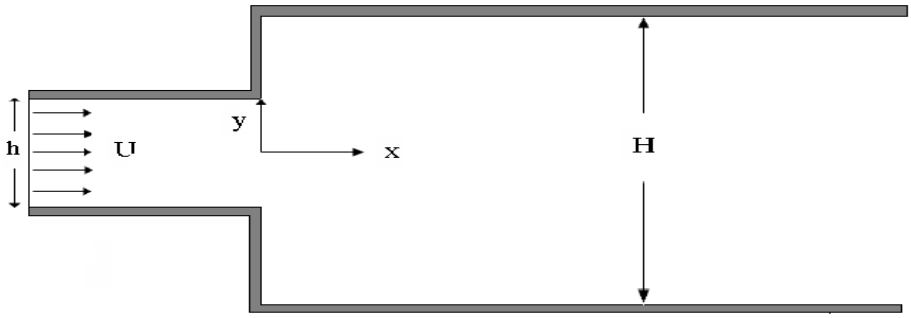

Figure 3-6 Channel with symmetric sudden expansion geometry.

Table 3-1 Critical Reynolds numbers calculating based on different definitions, with U(mean) being average inlet velocity.

Authors	Definition of Re	Critical Re (Re_{crit})
Sobey (1984)	U(mean), h/2	25.00
Fearn *et al.* (1990)	U(mean), h/2	40.45
Battaglia *et al.* (1997)	U(mean), h	53.80
Hawa & Rusak (2000)	U(max), h	53.80
Paulo & Oliveira (2003)	U(mean), h	54.00

3.3.2 Model setup and results

This study deals with incompressible Newtonian fluid flow with the Reynolds number at 80, defined as below, to investigate the refinement approach effects toward the flow numerical simulation.

$$Re = \frac{U_{mean} h}{\nu} \tag{3.10}$$

At this Reynolds number the flow is supposed to be steady and two-dimensional, the pitchfork symmetry breaking bifurcation has occurred. The time-dependent phenomena occurring at higher Reynolds number are not considered. The approach is adopted to focus

on the mesh refinement on the expansion region of the channel. Cartesian coordinate system (x,y) is used to described the flow field where x = 0 and y = 0 are the expansion section and the centreline of the channel respectively. The flow is introduced into the channel at $x = -x_0$ where $x_0 > 0$. To make sure that the channel length will not affect the solution, this study the suggestion of Hawa & Rusak (2001) was followed and it was done by setting x_0 and x_1 to be 5 and 50 responding to $h = 1$ (x_1 is defined as the distance from the original co-ordinate to the end of the channel in the positive end). Along the upstream section of the channel, $x < 0$, all velocities are normalized by U_{mean}. As a result, the flow is supposed to be full-developed with parabolic velocity profile, the *Poiseuille* flow, along the upstream section as well as the outlet flow far downstream of the channel. No-slip condition for velocity is adopted for all walls.

The investigation presented here is compared with the numerical solution from Oliveira (2003), whose results are in a good agreement with other numerical results, as well as with the experimental results from Fearn *et al.* (1990). The comparison is mainly concentrating on the x-velocity component along cross section lines $x/h = 1.25,\ 10$ and the bifurcation results, vortex length differences, of the flow. As mentioned above, the first and second gradient (curvature) of y-velocity and static pressure were taken into account as the testing refinement variables. A total of 8 simulations were performed starting with 2 different initial meshes as shown by Figure 3-7. A very fixed fine mesh with 25,800 cells was used initially to simulate the case in order to capture the flow basic feature at the relevant Reynolds numbers. Figure 3-8 shows a resulting solution for this mesh. The flow feature obtained from numerical calculation with this mesh illustrates upper and lower recirculation region which occurs at a bifurcation of the Navier-Stokes equations.

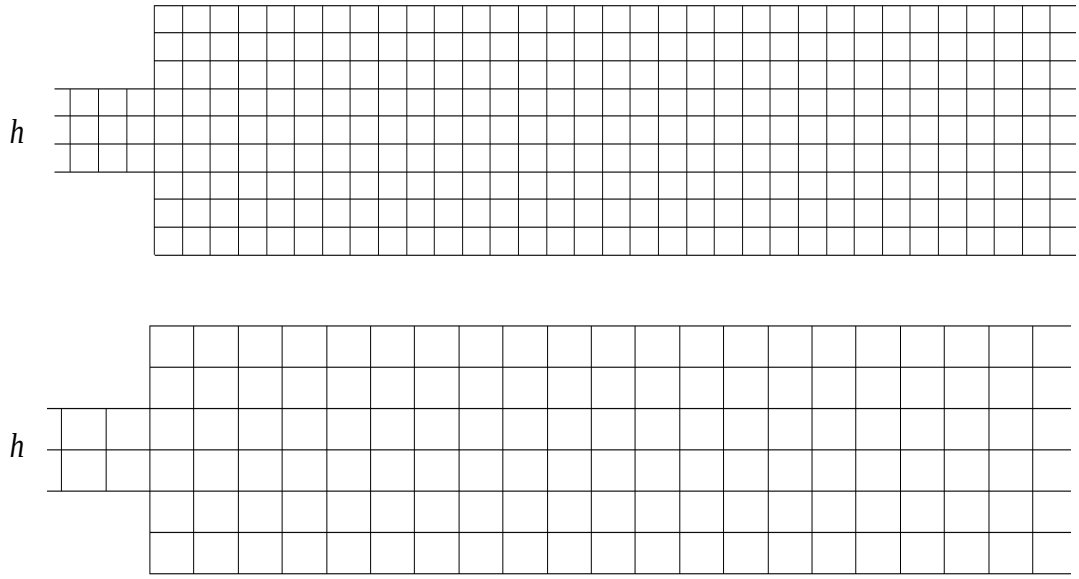

Figure 3-7 Above)Initial mesh-1: $\Delta x = \Delta y = h/3$, below)Initial mesh-2: $\Delta x = \Delta y = h/2$.

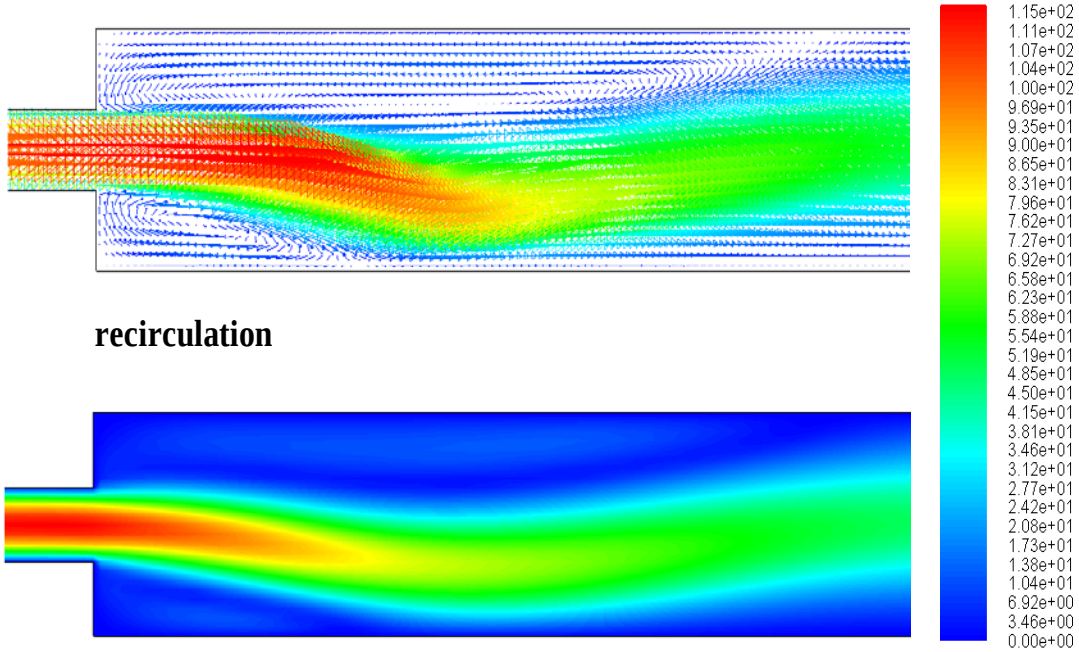

Figure 3-8 Feature of the flow in a two-dimensional channel with sudden expansion at Re = 80. Flow parameter shown: velocity magnitude.

The SAG based numerical simulation begins with two initial meshes with size $\Delta x = \Delta y = h/3$ (initial mesh-1) and $\Delta x = \Delta y = h/2$ (initial mesh-2), Figure 3-7. Two conventional meshes (one containing 12,400 cells and the other containing 24,800 cells) are adopted for the case of grid convergence and their results are shown in Figure 3-9. The initial mesh-1 creates 1,395 cells while 620 cells are generated by the latter. A variety in mesh resolution is establishing during the refinement process. In the case of adopting first gradient, grids are re-refined or re-coarsened mostly in the area following the flow further downstream, Figure 3-10, while mesh adaptation feature is more widely spreading for curvature cases, Figure 3-11. The maximum cells number of 3,999 occurs in the case of Y-velocity gradient which is approximately three times higher than the initial mesh-1 case. However, the maximum mesh density established in the case is still roughly 35% less than those utilized in the work of Oliveira (2003) while yielding acceptable result agreement. Figure 3-10(a) and (c) also reveal an evident supporting the normal flow aspect that further from critical Reynolds number the flow losses its stability and attach either side of the channel and this aspect seems to be sensitively affected by these two mesh dynamic refinements.

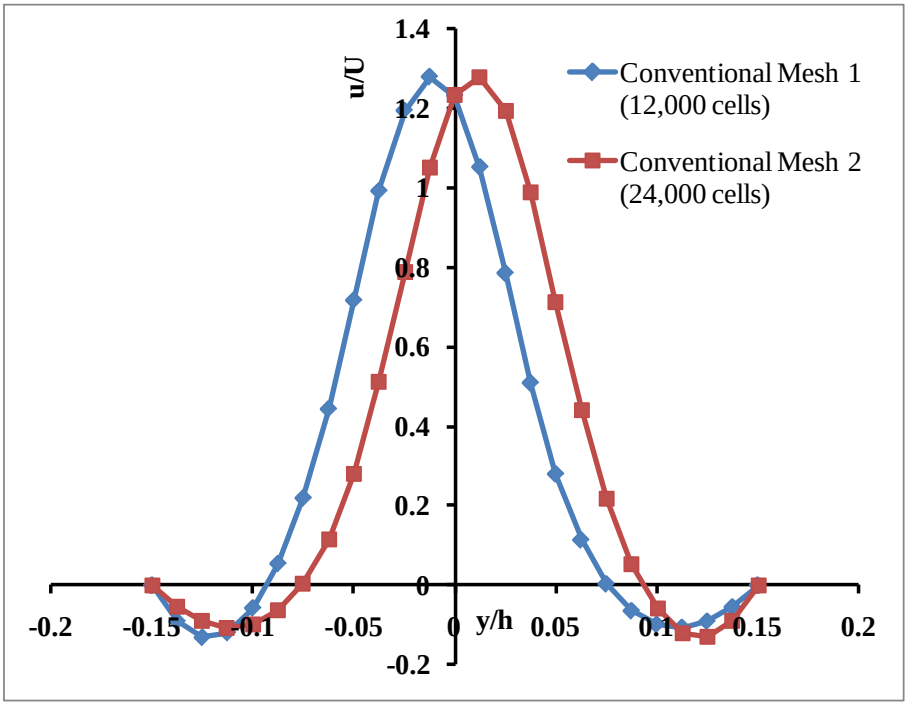

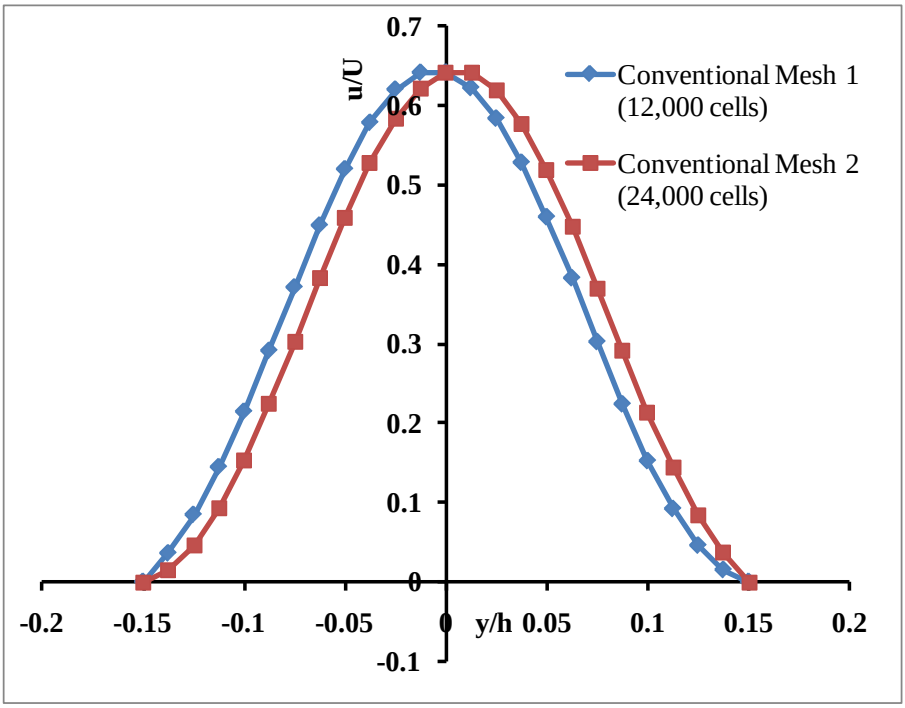

Figure 3-9 Grid convergence study cases : x-velocity profile on a cross section line x/h = 1.25 (above) and x/h = 10 (below).

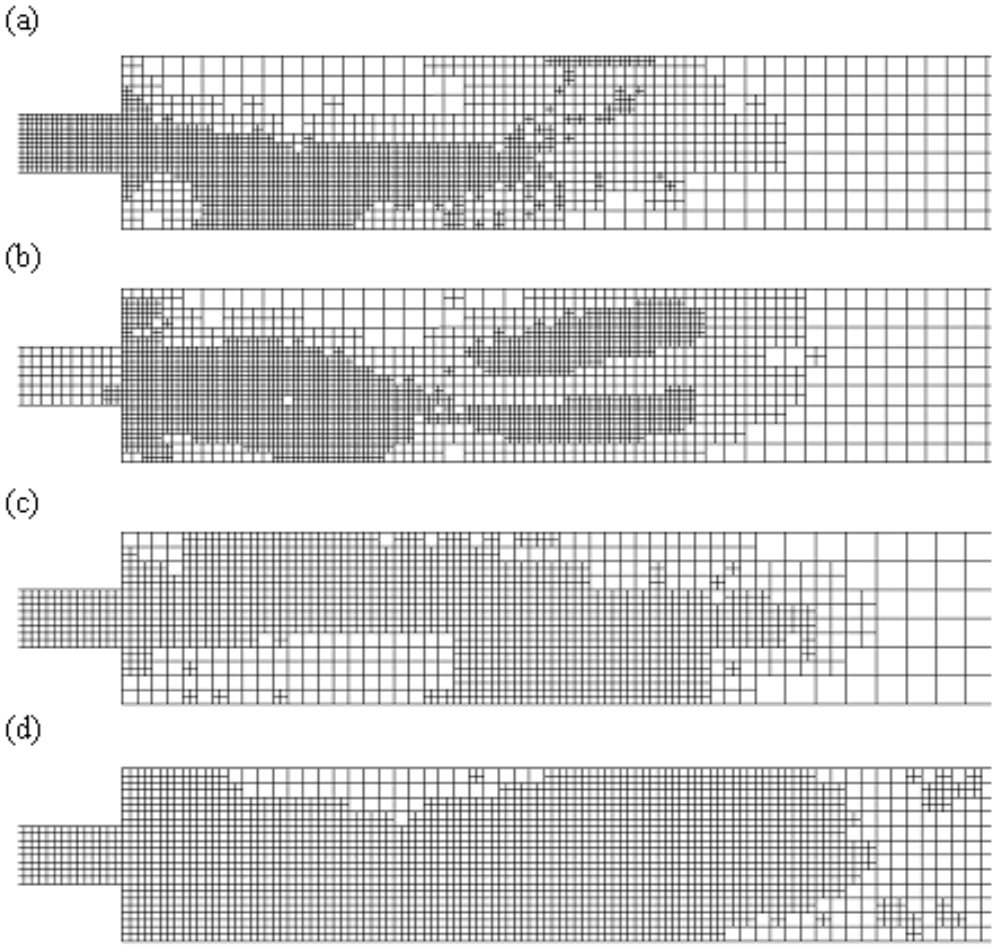

Figure 3-10 Mesh distribution after gradient adaptation of (a) Static pressure with Initial mesh-1, (b) Y-velocity with Initial mesh-1, (c) Static Pressure with Initial mesh-2 and (d) Y-velocity with Initial mesh-2.

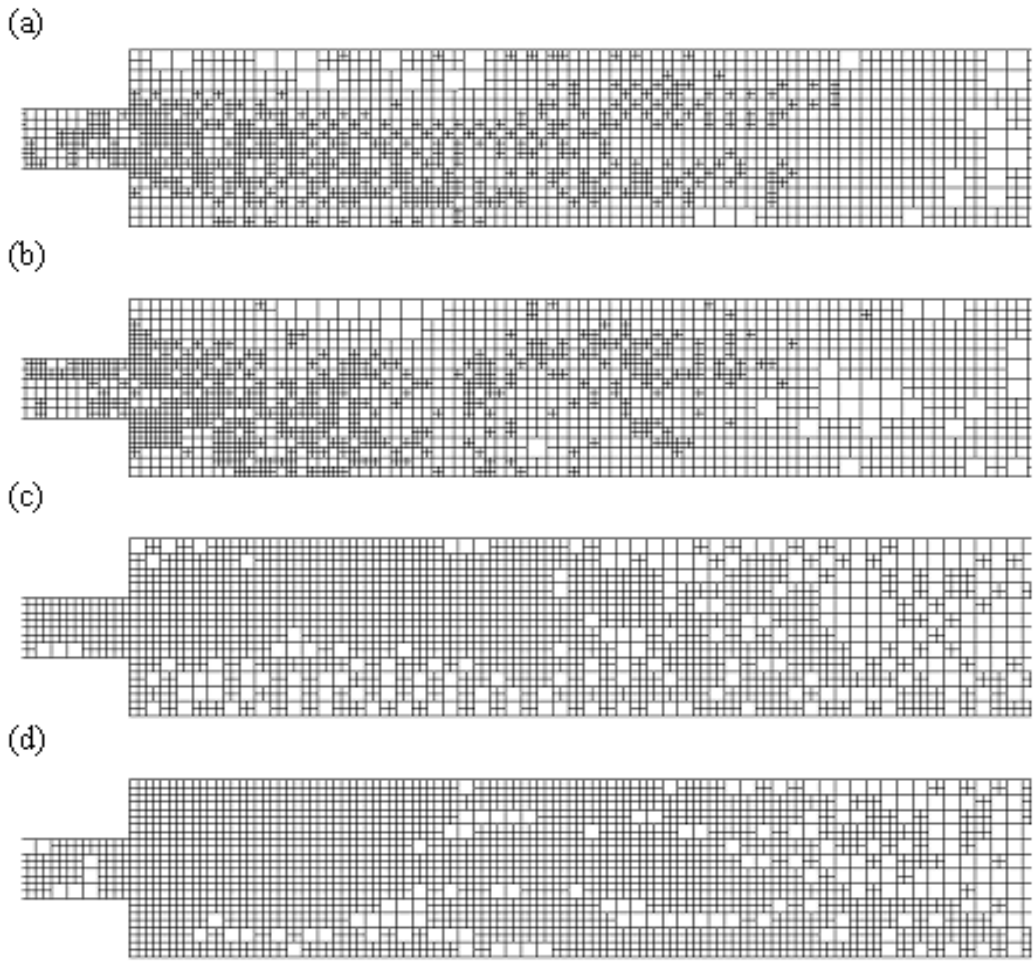

Figure 3-11 Mesh distribution after curvature adaptation of (a) Static pressure with Initial mesh-1, (b) Y-velocity with Initial mesh-1, (c) Static Pressure with Initial mesh-2 and (d) Y-velocity with Initial mesh-2.

Once again, with the initial mesh-2, even the highest mesh density created in the case of Y-velocity curvature is also lower than in the literature. Interestingly, regarding to Figure 3-13, Figure 3-14 and Figure 3-15, for both initial mesh cases, it can reach almost the same quality in result. The solutions have been very much improved after adopting the approach compared to those obtained from both initial meshes [Initial mesh-1 and Initial mesh-2]. The figures also show that the numerical solutions are in remarkable agreement with the measurement conducted by Fearn e*t al.* (1990) for both initial cases. It also should be mentioned here that the minimum cells number that can enable a good result to be reached is about a half of those in Fearn e*t al.* (1990). Figure 3-12 shows the predicted

bifurcation diagram comparison between experimental and predicted SAG based results. D_x represents the difference between primary and secondary vortex length. The result form the coarsest initial mesh is chosen for the comparison and the results are in good agreement with Fearn *et al.* (1990).

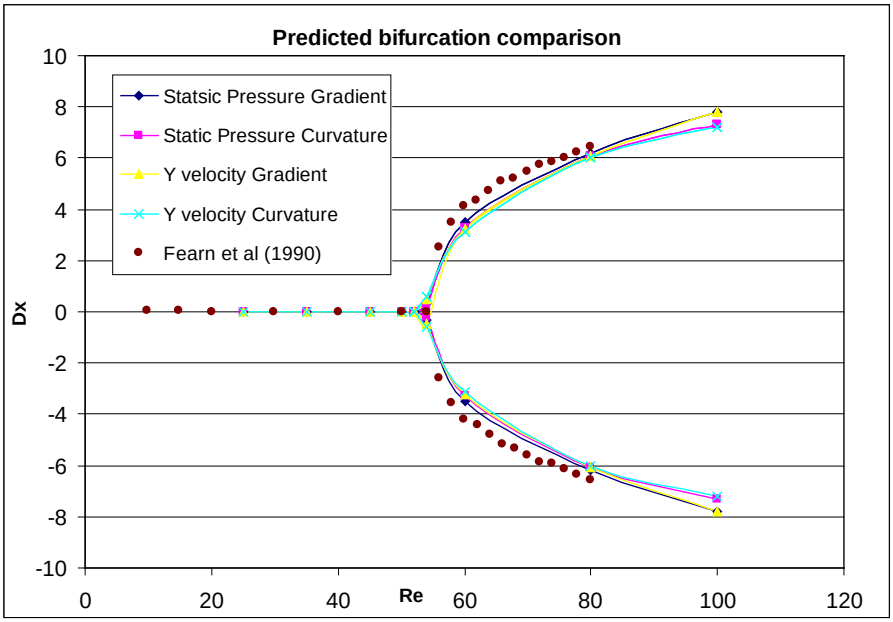

Figure 3-12 Predicted bifurcation comparison with experimental data from Fearn *et al.* (1990). Note : Dx is in the unit of channel inlet high (h).

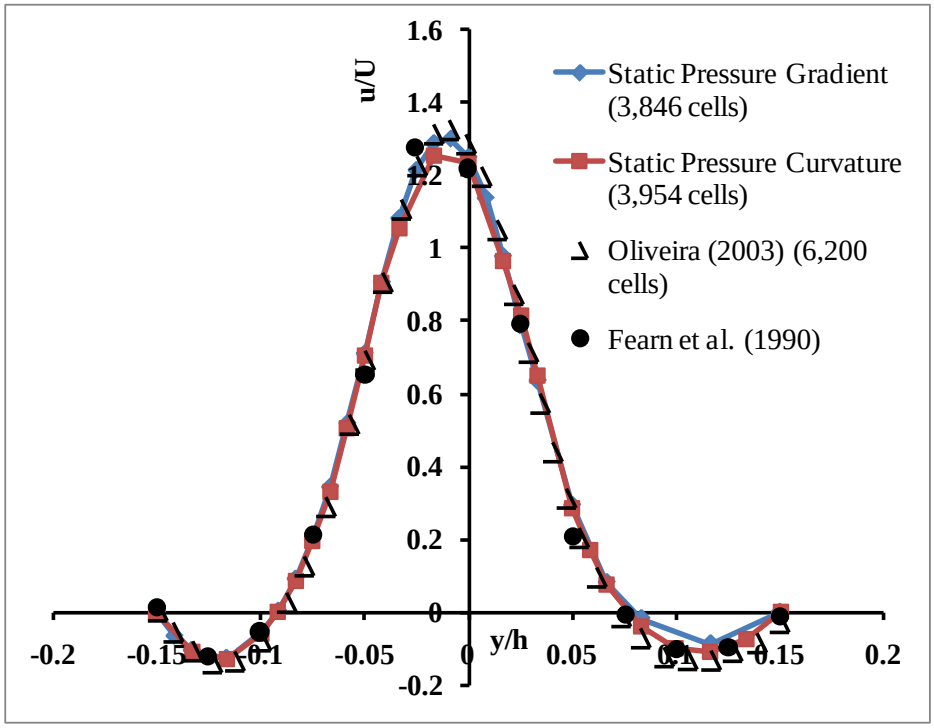

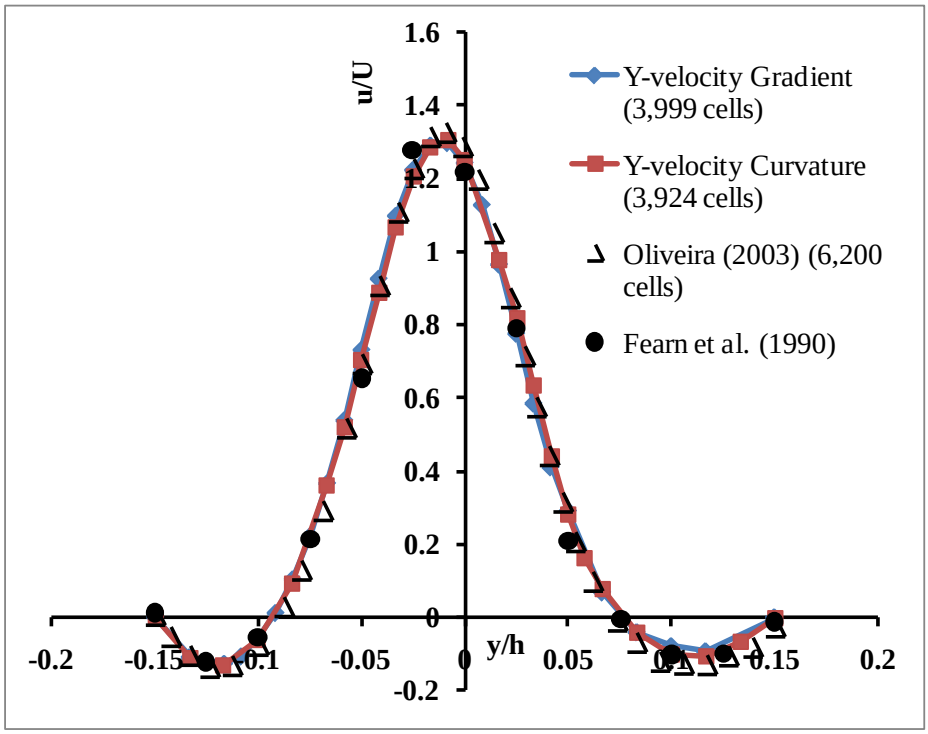

Figure 3-13 X-velocity profiles comparison on a cross section line x/h = 1.25 obtained from SAG application with initial mesh-1 and different refinement variables.

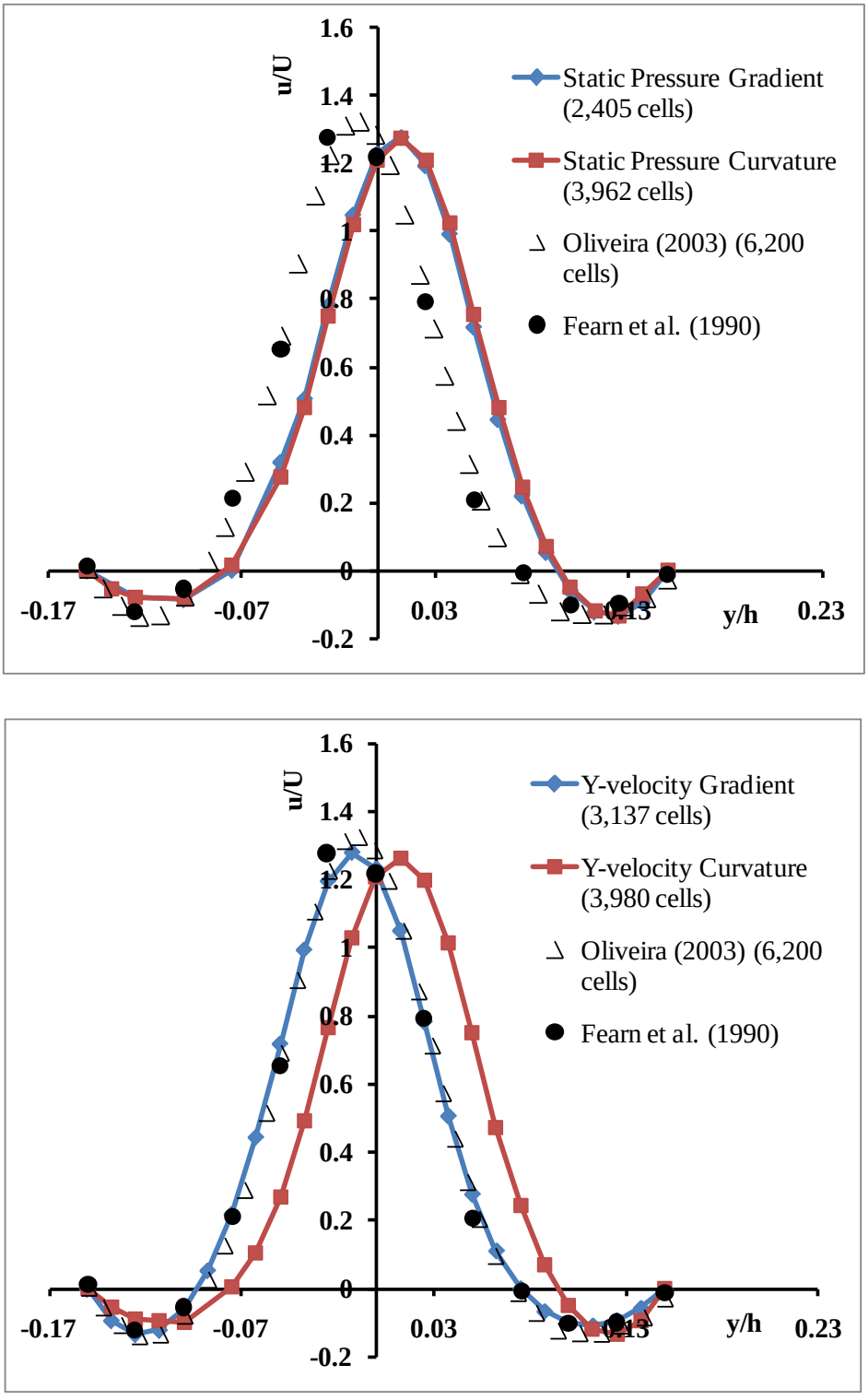

Figure 3-14 X-velocity profiles comparison on a cross section line x/h = 1.25 obtained from SAG application with initial mesh-2 and different refinement variables.

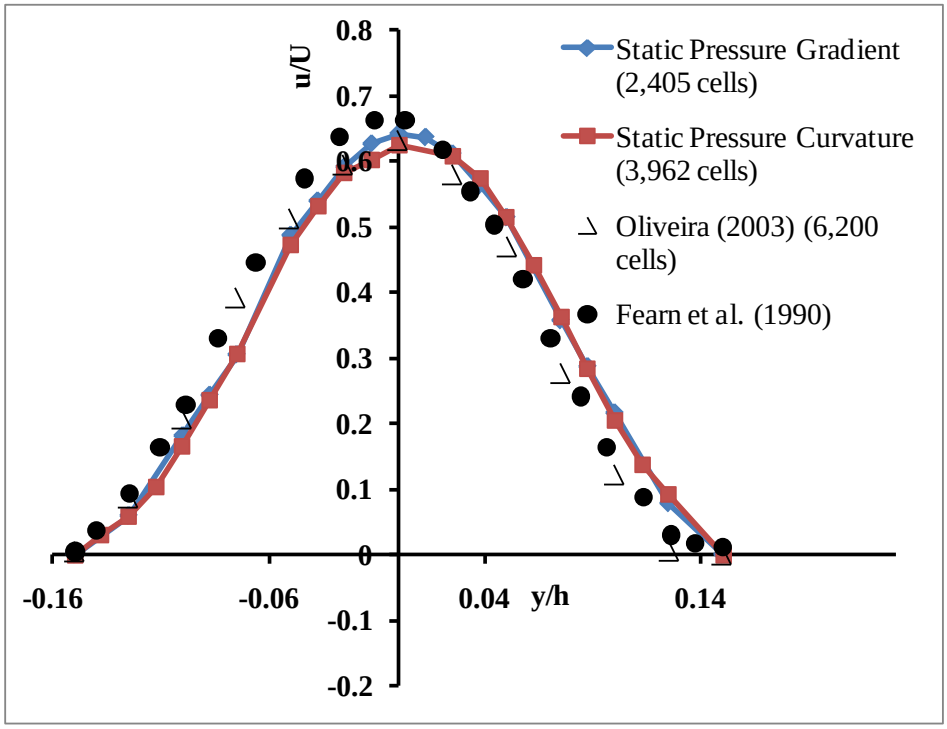

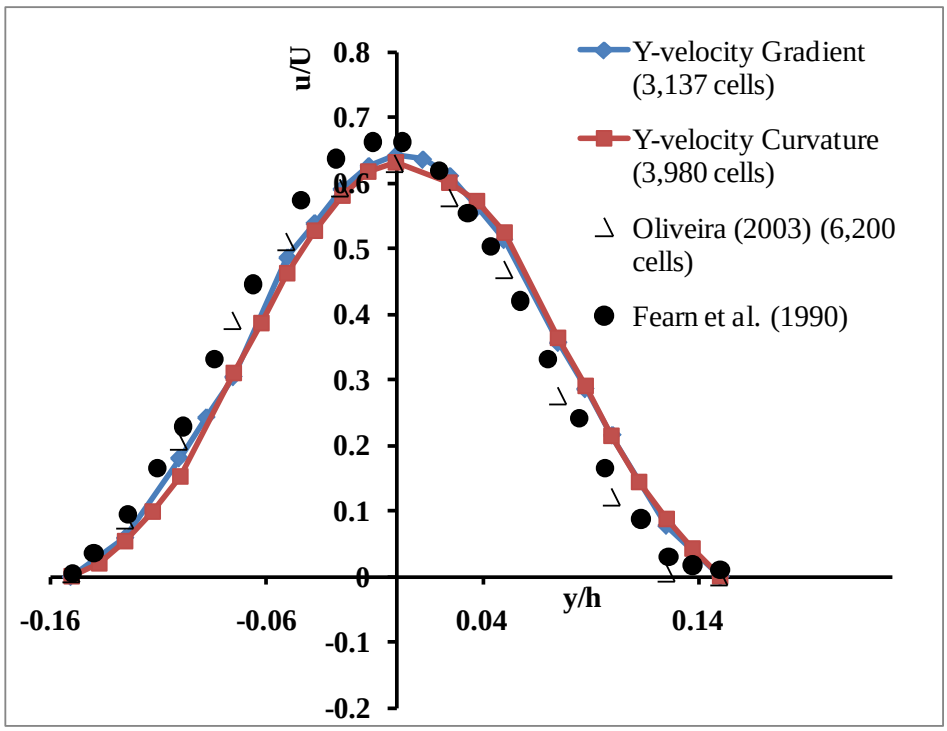

Figure 3-15 X-velocity profiles comparison on a cross section line x/h = 10 obtained from SAG application with initial mesh-2 and different refinement variables.

3.4 LID-DRIVEN CAVITY FLOW

3.4.1 Introduction

The third case study deals with the flow in a square cavity with a moving wall on the top and the rest are stationary, Figure 3-16. This kind of flows has been investigated by many authors for over twenty years. Interestingly, in the case of Reynolds number at 1000, many literatures have shown a very good agreement in the results from one author to another. Due to its simplicity to be investigated in numerical aspect, the lid-driven cavity flow has been extensively studied in the CFD field. Moreover, it also retains a rich fluid flow physics manifested by multiple counter rotating recirculating regions on the corners of the cavity depending on the Reynolds number.

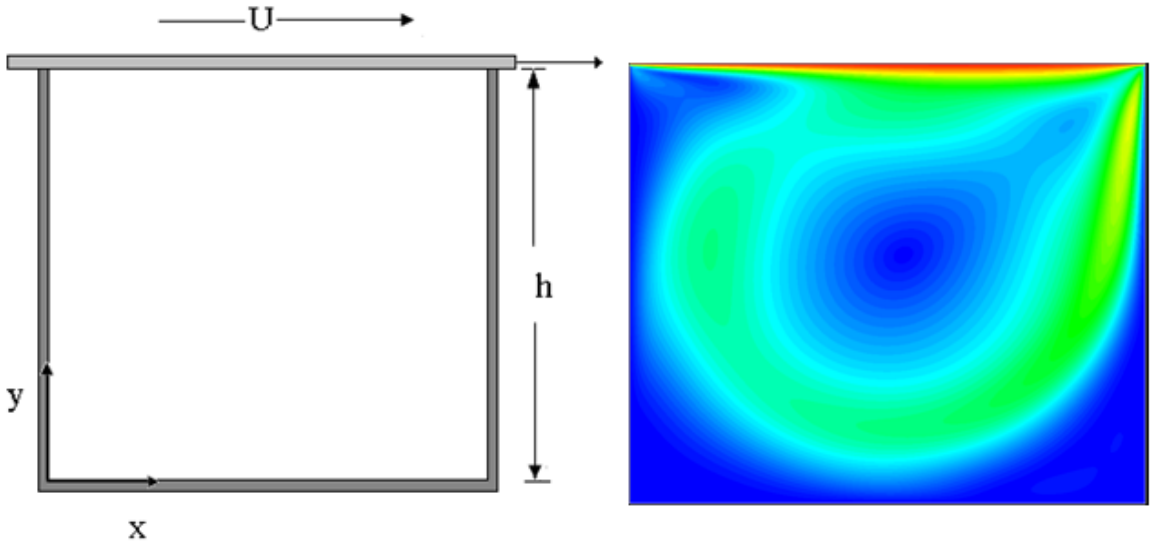

Figure 3-16 Computational configuration of lid-driven cavity together with its velocity magnitude contour; red being high and blue being low.

3.4.2 Model setup and results

To develop the refinement approach for this case, the case of the Reynolds number at 1000 is chosen. The cavity is of $hxh = 1\ m^2$ size with the top wall is moving with a velocity (U) in x-direction, while bottom and side walls are stationary.

In this case the investigation started with a very coarse mesh, $(h/10)^2$ (initial mesh-3) and continues by applying each refinement variable. Firstly, two cases with very fine mesh containing of 10,000 cells and 32,000 cells were investigated for a grid convergence purpose and the results are presented in Figure 3-17. In the study of SAG application, the level of refinement is set to be three which means that for an initial cell in the region of interest can be refined and increase the number of cells by a factor of 64. Mesh distributions are occurring following the counter rotating recalculating regions when performing both first and gradient of static pressure and concentrating more near the left and right wall due to its parameter feature, Figure 3-18. Here, velocity profiles on both horizontal and vertical line passing through the centre of the cavity are selected to justify the quality of the simulation results. For all cases, the solution was compared with the work of Chia & Shin (1982), whose result is acknowledged by many authors, and Fluent (2005). The comparison reveals a significant advantage of the dynamic grid adaptive application when those all are in very good agreement while the approach can cause a considerable reduction in mesh density. All cases conducted under the condition explained above produce less than 2,000 cells after refinement process which is approximately 7 times less than those adopted in the two references. The comparisons are shown in Figure 3-19 and Figure 3-20.

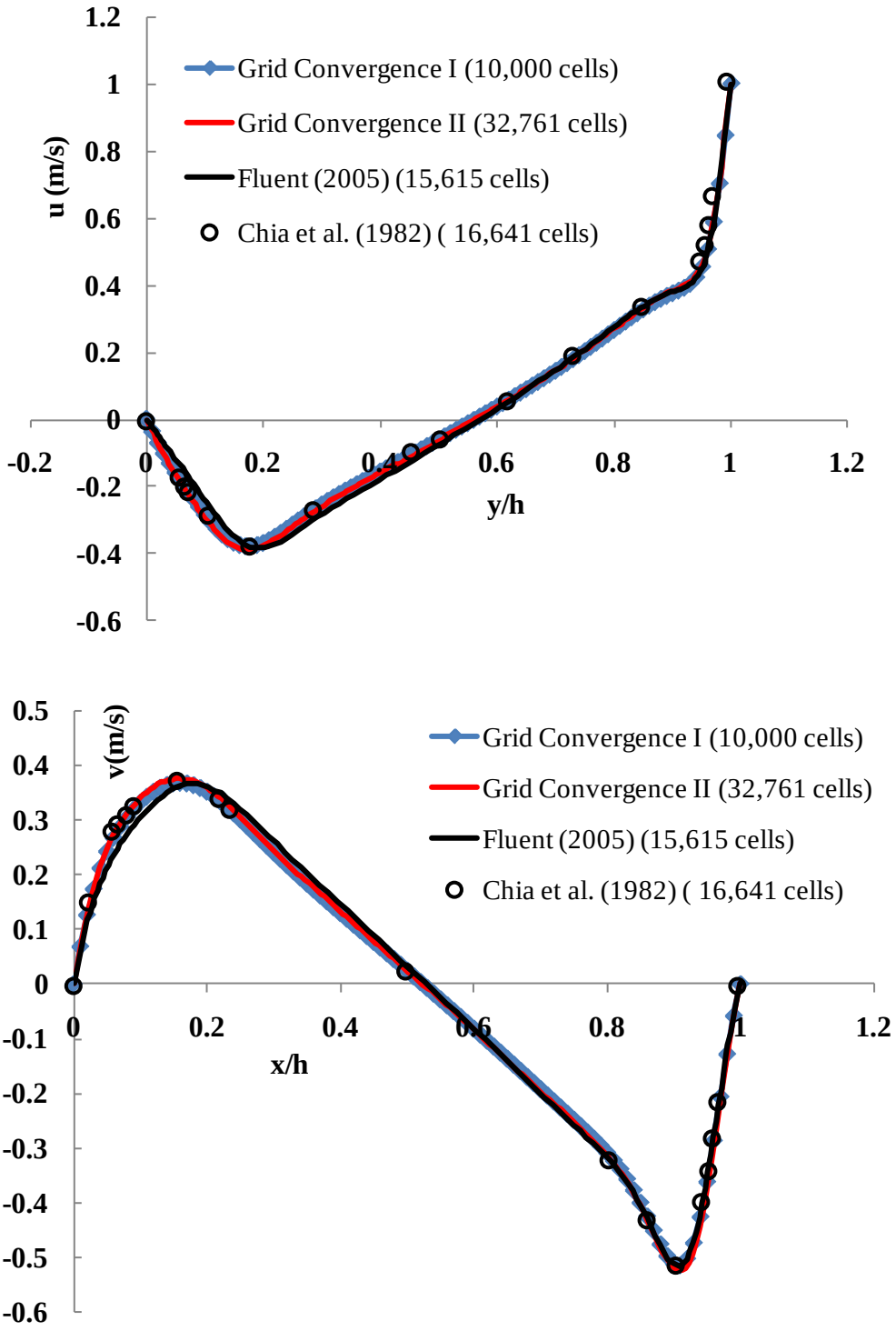

Figure 3-17 Velocity profiles comparisons for the grid convergence study cases : x-velocity (m/s) along the line x/h = 0.5 (above) and y-velocity (m/s) along the line y/h = 0.5.

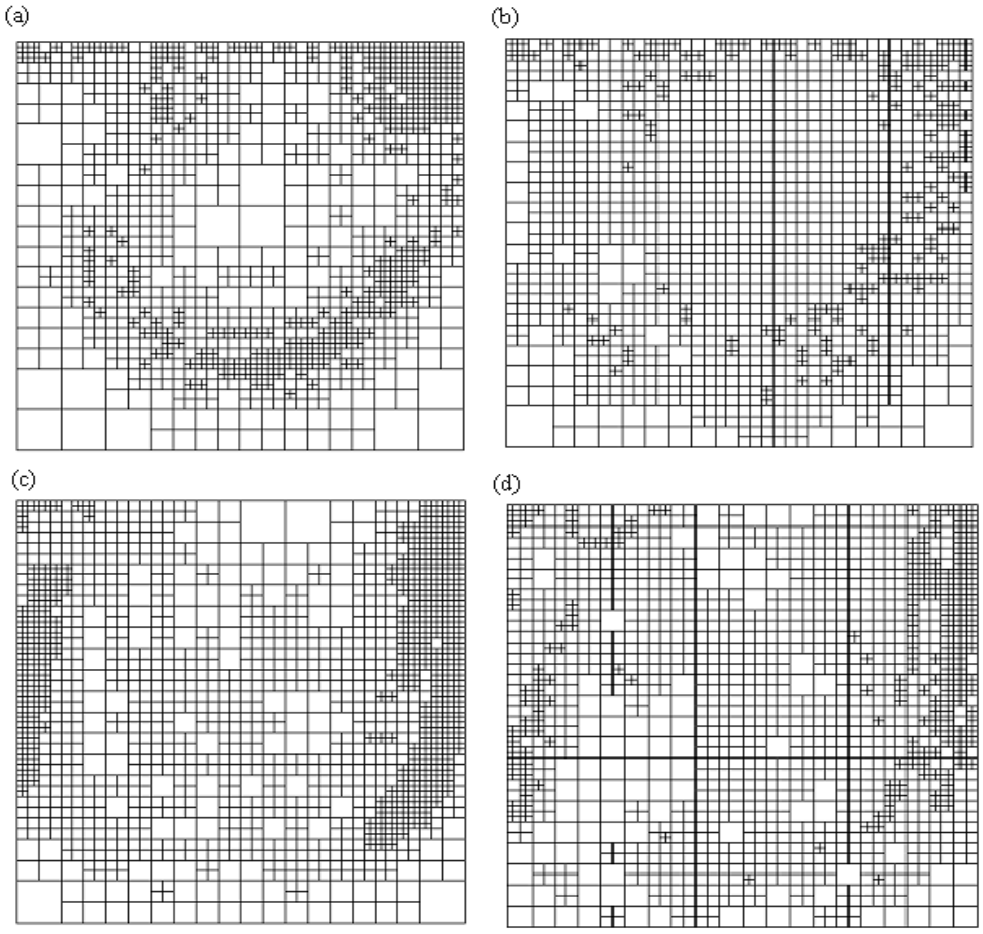

Figure 3-18 Mesh distribution after refinement regarding to each refinement variable (a) static pressure gradient, (b) static pressure curvature, (c) y-velocity gradient and (d) y-velocity curvature.

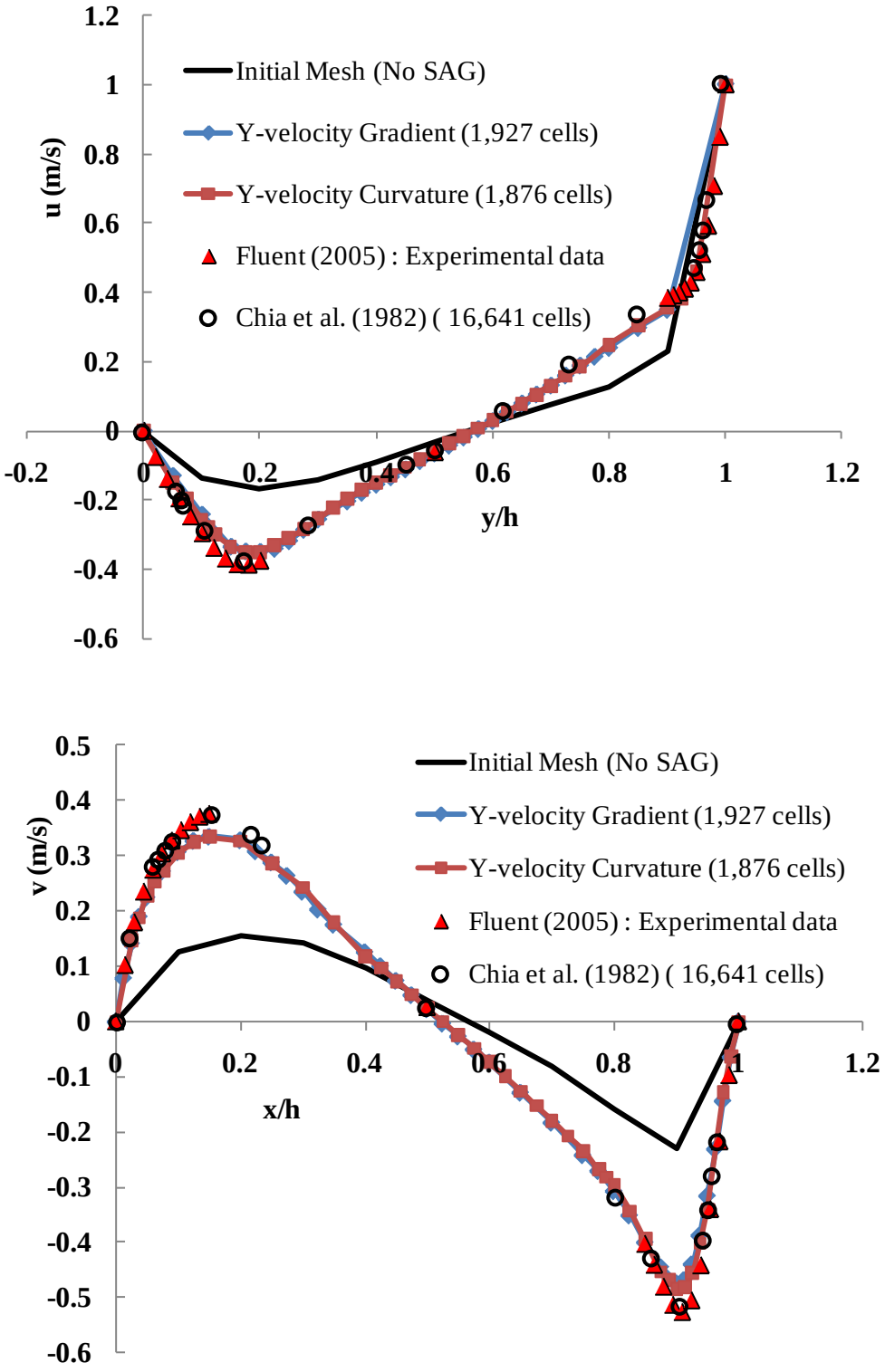

Figure 3-19 Velocity profiles for lid-driven cavity flow with refinement variable: y-velocity, compared against those from the referencing work both numerical and experimental.

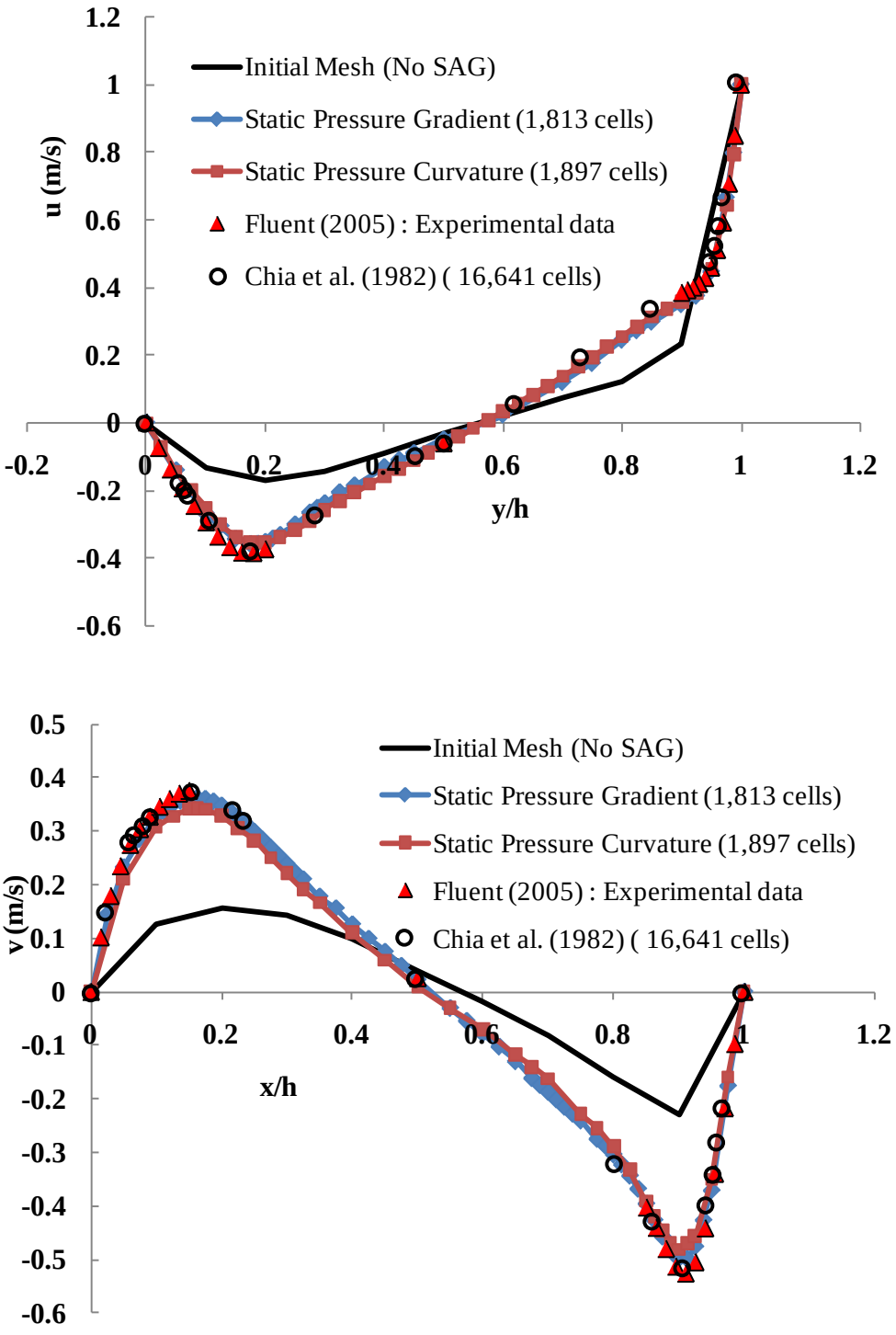

Figure 3-20 Velocity profiles for lid-driven cavity flow with refinement variable: static pressure, compared against those from the referencing work both numerical and experimental.

3.5 COMPUTATIONAL CPU TIME

One important aspect of the use of solution adaptive grid amongst several is concerned with the requirement of CPU time. It is ideal that with the use of SAG, computational time would be reduced and Table 3-2 provides information of this aspect.

Table 3-2 CPU time in minutes for adaptive refinement cases run on an Intel Pentium 4 computer with 3 GHz and 2 GB of RAM; approximately 8 minutes for grid convergence test case of the confined jet (12,400 cells) and 3 minutes for the lid-driven cavity (10,000 cells).

Refinement variables	Confined-jet, initial mesh- 2	Lid-driven cavity, initial mesh - 3
Static Pressure Gradient	6.14	2.10
Static Pressure Curvature	7.25	1.90
Y-velocity Gradient	8.00	2.25
Y-velocity Curvature	6.50	1.10

3.6 SUMMARY

Simulations of three low Reynolds number flows have been investigated with application of solution adaptive grids. The conclusions of the study are as follows:

1. Computing time for achieving good quality solutions are less for the solution adaptive grids than for the equivalent fixed grid counterparts. This is due to the lower overall grid size required for solution adaptive grids.
2. Initial grid configuration has a limited effect on final results in the present study.
3. The effect of refinement variable on the result depends on the problem studied.

- For the circular pipe, it is shown that once the flow is fully developed, the velocity gradient is the most suitable refinement variable.
- For the sudden expansion, it is seen that the velocity based and pressure based refinement variables gave similar results. It is also seen that the present results required significantly fewer cells than the study of Olivieria (2003).
- In the lid driven cavity problem, the effect of refinement variable was again seen to be small. The present results gave agreement with experimental values at grid sizes less than 2000, whilst Chia & Shin (1982) and Fluent (2005) used more than 15000 cells for similar results.

This confirms that the application of solution adaptive grid (SAG) together with appropriate refinement variables, achieves an acceptable simulation solution. The results are in good agreement with other works, and it is not always necessary to perform the calculation with very fine grids. This means that SAG leads to significantly lower computational cost and effort.

Regarding to the algorithm structure nevertheless, it has been shown that several requirements are needed. Even though the refinement variables selected and used with the chosen error indicator means and their corresponding normalization form have shown satisfactory results for simulation of laminar flows, choices for turbulence study might not be as straight forward. The level of refinement was also needed specifically to prevent the algorithm from producing redundant cells and user's judgment was still required to decide the stopping criteria.

An attempt to alleviate these downsides of typical h-refinement strategy begins with a development of components involved. In addition to this, another ultimate target is also to study the two types of error found under LES context and their interaction. This can lead to means to attain the maximum LES solution quality and all start in the next chapter.

CHAPTER 4 ALGORITHM DEVELOPMENT AND IMPLEMENTATION FOR TURBULENT FLOW APPLICATIONS

Chapter 2 has provided all the components that are involved in the main investigation of this work where Chapter 3 has provided an outlook of applications of SAG for low Reynolds number flow simulation. In this chapter an attempt to construct a new refinement algorithm for LES applications is made. Furthermore, the implementation in FLUENT of the new algorithm is also provided.

Before going into the details of the process of the algorithm construction however, a summary of the primary principal concept, challenges, factors involved as well as what is aimed to be achieved is first to be provided. This is important since they all have equal level of influence on the way in which the algorithm will be constructed. This is illustrated as a diagram in Figure 4-1.

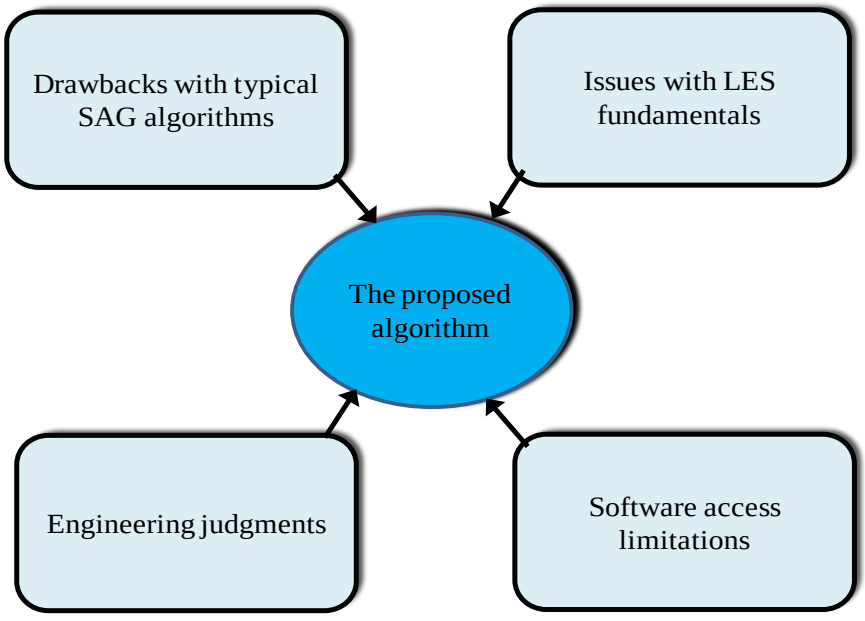

Figure 4-1 Aspects to take into consideration as well as factors encountered in the construction of the proposed algorithm.

The process begins with an attempt to simultaneously alleviate and improve both the problems frequently persist for the applications of typical refinement algorithms and the physically unclosed aspect of LES fundamentals. The main undesired figures that most existing mesh refinement algorithms (particularly h-refinement type) still consist of, deviate them away from meeting the requirements for the ideal algorithms stated in Chapter 2;

- Difficulties for finding proper means of error measurement, indicator and/or estimator for both locally and globally.
- Uncertainties in choosing adequate flow variables to play as the refinement variables, accordingly to the error measurement means selected and very often requiring high level of prior knowledge of the flow at hand.
- The requirement for adequate normalization schemes to prevent the algorithm from producing a strong change of the raw values during the computation.
- The need for suitable refined and coarsen thresholds corresponding to the chosen normalization method.
- The requirement for criteria to prevent the algorithm from producing redundant cells, i.e. the size of the smallest elements needed to be specified beforehand.
- Suitable stopping criteria as well as refinement frequency.

Two important issues regarding the principal concept of large eddy simulation are;

- Defining the smallest turbulence scales to be explicitly calculated by the grid does not take into account the actual nature of the scales.
- Finer mesh does not always guarantee a better result quality but still requires higher computational effort and time.

The process then continues into the details on how to carry out constructing and formulating an algorithm that takes into account all the aspects mentioned above. Here is where two main factors that strongly affect the procedure are being encountered. Firstly, the precise definition of the turbulence Taylor scale in which this study is focusing on has to be modified due to the necessity for allowing the algorithm to repeatedly take place. Secondly, it is also the lack of access into the software code that unavoidably leads to the

need for compromises to be made. Nevertheless, this step is carefully carried out by taking into consideration the judgment from an engineering point of view to preserve both the scale identity and the needs for real practical applications of the algorithm.

The chapter begins with classifying all the sources that equally determine the quality of LES result. This starts from the numerical error aspect in general as well as that under the context of LES to the physical error aspect for LES. A turbulence problem for which sufficient insight on flow parameters definitions involved are available in literature is primarily chosen (a free shear flow). Based on this, a new form of refinement variable is constructed. Another type of turbulent flow that provides distinct phenomena is then selected (a flow around bluff body with separation) and the formulation of the refinement variable previously defined is then generalized to cover this latter problem before the final form is proposed.

4.1 CFD ERRORS IN LES CONTEXT

Computational Fluid Dynamics can be seen as an art of representing a continuous problem by a discreet finite set of elements or cells. As previously stated, there are three main different types of error that can occur when dealing with large eddy simulation which are modelling error, numerical error and computer programming error (John & Anderson 1995). In this study, it is important to specify each part of the error type as well as point out which is to be looked out for and which can be assumed negligible.

4.1.1 Modelling error

In the process of attempting to represent the actual problems in nature, fluid flows for instance, by mathematical models, the first type of error known as modelling error arises. It describes the difference between the behaviour of the actual physical system and the exact solution of the mathematical model. In the context of large eddy simulation as in this work, the governing equations, the filter formulation, the boundary conditions, the computational domain and geometry as well as the means of subgrid scale (SGS) model used to account for effect of filtered smaller scales are all falling into this category of error (Breuer 1998). The judgment utilised to determine the level of magnitude of each of them

is predominately based on existing relevant researches. That is, for all the test cases chosen in this study, it is believed that the governing equations stated to represent their actual meaning has high level of accuracy and hence the error can be neglected. Concerns are, however, involving with the distinctions in the boundary conditions settings for which the experimental values are not always available. For this, some assumptions are unavoidably to be made. It then can be assumed that during a computation process this factor is fixed and not being significantly affected by the mesh size. Furthermore, for each simulation carried out this error type is believed to be of the same level and therefore no attempts are to be made to minimise it.

On the other hand, responsible for the influence of the small eddies filtered out by the filtering process to the resolved field is the chosen form of subgrid scale (SGS) models. Depending on the type and requirements used, it itself has an equally important role to play. In this work, the viscosity type of SGS model known as Smagorinsky SGS model is utilized and the turbulent eddy viscosity itself is written as a function of the grid spacing indicating that grid size has strong influence on determining its accuracy and error magnitude. When used in conjunction with solution adaptive grid where the grid size locally changes, this type of error varies locally and hence contributes to the global error. Therefore, its existence as well as its magnitude is acknowledged in this work.

4.1.2 Numerical error

After a mathematical model is selected to represent a problem at hand, unless that particular problem with well-posed boundary and initial conditions can be solved analytically, the model needs to be discretised for numerical calculation. The discretisation process can be seen as a function mapping certain points in the physical domain into a set of elements that is finite and by expanding a Taylor series around each of the points, its approximation can be obtained. By doing this the second type of the error known as the truncation error, defined as the difference between the discretised equation and the exact one (Ferziger & Peric 2000).

A Taylor series of a function f_i where the subscribe i represents a point in the domain, can be expanded as;

$$f_{i+1} = f_i + \left(\frac{\partial f}{\partial x}\right)_i \cdot \Delta x + \left(\frac{\partial^2 f}{\partial x^2}\right)_i \cdot \frac{\Delta x^2}{2} + \left(\frac{\partial^3 f}{\partial x^3}\right)_i \cdot \frac{\Delta x^3}{6} + \cdots \tag{4.1}$$

The series converges to the exact one under only two conditions which is both the summation carries on towards infinity and the spacing Δx tends towards zero. Clearly that neither of the conditions is feasible in practice and therefore, estimated values are instead looked for and error then inevitably arises.

In the numerical study of partial differential equations based problems, it is the derivative terms that is of great interest. From the above equation, the order of accuracy of the Taylor series used to represent a derivative is defined as the lowest order of Δx remaining in the part of the series that is to be neglected or truncated. For instance, the following equation has first order of accuracy because the lowest order term in the truncation error involves Δx to the first power.

$$\left(\frac{\partial f}{\partial x}\right)_i = \underbrace{\frac{f_{i+1} - f_i}{\Delta x}}_{\substack{finite\ difference \\ representation}} \underbrace{- \left(\frac{\partial^2 f}{\partial x^2}\right)_i \cdot \frac{\Delta x}{2} - \left(\frac{\partial^3 f}{\partial x^3}\right)_i \cdot \frac{\Delta x^2}{6} + \cdots}_{Truncation\ error} \tag{4.2}$$

It is obvious from the expression of the derivative representation that the more terms included, the smaller error magnitude becomes. This however, demands higher computational memory storage. In the study of LES, it is very often argued which costs more effort and/or gives better results between finer mesh and higher order of accuracy. Based on the definition described above of order of accuracy, the discretisation methods adopted to approximate the viscous term, convection terms of this study have second order of accuracy, whereas only the time derivative term is treated with a first-order of accuracy manner, as will be shown in the next section. Therefore, only certain number of terms in the Taylor series is included and the rest needs to be truncated. This indicates that the only option that remains available to be dealt with in order to improve the accuracy is to reduce the grid spacing Δx.

Another type of error that also belongs to this category is the iteration errors. Iteration process is needed to solve the algebraic equation system obtained from the discretisation.

It is also known as the convergence error arising out of the difference between the iterative and the exact solution of the discretised equations. This type of error is determined by the solver used as well as the convergence criteria involved. With the number of iterations chosen corresponding to the solution residual monitoring approach, equation (3.6), it is assumed that this type of error is relatively small and has the same level of magnitude for all the test cases.

4.1.3 Computation error

Another class of the errors is that caused by the computer software utilized. Two sub-components included in this type of error are as follows;

Computer round-off error : this can rise with the representation of floating point numbers on the computer and the accuracy at which numbers are stored. Generally, with modern computers available nowadays, it is commonly accepted in CFD community that this type of error is negligible.

Programming error : It renders from the difference between the ideal computer codes designed to represent the equation system and the actual code programmed by a user. For example, a small missing or incomplete routine embedded in a relatively lager one can trigger this type of error. The use of commercial code, which is the case in this study, it is impossible to have any active control over this error due to the access limitation to the codes. As a consequence, one can only rely on the reputation of the software used and assume that the error possibly rising from the error of the codes is minimized and negligible.

4.1.4 Main error types and their interaction

It is an ideal in any numerically study of PDE's based problems to be in control of determining the magnitude of each category of the error types stated above or at least to be able to tackle each of them separately. To be effective in the design and analysis of engineering systems, users of CFD tools need to know the level of accuracy of given simulations of realistic flows. However, as stated by Christopher (1999) it is not common practice to estimate errors in numerical simulations and moreover, error estimation is

difficult and time consuming. This is because in general they all are completely combined in the discrete solution of the physical problem and difficulties arise as unavoidable.

In the context of LES study, there are two main sources of error that have potential contribution with significant amount to the final outcome. They are the numerical type and modelling type. In this work, to study the application of the proposed mesh refinement algorithm in conjunction with large eddy simulation, one relies on the finite support of the computational mesh together with the low-pass characteristics of the discrete differencing operators to act as an implicit filter. It is well-known that this kind of filter makes it impossible to separate two error sources that greatly influence the final digital results from each other. This is always the case as long as no explicit filtering is involved. Furthermore, even though the quality of CFD simulations is normally assessable by performing grid refinement studies based on Richardson extrapolation (details provided in Roache 1998), this is neither valid nor straightforward under this context as such. The interaction of the two types of error occurs as a serious additional source of uncertainty.

Since it is practically impossible to separate one of another or monitor their magnitude separately, one is forced to instead come up with tools that potentially allow a study of the overall trend of their total interacting magnitude with varying some selected parameters. Obviously, these parameters shall not be dependent on the calculation process itself either but instead all be defined separately. Attempts to do so are one of the wide objectives of this work and will be demonstrated in the next section.

4.2 PHYSICAL AND NUMERICAL ASPECT OF LES

Over decades large eddy simulation (LES) has been used and developed to handle complex engineering applications. The approach has attracted more and more attention from CFD community due to its capability of capturing the main important flow feature occurring at large scales by the grid itself and only the small ones being modelled. This enables one to tackle problems with high Reynolds number where the means of direct numerical simulation (DNS) is not feasible due to computer capability limitations. Nevertheless, there is a price to pay when it comes to defining the smallest isotropic grid size for a LES calculation when finer mesh can no longer always guarantee better results.

In order to achieve the ultimate benefit of using LES, knowledge of the problem solved at hand as well as the numerical technique is often required. This section addresses the use of LES from both a physical and a numerical point of view.

As previously detailed in Chapter 2, the process of dividing scales in turbulence, i.e. large resolved scales from small modelled ones is done by applying a filter function with a filter width Δ to the governing equations. Generally speaking, by doing this, the eddies whose scales are larger than Δ are directly resolved by the grid whereas those with scales smaller than Δ are to be modelled by a subgrid scale (SGS) model. The resulting or filtered equations together with the additional closure term accounting for the small filtered out scales are then numerically solved on the mesh size or grid spacing Δ_{mesh}(= $\left(\Delta_x\Delta_y\Delta_z\right)^{1/3}$ in 3D and $\left(\Delta_x\Delta_y\right)^{1/2}$ in 2D). The closure term is then introduced to the calculating system via the turbulence model which in this study is the Smagorinsky model (details previously provided). As the importance of the modelling error caused by the chosen SGS model is as crucial as the numerical one, it is worth taking a closer look at its property.

Like other SGS model, Smagorinsky type has its own requirements and a crucial one has to do with the filter width Δ. Apart from the requirement to lie in the inertial subrange where the flow feature is diffusion dominated, the definition of the filter width Δ is to some extend arbitrary and very often is related to the grid spacing, $\Delta = \mathrm{f}(\Delta_{\mathrm{mesh}})$. There is then a similarity between the Smagorinsky model used in the context of LES and a mixing length model used in the context of RANS. A big difference however is that in LES the length scale is usually coupled to the filter width and therefore vanishes if the grid spacing converges to zero (Klein 2005). This simply implies that the two types of error introduced in solving LES equation; numerical and modelling error both are functions of the grid spacing Δ_{mesh}. In addition, by adopting the finite volume discretisation (as used in this study) defined in equation (2.21), each cell element in the computational domain itself implicitly acts as a filter width, i.e. $\Delta = \Delta_{\mathrm{mesh}}$. This kind of filtering process is known as the '*implicit filtering*'. It is then clear that the physical phenomena of the flow either to be picked up with the grid or to be left out for modelling are characterized directly by the grid size and therefore, their magnitudes are determined

by the grid size as well. It hence occurs that the grid spacing has an important role to play in LES and as a result the means of defining it is crucial.

It makes sense that more scales to be explicitly resolved will lead to more accurate results of the problem as the numerical error can considerably be reduced and by doing this the results are converging to direct numerical simulation (DNS). A preconception regarding this aspect can then be easily seen as the solution should converge towards a positive side and desired solution should be more likely to become achievable. Unfortunately, in the context of LES where the existing of the SGS still has an essential role to play, this is not always the case. By refining the mesh, even though the numerical error part should tends to zero, the modelling one could surprisingly and unexpectedly rise and eventually contaminate the final results.

It is interesting to observe that in general applications of LES the choice of choosing Δ is purely bounded by the computer power availability. This simply implies that the size of Δ is chosen to be as small as the computer can possibly handle with absolutely no physical aspects of the problem being taken into consideration when decision on the grid size is to be made. This figure, as a consequence, makes the system of large eddy simulation to some extend an 'unclosed' approach at least in a physical point of view and remains as a big hole of its principal concept.

With all of this in mind, this study then aims to address two questions concerning these aspects of LES;

1. When it is known that finer mesh leads to better results for general PDE's based problem but it is not always the case for a LES study, what can be done about this?
2. Having known that two key aspects that determine the LES result are both characterized with a grid size, would it then make more sense to also take into consideration some real physics of turbulence scales to be represented by the mesh correspondingly to a chosen SGS model when defining the mesh itself?

To answer these, the main attention of this study is then to relate the filter width (Δ) to some physics of turbulence and for this, the Taylor scale (λ) is now addressed in conjunction with the use of SAG.

4.3 SOLUTION ADAPTIVE GRID (SAG) WITH TAYLOR SCALE

4.3.1 Why the Taylor scale ?

It is one of the main objectives of this study to attempt to close the LES system by linking the filter width occurring in the scale decomposition process to some real physical scale of turbulence. As introduced in Chapter 2, that there are three main turbulence scales; Integral (L), Taylor (λ) and Kolmogorov (η) scale where $\eta \ll \lambda \ll L$. This suggests that the Taylor scale lies somewhere in the inertial subrange where the equilibrium between the production of turbulent kinetic energy and its dissipation is assumed. In other words, it is here that turbulent energy is transferred further down to smaller scales. Required for the model length scale Δ, i.e. Δ_{mesh}, by the derivation of the subgrid scale SGS model used in this study, the Smagorinsky model, it then occurs that the Taylor scale is the only physical turbulence scale meeting the requirement. Therefore, in this study an attempt to fulfill the LES physically closure problem by relating the subgrid scale Δ_{mesh} to the Taylor turbulence scale λ, equation (4.3), is carried out.

$$\Delta = \Delta_{mesh} \approx \lambda \tag{4.3}$$

From this, one might argue that with an increase of the Reynolds number in which as a consequence the inertial subrange expands proportionally to, it is then difficult to pin point exactly where the actual Taylor scale should lie. To alleviate this uncertainty, it will be shown later that an introduction of the so-called refinement variable, denoted by C^* as a key tool is useful.

Although the Taylor scale is always smaller than the integral once, it still does not represent the actual dissipative scales and in fact it is much bigger than that. In the framework of isotropic and homogeneous however, it is convenient to express the dissipation rate ε as a function of Taylor scale considering that the rate of strain of the dissipative scales can be evaluated based on it. Then it very often is written that $\varepsilon =$

$2\nu_t \langle (\frac{\partial u'}{\partial x})^2 \rangle$, as used to characterize the dissipation phenomenon, especially in experimental works (Tennekes & Lumley 1972) .

4.3.2 Why Solution Adaptive Grid (SAG) ?

It is known that flow features behave differently in both time and space. Small scales and turbulent activities may only occur at some parts of the domain whereas other parts the flow might be completely laminar. This aspect is very crucial particularly in flows with complex flow domains, involving additional complicated physics. Due to this difference in intensity of turbulent activities it makes sense to treat each of the regions differently and correspondingly to the main flow feature dominating that particular region. This is where the use of Solution Adaptive Grid (SAG) comes in. With the use of solution adaptive grid, it is possible to locally numerically tackle the problem at hand.

4.3.3 Taylor scale-like as the refinement variable

Refinement variable in grid adaption scheme is the pre-chosen key of flow variable used to locate the region of interest corresponding to some selected error measurement. In h-refinement where node points are inserted and taken out from the domain during the calculation process, it is unlikely for error estimator to be used due to its complicated procedure to obtain an adequate one and as a result an error indicator is more likely to be adopted. In this study however, for the main turbulence test cases, none of these schemes is used since the main attention is to drive the grid adaptation method based on a real physical scale of turbulence i.e. the Taylor scale.

By definition, the Taylor scale is constructed in a statistical sense which the time average values require a long period of flow time in order for the integrations to converse and hence for the definition itself to be mathematically well-defined. This implies that the exact value is technically obtained once a simulation has completed. The need of modified forms of the Taylor scale then comes in when applied with SAG since the scale has to be estimated during the calculation and as a function of space in order to accordingly and repeatedly adapt the mesh during the solution calculation processes. To do this, attempts to estimate the targeted scale locally are carried out by the use of the global estimation

relations of the three turbulence scales. As a result of this assumption, the approximated value of the local Taylor scale cannot technically completely represent the precise or exact one. Therefore, it is important to state here that in the context of this study the Taylor scale used is only the Taylor scale –like. Nevertheless, for the sake of simplicity it is still preferably referred to as Taylor scale.

As introduced in Chapter 2, the three well known turbulence scales; integral, Taylor and Kolmogorov can be related in Equation (2.11), (2.12) and (2.13). The relations allow one to estimate how big the Taylor scale should be from the pre-defined integral length scale and the Reynolds number based on it. To estimate the Taylor scale locally using this correlation, however, the task is very much flow phenomena-dependent. Amongst these turbulence scale relations, equation (2.12) seems to provide the most useful form. From this the global Taylor scale, λ, is then a function of two flow parameters; the global length scale, L and velocity scale U which, when locally defined, can be used to characterise local ratio of inertial and viscous forces.

For the investigation carried out in this work, two types of turbulent flows have been chosen; free shear flow and flow over a buff body. Turbulent free plane jet is chosen to represent the first category and the flow over a stationary circular cylinder with smooth surface for the second one. It has to be mentioned that attempts to analytically measure the local scale for each of selected flow types are beyond the scope of this work. Instead, the main investigation heavily relies on support from literature. Moreover, a survey of the literature has shown that there is only a small amount of work involved estimating local turbulence scales for certain type of flow such as turbulent free jets. As a consequence, the attempt to be made in this work first starts with imitating the locally estimated Taylor scale (λ_x) analyzed for free round jet in Dimotakis (2005) to apply for the first test case (turbulence free jet) and afterward expanding the idea to cover the second test case (circular cylinder flow).

Along this line, Equation (2.12) can then be rewritten following Dimotakis (2005), as follows.

$$\frac{\lambda_x}{\delta_x} \approx Cont.\left(Re_x^{-\frac{1}{2}}\right) \Longrightarrow \lambda_x \approx Cont.\left[\delta_x \left(\frac{\delta_x U_x}{\nu}\right)^{-\frac{1}{2}}\right] \tag{4.4}$$

The subscript x indicates function of position (local) and δ_x and U_x is the local integral scale and the local characteristic velocity, respectively. Taking into consideration three additionally important aspects; the presence of non-zero velocity field all over the domain as is the case for the circular cylinder flow, the lack of access to the commercial CFD software utilized and an attempt to maintain the statistical meaning of the exact Taylor scale, the form above is now modified to cover both flow phenomena and expressed as follows;

$$\lambda_x \approx C^* \cdot \left[\delta_x \left(\frac{\delta_x \left|\langle U_x \rangle - U_{dt}\right|}{\nu}\right)^{-\frac{1}{2}}\right] \tag{4.5}$$

Here $\langle \ \ \rangle$ represents time-averaged value and U_{dt} represents the velocity magnitude predominantly dominating the entire flow field. It has been added in order to prevent the algorithm from producing unnecessary cells to those regions with less level of interest as particularly the case for the flow over a circular cylinder. Table 4-1 gives definition of each parameter to be applied for each test case. Notice also that the constant is now replaced with C^* and is referred later on as ***refinement constant***.

Table 4-1 Parameters definition utilized for Taylor scale estimation for each test case.

Test case	Local δ_x	Local $\langle U_x \rangle$	U_{dt}
Plane jet	2 × (Jet half-width)	Cell centre value	0
Circular cylinder flow	Cylinder diameter D	Cell centre value	Inlet velocity

Unlike the use of h-refinement in conjunction with some chosen error indicator where it is necessary to introduce a normalization of the error indicator to prevent a strong change of the raw value of the refinement variable, as previously demonstrated in the

laminar cases, this study adopts no normalization means. Rather, since the main attempt is to adapt the local grid ($\Delta_{mesh,x}$) to be of the same size as the local Taylor scale (λ_x), it straightforwardly follows that a new form of refinement variable, E_x, can be defined as a function of the two parameters, expressed as;

$$E_x = f(\lambda_x, \Delta_{mesh,x}) = \frac{\Delta_{mesh,x}}{\lambda_x} \tag{4.6}$$

Notice also that defining a refinement variable this way has also an advantage of not needing any users' judgments for refinement bounds, normally required to prevent SAG from generating redundant cells. This is because the ratio can simply be set to vary around the value of unity.

4.3.4 Resolution requirement

By resolving only down to the Taylor scale instead of the smallest ones in this methodology, the requirement of computational effort can be approximated in terms of the Reynolds number. For a three dimensional flow field, the number of grid points required to resolve can be calculated as;

$$N_{p\lambda} \approx \left(\frac{L}{\lambda}\right)^3 \approx Re_L^{\frac{3}{2}} \tag{4.7}$$

In terms of time steps needed, the total number of time steps based on the Taylor time scale ($N_{t\lambda}$) can also be estimated as;

$$N_{t\lambda} = \frac{L_t}{\Delta t} = \frac{L}{U}\frac{U}{\lambda} \sim \frac{L}{\lambda} \sim Re_L^{\frac{1}{2}} \tag{4.8}$$

Where L_t is the turbulence integral time scale. Therefore, combining the above two requirements, the total computational effort, time and space, needed for solving turbulence down to the Taylor scale in this type of LES is promotional to Re_L^2 which readily is one order of magnitude smaller than those required for DNS. With the use of SAG moreover, the computational requirement can even be relatively reduced since not every part of the domain has to have the same level of resolution requirement.

4.4 FINITE VOLUME- LARGE EDDY SIMULATION (FV-LES)

The main feature of LES is the division of turbulence scales, the larger from the smaller. The larger ones are to be explicitly calculated by the mesh while the smaller ones are modelled by a subgrid scale (SGS) model. The process of separating the scales is called 'space filtering' and it can be done in either Fourier (wave-number) space or physical space.

There are two ways of filtering or decomposing the scales or eddies of turbulence in LES; explicit and implicit. The former requires an explicit form of a filtering operator with a specific filter width (denoted by Δ, normally related to the grid spacing (h)) available from the top-hat filter, Gaussian filter and sharp cut-off filter (Geurts 2004). The latter is carried out in such a way that the governing equations are directly solved assuming that the larger scales are calculated by the discrete representation nature of the selected numerical discretisation method. By doing this, it is automatically assumed that $\Delta \approx h$.

Even though it is known that the numerical error and the effect of the SGS model can be controlled by using explicit filtering, in conjunction with mesh adaptation extra treatment is required to take care of the commutation error (Geurts 2004), making mesh adaptation application rather difficult. Furthermore, due to the lack of a straightforward and robust filtering procedure for inhomogeneous flows, most LES performed to date have not made use of explicit filtering and for this reason this work focuses only on implicit filtering LES.

In finite volume type, as used in this study, a volume-averaging operation similar to Schumann (1975) of a flow parameter f is employed, defined as follows.

$$\bar{f} = \frac{1}{\Delta x \Delta y \Delta z} \int_{\Delta x} \int_{\Delta y} \int_{\Delta z} f(x', y', z')\, dx' dy' dz' \qquad (4.9)$$

This equation defined over a fixed control volume in space represents a function that maps a continuous and integrable function to its discrete value within a given cell volume. It has to be mentioned also that this operation is only similar to (but not the same as) the application of the top-hat filter where the continuity property of the function is preserved.

With the Gauss's divergence theorem that links the volume integrals to the surface integrals and by part integration technique, the (implicitly) filtered governing equations can be written as.

$$\overline{\mathrm{div}\, u} = \delta_j^{*}\, {}^{j}\overline{u}_j \tag{4.10}$$

$$\frac{\partial \overline{u}_i}{\partial t} + \delta_j^{*}\left({}^{j}\overline{u}_j\, {}^{j}\overline{u}_i\right) = -\delta_j^{*}\, {}^{j}\overline{p} + \delta_j^{*}\left(\nu\, {}^{j}\overline{\frac{\partial u_i}{\partial x_j}} - \tau_{ij}\right) \tag{4.11}$$

Where τ_{ij} is the subgrid-scale stress and is defined as.

$$\tau_{ij} = {}^{j}\overline{u_i u_j} - {}^{j}\overline{u}_i\, {}^{j}\overline{u}_j \tag{4.12}$$

Where ${}^{j}\overline{\emptyset}$ denotes the mean, surface-averaged value of a flow parameter $\emptyset$ over the surface in which its normal vector is in j −direction and δ_j^{*} is the usual finite difference operator.

The difference shown in equation (4.12) decreases towards zero and can be negligible, with only a minor approximation error, if the mesh is fine enough and the whole process turns towards DNS. If the mesh is not fine enough, as is very often the case for engineering applications however, the subgrid-scale stress needs to be modelled by the use of a subgrid-scale model (SGS) as details previously provided.

It has to be mentioned also that with the choice of finite volume discretisation, the conservation property of mess and momentum can be guaranteed within a cell volume. This, as a result, makes the structure of this proposed algorithm satisfy property **I** of ideal SAG algorithms stated in section 2.5.1.

4.5 NUMERICAL SCHEME

In the numerical study of laminar flows, as demonstrated in Chapter 3, it is known that the small ratio of magnitude between the convection and viscous term of the governing equation makes the choice of numerical scheme comparatively straightforward. For turbulence study on the other hand, adequate care must be taken to prevent the dissipative nature of the numerical discretisation used from excessively interfering and/or contaminating the role played by the subgrid scale part (see Sagaut 1998 for full details).

The central-difference is adopted to take care of the diffusion term where second-order accuracy can be attained. For the non-linear convection term, neither first-order accuracy scheme nor scheme in up-wind family can no longer be effective as pointed out by Kravchenko & Moin (1997) and Breuer (1998). For this, a second-order-accurate central-differencing scheme is used, i.e. in the momentum equations, the face value of a variable $\emptyset_f$ can be calculated as follows:

$$\emptyset_{f,CD} = \frac{1}{2}(\emptyset_0 + \emptyset_1) + \frac{1}{2}(\nabla\emptyset_o \cdot \overrightarrow{r_o} + \nabla\emptyset_1 \cdot \overrightarrow{r_1}) \tag{4.13}$$

Where the indices refer to the cells that shear the face f, see Figure 4-2. The reconstructed gradients, denoted by ∇, are approximated using the Green-Gauss cell-based method defined as.

$$(\nabla\emptyset)_{c0} = \frac{1}{V}\sum_f \overline{\emptyset}_f \overrightarrow{A}_f \tag{4.14}$$

$$\overline{\emptyset}_f = \frac{\emptyset_{c0} + \emptyset_{c1}}{2} \tag{4.15}$$

Using the central-differencing schemes can very often produce unbounded solutions and non-physical wiggles leading to stability problems for the numerical procedure. This problem is overcome with using a deferred approach where the face value is calculated by:

$$\underset{[\text{implicit}]}{\emptyset_f} = \underset{[\text{implicit}]}{\emptyset_{f,UP}} + \underset{[\text{explicit}]}{(\emptyset_{f,CD} - \emptyset_{f,UP})} \tag{4.16}$$

The upwind part, denoted by UP, is treated implicitly while the difference between itself and the central-difference, denoted by CD, is treated explicitly.

For transient simulations, in this work we use a fist-order implicit discretisation where all the unknowns are evaluated from the fields for time level $n + 1$, as it can be seen in general form as.

$$\int_V \frac{\emptyset^{n+1} - \emptyset^n}{\Delta t} dV + \oint \emptyset^{n+1} \vec{u}^{n+1} \cdot d\vec{A} = \oint {\Gamma_\emptyset}^{n+1} \nabla \emptyset^{n+1} \cdot d\vec{A} - \oint P^{n+1} \cdot d\vec{A} \tag{4.17}$$

For a given time step, the stopping criteria defined as residual of flow parameters, as expressed in equation (3.6) is adopted where at least a tolerance of 10^{-3} in residual is met for all test cases.

The discretisation of the continuity equation proceeds in the similar way to that of the momentum equation. Integrating over a control volume reads;

$$\sum_f^{N_{faces}} M_f A_f = 0 \tag{4.18}$$

Where $M_f = u_n$ is the mass flux across face f. A linear interpolation is used to link the surface values to the centre ones. This process usually results in unphysical checker-boarding of pressure. To avoid checker-boarding of pressure, a procedure similar to that outlined by Rhie & Chow (1983) is employed. The scheme interpolates the pressure values at the face using momentum equation coefficients. Using this procedure, M_f can then be written as.

$$M_f = \rho_f \frac{a_{P,c0} u_{n,c0} + a_{P,c1} u_{n,c1}}{a_{P,c0} + a_{P,c1}} + d_f\left((P_{c0} + (\nabla P)_{c0} \cdot \vec{r_0} - (P_{c1} + (\nabla P)_{c1} \cdot \vec{r_1})\right) \tag{4.19}$$

Where P_{c0}, P_{c1} and u_{c0}, u_{c1} are the pressures and normal velocities respectively, within the two cell sharing the face and $\widehat{M}_f$ contains the influence of velocities in these cells.

In the linearisation process, each discrete equation will be linearized implicitly with respect to that equation's dependent variable. This results in a system of linear equations with one equation for each cell in the domain. A point implicit (Gauss-Seidel) linear equation solver is used in conjunction with an algebraic multigrid (AMG) method to solve the resultant scalar system of equations for the dependent variable in each cell. Pressure-velocity coupling is achieved by using a well-known semi-implicit method for pressure linked equations (SIMPLE) algorithm.

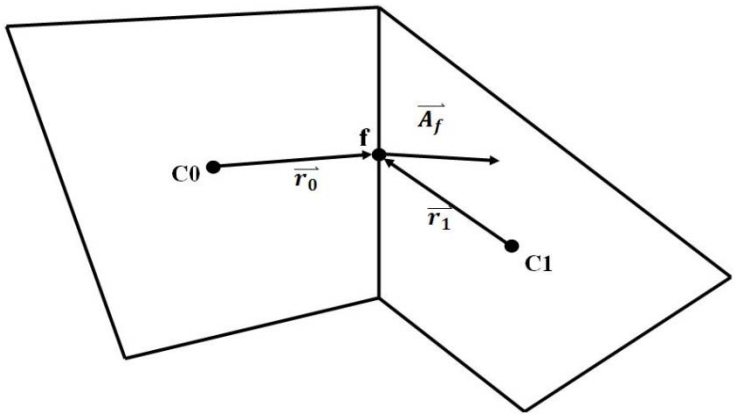

Figure 4-2 Control volume illustrating the discretisation of a scalar transport equation.

4.6 THE PROPOSED SAG ALGORITHM

A simple process of adding and removing the grid points shown in Figure 4-3 is used with a uniform rectangular shape mesh. The algorithm consists of 5 main steps, listed as:

1) Calculating the refinement variable defined in Equation (4.6) using the initial condition obtained either from the initial condition or the calculation previously carried out, for each control volume all over the domain.
2) Comparing the value obtained from the first step for each cell with the unit value of one. Those cells with $E_l > 1$ are marked and subjected to refinement activity and only one level of refinement is allowed to perform for those cells

with $E_l < 1$. Therefore, those cells that require more than one level of refinement are subject to undergo a coarsening process.

3) Performing a mesh adaptation in such a way as shown in Figure 4-3.
4) Interpolating flow parameters' values from parent to child cells.
5) Continuing the calculation for the next time step.

To maintain accuracy, neighbouring cells are not allowed to differ by more than one level of refinement. This helps preventing the mesh adaptation from generating excessive cell volume variations. In addition, this also ensures that the position of the parent (original) and child (refined) cell centroids are similar (reducing errors in the flux evaluations). Using this adaptation scheme, mesh that is coarser than the original ones is not allowed to be generated.

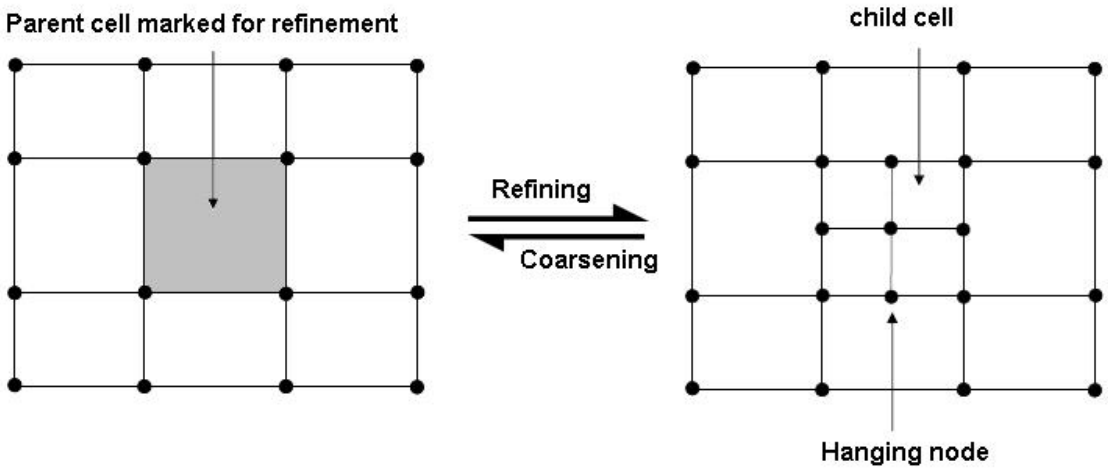

Figure 4-3 Refining and coarsening process for one level of refinement.

4.7 IMPLEMENTATION IN FLUENT

The commercial meshing software, namely, GAMBIT version 2.2.30 was used to construct the computational domain and to generate mesh. The file was then exported to FLUENT version 6.2.16 for the calculation process.

The implementation of the refinement criterion described in section 4.3 and its algorithm in section 4.5 into the CFD software FLUENT consists of two steps;

- Setting up the refinement variable.
- Introducing the refinement variable defined to the process of grid adaptation.

The new refinement variable proposed in this work is defined as in equation 4.6 and its combining form as in equation 4.5. This refinement variable cannot be directly selected from the **Gradient Adaptation** panel, Figure 3-1, as it is not explicitly provided by FLUENT. Therefore, it has to be defined via the **Custom Field Function Calculator** panel, shown in Figure 4-4, which is accessible directly from the main console window of FLUENT. Underneath the **Definition** section of the panel is where the refinement can be defined. Shown in Figure 4-4 is an example with all parameters corresponding to equation 4.5 and their definitions in Table 4-1. For this example, the refinement variable is named as **custom-function-10**.

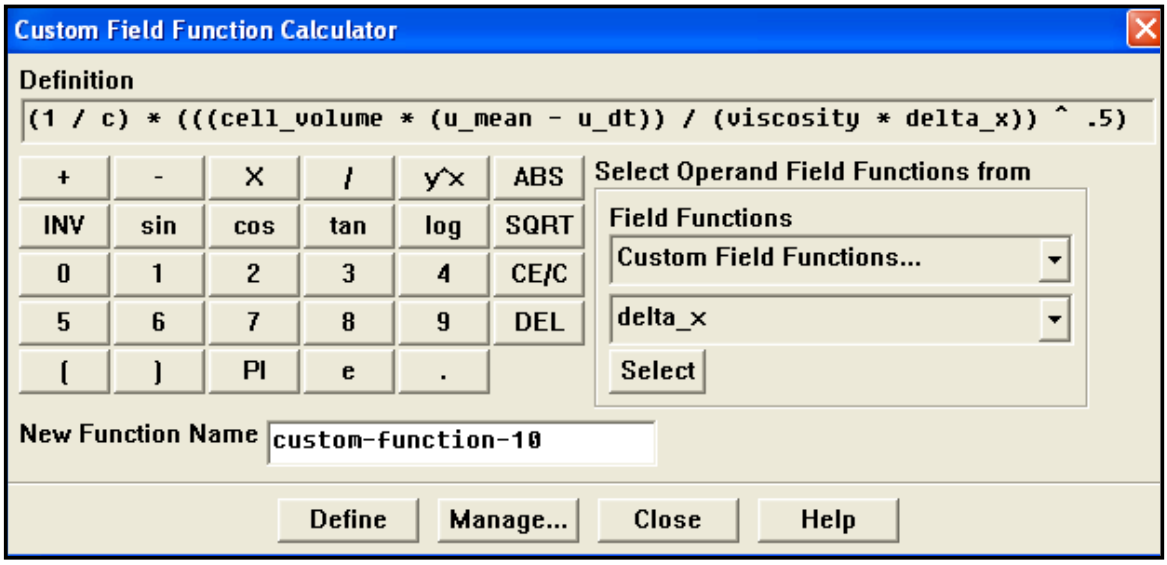

Figure 4-4 The Custom Field Function Calculation panel in FLUENT.

The custom-function-10 is then introduced to the **Gradient Adaptation** panel and used as the main refinement variable, see Figure 4-5. Underneath the **Method** section of the panel, the **Iso-Value** is chosen in order not to modify the refinement value based on either its gradient or curvature. The **Standard** type of **Normalization** is ticked in order not to scale the value, instead it is kept to vary around the value of 1 as indicated by the lower bound of 0.8 and upper bound of 1.2. The **Dynamic** option is also ticked to allow the mesh adaptation process to perform automatically without any user's interference and

it is set to perform at every 20 time steps, as indicated underneath the **Interval** section. Once everything is set, by clicking 'Apply' button, the mesh adaptation can now be carried out simultaneously with the process of solving the governing equation.

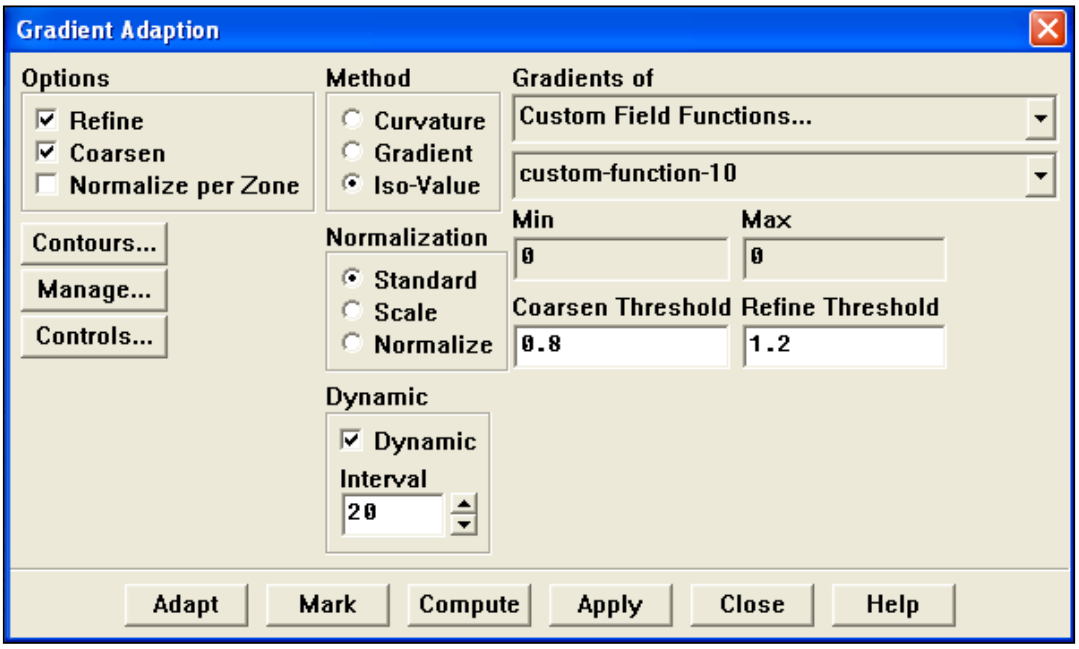

Figure 4-5 The Gradient Adaptation panel in FLUENT with the refinement criterion used for turbulence case studies in Chapter 5.

4.8 SUMMARY

In this chapter, an attempt to construct a new solution adaptive grid algorithm has been made. The process started with stating all the factors involved in the procedure. A new refinement variable has been defined taking into consideration several aspects from the Taylors scale, the nature of the turbulence cases to be chosen for its capability assessment as well as restrictions from the software access. The fundamental of large eddy simulation with implicit filtering supported from the nature of the finite volume discretisation has also been detailed. The whole numerical scheme consisting of treatments for each term in the governing equations has then been given before all components mentioned were put together in a new simple solution adaptive grid algorithm. The implementation of the algorithm in the commercial software used, FLUENT, was then provided for future reference.

Next chapter will demonstrate the effectiveness of the algorithm. This is done by testing out with two turbulent flow problems; plane jet and circular cylinder flow.

CHAPTER 5 SOLUTION ADAPTIVE GRID (SAG) WITH TURBULENT FLOWS

Chapter 3 has given some idea of how beneficial the use of Solution Adaptive Grid (SAG) can be for numerical simulation of some selected low Reynolds number flows. It was demonstrated that with an adequate refinement criterion, flow simulation can produce acceptable results without significant computational cost and effort. In this chapter application of SAG to turbulent flow simulations will be explored. This is to investigate how efficient SAG can be when dealing with turbulent flows. It is known that computation cost of turbulent flows is much higher as they consist of phenomena with an extensive range of scales. Therefore, it is of great interest to investigate the use of SAG for this kind of flow as well as to develop a suitable refinement algorithm and criteria.

In Chapter 4 a new h-refinement algorithm was proposed as well as provided the fundamental and principal concept behind the construction of the approach. In this chapter an attempt to test out the efficiency as well as limitations of the algorithm is made. For this, two turbulent flow problems that represent important categories of turbulence; free shear flow and flow over bluff bodies with separation layers, are selected for validation of the proposed grid refinement algorithm.

Provided in the first part of the chapter is an application of the proposed SAG algorithm with a turbulent plane jet at Re = 4,000. Presented later in the second section of the chapter is an application for a circular cylinder at Re = 140,000. It is worth pointing out that the main differences between the two chosen test cases that make it challenging to validate the algorithm include the existence of the dominant velocity field and the interaction of the viscous effect at solid wall. Experimentally, in free shear type of flows like free jet, there exist regions with zero or nearly zero velocity field whereas this is not the case for flows around bluff bodies (except for the surface area, stagnation point and the end of the recirculation region in the near wake). Furthermore, no wall treatments is required for the plane jet while the most crucial mechanism of flow over circular cylinder

takes place at the circular wall (the existence of boundary layer) implying that adequate strategies are needed to deal with flow around this area.

Before going further, some important remarks concerning the effectiveness of the proposed algorithm have to be first stated. Since there are several issues that the algorithm is designed to tackle, the assessment/judgment of its success will equally take into consideration several main aspects;

- Predicted solution statistics; local velocity components, turbulent intensity and turbulent kinetic energy, in which benchmark experimental data is adopted for solution validation.
- Capability of adapting the mesh when applied with a simply generated initial mesh.
- Simplicity in defining all relevant parameters involved in the algorithm for each turbulence case selected.
- Requirement for user's interfering during the calculating process of a simulation.
- The number of final grid points as well as CPU time required in simulations with fixed mesh, carried out alongside for comparison.

5.1 TWO DIMENSIONAL FREE PLANE JET FLOW

Its appearances in many industrial systems and engineering applications have made the study of turbulent jets, Figure 5-1, one of the most challenging and important phenomena. The jets are of practical interest due to their presence in a broad range of engineering application such as combustion, propulsion and environmental flows. Previously Stephane *et al.* (2000) have documented a variety of applications of jets, particularly of those issued from rectangular orifice shape type. This includes air curtain devices which work on the basic principle of blowing a plane air jet between two environments to isolate one volume from the other, thus reducing heat and mass transfer. Its crucial application is also found in biological area such as its assistance in the reduction of chemical species, odors, bacteria, dust, insects etc.

Jets may be designed for specific functions or they may be present due to system failure. In many cases jets emanate from specifically designed orifices and in such cases

the orifices are nearly always of an axis-symmetric design. However, in the case of jets caused by rupture of seals or gaskets the resulting jets are unlikely to issue from smooth, axis-symmetric orifices (Holdø & Simpson 2002). Jets represent a benchmark for research into the physics of turbulent fluid flow and they have been used for evaluating numerical turbulence models. For these reasons, a plane jet has been selected to be the first test case for testing out the new proposed SAG algorithm.

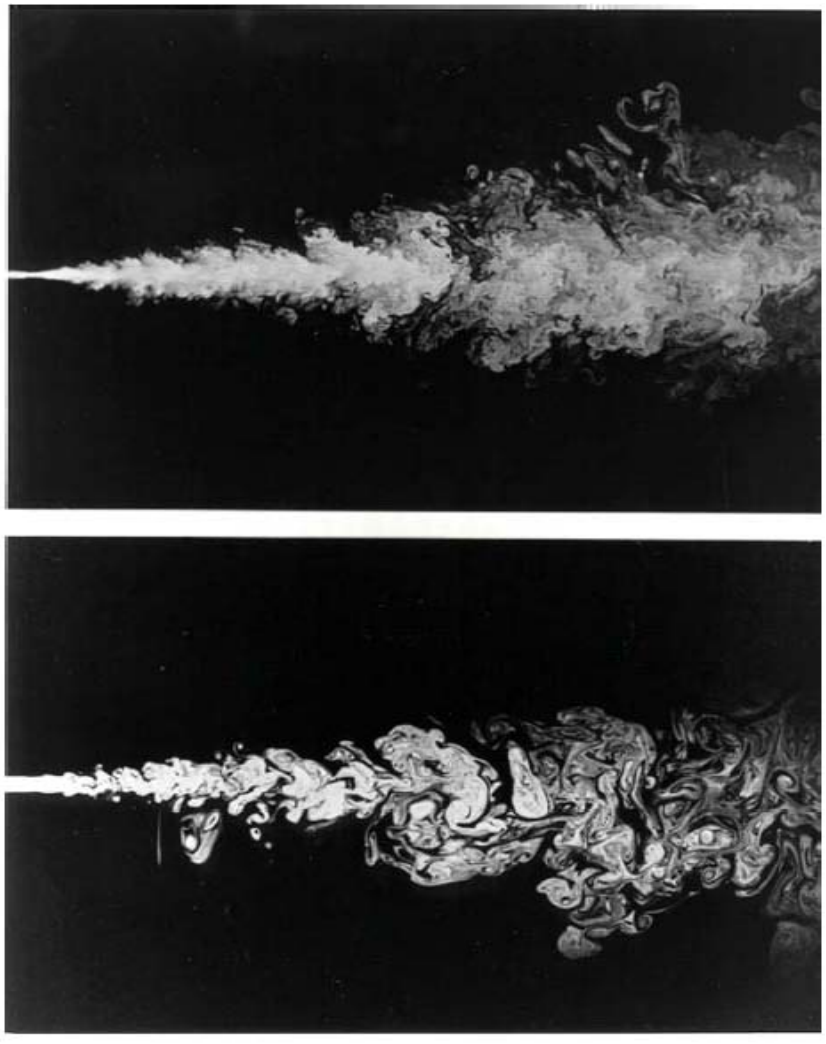

Figure 5-1 Turbulent jets issued from a round shape orifice at different Reynolds numbers, above) Re $\approx 10^4$ and below) Re $\approx 2.5 \times 10^3$ with flow direction from left to right. Data from Dimotakis *et al.* (1983).

5.1.1 Plane jet configurations and its recent simulation history

Free jets are defined as jets that have no obstacles disrupting the traveling fluid and can be categorized into three groups based on the shape of the orifice; round, rectangular and plane (or planar) jet. The first two have, by nature, three dimensional structures while the latter can be seen as statistically two-dimensional flow. This aspect is only valid if a sufficiently large aspect ratio is used. In the past, there have been a number of experimental investigations carried out on jets of all shapes of orifice (Gutmark & Wygnanski 1976, Quinn *et al.* 1983, Browne *et al.* 1983, Namer & Otugen 1988, Thomas & Chu 1989, Ravinesh *et al.* 2008). It is interesting, however, to see that there are only a relatively small number of numerical studies of this kind of flow phenomena. As a consequence, it suggests the necessity of further numerical investigations of turbulent plane jets.

Figure 5-2 illustrates a sketch of a plane jet together with all related parameters. The fluid is discharged from a narrow nozzle into an open space. Its well known flow structures include the presence of vortex rollup in two shear layers, having vorticity of opposite signs, separated by the first identifiable region of the jet namely *potential core region*. In this potential core, the mean centreline velocity ($\overline{U}_{cl}$) is approximately equal to that of the inlet (U_0) and occurs in the near-field of the jet nozzle. Further downstream, next to the potential core region is the *transition region* where the two shear layers merge into each other. Here large scale vortices interact and facilitate momentum transport resulting in the statistical velocity decay before the flow eventually reaches the *self-preserving* state (also known as self-similarity state and defined as when the time averaged flow parameters become independent of distance x in the flow direction for each streamwise section, i.e. $y =$ constant.)

Like other kinds of jets, there are so far only a few numerical simulations done on free plane jets. In the early days when computers had begun to play a significant role in CFD community, one of the primary works on two dimensional numerical study of jet is that of Comte *et al.* (1989). Then in 1994, Dai *et al.* (1994) performed the first three dimensional simulation of plane jet involving subsonic with large-eddy simulation. Even though in their study the mean profiles of predicted flow parameters remained in a good

agreement with experimental data, it was the turbulent intensities that were found to deviate by approximately 40% from the experimental ones. Stanley *et al.* (2002) and Klein *et al.* (2003) have used direct numerical simulation (DNS) to study the mixing structure and the effect of the Reynolds number respectively. The former considered a relatively low Reynolds number, $4{,}000$ and only up to $6{,}000$ for the latter when compared with existing experimental work. The main factor determining this range of Reynolds numbers is the limitation in computational facility. The use of LES on the other hand allows one to tackle jet simulations with considerably higher Reynolds number as conducted by Ribault *et al.* (1999) with a Reynolds number of 3×10^4 and with different SGS models. They found that the standard Smagorinsky model is excessively dissipative even with comparatively fine mesh. Recent LES study by Liu *et al.* (2008) at a lower Reynolds number of $4{,}000$ has used both linear and non-linear SGS models. Even though the results from these testing models do not reveal any significant differences, it is recommended in this work that a model that is well-conditioned, efficient, and easy to implement is a better choice.

From this brief history of free plane jet numerical simulation, it then suggests that a strong influence of computational capability still persists and remains the main factor even for LES simulations. Therefore new alternatives to treat high Reynolds number flows in conjunction with LES would be effectively desired and should be put forward.

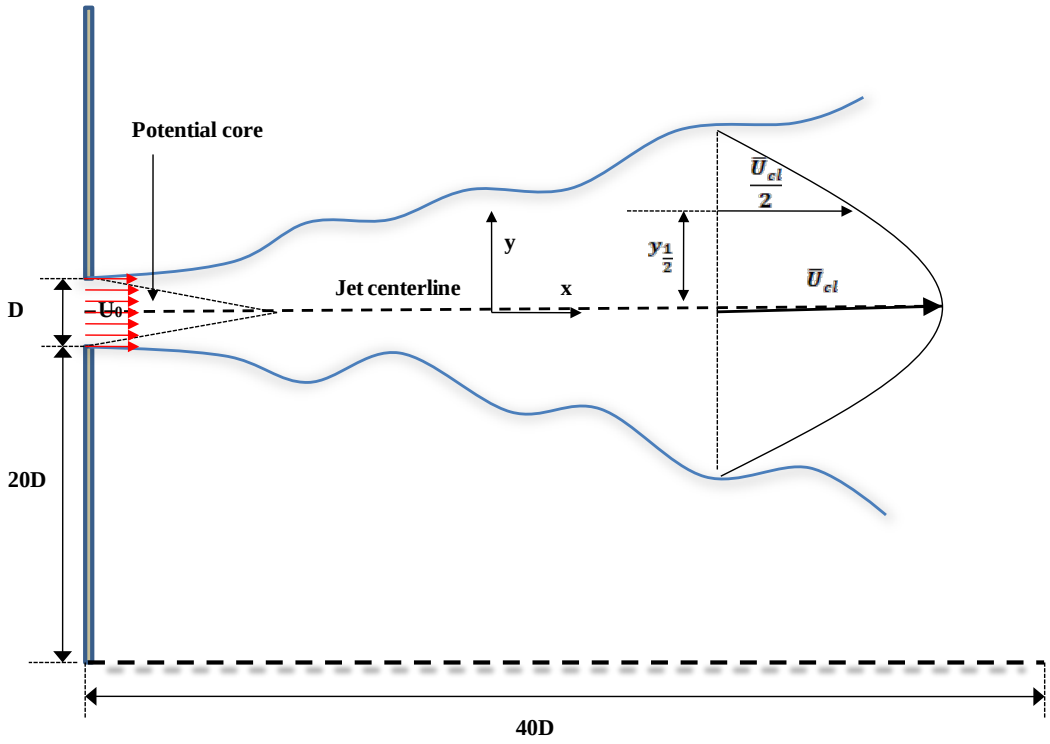

Figure 5-2 Sketch of a turbulent plane jet with related parameters and dimensions.

5.1.2 Numerical and simulation details

- **Governing Equations**

The investigation carried out in this work deals with a statistically two-dimensional plane jet, assuming that the third dimension is sufficiently large. The chosen Reynolds number is 4,000, based on the nozzle width (D) and the inlet velocity (U_0) in which experimental data as well as alternative numerical study are available for validation. Only conservation of mass and momentum were applied as the flow was assumed to be in the incompressible range and without any heat transfer. The governing equations were then discretised using the finite volume. The normalized time step was fixed to $\overline{\Delta t} = \Delta t \cdot U/D = 0.019$ for all simulations.

- **Computational domain**

A two dimensional computational domain with the size of $40\mathrm{D} \times 41\mathrm{D}$, same as those adopted in Klein *et al.* (2003) and Liu *et al.* (2008) is constructed and used for all

the simulations. It is one of the wider objectives of this work to investigate the necessity of having extremely fine grids, which is a reason why LES has traditionally been regarded as inaccessible. In using LES for high Reynolds number flows, only the locally isotropic, smaller, dissipative scales should be modelled by the SGS model although this is not always practical. For this reason, the first three conventional simulations were carried out with three different mesh sizes. The first contains 33,000 cells (referred to as NO-SAG-1) and is termed as very large eddy simulation (VLES). The medium mesh has 96,000 cells (referred to as NO-SAG-2) and the finest one consists of 133,000 cells (referred to as NO-SAG-3). All three were constructed based on the information given by Ribault *et al.* (1999) and Klein *et al.* (2003). In the x-direction, the rectangular mesh was refined in the vicinity of the jet exit and smoothly expanded towards the entrainment and outflow boundary and this is also the case in the lateral direction, see Figure 5-4. This is to ensure that more grid points are placed in the area where high velocity gradients are expected.

For study of application of the proposed mesh adaptation algorithm, a very coarse mesh consisting of 6,800 rectangular-shape cells was generated and used as the initial mesh for SAG application, Figure 5-5. Constructing the initial mesh this way is made specifically to demonstrate the efficiency of the algorithm in alleviating the need for prior knowledge of the flow at hand in the meshing process. This is crucial particularly for engineering applications where meshing as well as mesh testing normally requires significant efforts in order to achieve the desired accuracy.

- **Inlet and boundary conditions**

Following Klein *et al.* (2003), a hyperbolic-tangent velocity profile was constructed and imposed at the inlet, displayed in Figure 5-3, and expressed as below.

$$\bar{U} = \frac{U_0}{2} + \frac{U_0}{2} tanh\left(\frac{-|y| + 0.5D}{2\theta}\right), \quad \bar{V} = 0 \tag{5.1}$$

Where θ is the momentum thickness and is set to $D/20$. The nature of jet flows which is evolving in both time and space in all directions has made the use of periodic boundary conditions impossible. Instead, for all the outflow sections the conditions were set with zero gauge pressure and the negative velocities normal to each outflow were clipped.

Another investigation was also carried out to study the effect of boundary conditions at the outflows when a zero normal gradient of all flow variables except pressure was assumed. It occurred that this condition gave rise in numerical instabilities. For this reason, the former inlet condition was applied for all the test cases.

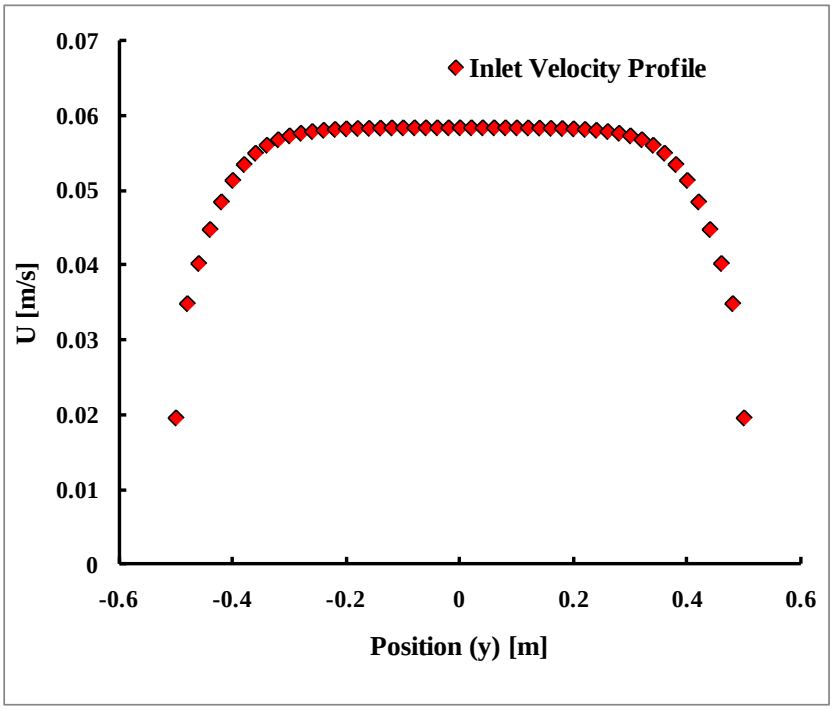

Figure 5-3 Streamwise velocity profile imposed at the inlet of the plane jet.

The level of strength of co-flow imposed at the upper and lower wall-like areas is also not to be omitted. Everitt & Robins (1978) and Larue *et al.* (1997) have studied the effects of co-flow and found that its presence can slow the development of the jet to a self-preserving state. In this work we applied a no-slip condition with the subgrid length scale $l = \min(\kappa d, C_s\Delta)$ with κ, d being the Karman constant ($= 0.4187$) and the distance to the nearest wall respectively. The effect of the length scale however is negligible since the first element adjacent to the walls is set with sufficient distance d from the wall. Therefore it results in $l = C_s\Delta$ everywhere and therefore, the SGS acts similarly to other regions of the domain.

- **Simulation data integration**

Unlike the turbulence modelling based on time averaging such as RANS, flow simulations using LES produce time dependent solutions. To obtain the mean flow characteristic therefore, a simulation needs be run for sufficient amount of time.

To obtain a more physical velocity field, simulations were initially run with the standard $\mathrm{k}-\varepsilon$ model and the results were used as the initial condition for all the LES simulations. The primary data established from this simulation was also used to provide the local estimated characteristic length scale, δ_x in equation (4.6), which in this case is the jet half-width, defined as the distance from the jet centreline to the point at which the mean streamwise velocity is half of the centreline velocity. The length scale was then set to this simple linear approximated form expressed as below and independent of y.

$$\frac{\delta_x}{D} = 0.125\ \frac{x}{D} + 1 \tag{5.2}$$

All the LES simulations, both those with conventional mesh and those with applications of SAG, were performed for 16 flow-through times, based on D and U_0. The first 6 flow-through times were required in order for numerical transients to pass through the domain and not to be affected by the initial conditions. All the results presented in this work are time-averaged over the remaining 10 flow-through times.

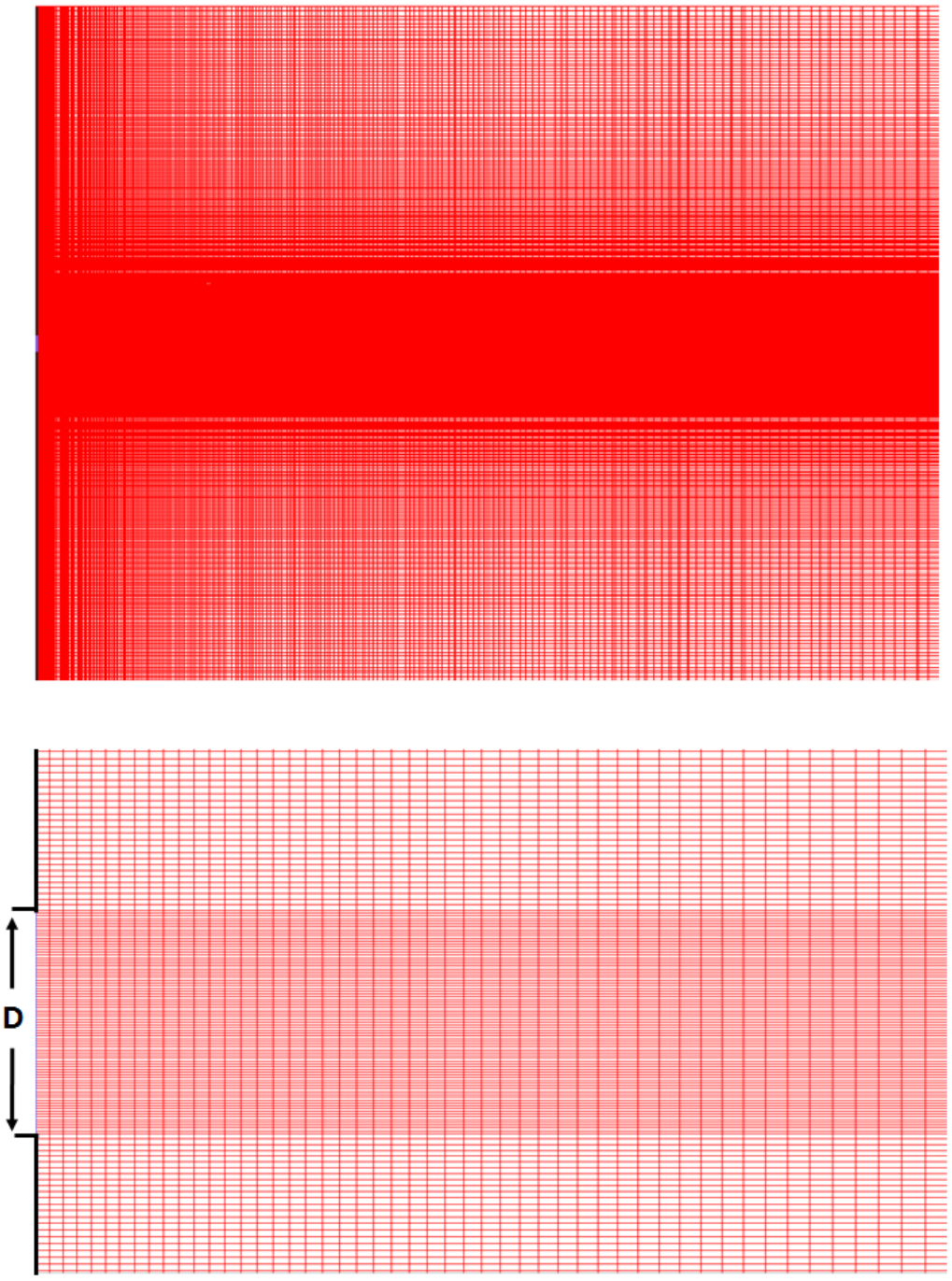

Figure 5-4 Global mesh distribution for a conventional mesh case, NO-SAG-2 (above) with its magnified image at the inlet and near field (below).

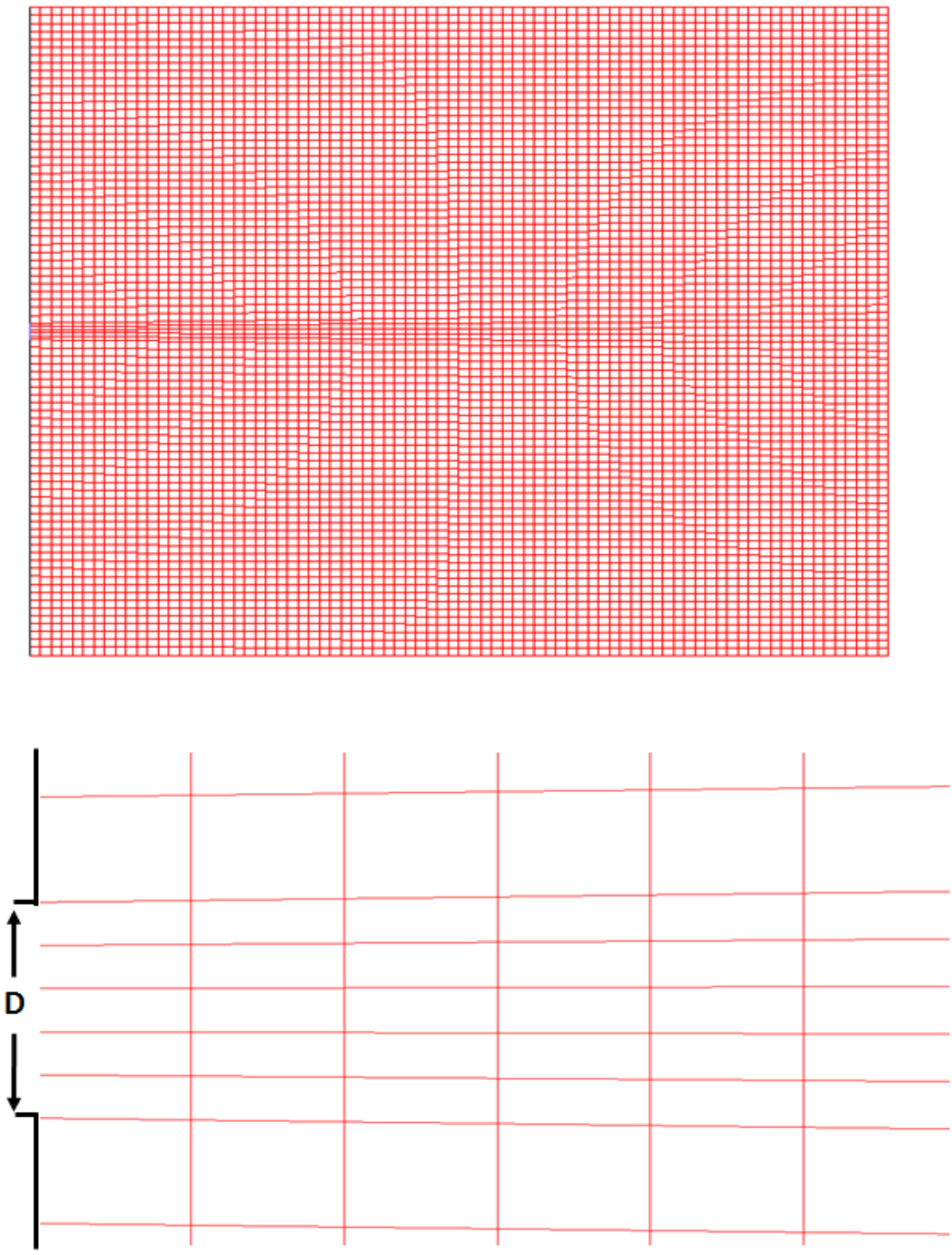

Figure 5-5 A coarse mesh distribution to be used as an initial mesh with application of the SAG algorithm (above) with its magnified image at the inlet and near field (below).

5.1.3 Results and general discussion

For studies of solution adaptive grid with large eddy simulation for a 2D plane jet, a total of seven simulations were performed. The first three simulations were carried out with the three conventional meshes, NO-SAG-1, NO-SAG-2 and NO-SAG-3, with mesh density details previously provided. This is also to emphasize and demonstrate the complication of grid refinement when applied with LES where a better result cannot always be achievable by refining the mesh. The other four were carried out with the initial mesh in conjunction with the proposed SAG algorithm. The results presented are compared against available measurements of Browne *et al.* (1983) ($\mathrm{Re} = 3{,}000$), Thomas & Chu (TC) (1989) ($\mathrm{Re} = 8{,}300$), Namer & Otugen (NO) (1988) ($\mathrm{Re} = 1{,}000 - 7{,}000$) and Gutmark & Wygnanski (GW) (1976) ($\mathrm{Re} = 30{,}000$) as well as alternative numerical works where appropriate.

- **Difficulties in numerical study of a plane jet in 2D**

As studied by Stanley & Sarkar (1997), as well as those carried out before that, and later pointed out by Stanley *et al.* (2002), numerical work on turbulent plane jets in two dimensions is known not be a success. The absence of spanwise instabilities in two-dimensional simulations leads to a phenomenon that is not seen in experimental work namely 'dipoles', jet breaking down to vortex resulting in incorrect mean velocity profile. It is consequently quite a big challenge, in general, to numerically study plane jets in two dimensions.

The difficulties in simulating plane jets in general are also known to be caused by several factors: special treatment of inlet conditions, computational domain size, boundary conditions which are not always known a *priori*. Another important one is the local complexity of the flow itself, consisting of a wide range of physical turbulence scales where most of which are strongly determined by the mesh intensity in reproducing the physical dynamics. Another relevant imperfective assumption to this work is the zero turbulent level at the inflow which is not feasible in any real experiments. Experimentally, this was confirmed by Gutmark & Wygnanski (1976) where hot-wire anemometry was used to measure the mean and fluctuating fields in the self-similar region of plane jet. In

this work they found that the evolution of the fluctuating velocity fields as well as the jet spreading rate and centreline velocity decay were strongly affected by the initial condition at the nozzle and the external conditions in the laboratory. Furthermore, the wide range and scatter between existing experimental measurements has also made the validation of numerical study rather difficult. All these contribute to deviation of the results obtained from this work from the references and should be kept in mind.

- **Refinement constant and mesh distribution**

With an increase of Reynolds number, it is the inertial subrange on the energy spectrum that expands proportionally to the Reynolds number. One then can argue that defining the Taylor scale may be difficult. The use of refinement constant C^* aims at responding to this difficulty. Based on equation (4.2), the only controlling parameter is the refinement constant C^*.By varying this constant, differences in results as well as mesh distribution behaviour can be observed.

Figure 5-4 to Figure 5-9 illustrate the mesh distribution and density of all the study cases along with one from the conventional mesh cases. Each figure also provides a clearer picture of the mesh gathered at the inlet area as well as its near field. As can be seen, the smallest grid size at the inlet of the shown conventional fixed mesh NO-SAG-2 is of approximately $D/80$ which is comparatively finer than those of the SAG cases. As shown in Figure 5-5, the grid to be used as the initial mesh for SAG application has the smallest grid size at the inlet of only approximately $D/5$ which is more than 10 times coarser than that of NO-SAG-2.

Changing of the refinement variable C^* leads to the mesh adaptation taking place in three noticeable areas. These are the potential core region, the thickness of mesh adaptation area of each cross section downstream and the area near the end of the computational domain. It should be noticed that when the refinement variable increases, less grid points are added in the far-field region, which can be anticipated beforehand according to the strong decay in time integrated local velocity in that area. Nevertheless, it is evident that for all SAG cases, the mesh at the areas adjacent to top and bottom jet edge at the inlet where shear layers are expected to take place is reasonably refined. It is in the

near field where capability of capturing main flow mechanism has strong effect on the flow behaviour downstream.

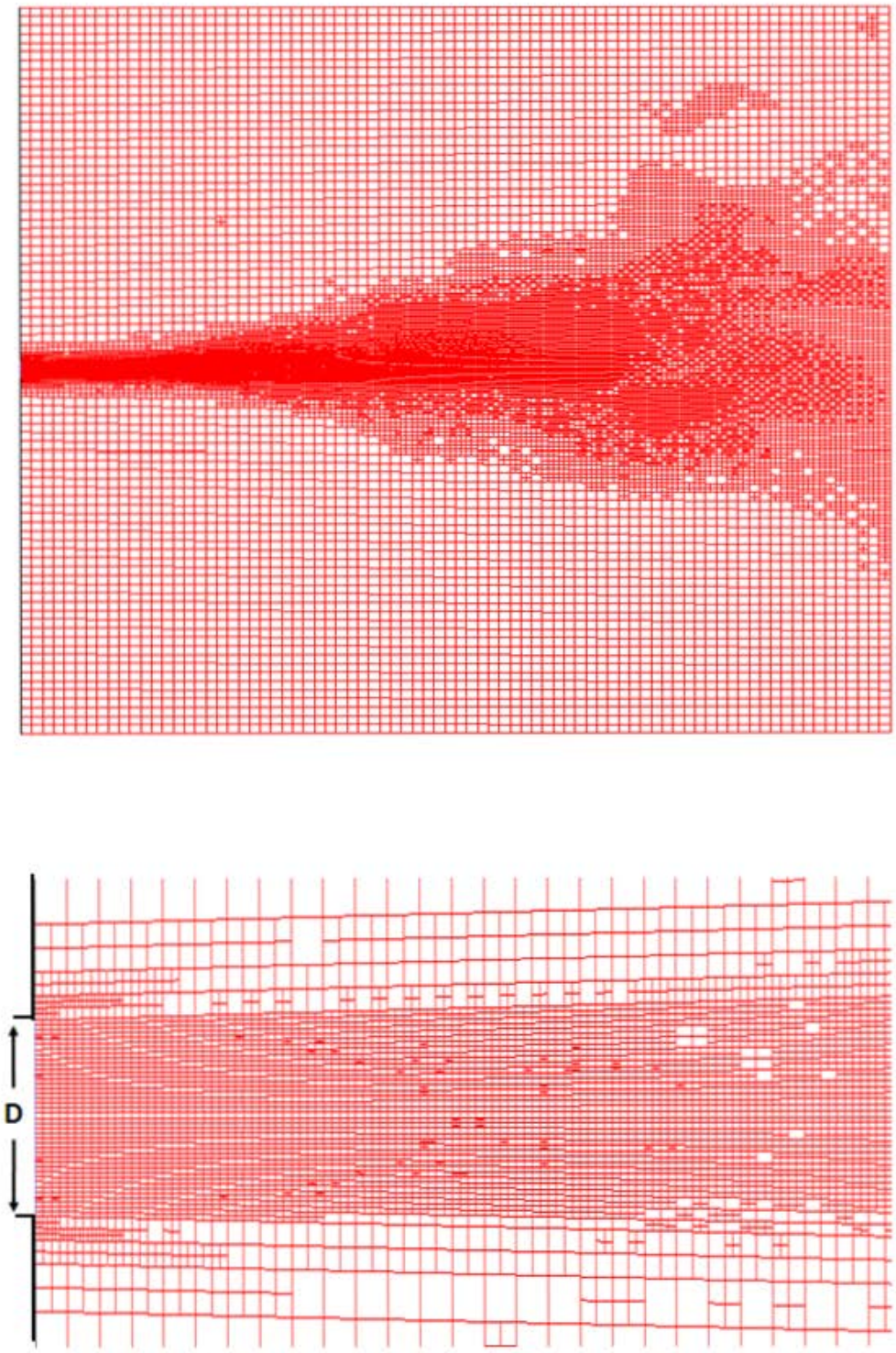

Figure 5-6 Final mesh redistribution when applied with the SAG algorithm with $C^* = 2$ (above) and its magnified image at the inlet and near field (below).

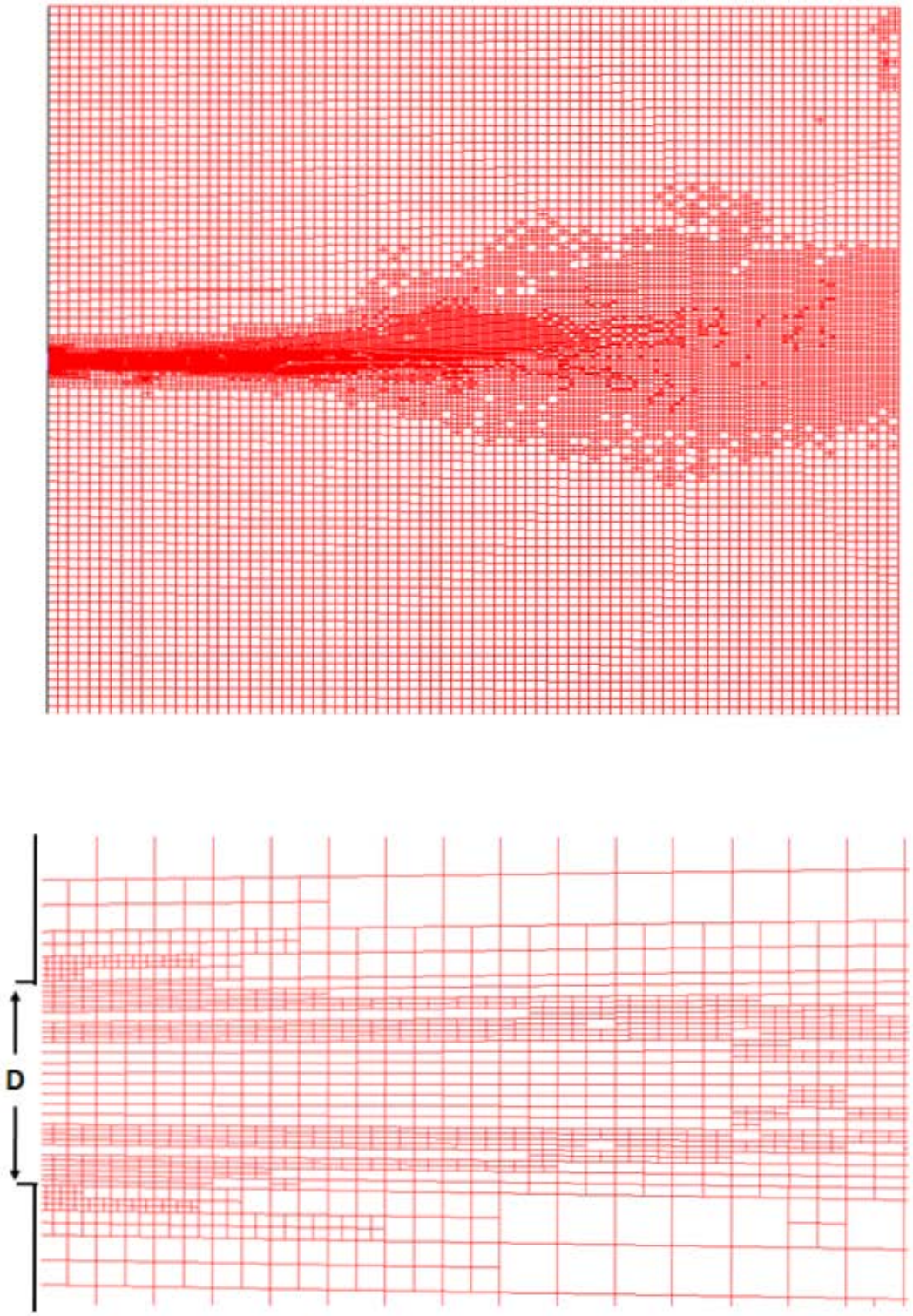

Figure 5-7 Final mesh redistribution when applied with the SAG algorithm with $C^* = 3$ (above) and its magnified image at the inlet and near field (below).

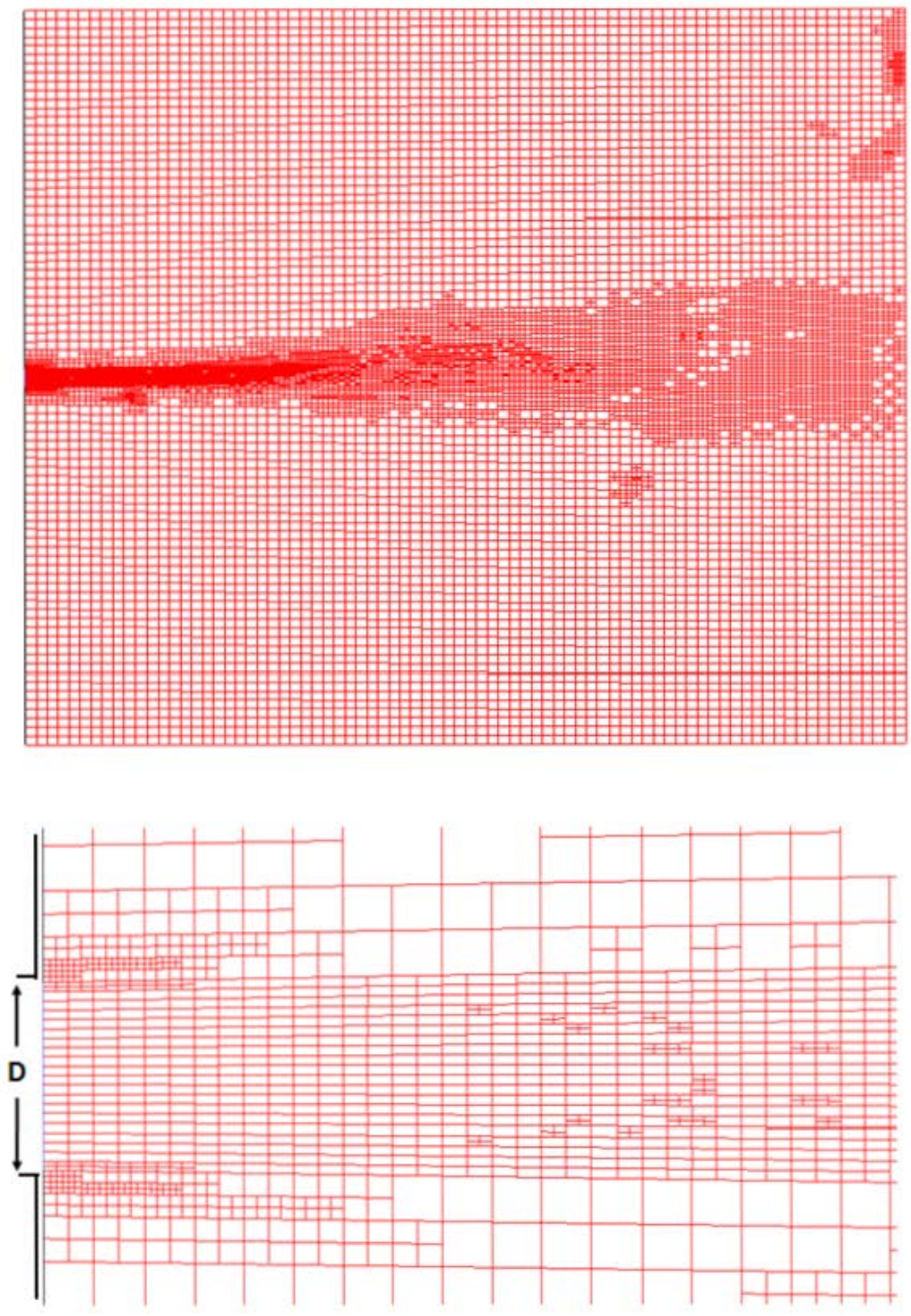

Figure 5-8 Final mesh redistribution when applied with the SAG algorithm with $C^* = 4$ (above) and its magnified image at the inlet and near field (below).

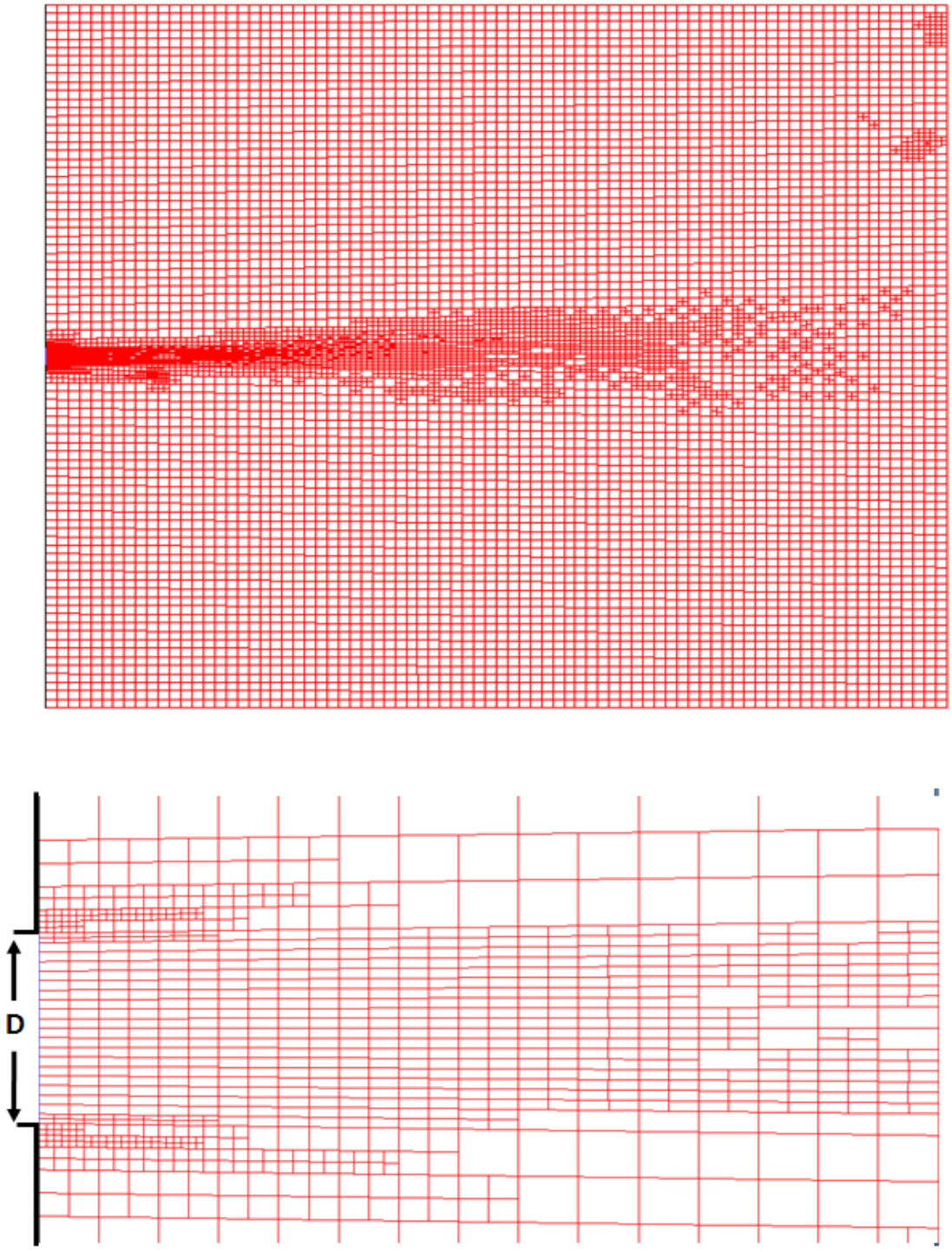

Figure 5-9 Final mesh redistribution when applied with the SAG algorithm with $C^* = 5$ (above) and its magnified image at the inlet and near field (below).

- **Instantaneous flow motion**

Figure 5-10 shows the magnitude of the vorticity obtained from each simulation with SAG algorithm. It can be clearly seen an indication of the presence of vortex roll-up in both the upper and lower shear layers. These layers then gradually develop and start breaking down into small scales. One obvious difference regarding the onset of the first rollup formed in the shear layer areas is the delay farther downstream as the refinement constant C^* increases. Based on the difference in mesh density and distribution for the cases with higher C^* and those with lower as previously illustrated, this behaviour in vortex forming delay can then be a result of less turbulent intensity at the inlet with higher C^*. When the mesh gets coarser, it should be expected that the turbulent viscosity would be increased, causing a decrease of the growth rates of instability waves by viscosity. The instability waves thus grow more slowly and lead to a development of the shear layer that takes place farther downstream. This is in good agreement with the recent observation of near field instability of round jet made by Bogey & Bailly (2006) as well as the study of the inflow turbulent fluctuations effect carried out by Ribault *et al.* (1999).

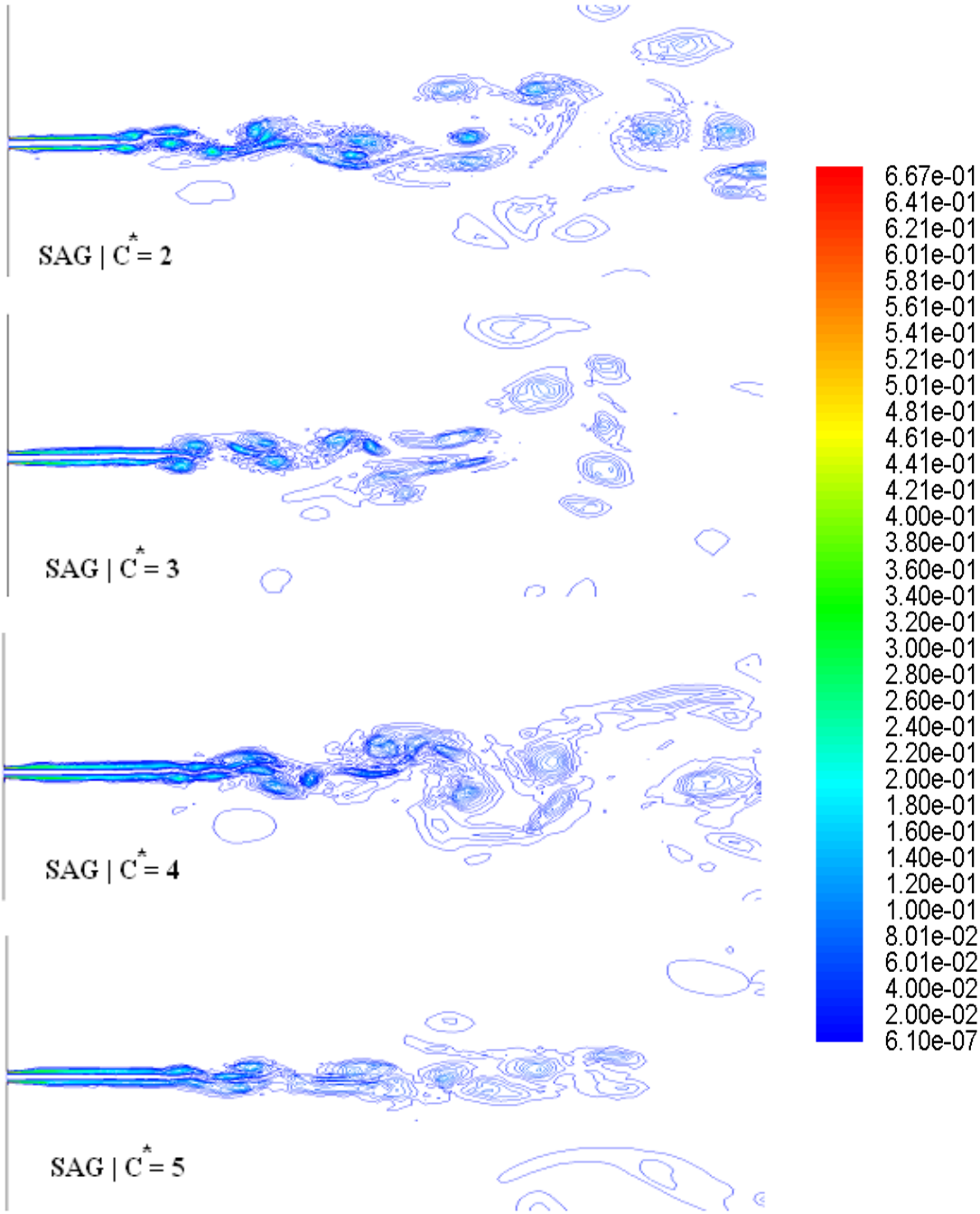

Figure 5-10 Snapshots of vorticity magnitude contour obtained from each case of SAG applications with red representing high values and blue representing low values.

- **Self-similarity state prediction**

Figure 5-11 shows the longitudinal centreline fluctuation intensities obtained from the application of SAG for $C^* = 5$ against the experimental work as well as those from Ribault *et al.* where the same SGS model was used. It is found that for the near-field, $x < 7D$, the results obtained from the chosen SAG case is significantly under-predicted whereas a good agreement still remains for the conventional mesh and the experimental data. However, when compared with the same SGS model as used in Ribault *et al.* (1999), the use of SGA algorithm is seen to rapidly enhance the fluctuation intensity level where the both shear layers start to merge at the end of the potential core, $7D < x < 10D$, and eventually reaches the similarity at $x = 10D$. From here an approximation of 20% over-predicted in turbulent intensity can be found, till the end of the domain. Results from the other SAG cases follow the same trend (not shown). The location of this sudden increase in turbulent intensity corresponds to the location where the shear layers merge at the end of the potential core.

Figure 5-12 illustrates the time-averaged streamwise velocity profiles normalized with the local centreline one, U_{cl} alongside with the experimental ones. The Figure confirms the existence of the self-similarity state of the jet where the velocity profiles fall in a singular curve roughly 10 jet-slot widths downstream the inlet in good agreement with the experimental measurements. Therefore, values at cross section $x = 11D$ are chosen for self-similarity data comparison. Figure 5-13 gives the normalized streamwise velocity profiles of the similarity state at $x = 11D$ of the jet of all the SAG cases and they are in a good agreement with the reference. Most of the data, in similarity state, is then normalized with the local centreline velocity U_{cl} and the jet half-width $Y_{(\frac{1}{2})}$.

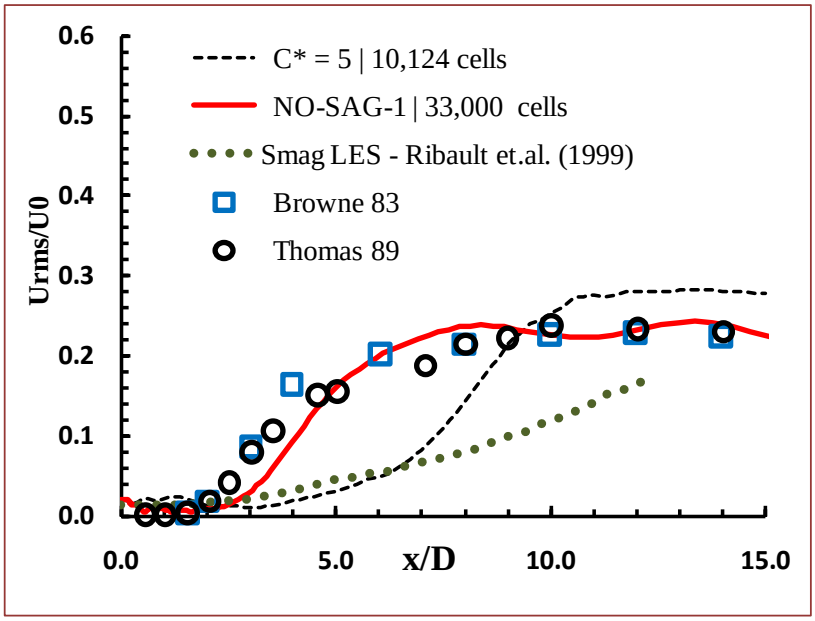

Figure 5-11 Centreline velocity fluctuation comparison; values obtained from numerical work with and without SAG as well as experiments.

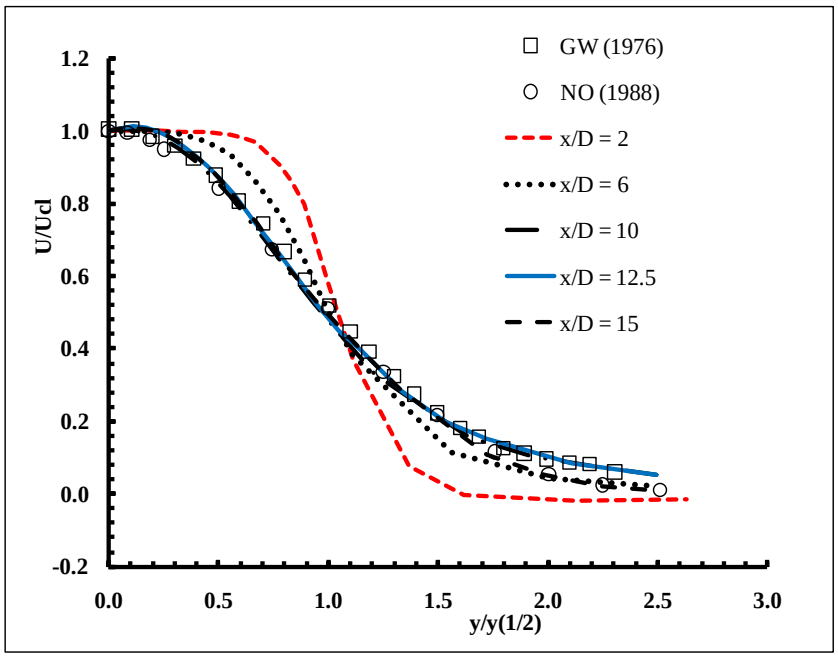

Figure 5-12 Normalized velocity measured at different cross sections downstream, data obtained from the SAG case with $C^* = 4$. Note: GW = Gutmark & Wygnanski (1976), NO = Namer & Otugen (1988).

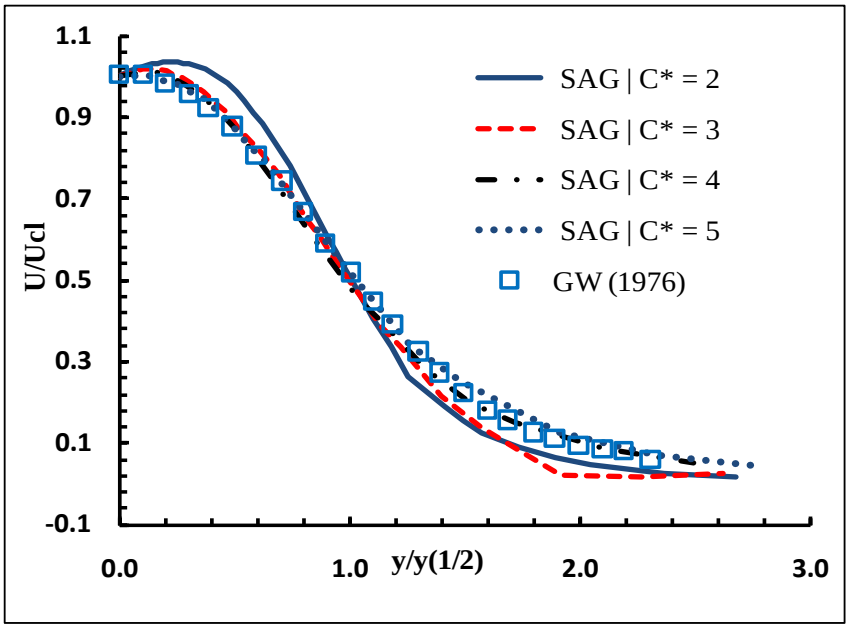

Figure 5-13 Normalized longitudinal velocities along = 11D ; values obtained from SAG with different refinement constants compared against the corresponding experimental data. Note: GW = Gutmark & Wygnanski (1976).

- **Jet downstream development**

The evolution of the inverse square of the jet velocity at the centreline measure from the inlet to just after where the jet reaches its self-similarity state, approximately $x \approx 11D$ (Klein *et al.* 2003)), is shown in Figure 5-14 and Figure 5-15. It can be seen from the results obtained from conventional mesh NO-SAG-3 that the increase in mesh density can lead to an unexpected result. Here a significant deviation from the experiment data of this case is clearly noticeable. Those from applying SAG on the other hand, are approximately 25%, on average, lower than the measurement. This under-prediction is a result of the prolonged potential core region length with higher C^*.

The jet half-width growth downstream, $\mathbf{y}_{\frac{1}{2}}$, as illustrated in Figure 5-16 and Figure 5-17 have shown a monotonic trend for all the SAG cases. With the highest refinement constant, the jet shows comparatively higher level in the half-width growth and the growth is slightly declining with smaller C^*. Once again, the location where the shear layers instabilities start to kick in seems to have had influenced the jet half-width growth. The results obtained from the fixed mesh cases have shown some interesting trends. It is

actually the case with medium mesh density, NO-SAG-2 that gives the relatively better agreement with the experimental measurements in this region. The other two cases, NO-SAG-1 and NO-SAG-3, on the other hand, remain close to each other with a gradual increase in the deviation from the measurements.

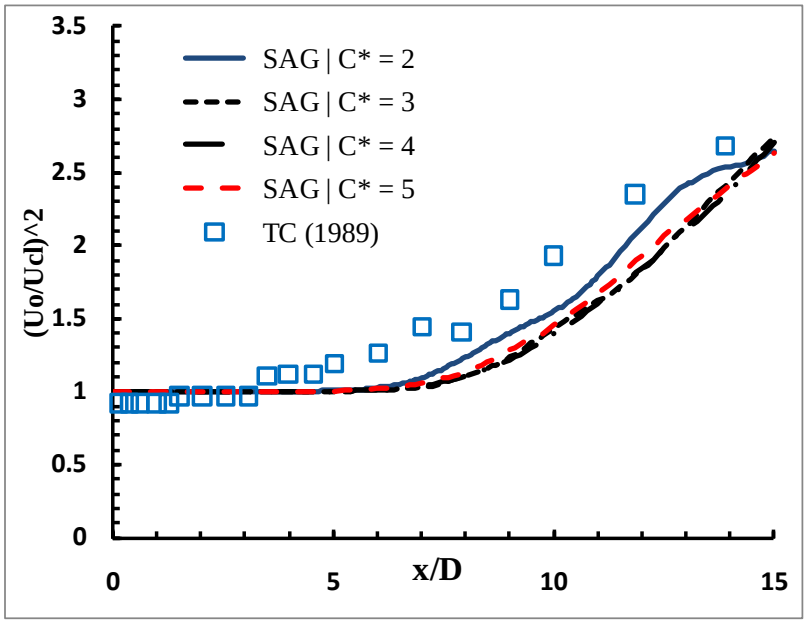

Figure 5-14 Centreline inverse square of the jet velocity; values obtained from SAG with different refinement constants compared against the corresponding experimental data. Note: TC = Thomas & Chu (1989).

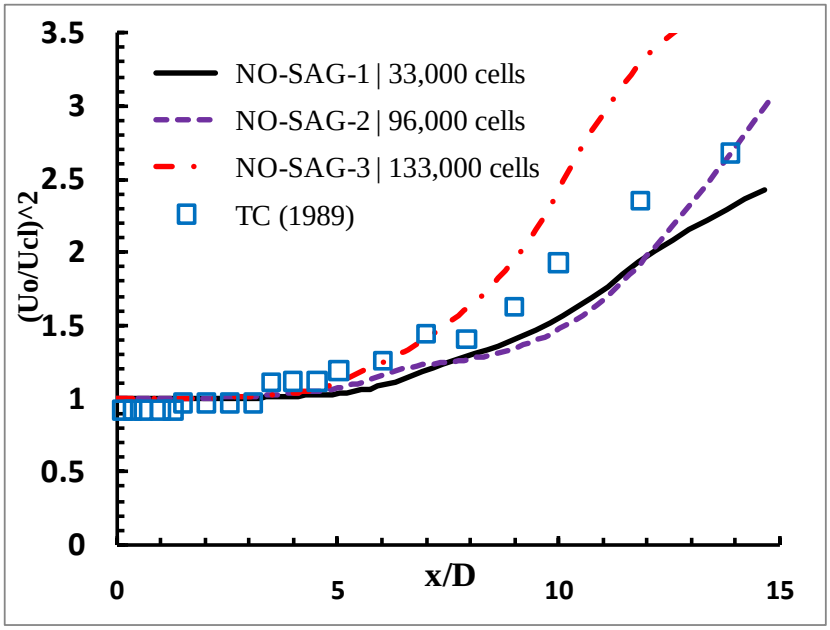

Figure 5-15 Centreline inverse square of the jet velocity; values obtained from the conventional mesh cases compared against the corresponding experimental data. Note: TC = Thomas & Chu (1989).

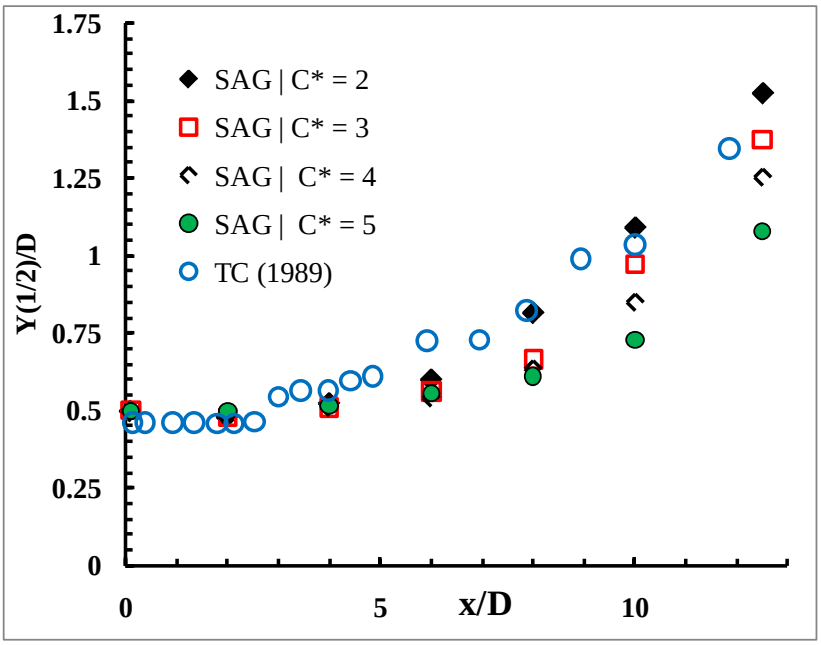

Figure 5-16 Downstream jet half-width growth $y_{\frac{1}{2}}$; values obtained from SAG with different refinement constants compared against the corresponding experimental data. Note: TC = Thomas & Chu (1989).

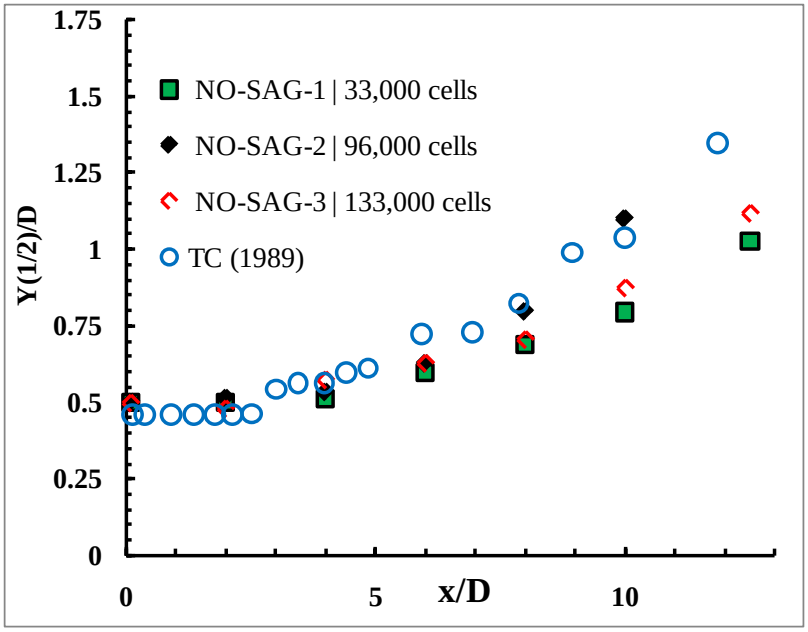

Figure 5-17 Downstream jet half-width growth $y_{\frac{1}{2}}$; values obtained from the conventional mesh cases compared against the corresponding experimental data. Note: TC = Thomas & Chu (1989).

For the jet evolution in the self-similar region, $x > 10\ D$ in this simulation, the jet half-width $y_{\frac{1}{2}}$ is believed to grow linearly with the distance downstream x, expressed as:

$$\frac{y_{\frac{1}{2}}}{D} = K_1\left(\frac{x}{D} + C_1\right) \tag{5.3}$$

Furthermore, the well-known similarity relationship for a plane jet defined below is also anticipated.

$$\left(\frac{U_0}{U_{cl}}\right)^2 = K_2\left(\frac{x}{D} + C_2\right) \tag{5.4}$$

Where K_1 , K_2 are the jet spreading and centreline velocity decay rate respectively. Table 5-1 shows their values obtained from this work and other numerical and experimental works. C_1 and C_2 are known as virtual origin and velocity decay coefficient of the plane jet and are strongly affected by the conditions at the nozzle inlet. Therefore, their values

are expected to vary and are not of significant interest, as pointed out by Stanley & Sarkar (2000).

According to Table 5-1, with higher refinement constant, the result reveals a gradual decline in the jet half-width spreading rate whereas a nearly negligible centreline decay rate is noticed. An overall agreement can be observed especially for the SAG case with $C^* = 5$, with less than 2% difference from the average measured value for K_1 and less than 4% for K_2. While an observation in result tendency can easily be made for the SAG cases, those from the fixed mesh show a nonlinear relationship between the results and the mesh density. Rending from the highest steep initialized at the end of the potential core for the NO-SAG-2, this case still provide a very satisfactory result for K_1 and fairly good result for K_2, in this self-similarity area.

The increase in jet spreading rate, K_1, with the decrease of the refinement variable, once again suggests a crucial role played by the inlet condition. The comparatively less turbulent intensity reproduced in the resolved field by a coarser mesh results in a longer potential core region. The same aspect was found in the findings of Goldsschmidt & Bradshaw (1981) where their result revealed a larger jet-spreading angle for jet with higher exit turbulence intensity. Nevertheless, the results from the fixed mesh cases do not follow this assumption, suggesting potential change in the error sources interaction when the mesh density reaches a certain level and changes the results tendency accordingly.

- **Time-averaged velocity and turbulent intensity predictions**

Normalized transverse velocity profiles numerically calculated from SAG application at $x/D = 11$ are compared with the conventional mesh NO-SAG-2 and the experimental data (Figure 5-18 and Figure 5-19). For these comparisons, only the case of NO-SAG-2 has been chosen amongst all the three fixed mesh cases since it provides the best prediction.

Table 5-1 Spreading and centerline velocity decay rates

Case	K_1	K_2
$C^* = 2$	0.15	0.16
$C^* = 3$	0.15	0.18
$C^* = 4$	0.13	0.18
$C^* = 5$	0.11	0.19
NO-SAG-1	0.075	0.17
NO-SAG-2	0.098	0.25
NO-SAG-3	0.081	0.45
Browne *et al*. (1983)	0.104	0.143
Thomas & Chu (1989)	0.11	0.22
Gutmark & Wygnanski (1976)	0.1	0.188
Smagorinsky LES of Liu *et al.* (2008)	0.12	0.20

According to the graphs, there are two noticeable regions along the cross section that yield distinct results. The first region is from the centreline to where $y / y_{1/2}$ is approaching the value of 1.25 and the second region starts from there to the end point of the measurement, $y / y_{1/2} \approx 2.2$. For both sections, it is clear from the graphs that, amongst all the SAG cases, it is actually the one with the highest mesh that mispredicts the parameter with a significant over-prediction revealed in the first region and under-prediction in the second region. In fact, in overall trend, the smaller the refinement variable C^*, the worst agreement with the experimental one. Solution obtained from the case of $C^* = 5$, for both regions along the cross section, provides the best agreement with both NO-SAG-2 and Gutmark & Wygnanski (1976) results.

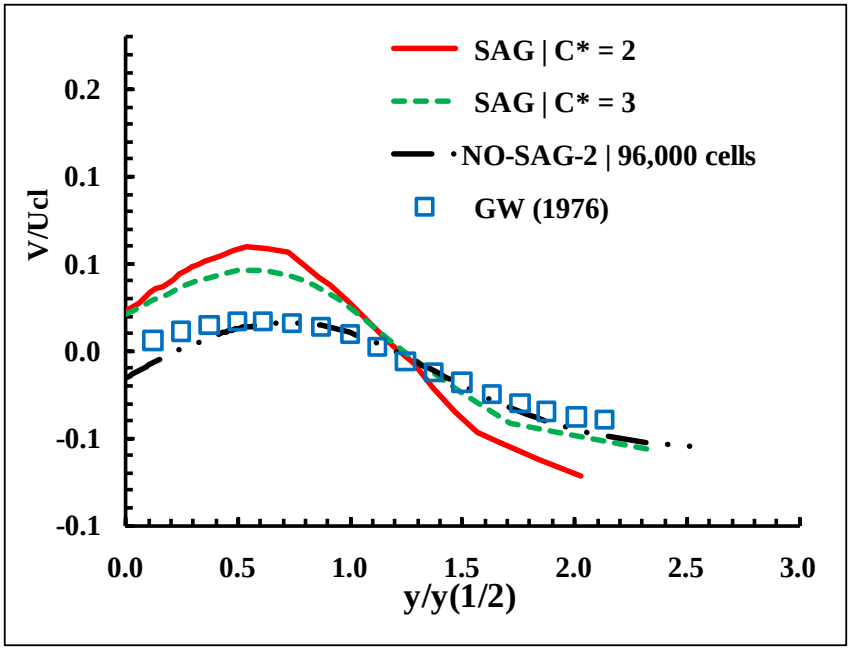

Figure 5-18 Normalized transverse velocity along x = 11D; Note: GW = Gutmark & Wygnanski (1976).

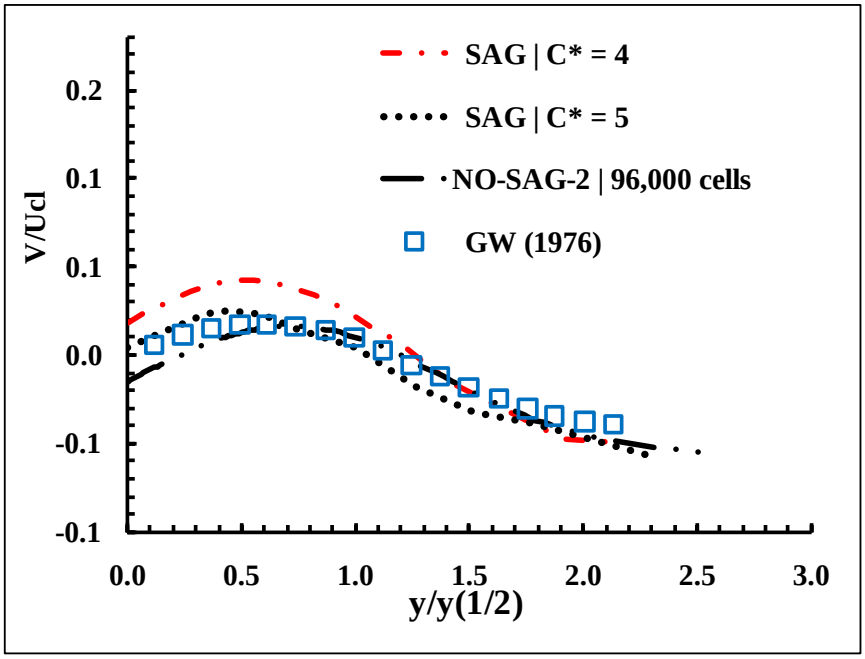

Figure 5-19 Normalized transverse velocity along = 11D ; Note: GW = Gutmark & Wygnanski (1976).

Figure 5-20 and Figure 5-21 show the streamwise fluctuation, *Urms*, along the cross section x = 11D. The results show that all the SAG cases provide reasonably good predictions for the turbulent intensity, at this location, when compared to an overall solution quality predicted by the conventional fixed mesh cases. While the rest of the cases yield the results that remain approximately 30% over-predicted along the cross section from the measurement of Gutmark & Wygnanski (1976), it is of great interest to notice that the prediction with comparatively highest level of error is provided by the finest mesh NO-SAG-3, particularly at the centreline $y / y_{1/2} = 0$.

The fluctuations in the lateral direction, Vrms, obtained from all the cases are shown in Figure 5-22 and Figure 5-23. The same figure as previously seen in the streamwise fluctuation in the case with the finest mesh NO-SAG-3 can be clearly seen. In addition to this, it should be noticed that the finest mesh case amongst SAG applications also gives roughly the same level of over-prediction percentage. On the other hand, it is the case with the largest C^* that provides the most satisfactory result particularly at the centreline where only 10% error difference from the reference data is found.

In terms of the Reynolds shear stress $u'v'/Ucl^2$, all the cases have shown distinctively different trends of results, Figure 5-24. Those predicted with the fixed mesh have revealed differences in both the peak values and their position on the selected cross section. NO-SAG-1, with comparatively coarser mesh, provides the peak value with a significant error when compared to the experimental measurement while the location of the peak is in good agreement. On the other hand, the finer mesh case, NO-SAG-3, has a better predicted peak shear stress value but with the location closer to the centreline. While the results obtained from the two fixed mesh cases give a difference in solution tendency, those obtained from the application of the SAG algorithm interestingly provide the same result behaviour along the cross section. The peak points predicted by all the SAG cases are approximately the same as that of NO-SAG-1 and take place at approximately the same location as that of NO-SAG-3. After reaching the peak point, the solutions then drop rapidly, especially in the interval $0.6 \leq y / y_{1/2} \leq 1.1$ before beginning to stay stable around the value of zero. Unlike the case of $Urms$ and $Vrms$, it is unclear which case is superior for prediction of the Reynolds shear stress.

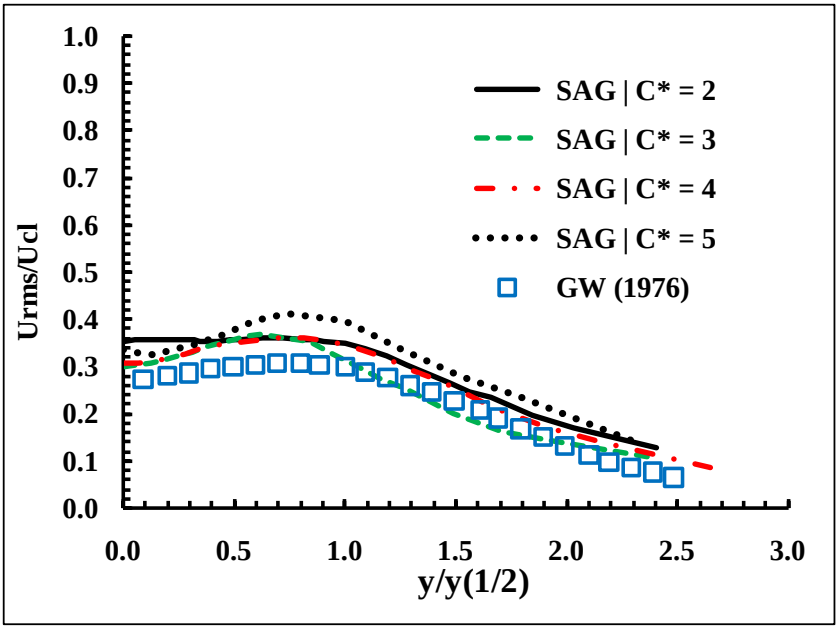

Figure 5-20 Streamwise fluctuation along x = 11D. Note: GW = Gutmark & Wygnanski (1976).

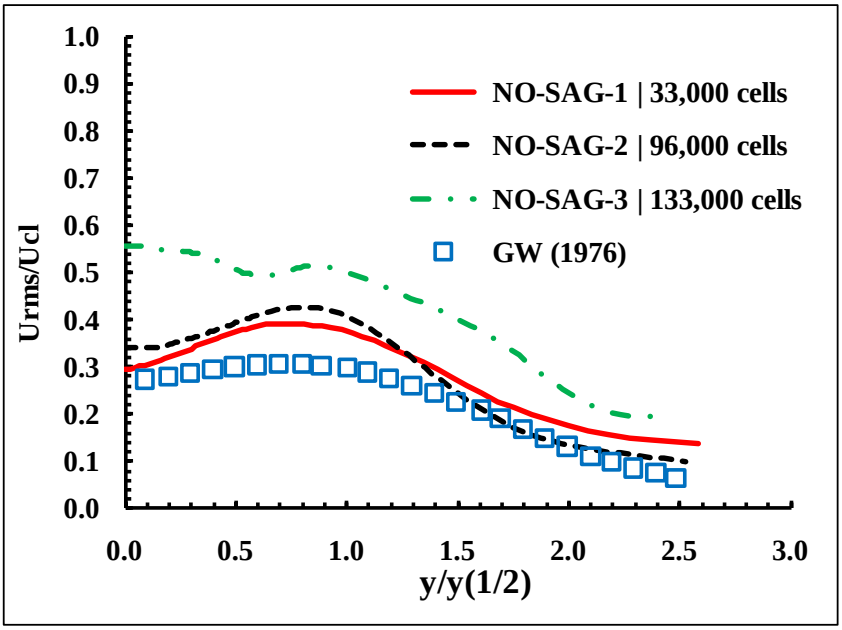

Figure 5-21 Streamwise fluctuation along x = 11D. Note: GW = Gutmark & Wygnanski (1976).

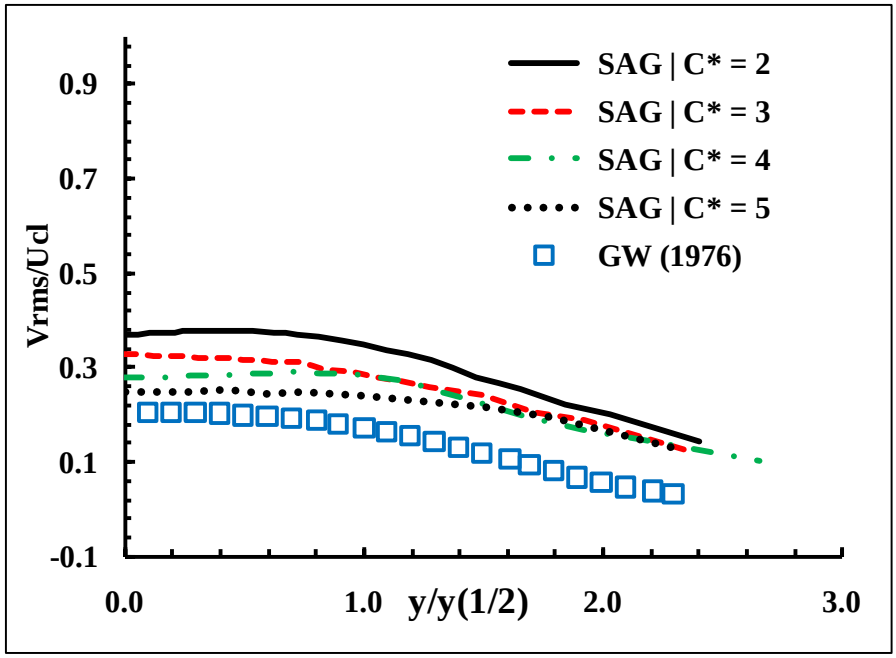

Figure 5-22 Lateral fluctuation distributions at x = 11D. Note: GW = Gutmark & Wygnanski (1976).

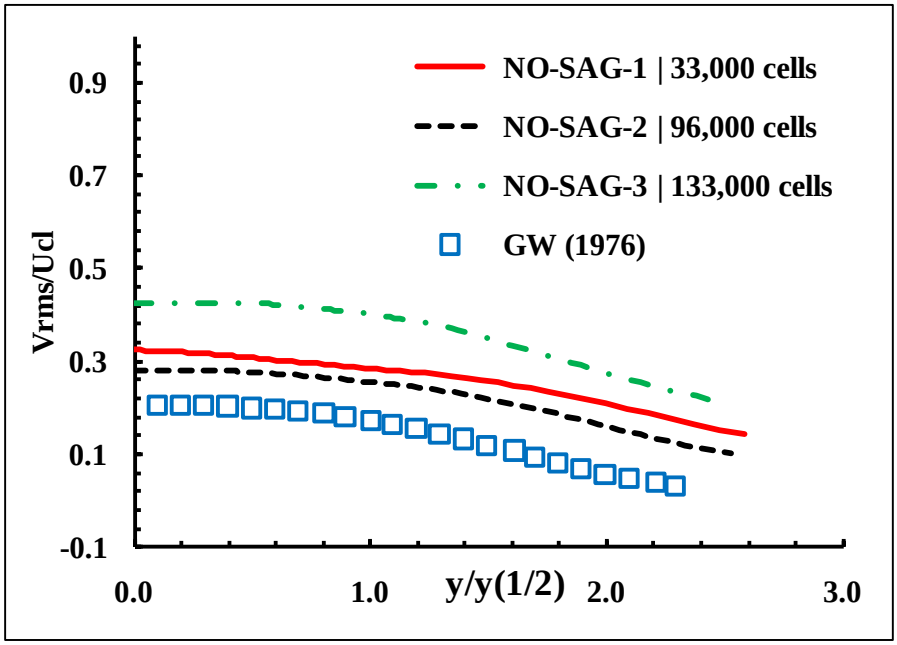

Figure 5-23 Lateral fluctuation distributions at x = 11D. Note: GW = Gutmark & Wygnanski (1976).

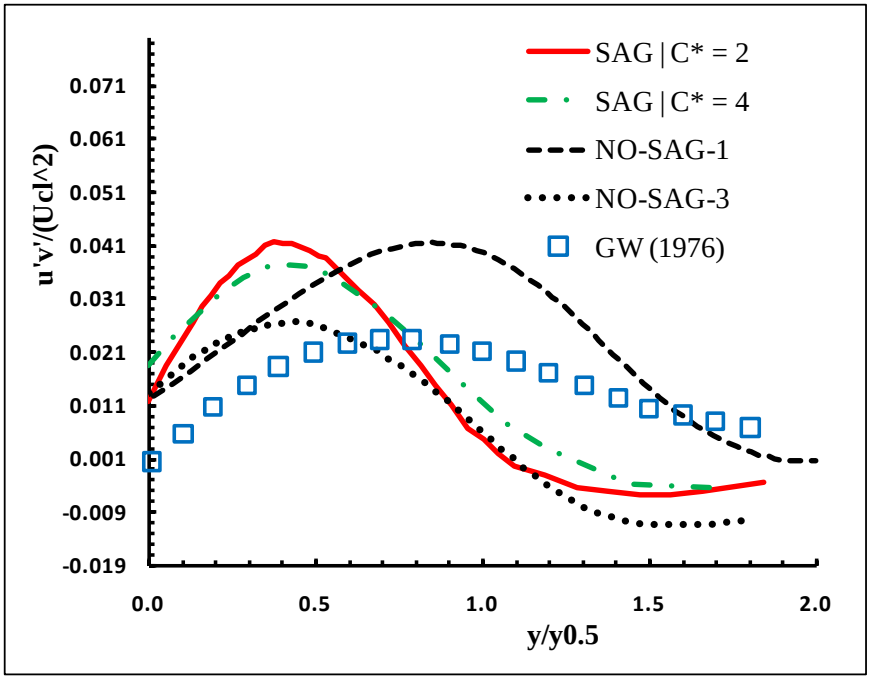

Figure 5-24 Lateral Reynolds shear stress at x = 11D. Note: GW = Gutmark & Wygnanski (1976).

On the overall image of the solution of this two dimensional plane jet predicted by the algorithm, it is evident that mesh resolution level at the inlet has a crucial role to play in generating and maintaining turbulent intensity and thus accounting for the upstream flow dynamics. The direct and obvious effect of this inlet condition appears in every flow parameter prediction, strongly suggesting a requirement for proper flow mechanism to be correctly generated at the flow upstream near field.

As numerically studied by Holdø & Simpson (2000) and With & Holdø (2005), it has become known that turbulent mechanisms prescribed at the inlet has sensitive influences on the flow downstream. Generally, the most suitable approach is to construct the turbulent structures at the inlet boundary in an artificial manner. One of the most popular choices for plane jet simulation is a three-dimensional energy spectrum broadband inflow forcing as utilised by Stanley *et al.*(2002). In order to generate initial velocity and turbulent intensity profiles that mimics as much as possible the actual 'known' condition involved in the corresponding experimental work, alternatively, researchers also perform a simulation separately in order to establish a turbulent field before imposing to the jet inlet upstream. Even though the procedure might involve some sophisticated mathematical

formulation, the former choice of turbulent flow conditions generation will then account for the upstream flow dynamics and hence the need to perform a jet simulation with high resolution separately can be reduced. It is important to remark that effective use of turbulent inflow conditions under LES context is subject to grid resolution and turbulence modelling. That is the grid resolution together with the dissipative nature of the corresponding turbulence modelling should correctly preserve reasonable amount of the turbulent intensity. In other words, inlet conditions, which are equipped with small-scale turbulent structures, do require a mesh resolution which can maintain these structures. If the mesh has insufficient mesh resolution, high frequency turbulent statistics included in the boundary conditions will be filtered and will not make an impact on the downstream flow filed. In this work, even though the inlet velocity profile is imposed with zero level of turbulent, higher mesh resolution, clustering at the inlet or the beginning of the potential core, as evident from the fixed mesh cases, is clearly responsible for reproducing the smaller scale turbulent structures. It then strongly indicates that without any turbulent structures constructed in an artificial manner and imposed at the inlet boundary, the requirement for high mesh resolution persists.

Another aspect of the overall results concerning the mesh density and turbulence fluctuation level is the potential role played by the numerical error. Despite the nonlinear correlation between the mesh density and the result behaviour, the solution tendency obtained from all the SAG cases suggests a limited level of contribution of numerical error. This could mean that a reasonably high level of the turbulence viscosity property in the Smagorinsky model has been well preserved. This is confirmed by the relatively coarser mesh producing lower turbulent mechanism leading to longer potential core region length as well as lower amount in jet spreading rate.

- **Computational demand**

To demonstrate the advantage of using the proposed SAG algorithm in terms of computational requirement, Table 5-2 gives CPU time in minutes needed to complete one flow-through time, based on U_0 and D. It is clear that the number of grid points (or cells) involved in the calculation is proportional to the amount of computational time needed. In this study an approximate 10 times factor in the number of cells between SAG case with

$C^* = 5$ and NO-SAG-2 was obtained, at equal level of overall result accuracy. This emphasises the benefit of adopting SAG algorithm in CFD community.

Table 5-2 CPU time in minutes spent for running one flow-through time (≈ 2,000 time steps) for each case, run on an Intel(R) Xeon(R) computer with 2.66 GHz and 4 GB of RAM.

Case	Final number of cells [*initial mesh: 6,800 cells*]	CPU time (minutes)
$C^* = 2$	31,838	42
$C^* = 3$	17,528	35
$C^* = 4$	12,830	22
$C^* = 5$	10,124	19
NO-SAG-1	33,000	51
NO-SAG-2	96,000	94
NO-SAG-3	133,000	147

5.1.4 Summary for plane jet simulations

The new simple Solution Adaptive Grid (SAG) algorithm proposed in Chapter 4 has been tested out by applying with simulations of a turbulent plane free jet at Re = 4,000 in two dimensions. The final results are compared with both those obtained from the conventional fixed mesh and the measurements available in literature. Taking into consideration all the aspects involved, some main conclusions of this investigation can now be drawn as follows;

- It has been emphasised by the results from the conventional mesh cases that in LES, finer mesh does not always lead to better results. This indicates the necessity to have higher mesh density only where needed.

- By increasing the refinement variable C^*, the results are improved. This could be explained by the fact that with coarser mesh the two types of error more effectively cancel each other.
- The nonlinear relationship between the result tendency with the mesh density obtained from the conventional mesh cases strongly suggests a potential change in the interaction of the two errors at a certain mesh density. This indicates the benefit achievable from being able to define the smallest grid size where the most suitable interaction of the errors occurs.
- With a very simple initial mesh, the refinement algorithm is capable of adapting the mesh locally and capture flow effectively, leading to improvement in final results. This can have a significant effect in real industrial engineering applications where mesh generation and testing is still a big issue and takes significant engineering time.
- Despite the difficulties in dealing with numerically study of plane jet in two dimensions, the chosen solver used in conjunction with the proposed mesh adaptation algorithm is proven to give an overall acceptable level of results accuracy.
- With this SAG, a considerable reduction in both computational time and the number of cells required to reach the certain level of accuracy is clearly seen. This strongly suggests the favorable benefit of adopting SAG for CFD problems.
- It is clear that the amount of turbulent intensity at the inlet has strong effect on the flow downstream and without introducing any means of turbulent generator, high mesh resolution is important. It then suggests that with an introduction of turbulent generation to the inlet, further reduction in the degree of freedom can be anticipated.

5.2 TWO DIMENSIONAL CIRCULAR CYLINDER FLOW

Amongst those known as classical problems in fluid mechanics is the flow around bluff bodies and regarded as an idealised bluff body flow is a flow over a circular cylinder. This is due to its wide range of applications in the engineering world such as marine pipelines, risers, offshore platform support legs, hydrodynamics etc. (Ong *et al.* 2009). From the point of view of the numerical study of fluid dynamics, this flow phenomenon is known as one of the benchmark and most challenging test cases especially at high Reynolds number. Furthermore, as far as large eddy simulation is concerned, the treatment at the wall still remains the most critical issue.

Like other types of flows past bluff bodies, a cross-flow normal to the axis of a stationary and smooth circular cylinder exhibits several complex phenomena including vortex shedding, reattachment and separation. Figure 5-25 shows typical features of this flow phenomenon at two different Reynolds numbers. The flow phenomena can be categorised based upon the Reynolds number ($Re = \frac{UD}{\upsilon}$), with the upstream velocity (U), the diameter of the cylinder (D) and the kinematic viscosity (ν). Based on the Reynolds number defined this way, amongst the few, Achenbach (1971) had stated a terminology used to classify different flow regimes:

i. Subcritical flow with $2.0 \times 10^2 < Re < 1.5 \times 10^5$
ii. Critical flow with $1.5 \times 10^5 < Re < 4 \times 10^5$
iii. Super critical flow with $4 \times 10^5 < Re < 1.0 \times 10^7$
iv. Transcritical flow with $Re > 1.0 \times 10^7$

Each of these flow regimes have their own range of parameters and behaviour. Such parameters are the Strouhal number, the location of separation, the drag coefficient and position of the flow transition from laminar to turbulence. Brief details regarding all this can be found in Celik & Shaffer (1995). In this thesis however, the author has focused only on the flow with subcritical regime with the chosen Reynolds number of 1.4×10^5. Their important phenomenon of their flow regime is the separation of the boundary layer that takes place in the laminar mode.

There are two factors why the flow over a circular cylinder has been chosen to test out the proposed SAG algorithm; one, the non-zero dominant velocity field and two, the existence of the solid wall both require that the flow mechanism in the region have a strong effect in the flow downstream. As it is known that the current limitation of applying LES to engineering problems lies in the tremendous number of grid points needed to effectively resolve the thin boundary layers found at high Reynolds number. It is extremely challenging to validate the algorithm with this flow phenomenon.

Figure 5-25 Schematic diagram of flow over a circular cylinder and vortex shedding at Reynolds number Re = 10,000 (above) and Re = 140 (below) with the flow direction from left to right. Source: Potter *et al.* (1997).

5.2.1 Subcritical Flow configurations and simulations

Adjacent to the circular cylinder boundary appears a thin region in which the viscous effects are dominant. The velocity on the surface is zero and increases towards the main flow stream further away. This thin region is known as the boundary layer where a large velocity gradient is found and hence increased shear stress levels. From the front part of the cylinder towards downstream direction the boundary layer thickness is growing and presenting different sub-regions starting with laminar up to a certain point where a transition to turbulence is triggered by unstable flow disturbances. The location of the transition point depends on several factors such as turbulent level of the flow outside the boundary layer, the Reynolds number and the roughness of the surfaces, etc.

At the stagnation point where zero velocity occurs, the pressure distribution has the value of unity according to Bernoulli's theorem. At the front, the flow speed increases resulting in an adverse favourable gradient before the opposite state of both velocity and pressure takes place around the rear of the cylinder. As a result, the adverse pressure gradient along the rear of the cylinder, the flow here then separates from the cylinder surface, rolls up into swirling eddies and eventually forms alternate shedding of vortices in the wake regions, known as Kármán vortex street, see Figure 5-26. The vortex shedding phenomenon in the wake is characterized by a dimensionless parameter namely Strouhal number (St), defined as follows;

$$St = \frac{f \cdot D}{U} \tag{5.5}$$

Where D is the diameter of the cylinder, f is the shedding frequency of vortices and U is the free stream velocity.

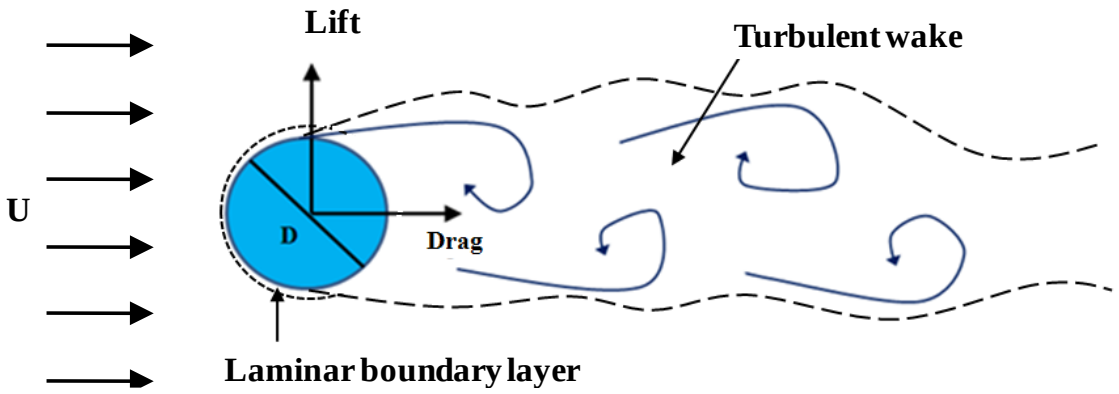

Figure 5-26 Basic feature of a flow past a circular cylinder in the subcritical regime.

A consequence of this is the occurrence of the additional time-dependant body forces, drag force (F_D) and lift force (F_L), due to the pressure variation. It is convenient to characterize these forces using dimensionless parameters which are the drag coefficient (C_D) and the lift coefficient (C_L) and with A being the reference area, can be expressed as;

$$C_D = \frac{F_D}{\frac{1}{2}\rho U^2 A} \quad , \quad C_L = \frac{F_L}{\frac{1}{2}\rho U^2 A} \tag{5.6}$$

Despite a significant number of studies on flow over circular cylinders (both experimental and numerical) at relatively low Reynolds number, the amount of investigations carried out at higher Reynolds number are limited, this is particularly true of numerical studies. Over the past two decades, only a limited number of numerical investigations of circular cylinder flow at high Reynolds number, i.e. $Re \geq 10^4$, have been carried out and some recent ones are Charles & Mingshun (1990), Kato & Ikegawa (1991), Zhang & Dalton (1996), Breuer (2000), Tutar & Holdø (2001), With *et al.* (2003), Kakuda *et al.* (2006). This is due to the presence of several complex flow phenomena that strongly influence the numerical study. The difficulties that numerical simulations of this type of flow have experienced involve the boundary conditions setup, proper treatment for the wall, suitable and effective turbulence modelling as well as the search for robust numerical schemes.

Beginning from the early days, works using method of time-averaged turbulence model have shown several drawbacks. Majumder & Rodi (1985) used the standard $k-\varepsilon$

turbulence model to simulate these flow phenomena where they failed to capture the separation point and under predicted the drag coefficient and more over the incorrect prediction of the recirculation length in the wake was also found. Their results suggested that separated turbulent flow past a cylinder cannot be predicted realistically with a steady state flow simulation ignoring the unsteady separation involving periodic motion. This is due to the fact that the overall predicted flow structure both near field and in the wake far field is strongly determined by the alternating periodic shedding of the vortices formed at both the upper and lower surface of the cylinder.

Along this line, several attempts to tackle the problem using modified versions of the standard $k-\varepsilon$ turbulence model have been made but still lack of success (Launder & Spalding 1972, Speziale 1978, Franke *et al.* 1989). Franke et al. (1989) concluded that based on the over-prediction of the turbulence kinetic energy, the isotropic eddy-viscosity assumption used in the $k-\varepsilon$ is not effective. In addition, the results also indicated that the model had a lack of capability of picking up the effects of the individual Reynolds stress components. Approximately five years later nevertheless, Celik & Shaffer (1995) combined the standard $k-\varepsilon$ model with an empirically imposed transition criteria and a good agreement in results was obtained for flow parameter prediction of up to and including the separation point. This is a result of having sufficient number of grid points placed in the thin boundary layer of the cylinder. Beyond this region however, the quality of results is not as good and they concluded that the model does not account for the presence of vortex shedding, the influence of which should be seen immediately after the separation point.

At the particular Reynolds number of 1.4×10^5, as chosen in this thesis, the first attempt to investigate and compare the efficiency of several turbulence models is that of Tutar & Holdø (2001). Their main conclusion was that the large eddy simulation (LES) provided the best results compared to the non-linear $k-\varepsilon$ model with extended models, such as renormalization group (RNG) and the anisotropic model. Prior to this work, an investigation was carried out by Breuer (2000) to study the effect of subgrid scale modelling (SGS), mesh density and the presence of the third dimension. Regarding the chosen subgrid scale modelling which were the standard Smagorinsky and its dynamic

version, their results did not give clear suggestion on which should be preferred. The key parameter for this seemed to be the Smagorinsky constant. The same observation of the unclear superiority of taking into account the third dimension was also concluded. Regarding the effect of mesh density, the results obtained in this work have shown that grid refinement does not improve the solution when employing LES.

The very first attempt in combining the methodology of solution adaptive grid and simulation of high Reynolds number circular cylinder flow was made in the work of With *et al.* (2003). They adopted the h-refinement type with the refinement variable defined to mimic the turbulence viscosity formulation. Even though most numerically predicted flow parameters obtained in this work remained in a good agreement with experiments, the main uncertainties are still concerned with the criteria that are required to *priori* setup the algorithm. This includes the proper form of refinement normalization means, their corresponding threadholds as well as the size of the smallest element allowed. This figure confirms the typically undesired aspects of solution adaptive grid methodology in which a large amount of user's judgment is still needed. In addition to this, they also found that finer mesh did not lead to a better result and no explanation is provided in their work. Nevertheless, the explanation proposed by Breuer (2000) was that in the LES context, with implicit filtering, the modelling and numerical error may cancel each other on a coarse grid much better than on a fine grid. This confirms the complications of the effect and interaction between both sources of error. It is then worth taking a closer look at this feature of LES with mesh refinement.

5.2.2 Numerical and simulation details

- **Governing equations**

Like the previous investigation on a plane jet, the investigation was carried out in this section deals with a statistically two-dimensional flow pass a circular cylinder, assuming that the third dimension is sufficiently large. The chosen Reynolds number is 1.4×10^5, based on the circular diameter (D) and the inlet upstream velocity (U) in which experimental data is available for validation. At this Reynolds number, the flow is characterized as sub-critical, i.e. the boundary layer on the cylinder wall separates in a

laminar mode and the transition to turbulence takes place in the free shear layer. Only conservation of mass and momentum were applied as the flow was assumed to be in the incompressible range and without any heat transfer. The governing equations were then discretised using the finite volume. The normalized time step $\overline{\Delta t} = \Delta t \cdot U \ /D = 0.01$ is used for all simulations.

- **Boundary conditions**

Figure 5-27 provides the computational domain and the boundary conditions used in this work. A parameter, D, is used to represent the cylinder diameter and all other relevant parameters are defined based on it. A uniform velocity in the x-direction is imposed while at the outlet boundary pressure is used and both velocity components are set free. Y-velocity component is set to zero for both upper and lower boundary while the streamwise component is set to equal the free stream inlet. No extra perturbations are introduced at the inlet and therefore no turbulence activity is initialized. No-slip condition is applied to the cylinder surface ($u = v = 0$).

The wall effect is treated in such a way that no wall functions are adopted. As suggested by Rodi *et al.* (1997) that simulations that use of 'law of wall' boundary conditions do not seem to be reliable enough to be used with confidence in separated flows, and the best treatment will be to use a sufficiently fine mesh to resolve the near-wall flow with no slip condition. This however implies that extra computational afford is unavoidable which simply goes against the main concept of this work. As a result, to account for this, the length scale in the vicinity of the cylinder wall up to some distance away from it was chosen from the minimum value between the von Karman constant (κ) and $C_s\Delta$, or;

$$l = \min(\kappa d, C_s\Delta) \tag{5.7}$$

Where d is distance to the nearest wall and C_s is the Smagorinsky constant ($= 0.1$ in this work).

- **Computational domain**

For the investigation of the proposed SAG algorithm on circular cylinder flow, a total number of 6 simulations were performed. The first two are classified as conventional mesh cases with no grid adaptation involved; one containing of 88,247 cells (named as NO-SAG-4) and the other containing of 65,207 cells (named as NO-SAG-5). The other four simulations were carried out with application of SAG with different refinement constants C^*. Figure 5-29 and Figure 5-30 shows respectively the distribution of the mesh in the case of NO-SAG-4 as well as the mesh used as the initial mesh for SAG cases (containing 15,380 cells). Both meshes shown were constructed in a similar way but the mesh in the vicinity of the wall was approximately 5 times finer in the NO-SAG-4 case than those in the initial mesh case. The mesh size then increases with respect to the distance from the cylinder wall. NO-SAG-5 mesh case was similar to NO-SAG-4 everywhere except for the area closer to the wall ($\approx D/5$ away from the wall) where a two-time coarser mesh is found. For the NO-SAG-4 mesh case, the distance of the first cell centre from the cylinder wall was approximately 0.15 per cent of the cylinder diameter D.

Table 5-3 Test cases and their details for the study of circular cylinder flow.

Case Name	With SAG ? (if yes, $C^* =$)	Initial Number of Cells
NO-SAG-4	No	88,247
NO-SAG-5	No	65,207
SAG | C* = 3	Yes, $C^* = 3$	15,380
SAG | C* = 5	Yes, $C^* = 5$	15,380
SAG | C* = 8	Yes, $C^* = 8$	15,380
SAG | C* = 10	Yes, $C^* = 10$	15,380

- **Simulation data integration**

Each of the simulations was run at least $\frac{25D}{U}$ time units before the statistical data was recorded over approximately 100 vortex shedding cycles. Even though no investigation has been conducted to investigate the effect of convergent statistics with different time-period of recording, it can be clearly seen from Figure 5-28 that data with fluctuations containing different amplitudes requires a sufficient long period of time for the statistics to converge.

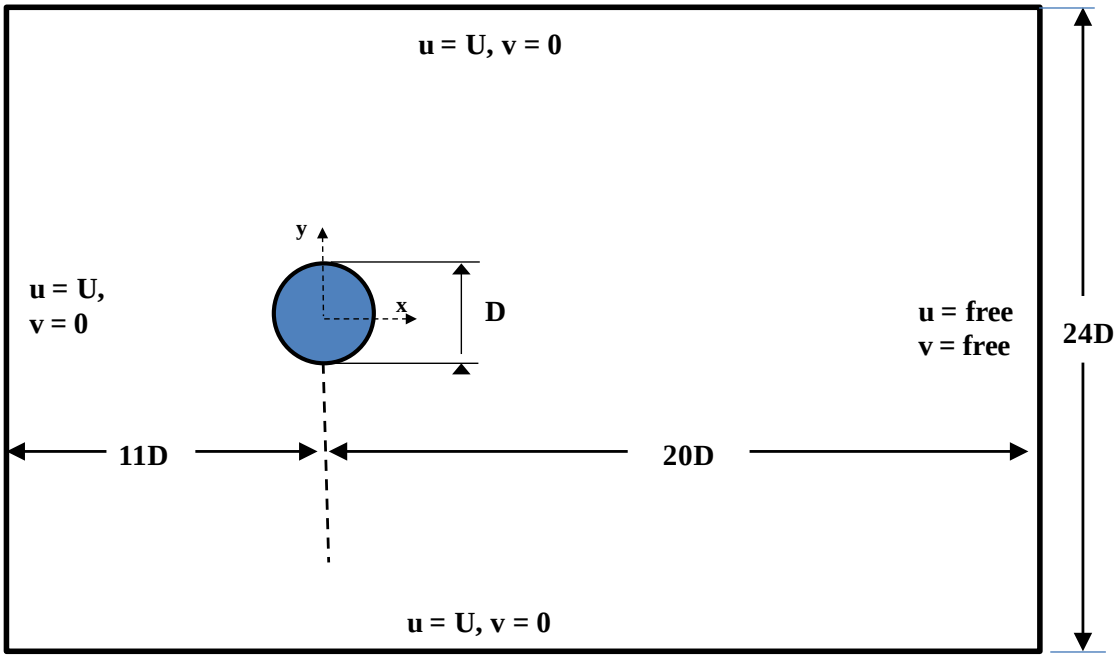

Figure 5-27 The geometric size of the computational domain and the boundary conditions used for the investigation of both conventional cases and SAG application.

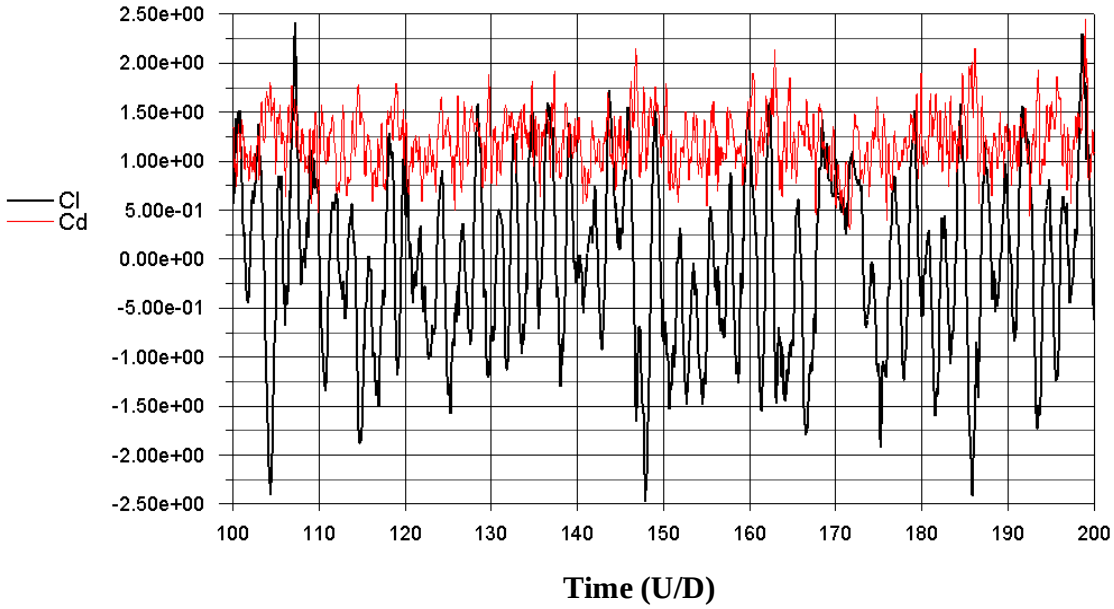

Figure 5-28 Time history of the drag coefficient (Cd) and life coefficient (Cl) obtained from the NO-SAG-4 case.

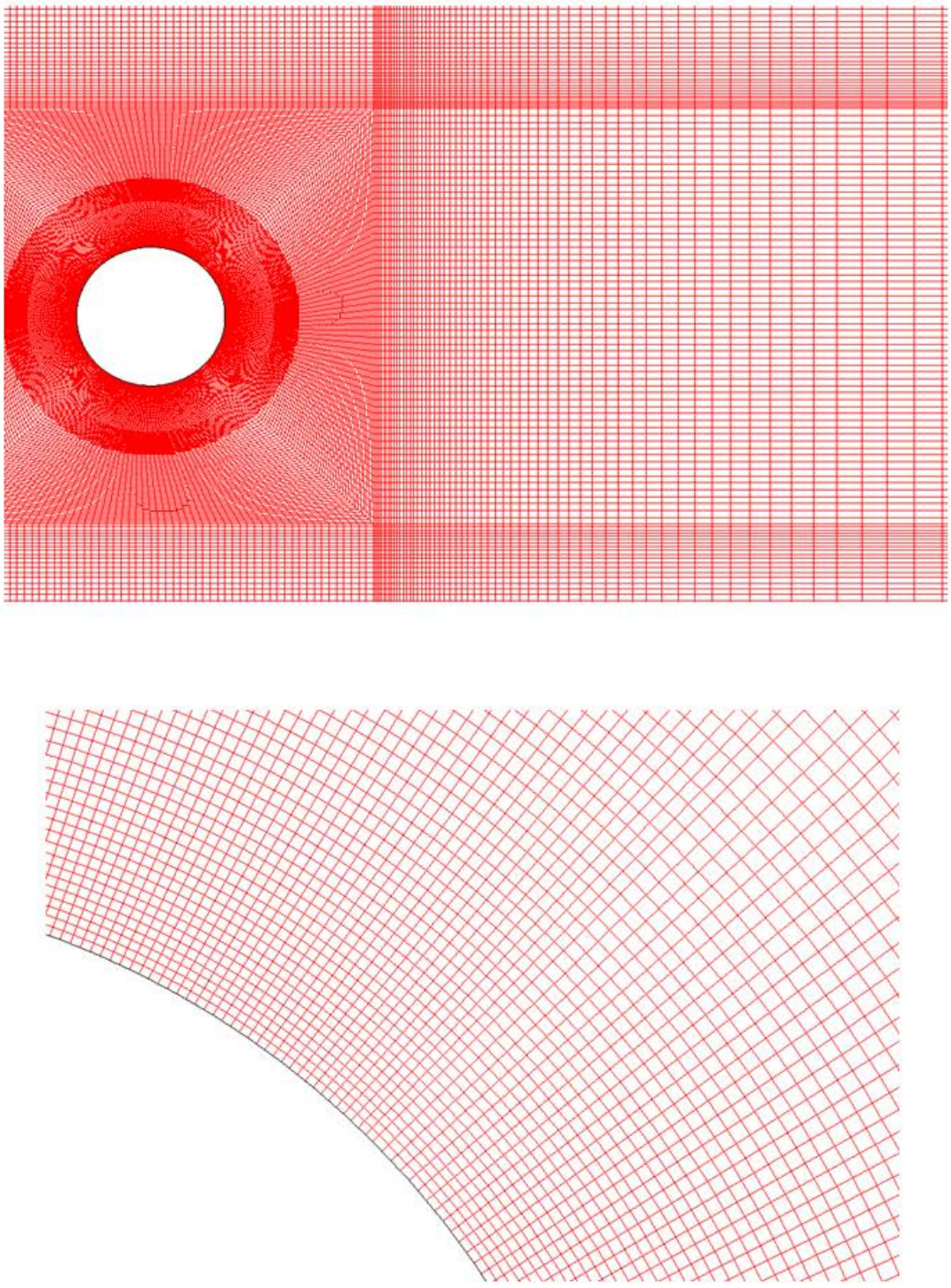

Figure 5-29 Mesh distribution with its mesh density near to the cylinder surface of the conventional test case NO-SAG-4.

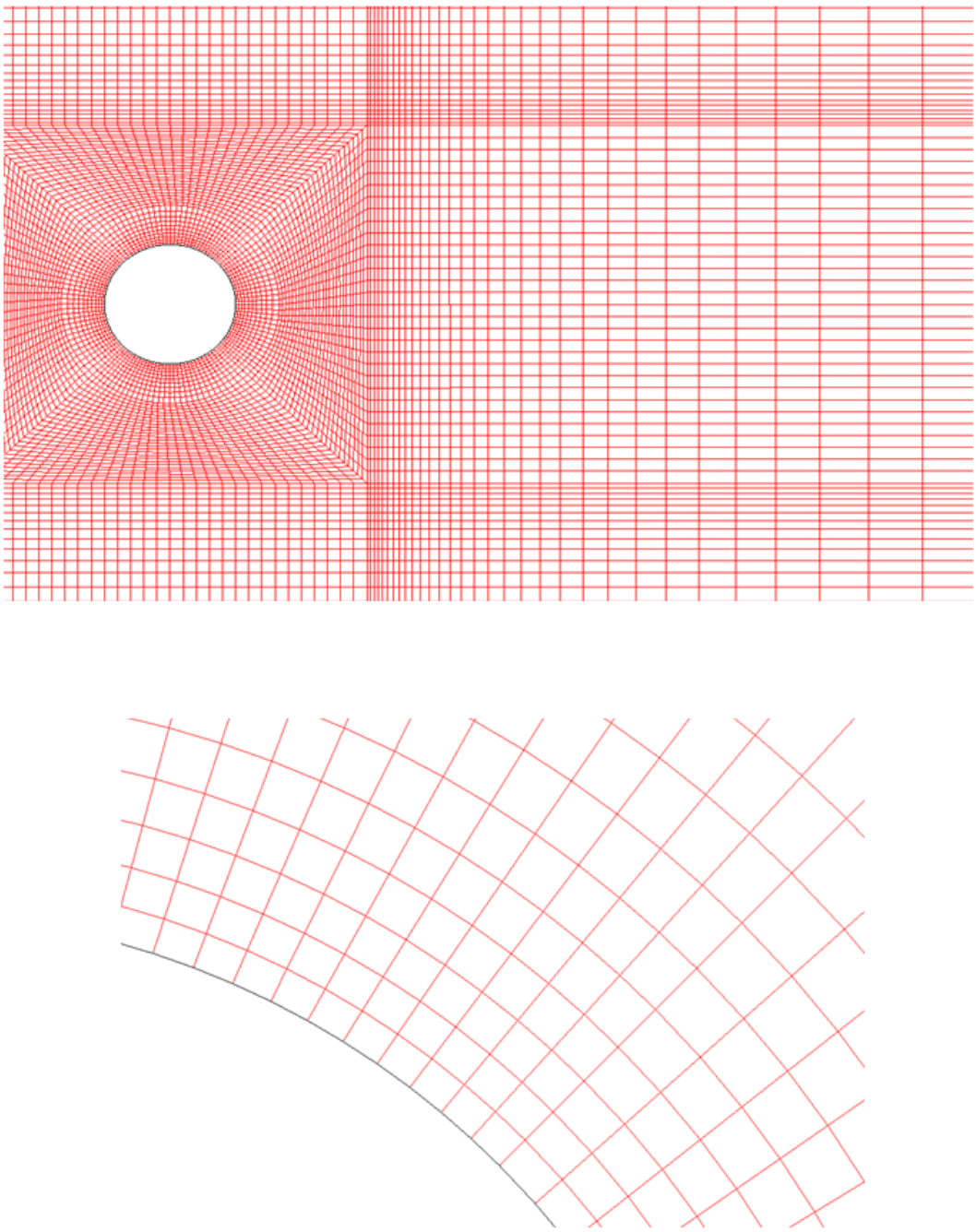

Figure 5-30 Initial mesh, together with its mesh density near to the cylinder surface, to be used with SAG application.

5.2.3 Results and general discussion

All the results obtained from the investigation carried out in this work are validated by comparing against the benchmark experimental data provided by Cantwell & Coles (1983). Even though this has been accepted as the standard validation for general computational fluid dynamics study, some critical remarks need to be made.

It is well known that the turbulent flow around a circular cylinder is sensitive to several factors and each of which has equal role to play in determining the solution quality. They are the Reynolds number, the ratio between the length and diameter of the cylinder, the blockage ratio of the cylinder, the end conditions, the roughness of the cylinder and the turbulence level at free stream. A widely scattered experimental data particularly for two critical flow parameters; the drag coefficient and the Strouhal number, gathered by Cantwell & Coles (1983) confirms this analysis.

In this study, amongst all the factors mentioned above, the most relevant ones are the 2D simplification and the zero turbulence level at the inlet which is obviously not feasible in any actual experiments. Consequently, distinctions between the results achieved from this work and their corresponding experimental ones can be expected.

- **Final mesh distribution after SAG**

Figure 5-31 and Figure 5-34 depict the final mesh distribution obtained after applying the SAG algorithm to the initial mesh with $C^* = 3, 5, 8$ and 10 respectively. It can be clearly seen that there are two areas that show obvious difference in mesh density and distribution; the vicinity of the cylinder wall (including the near field approximately one cylinder diameter away from the cylinder rear) and in the wake downstream far-field. Nevertheless, the same trend of mesh density in each area of the domain can be easily established for all the refinement variable C^* cases. For smaller refinement constant C^*, grid adaptation is more sensitive to the local velocity by definition resulting in higher mesh adaptation activity all over the domain in general. Closer to the cylinder surface, on the other hand, only the cases $C^* = 3$ and $C^* = 5$ exhibit a slight adaptation of the mesh while it can be easily noticed in the flow downstream section for all the cases. Further downstream towards the outflow boundary, following the definition of the estimated form

of the local Taylor scale adopted, the figures show that comparatively high mesh adaptation level takes place due to the increase of the local mean velocity component. This mesh distribution behaviour gives rise in differences in flow prediction accuracy.

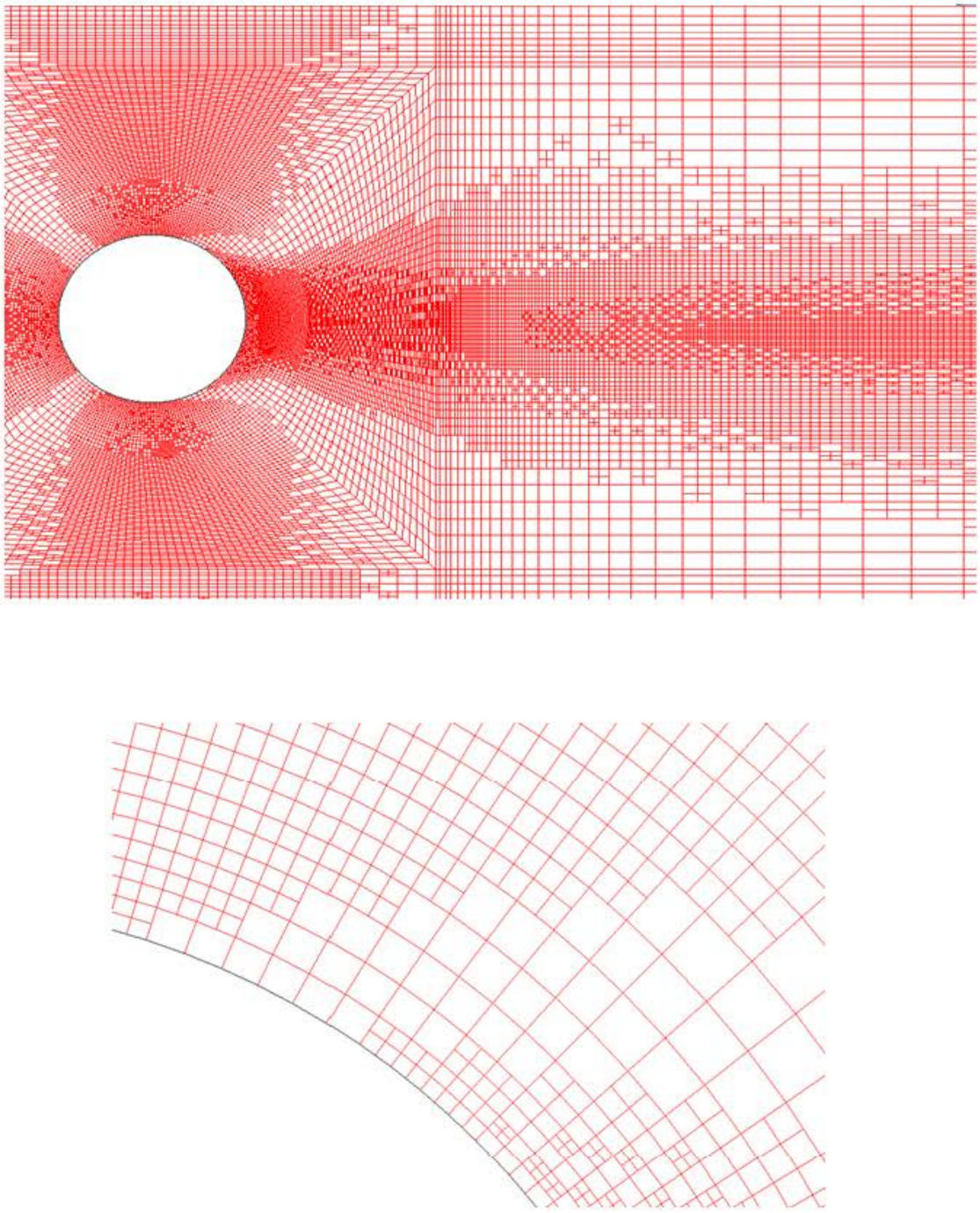

Figure 5-31 Final mesh distribution for SAG application with $C^* = 3$ (above) and its near wall region (below).

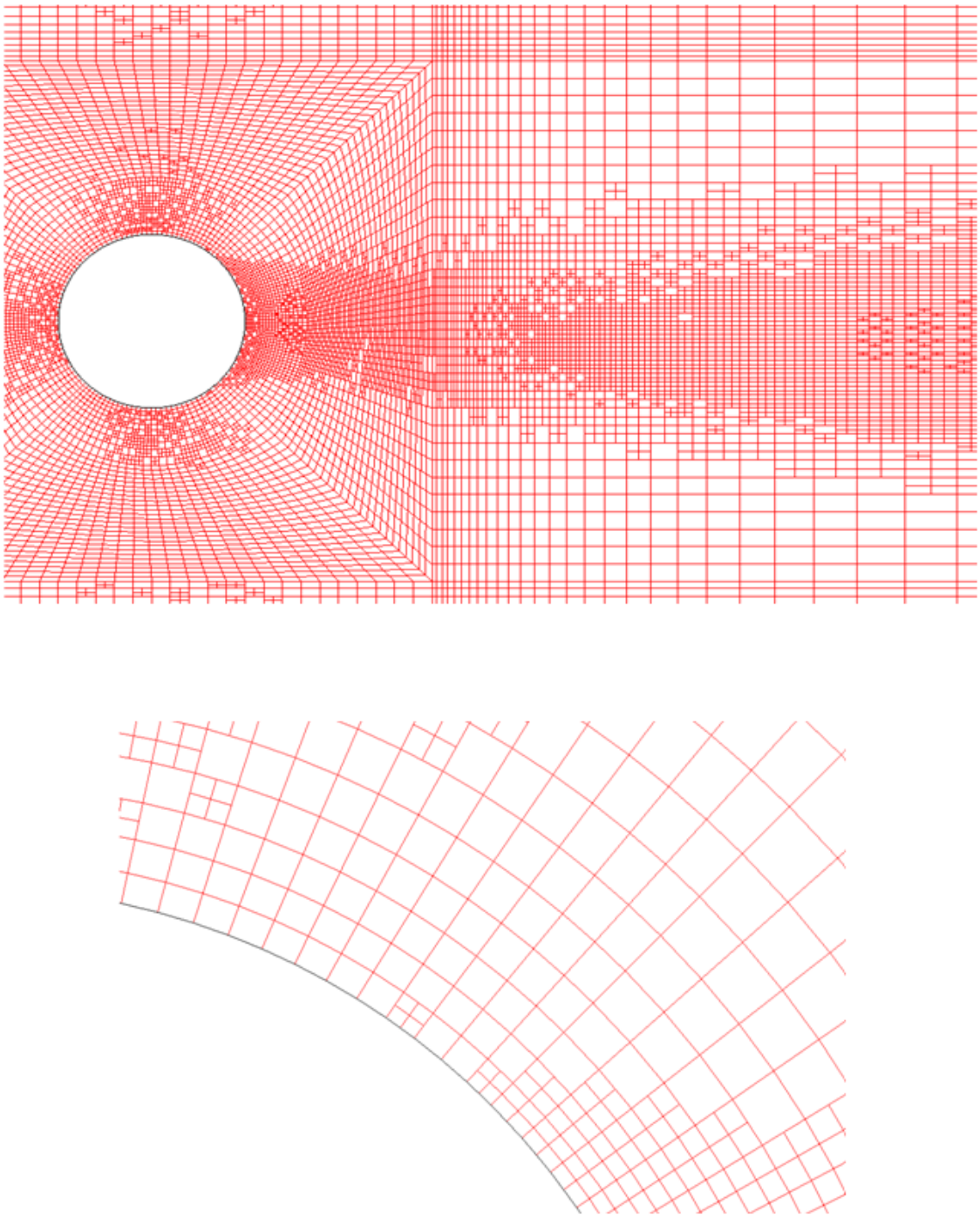

Figure 5-32 Final mesh distribution for SAG application with $C^* = 5$ (above) and its near wall region (below).

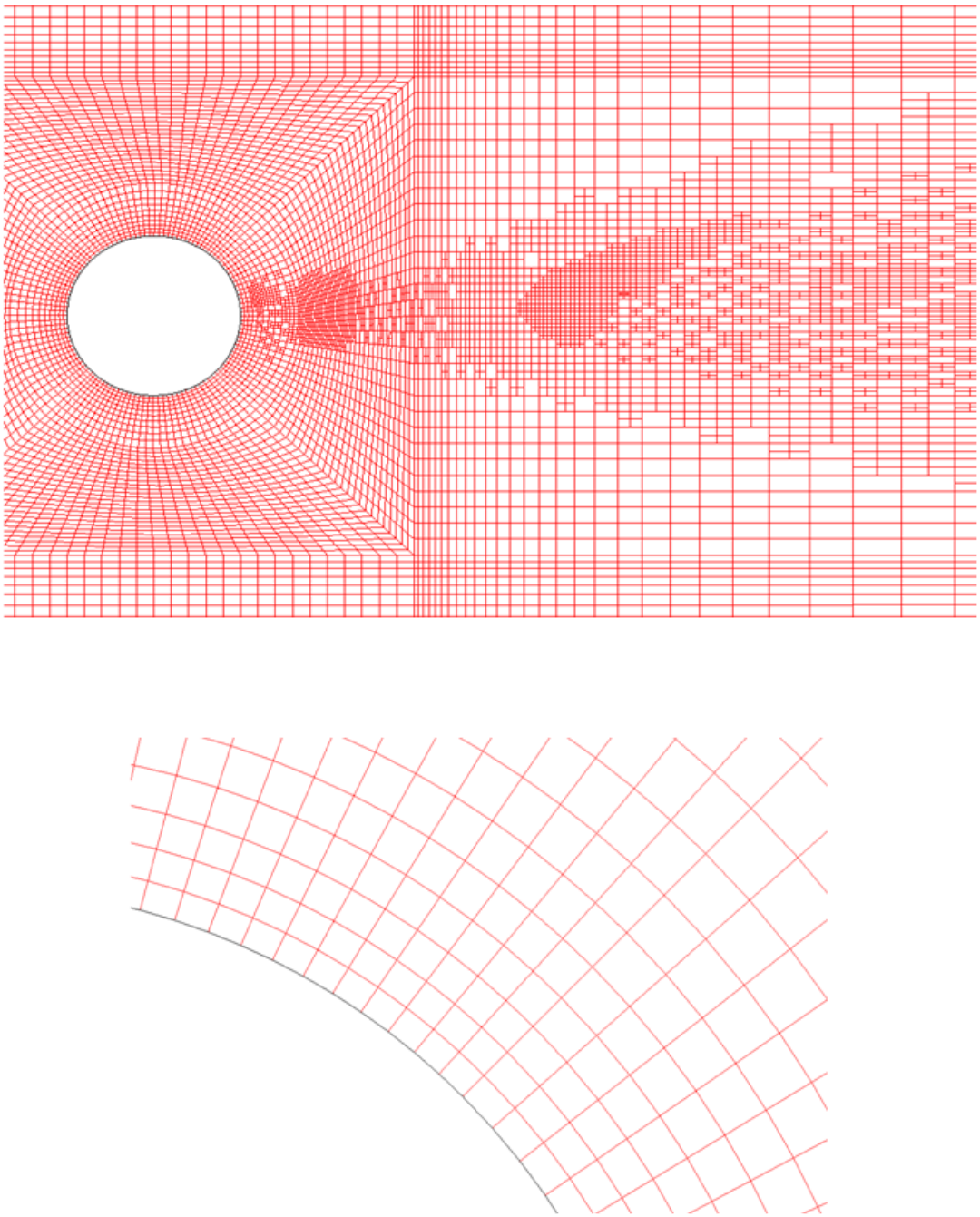

Figure 5-33 Final mesh distribution for SAG application with $C^* = 8$ (above) and its near wall region (below).

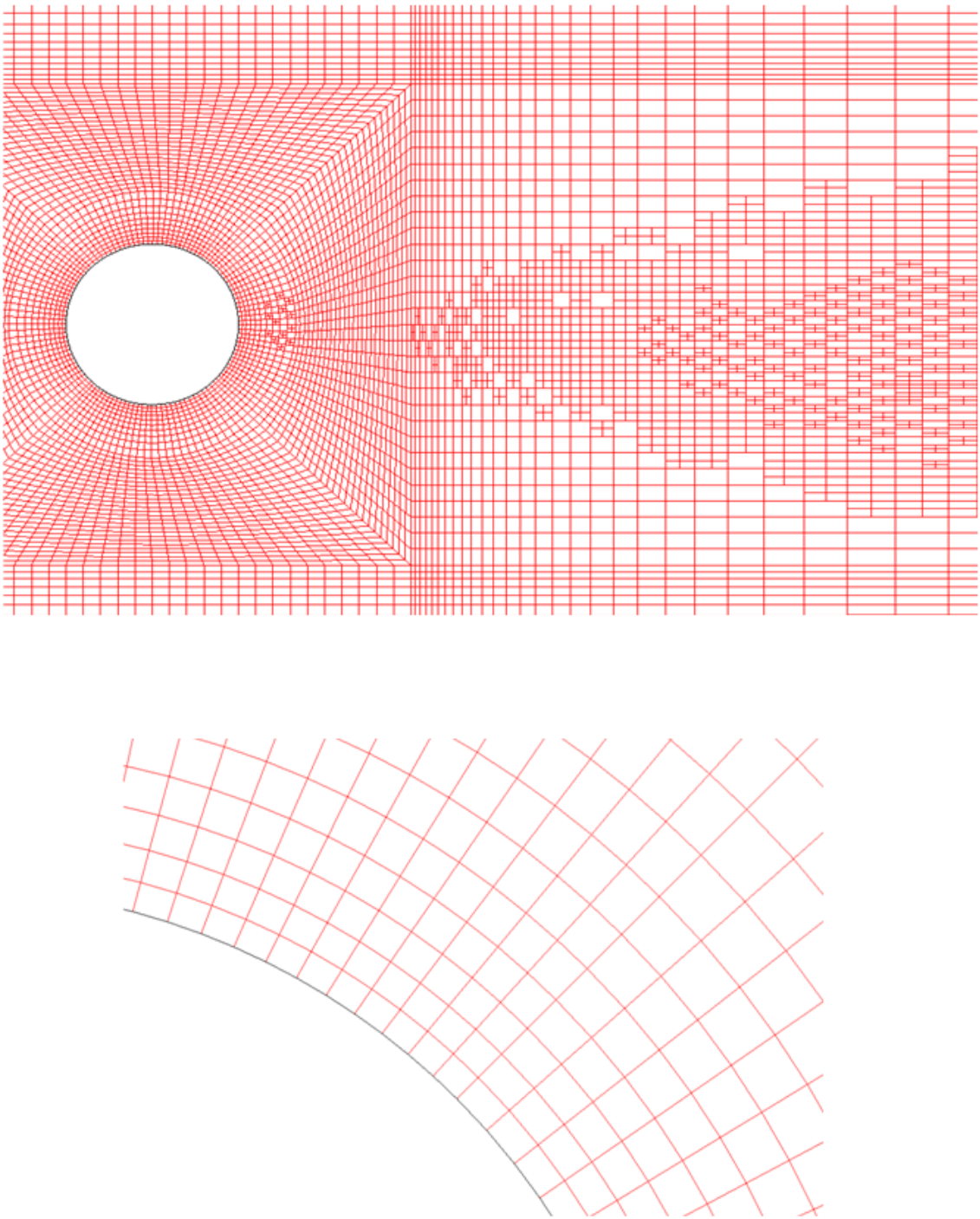

Figure 5-34 Final mesh distribution for SAG application with $C^* = 10$ (above) and its near wall region (below).

- **Critical flow parameters predictions**

Table 5-4 provides the critical flow parameters which are time-averaged drag coefficient ($\overline{C_p}$), normalized recirculation length (L_r/D), mean separation angle (θ_S), mean back-pressure coefficient $\bar{C}_{P_{back}}$ and non-dimensional vortex shedding frequency (the Strouhal number, St) obtained from all the cases and compared against the reference experimental data from Cantwell & Coles (1983). The experimental result for separation angle is not provided in the table. This is due to the fact that this flow parameter is extremely difficult to measure experimentally. Cantwell & Coles (1983) instead provided a value for the inflection point of the mean pressure coefficient of about 77° which is not the same as the separation angle. Nevertheless, Son & Hanratty (1969) has provided a value of $\theta_S = 78^{\circ}$ for flow at $Re = 10^5$ from their experimental work. In addition to this, it was Achenbach (1968) who revealed some interesting observation on this particular flow parameter. Here he found that $\theta_S = 78^{\circ}$ was where the laminar boundary layer separated at $Re = 10^5$ whereas this value jumps dramatically to $\theta_S = 94^{\circ}$ for $Re = 2.6 \times 10^5$. At $Re = 1.5 \times 10^5$ however, the separation of $\theta_S = 72^{\circ}$ was found. The figure strongly indicates a non-linear relationship between the separation angle and the Reynolds number in this Re range. Consequently, for flow over a circular cylinder at subcritical regime it is accepted that there is no fixed value for separation point.

The first critical flow parameter to take a look at is the separation angle of the boundary layer, θ_S. The numerical estimation for this parameter decreases with the increase of the refinement variable starting from one with the largest value of 120° in the $C^* = 3$ case to the lowest one of 109° in the case with $C^* = 10$. All the SAG cases have, as can be seen, yielded the angle of separation taking place behind the maximum thickness (90°). This behaviour is expected to occur only in cylinder circular flow in the critical regime not in this subcritical regime. The results from the two conventional mesh case nevertheless are in a much more reasonable agreement with the literature with the value of 81° for NO-SAG-4 and 84° for NO-SAG-5.

Table 5-4 flow parameters; time-averaged drag coefficient ($\overline{C_p}$), normalized recirculation (L_r/D), separation angle (θ_S), mean back-pressure coefficient ($\bar{C}_{P_{back}}$) the mean Strouhal number (St), obtained from all the cases and compared against the reference experimental data.

Case	$\overline{C_d}$	L_r/D	θ_S	$\bar{C}_{P_{back}}$	St
$C^* = 3$	0.567	0.217	120	-1.05	0.361
$C^* = 5$	1.062	0.221	118	-1.64	0.308
$C^* = 8$	1.526	0.312	111	-2.06	0.277
$C^* = 10$	1.558	0.326	109	-2.21	0.229
NO-SAG-4	1.221	0.565	81	-1.15	0.221
NO-SAG-5	1.524	0.491	84	-1.64	0.163
Cantwell & Coles (1983)	1.237	0.44	-	-1.21	0.179

The predictions for the recirculation length, defined as the distance from the circular wall in the backside to where the time-averaged velocity changes from negative to positive value and denoted by L_r, has revealed some interesting trends. The shortest recirculation length is obtained from SAG with the smallest refinement variable at $C^* = 3$ with approximately 50% under-predicted. The percentage of under-predicted result then decreases when the refinement variable increases and the best prediction for the SAG cases is that from $C^* = 10$ with only about 25%. An over-prediction of approximately 28% is also found for the conventional mesh cases NO-SAG-4 whereas only around 11% over-predicted in the NO-SAG-5 case. From this trend, an interesting observation can be made and that is the relatively higher mesh density clustered in the near wall region as is the case for NO-SAG-4 as well as those with smaller C^* do not seem to result in any more impressive prediction for recirculation length. On the other hand, despite the other fine mesh case of NO-SAG-5, it is the case with the coarsest mesh, $C^* = 10$, that is more comparatively successful.

In terms of the Strouhal number St for this circular cylinder flow at $Re = 1.4 \times 10^5$, before a determination of the accuracy obtained from this work can be made, a crucial remark needs to be mentioned. The value of $\mathrm{St} = 0.179$ from the reference work as shown in Table 5-4 is widely observed and accepted to be distinctively lower when compared to other works experimentally carried out in the past in which all of these provide the value at approximately of 0.2 (Son & Hanratty 1969, Zdravkovich 1997, Fay *et al.* 1998). Based on this widely accepted value of St, it can then be seen that there are only three cases from this study that provide the results within 15% differing from the experimental one. These are those from the two cases with conventional mesh, NO-SAG-4 and NO-SAG-5, and only one from the application of SAG, with $C^* = 10$. The St then tends to get smaller with a decrease of the refinement constant with the comparatively worst one corresponding to $C^* = 3$.

Another parameter to look at is the mean drag coefficient, $\overline{C_d}$. The same pattern of the predicted values obtained from all the SAG cases as the case of recirculation length can also be found for this when the predicted value tends to increase with the increase of the refinement variable. The lowest one predicted is 0.567 obtained from the $C^* = 3$ case which is approximately 54% away from the measurement of Cantwell and Coles (1983). The best agreement is that of NO-SAG-4 case with only less than 2% under-predicted. Results obtained from NO-SAG-5, $C^* = 8$ and $C^* = 10$ are very close to each other and approximately 25% over-predicted whereas the mesh distributions as well as densities amongst them are noticeably different. For these numerical predictions, Sampaio & Coutinho (2000) stated that with this range of percentage of error it can be assumed that the prediction is accurate enough for most engineering purposes.

Regarding the flow parameter, a collection of its values, gathered from a number of experimental studies by Cantwell & Coles (1983), reveals that there is a vast scatter of the measurements. This is the result of the fact that the flow is sensitive to several factors such as aspect ratio, blockage ratio, end conditions, roughness of the cylinder, free stream turbulence level, Mach number and so on. This all equally makes it difficult to state a definite value. Nevertheless, the value of approximately 1.2 is a widely accepted value of $\overline{C_d}$ for $Re = 1.4 \times 10^5$.

Last but not least is the back-pressure coefficient integrated over time, $\bar{C}_{P_{back}}$. For this flow parameter overall results yielded from all the SAG test cases show a unimpressive prediction with the highest percentage of over-prediction of approximately 80 % as in the case of $C^* = 10$, with the coarsest mesh density. In the case with $C^* = 5$, the result nevertheless remains in the same level of accuracy as that of the finest mesh NO-SAG-5 with about 35% under-predicted. The best prediction for this flow parameter is that of the case with conventional mesh NO-SAG-4 with only 5% over-predicted. The decrease in predicted value of this parameter corresponds well with a higher prediction of the recirculation region. This is consistent with an experimental work of Gerrard (1966) as well as the numerical investigation of Kravchenko & Moin (2000), where authors concluded that this is more likely to be the case with simulations with coarse mesh.

From the overall prediction of the critical flow parameters, even though a high level of differencing with experimental values still exists, a very good correlation amongst the parameters predicted can be found. The small dimensions of the recirculation region are in accordance with the presence of the delay in separation angle (higher θ_S) indicating the existing of a narrow wake, at least in the flow near field. As the wake is decreasing in size, a reduction of the drag coefficient with the decrease of C^* would be expected and clearly seen in the Table 5-4. Moreover, the increase in the Strouhal number St also corresponds well with the decrease of drag coefficient $\overline{C_d}$ and therefore also the increase the back pressure, $\bar{C}_{P_{back}}$. This is all in accordance with the findings of literature (Tutar & Holdø 2001, With *et al.* 2003).

Next to this, there are also some noticeable figures revealed from simulations with conventional mesh as well as from the application of the algorithm. Firstly, with all the cases with SAG application it is clear that the trend of all predictions for these critical flow parameters is monotonic. i.e. all the results behave correspondingly to the change of the refinement variable in the same direction. This aspect emphasizes the advantage of the algorithm where the existence of the refinement variable can be seen as a tool for real engineering applications and also can enable one to be more control in the mesh distribution.

Secondly, the overall predictions obtained from the SAG case with $C^* = 10$ and those from the conventional mesh NO-SAG-4 in which they reveal comparatively the closest results. The most interesting one is the predicted frequency of the vortex shedding where nearly the same values were predicted, despite the difference from the experimental one. This is surprising, considering their significant difference in mesh density. Here, an approximately 5 times finer mesh is utilized in NO-SAG-4 case than those in SAG with $C^* = 10$ to model small turbulent structure closer to the wall where it is believed to strongly effect the vortex shedding. From this figure, it is then difficult to state whether or not the formation of vortices is always highly dependent on the resolved small scales in the free shear layer. Alternatively, it could also be a result of the numerical error produced with the coarse mesh that potentially contributes to the instabilities of the shear layers and hence the formation of the vortex street.

- **Instantaneous flow motions**

Figure 5-35 displays the contour of vorticity magnitude snap shot taken at different flow times. Two shear layers formed at the top and bottom surface of the cylinder can be clearly seen. These layers begin to separate themselves from the cylinder with the thickness approximately the same size as the laminar boundary layer and form the Karman vortex in the wake region. The lengths of the shear layers are shown to be strongly sensitive with the mesh resolution around where they take place as well as the boundary layer. It can be observed that with coarser mesh the length of the shear layers tend to increase. This is corresponding well with the relatively increase in the circulation length L_r/D as previously discussed.

Regarding the formation of the vortices downstream, it is shown that with high mesh density, as with smaller C^*, each vortex generated at the free shear layer can be better maintained further downstream. Nonetheless, as expected, it is shown that the vorticity contour of the NO-SAG-4 illustrates well the existence of the secondary eddies, as observed in the experiment conducted by Bouard & Coutanceau (1980). On the contrary, no strong secondary vortices, for all SAG cases, are obviously noticed before or around the highest/lowest point of the cylinder. Nevertheless, further to the rear of the cylinder these flow phenomena can still be found but comparatively weak in magnitude.

As the flow develops these small eddies move forwards and embedded themselves with the primary once forming larger eddies. The delay of onset of these small eddies as obtained in the SAG cases, closer to the primary ones as well as those being formed at the other side of the cylinder, perhaps forces the interaction of the primary eddies generated from both sides to take place more frequently. It then results in higher vortex shedding frequency (hence relatively higher the St) when compared with the experimental data. This is confirmed by the correlation that can be easily observed from this study of the separation angle θ_S and the Strouhal number St obtained from all the SAG test cases.

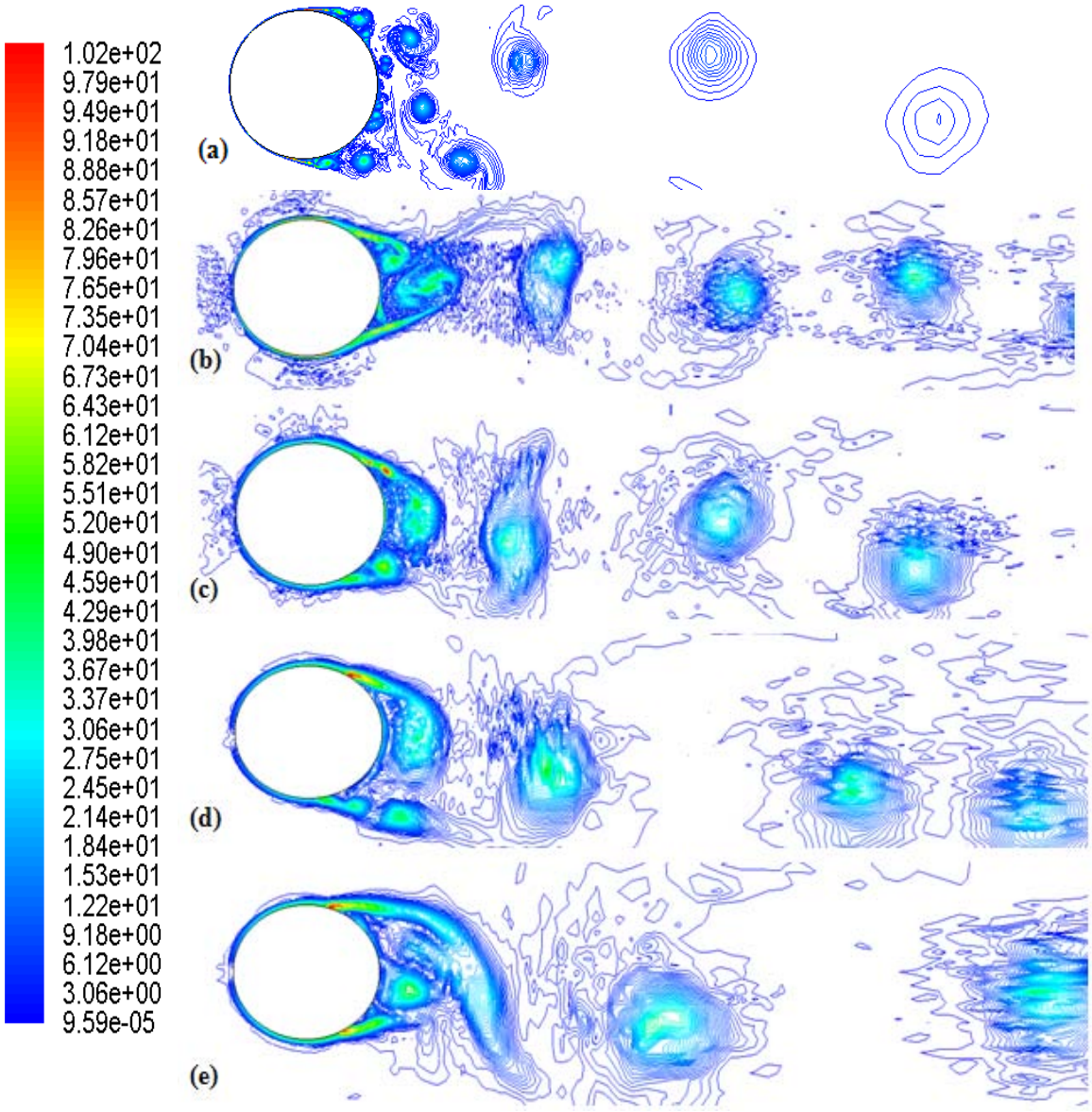

Figure 5-35 Snap shot of predicted vorticity magnitude, demonstrating vortices formed behind a circular cylinder provided from different test cases; a) NO-SAG-4, b) SAG | C*=3, c) SAG | C*=5, d) SAG | C*=8 and e) SAG | C* = 10.

- **Time-integrated velocity predictions**

Figure 5-36 shows the normalised time-averaged streamwise velocity of some selected cases along the symmetry axis ($y = 0$) of the cylinder. Some information of the distribution of the profile near the wall of the cylinder and the wake ($x \leq 2.5D$) can also be observed from the recirculation length measurement as previously shown. On overall

image, despite the short recirculation region as in both SAG cases shown, predictions on this region remain in good agreement with the measurement of Cantwell & Coles (1983). Further downstream approximately $2.5D \leq x \leq 4D$ there is a small deviation of the results obtained from SAG with $C^* = 8, 10$ with the highest of approximately 18% under-predicted around $x/D = 3$. The trend of both lines then starts to get closer to the experimental one further downstream. For this time-averaged velocity component, it is the NO-SAG-5 case where the comparatively best agreement with the reference work is found.

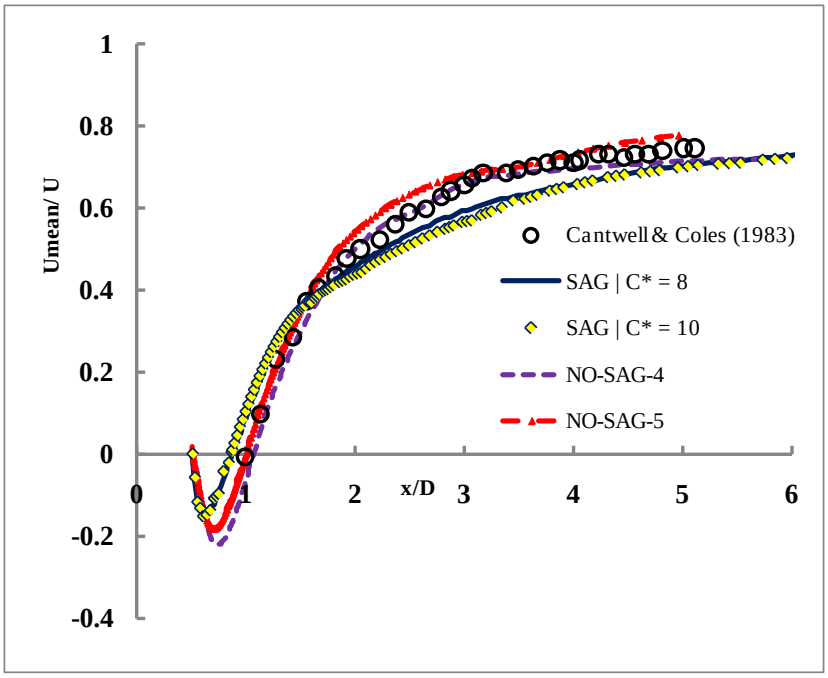

Figure 5-36 Time-averaged X-velocity distribution along the centreline of the cylinder for selected cases both those from conventional mesh and those from SAG study.

Figure 5-37 shows the streamwise normalized time-averaged streamwise velocity component, U_{mean}/U, in the near wake region along the vertical line $x = D$. Amongst the cases with application of SAG, it is the relatively finest mesh, with $C^* = 3$, that provides the worst prediction while the other two remain close to each other. At the centreline position of the cylinder ($y = 0$) this case gives more than 40% over-prediction. Further away towards the edge of the wake at the cross section all the predictions show the same trend of getting closer to the experimental measurement but fail to reach the peak

value of 1.18. The finer mesh, NO-SAG-4, shows a very good agreement with the reference nearly everywhere along the cross section but is still about 10% under-predicting the peak value. Towards the outside the wake nevertheless, all simulations show good agreement.

Figure 5-38 illustrates the transverse normalised time-averaged component, V_{mean}/U, along the vertical line $x = D$. In contrast to the streamwise component as explained above, the graph shows that the numerical solutions of this transverse component have an increase in accuracy as the mesh density increases, i.e. smaller C^*. The case with the coarsest mesh, C^* = 10 has predicted the lowest value of the normalized velocity by approximately 45% away from the experimental data. The best numerical solution for this flow parameter is that of the case NO-SAG-5 with relatively highest mesh resolution. Nevertheless, the point at about $0.5D$ away from the centreline in the wake where the lowest value of V_{mean}/U is measured experimentally, is not reproduced by any of the numerical cases.

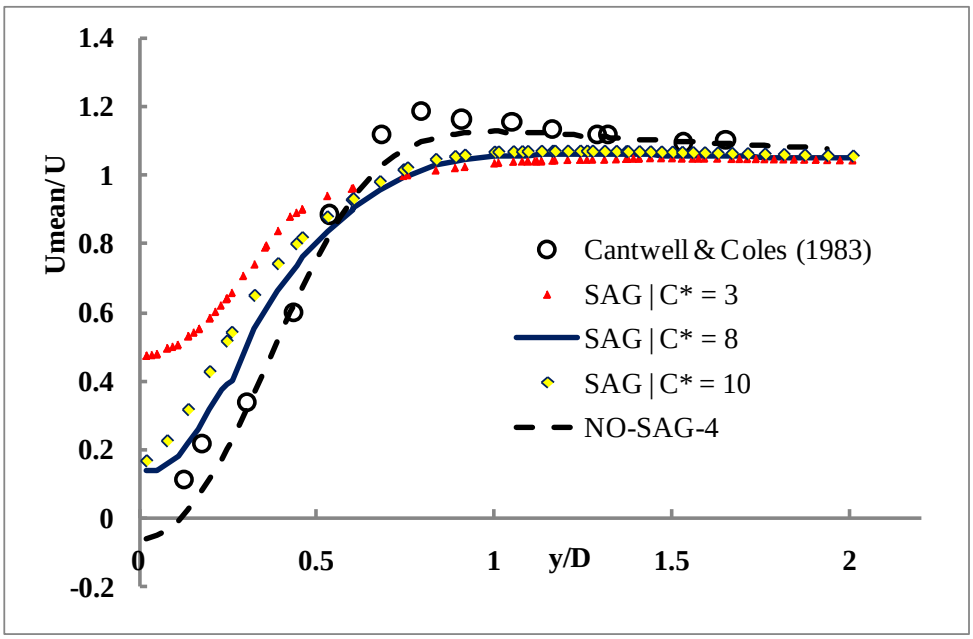

Figure 5-37 Time-averaged X-velocity distribution along the line x = D of the cylinder for selected cases both those from conventional mesh and those from SAG study.

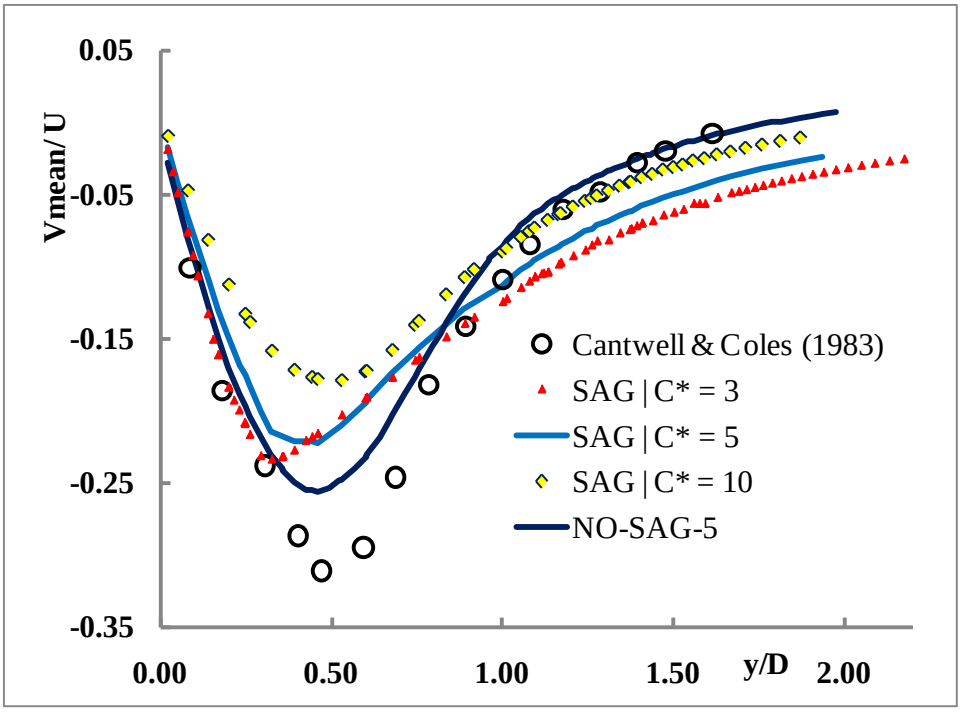

Figure 5-38 Time-averaged Y-velocity distribution along the line x = D of the cylinder for selected cases both those from conventional mesh and those from SAG study.

From the result quality obtained from NO-SAG-4 in the first graph and NO-SAG-5 in the second one, it can be assumed that the flow parameters predictions are strongly influenced by the level of mesh resolution around the cylinder surface and in the shear layers. From this observation, however, there is a contradiction appearing in the case of SAG with $C^* = 3$ for the prediction of the two normalised parameters. With the same density of mesh and assumingly the same level of turbulence produced, the mean transverse cross section velocity has lied in better agreement with the experimental one whereas the opposite trend is seen for the streamwise mean velocity. Nevertheless, in general it can be seen that due to the insufficiency in mesh density in such critical areas, for all the SAG cases, the results far away from the cylinder are sensitively affected.

- **Turbulence intensity predictions**

In terms of numerical predictions for turbulent intensity, Figure 5-39 shows the normalized Reynolds stress $u'u'/U^2$ along the centreline and reveals differences in magnitude of the flow parameter. Despite the good agreement in terms of the position in

the wake, $\approx 1.2D$, where the peak in Reynolds stress is found for all cases, the peak value of each case needs a closer look. Consider where $x \leq 2D$, results obtained from the only conventional mesh case shown, NO-SAG-5 has given the largest deviation from the reference. From this, it should be expected that with higher mesh resolution taking place close to the vicinity of the cylinder surface, the Reynolds stress would as a result be increasing. Observation taken at all the SAG cases, however, reveals an opposite trend. The further decrease in the mesh density as C^* increases has led to a falling trend in result quality. For the case of SAG with $C^* = 3$ nevertheless, the relatively satisfactory agreement can be found. The Figure 5-39 could be a good demonstration of the crucial role played by the model part of LES, where the finest mesh does not provide better results, assuming that the numerical one is sufficiently minimized. Further downstream, all the cases are seen to have the same level of discrepancy from the reference. This indicates that higher mesh resolution given in the SAG cases does not improve the results downstream either.

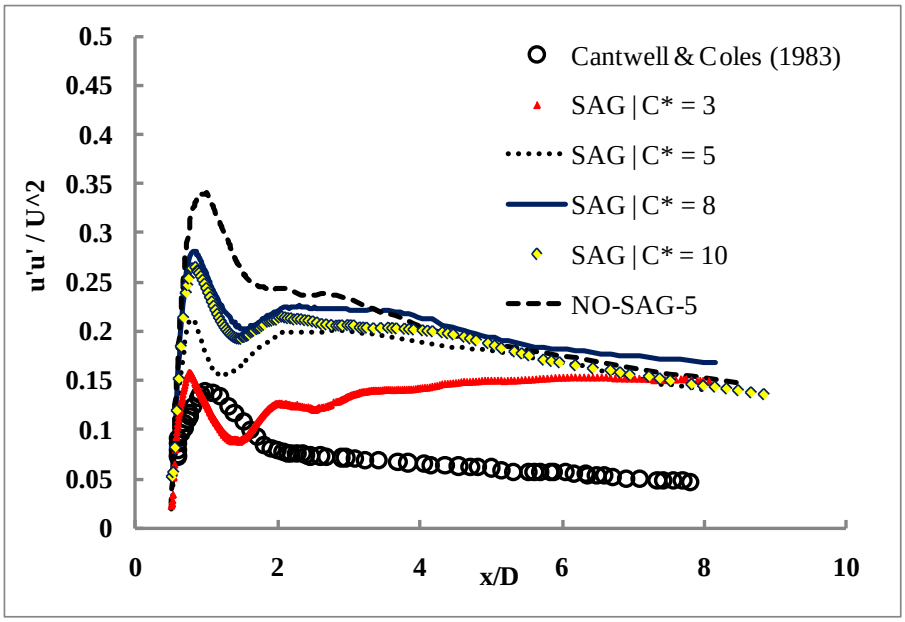

Figure 5-39 Time-averaged Reynolds stress $\mathrm{u'u'}$ along the centreline of the cylinder for selected cases both those from conventional mesh and those from SAG study.

The normalised cross-stream Reynolds stress $v'v'/U^2$ along the centreline, as shown in Figure 5-40, shows different aspects of prediction quality behaviour. While the magnitudes of the peak points are in fairly good agreement, they take place in slightly different regions. For both chosen SAG cases, the values reach the peak points at approximately $x = D$, which is roughly a cylinder diameter away from that of the experiment. The result in the NO-SAG-5 case provides a closer peak point to the experimental work. Similar figures can also be seen for the resolved shear stress, $u'v'$, shown in Figure 5-41.

The numerical results for the second moment of flow statistics, i.e. the Reynolds stress components, have shown a dramatically over-predicted trend compared to the experiments. It has to be mentioned, nevertheless, that this is not out of ordinary when taking into account the findings obtained from alternative numerical works, for example, that of Breuer (2000) where error reached 100% (over-predicted). It has gradually been known that it is extremely difficult to accurately predicts these stresses. The same also goes to simulations of another most widely studies subcritical regime circular cylinder flow at $\mathrm{Re} = 3{,}900$, as can also be seen in Franke & Frank (2002).

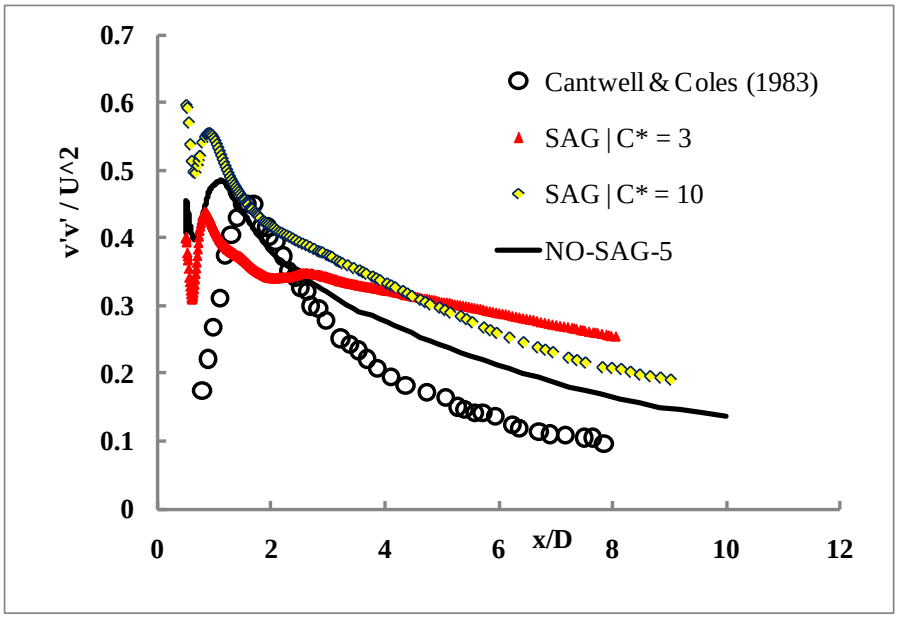

Figure 5-40 Time-averaged cross-stream Reynolds stress $v'v'$ along the centreline of the cylinder for selected cases both those from conventional mesh and those from SAG study.

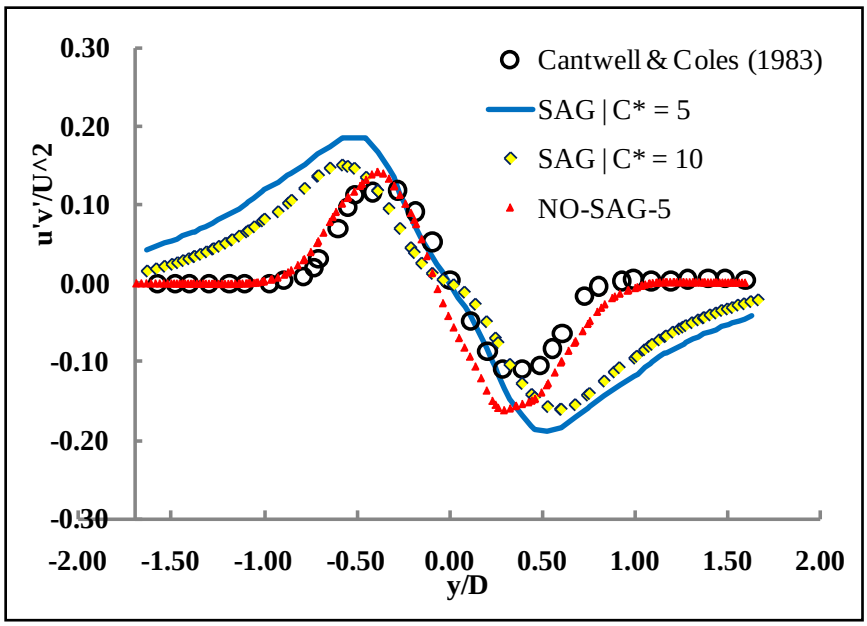

Figure 5-41 Time-averaged shear stress $u'v'$ along the vertical line $x = D$ of the cylinder for selected cases both those from conventional mesh and those from SAG study.

It can be noticed in the case of the shear stress, as predicted in Figure 5-41, which can be attributed to the over-predicted of the normal shear stress components, that not only do the predictions give higher peak values but also indicate a comparatively wider wake width. This contradicts the results of the predictions for the critical parameters as previously discussed. It then indicates that there is a mechanism driving and expanding the wake as soon as the primary vortex begins to form at about one circular diameter downstream. These over-predicted shear stresses for all SAG cases are also in contrast with the finding of With *et al.* (2003) where they concluded that the stresses increase with the increase of mesh resolution in the shear layers. With comparatively coarse mesh as seen in all the SAG cases nevertheless, this does not seem to be the case. This behaviour of the results probably implies effects on the numerical side. The interaction between the modelling error, arising from an excessively large subgrid length scale, and the truncation error, arising with coarse mesh, can well result in unexpected outcome.

From this aspect, with the mesh getting coarser, the turbulent viscosity would theoretically increase and more turbulent level would hence be compressed. However, one must not forget that the dissipation of the energy from this mechanism of turbulent viscosity can theoretically only take place in three dimensions. Therefore, it is also another

plausible conjecture that the absence of the third dimension, as in this work, results in the energy being transferred back to the mean flow and hence higher turbulent level would then be expected, as also conjectured in With *et al.* (2003).

To fully understand this interesting behaviour and to be able to pin point what exactly causes this requires a significant amount of work to cover all aspects that potentially affect the results. This is beyond the scope of this work but might well be, nevertheless, worthwhile subjecting to further investigation. Moreover, distinctions and contradictions in some certain aspects of numerical study of this flow problem can still be found in literature making drawing universal conclusion practically impossible.

- **Computational time efficiency**

It is one of the wide objective of this study to investigate the efficiency of the propose grid refinement algorithm in term of computational CPU time. Table 5-5 gives both the total number of grid cells generated after applying SAG and the CPU time in hours spent on each simulation. The measurement took place on a stand-alone computer with 2.66 GHz and 4 GB of RAM. The CPU time is shown in the total number required in order to complete a simulation. According to the flow prediction previously discussed together with the time consuming aspect, the application of SAG with $C^* = 8$ has shown the best result. Unlike in the case of turbulence plane jet, no obvious advantages can be observed with the use of SAG.

Table 5-5 CPU time in hours needed for running each simulation (run on an Intel(R) Xeon(R) computer with 2.66 GHz and 4 GB of RAM) as well as the final number of computational cells; the time measurement takes place from the start of each calculation to the end.

Case	**Final number of cells** [***initial mesh: 15,380cells***]	**CPU time** [***hours***]
$C^* = 3$	144,539	216
$C^* = 5$	74,666	154
$C^* = 8$	47,066	113

$C^* = 10$	34,052	97
NO-SAG-4	88,247	178
NO-SAG-5	65,207	135

5.2.5 Conclusions for circular cylinder case

The proposed SAG algorithm details provided in Chapter 4 was tested out with a circular cylinder flow at Reynolds number of 140,000. The results then were validated against experimental data. The existence of the wall region as well as the presence of the dominant non-zero velocity field makes this flow type a challenging test case. Six simulations were carried out and the main conclusions can be drawn as follows;

- The mesh distribution and refinement in the supposingly critically regions, i.e. the boundary layer as well as shear layer is shown not to be sensitive to the proposed algorithm. More mesh density takes place in flow downstream towards the outflow boundary.
- By varying the refinement constant C^*, it can be noticed that the monotone tendency in flow predictions, particularly for the critical ones, is obtained. This can be considered an advantage in observing different result behaviour and tendency correspondingly to the change of mesh density.
- The mean flow parameters predictions fall into a fairly acceptable range of agreement with the experimental work, despite the comparatively insufficiency in mesh density in the vicinity of the wall as well as in the wake near field.
- The insufficient mesh density around the cylinder surface as well as in the shear layer regions as found in all the SGS cases causes a significant low level of turbulent activity. As a consequence, the turbulent small vortices are not being picked up by the mesh leading to the delay of the occurrence of the pressure gradient and hence to the increase of the separation angle. This confirms the

sensitivity to the resolution around these critical regions of the body force prediction.

- Overall figure of mesh distribution obtained from all the SGS cases has shown strong discrepancy in the location where high level of mesh adaptation and the areas where strong turbulent activity and vortices with different sizes would be expected. This can be explained as a result of the proposed formulation of the locally estimated Taylor scale.
- Despite the potentially miscalculated local Taylor scale, and purely based on the results obtained, it is observed that the two sources of error show a high possibility of having the same trend of magnitude; amplifying each other rather than canceling each other when the mesh is getting coarsened.
- Previously seen in the case of free plane jet, as well as the literature for this case, the case of finer mesh not providing more satisfactory results can still be found.
- The computational CPU time required for all simulations with SAG is not outstandingly different from the conventional fixed mesh cases. This is due to the unnecessarily excessive mesh adaptation taking place further downstream with the change of C^*.

CHAPTER 6 DISCUSSION

6.1 LAMINAR FLOWS SIMULATIONS

It is one of the wide objectives of this work to demonstrate the advantages one can achieve with the use of solution adaptive grid for flows at low Reynolds number.

The present study shows that SAG can be successfully used for some classes of low Reynolds number flows. The first two cases are based on flow in pipes which are dominated by a balance between pressure gradient and viscous losses. In such cases it is found that the use of velocity gradient or pressure gradient gives acceptable results. When the flow is fully developed, the velocity curvature is constant and does not yield any differentiation in grid density when used as grid refinement variable. The effect of initial grid dimension is also seen to be small, but it may be useful to test this finding for a wider range of grid dimensions. The final grid sizes for SAG based computations are seen to be of the order of three times smaller than the fixed mesh computations achieving results of similar agreement with experimental or analytical values. In the cavity, the effect of the refinement variable on computational results is also found to be small. In this case the difference in resulting mesh size between the SAG based and fixed mesh computation is of the order of ten. This is likely to be due to the concentration of flow activity in the vicinity of the moving plate, thus leaving most of the cavity with regions of near stagnant flow. Nevertheless, the important vortex regions are still picked up by the SAG simulation.

It can be seen that for laminar flow simulations, choosing flow parameters to be the refinement variable is not complicated. Velocity and pressure are good candidates as shown in the results. It has to be mentioned also that the error indicators chosen in this study; the first and second gradient, do not show any distinctions in the result either. The sensitivity of mesh adaptation for some cases still show some shortcoming in picking up and representing some flow phenomena at certain regions as previously discussed.

Parameters selected to test out in this laminar cases show no significant differences. This can be the result of the nature of the governing equations where the level of truncation error play the major part in determining the results and this error can effectively be reduced with mesh refinement. Based on first and second gradient it can then be clearly seen that SAG can be successfully employed for differing low Reynolds number flows with success in reducing computer time and mesh sizes.

6.2 TURBULENT FLOWS SIMULATIONS

6.2.1 Final mesh distributions and their local corresponding scales estimation

The algorithm has shown differences in final mesh redistribution when applied at the flows chosen. Mesh density varies with the change of the refinement variable C^*. Despite the satisfaction obtained for numerical predictions of most for the flow parameters as shown in Chapter 5, it is still of great interest to question how well the primary objective of the algorithm has been met in terms of local scale estimation. To assess this aspect of the algorithm, it is then important to take a closer look at the mesh behaviour taking place locally and its correspondingly analytical estimation supported from literature available.

- **Turbulence plane jet**

An analytical work on turbulence local scale for mixing shear layer and plane jet flow is well documented by Tennekes & Lumley (1972). In their work they have estimated the local scales by monitoring the order of magnitude of the convection term and viscous term in the governing equations. They concluded that the local ratio between the inertial and viscous force increase with an increase of the distance downstream of the jet, L_J, see Figure 6-1, indicating a decrease in the corresponding local Taylor scale λ_x. Nevertheless, it has to be stated that this conclusion is to be valid only under two strong conditions; the flow has to have sufficiently high Reynolds number and $\frac{\delta_2}{L_J} \ll 1$. Based on this, when related to this study of SAG, it can then be conceived that with an increase in the refinement variable the flow downstream is more likely for the mesh to remain

relatively fine when compared to the potential core region and upstream. This explanation seems to contradict to the mesh behaviour obtained in this work. To explain this discrepancy, several facts concerning the refinement variable have to be taken into consideration. To do this, the computational domain used in this investigation is now divided into two main regions; **R-I** covering from the jet inlet to the end of the potential core, **R-II** covering from this point to the end of the computational domain, 40 jet slot-widths and illustrated in Figure 6-1..

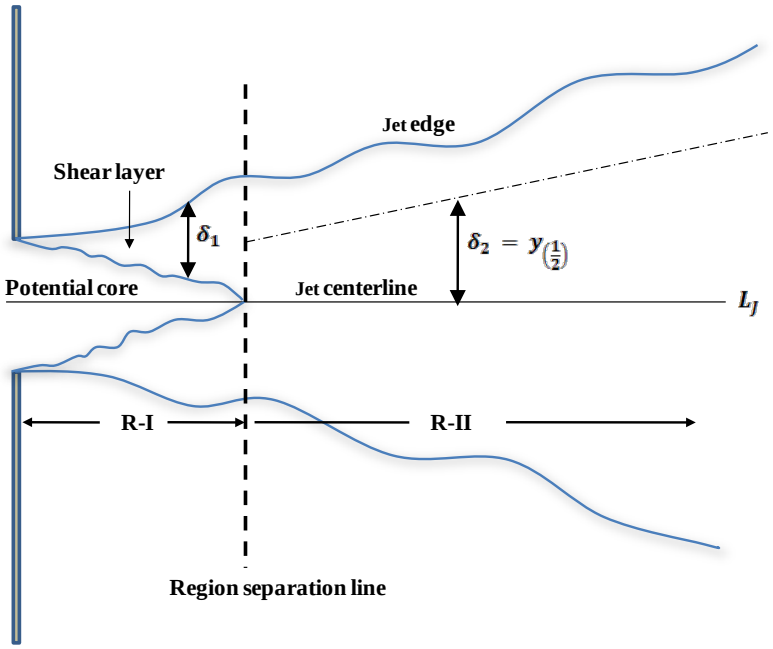

Figure 6-1 Schematic of a turbulent plane jet in two dimensions.

Firstly, the local Taylor scale used in this work is estimated following the work done for turbulent round jet of Dimotakis (2005). The exact form of this estimation documented in this reference work, is based on and for the jet parameters far field (no definite distance specified) i.e. **R-II.** For the near field including the region **R-I**, nevertheless, no information is provided. For this far field region, there are differences in defining the two local parameters; δ_x and U_x. Even though this work and the reference have the same local length scale, which is the jet half width $y_{(\frac{1}{2})}$, the one used in this work is defined beforehand using the rough estimation provided by a $k-\varepsilon$ turbulence and is kept fixed during a computational process. Another difference is the local velocity U_x. The

original form defines this value as the one on the jet centreline whereas this work used the cell-centre value for each control volume and therefore, provides distinct values for each vertical cross section. Consequently, it is not entirely certain if the jet downstream should really be expected to behave similarly in both studies.

Secondly, in the region **R-I** the ideal local characteristic length scale is the mixing layer width δ_1, according to Tennekes and Lumley (1972), but the value used in this work is still the estimated jet half width. Based on the mesh distribution in this area nevertheless, the consequence of this difference seems insignificant.

Last but not least are the conditions strongly required to support the analytical work of Tennekes and Lumley (1972), as stated previously. However, no specific values are quoted. Consequently, the Reynolds number of 4,000 and the size of computational domain of $40D$ as used in this work are in doubt to satisfy the conditions.

With all these in mind, the slight discrepancy in the final mesh distribution generated by the SAG algorithm and the analysis of fully-developed turbulence plane jet could be acceptable.

- **Turbulence circular cylinder flow**

Unlike the application with free plane jet, to the best of author's knowledge and at the date of this investigation, there had not been any analytical work done on local turbulence scale of this kind of flow. The reason for this is possibly the complexity of the flow that consists of distinct flow activities; laminar boundary layer, shear layer, near field wake as well as far-field wake, see Figure 6-2. The judgment on mesh distribution is then to be made in this section purely based on the actual local dominant flow mechanism. To do this, several regions revealed in a typical flow pass a stationary circular cylinder at the Reynolds number of 1.4×10^5 are divided including; the laminar boundary layer, the top and bottom shear layers, wake near-field region including the recirculation region (L_r) and wake far-field. Figure 6-2 depicts all the regions with L_r being the recirculation region length and δ_x the local characteristic length scale which is the wake width in this case.

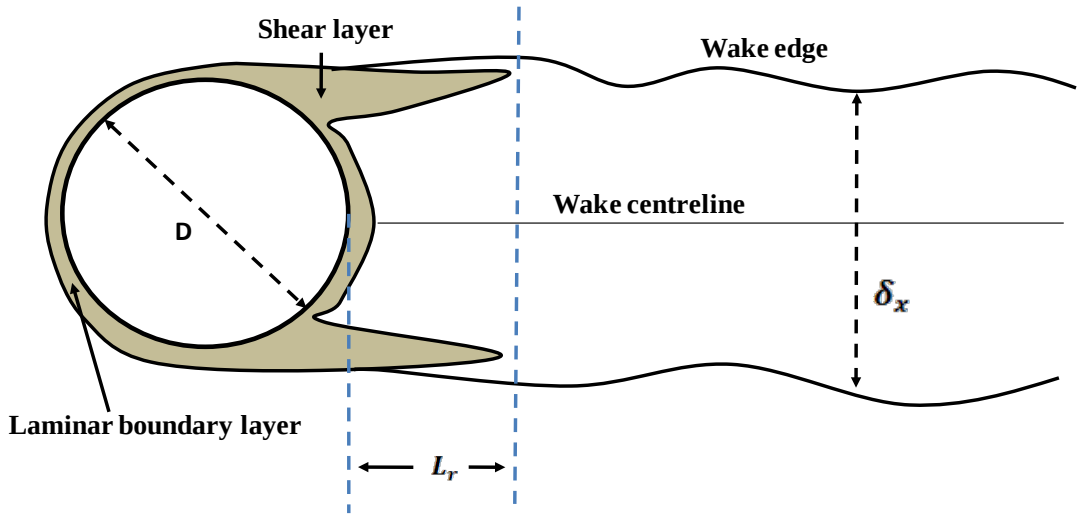

Figure 6-2 Schematic of a turbulent flow pass circular cylinder in two dimensions.

The rapid change in velocity, i.e. high gradient, towards the solid wall to satisfy the no-slip condition in the boundary layer requires a certain level of mesh refinement. The laminar mode also distinguishes itself from other regions when it comes to local turbulence scale estimation. Instead, the boundary thickness with the size proportional to $1/\sqrt{Re}$ would be more appropriate. The mesh distributions obtained from all the SAG cases have shown strong weakness of the algorithm for this layer. The slight mesh refinement that takes place in the front, top and bottom of the cylinder, obtained in the case with $C^* = 3$, is a result of the velocity difference, local one being deducted with the inlet one as by the definition of the refinement variable, equation (4.6). Nevertheless, based on the results obtained from this case, it indicates a lack of improvement. Together with the results from the fixed mesh, this then suggests a strong requirement for proper mesh treatment not only in this region itself but also the shear layer where the transition to turbulence takes place.

Recommendation made by With et al. (2003), apart from sufficient care needed for laminar boundary layer treatment, concerns layer where high rate of strain is maintained and the region of transition to turbulence. The consequence of the velocity component deduction (reduction) of the algorithm has once again revealed limitations in mesh refinement. The local Reynolds number would be expected to rise if high mesh density is

to take place based on the refinement variable formation, equation (4.6). For this regard, since the formation fixes the local length scale δ to the cylinder diameter D (Table 4-1) and the velocity scale is low in magnitude, the calculated Reynolds number is not sufficiently high to force the algorithm to refine the mesh. This suggests once again that this region should not be driven with the proposed refinement variable formation but instead an extra criterion should be introduced.

Towards the rear of the cylinder, the recirculation region and the wake near field (up to approximately $x = 2D$), only the mesh refinement in the case of $C^* = 3$ and 5 that a level of refinement of approximately two can be seen (n level of refinement, Figure 2-5, can increase the number of cells by the factor of 2^{2n} in 2D domain). The transition to turbulence of the flow that takes place in the shear layers generates secondary vortices before moving evolving into primary vortices in the recirculation region. This implies that a constantly increase in velocity fluctuations would be expected to take place and so would the kinetic energy suggesting a requirement for sufficiently high mesh density. Although the mesh refinement activity that is obtained from the smallest C^* might seem corresponding well with this requirement, the final result quality does not show any obvious superiority over the other cases. An explanation for this is the flow resolution in the laminar boundary layer as well as the shear layers, which have not been properly resolved, that strongly influence the downstream flow mechanism.

Experimentally, in this near field region, the mean streamwise velocity component is expected to remain negative with small magnitude when compared to the flow far-field. This should also indicate small local Reynolds number. However, without any obvious determination for the local length scale, it is difficult to measure the change in local Reynolds number and hence the local Taylor scale.

For the mesh refinement further downstream, $x > 2D$, a gradual increase in mesh density proportionally with the distance x is found for all the SAG cases despite the reduction of local velocity. This figure is a result of the increase in local mean velocity as obtained from this work and confirmed experimentally by the references. Consequently, an increase in high Reynolds number would also be expected and hence decrease in local Taylor scale. The excessively high mesh refinement that takes place in this region gives

rise to excessive turbulent intensity as shown in Figure 5-39 and Figure 5-40 when compared with the experimental data. The small magnitude of the turbulent viscosity generated by the Smagorinsky subgrid scale model does not seem to dissipate the amount of energy with this fine mesh. It then prompts a question whether or not the definition of local Reynolds number based on the local mean velocity, if the length scale is to be kept constant as the diameter D, is adequate to represent the smallest isotropic turbulence scale when used in conjunction with the Smagorinsky SGS model. This is well worth further investigation.

In summary, suggestions made by several numerical works found in literature on local meshing for stationary circular cylinder with smooth surface flow over a wide range of Reynolds numbers have pointed to the same direction. The first critical area that requires proper treatment is the near wall region where the boundary layer is present. Next to this is the shear layer in which its length and thickness depends heavily on the Reynolds number and also the resolution quality established in the upstream boundary layer. Another area is the recirculation region including wake near-field. This is also of great importance to preserve and maintain the formation of vortex street from the shear layers. The turbulent activity and the existence of small scales turbulence (and their locations) downstream beyond this point are still under debate (see Kravchenko & Moin 2000, Beaudan & Moin 1994). It can then be concluded that despite the overall acceptable solutions, the attempt to generalise the algorithm originally designed for free shear layer flows in this work is not capable of satisfying mesh requirement for all the regions occurring in a flow with boundary layer separation. For this to be fulfilled, extra intrusions into the main built-in mesh refinement structure provided by the software have to be made and without a proper level of access, this cannot be done and remains the case in this work.

6.2.2 Inadequate mesh distribution and software access limitations

Presented by the results from both cases, the importance of the local estimation form of the Taylor scale in which the mesh adaptation is taking place based upon is confirmed. While there is only a slight discrepancy between the actual estimated local Taylor scale and one actually adopted in the simulation of plan jet, a severe consequence

is clearly seen in the case of circular cylinder where mesh adaptation takes place in the wrong region. This is all subject to two factors; the limitation in capability of manipulating and implementing the software within a commercial code and the lack of analytical work on local turbulence scale for the flow pass circular cylinder case.

- **Limited access to software program structure**

In the case of the plane jet, the estimation of the local Taylor scale is adopted from Dimotakis (2005). The work provides details of each parameter contained in the approximation form. Nevertheless, small modification took place in which one necessary criterion had to be left out. In the Taylor scale equation used in this case, it is the mean velocity on the centreline that was supposed to be adopted for each cross section $x = constant$. The problem kicked in where it was not possible to specify the certain location of the cell volume in each cross section and for this the mean velocity of each cell volume was used instead (details provided in the previous section). Observing from the mesh redistribution after applying SAG, however, no serious damage is found. The mesh still behaves in a reasonable manner and as a result, good solution has been achieved where another story is found for the case of circular cylinder.

For the case of circular cylinder simulation, it was initially to be the exact same form previously used for the plane jet before the existence of the non-zero field of this case was identified. It can be easily seen that the characteristic velocity which was chosen to be the mean velocity $\langle U \rangle$ leads to high local Reynolds number nearly everywhere in the whole domain. As a result, based on the same refinement criteria the mesh adaptation will take place equally everywhere which is obviously not desirable.

There were initially two solutions for this undesired mesh behaviour. The first remedy was to insert a criterion designed separately at the beginning of the algorithm to decide roughly the regions to be or not to be subject to mesh refinement activity. A simple form of velocity gradient in either time or space would have been sufficient for this task. Unfortunately, no attempt was successful as long as it involved interfering with the main mesh refinement structure already built-in. As a result, an alternative means to do the same task had to be taken into consideration but it also has to be embedded in the main algorithm. For this, in order to prevent the mesh from taking place in the regions where it

should not as much as possible, a deduction in local velocity; the value of the inlet from the mean local one velocity, $|\langle U\rangle - U_{inlet}|$ was implemented. With this in mind, it is assumed that there is no significant difference between the mean value and the inlet on in those areas with virtually no turbulence. Even though it was a success by doing this, one must not forget that for the regions where mesh adaptation is still expected to occur, it is now only part or the remaining part of the deduction that is used to calculate the local Taylor scale and severe consequence can be clearly seen.

- **Insufficient support of analytical work**

An insufficient amount of work dedicated to analytically investigating the changing of turbulence scales locally is highly believed to make a substantial effect on the results. As discussed previously, it is indicated that although no analytical work has been available, it is still possible to remedy this by designing a separate criterion for each flow region according to the local flow dominant activity but it has not been possible either. Therefore, as far as the estimation of the Taylor scale is concerned for this case, it is still difficult to expect any improvement in the resolution.

Up until now, one might be able to question that if the estimation form of the Taylor scale is as important for different kinds of flow then why not pay more attention to its exact form instead. The ratio between two of the time-averaged second order parameters; the velocity fluctuation ($\langle u'^2\rangle$) and its space derivative ($\langle(\frac{\partial u'}{\partial x})^2\rangle$), following equation (2.9), then comes up in mind. To do this nevertheless, several difficulties then arise;

- It is unfortunate that the solver used, Fluent 6.2.26, in this work only provides the mean velocity fluctuation $\langle u'^2\rangle$ but does not directly provide the calculation of it mean space gradient and nor their ratio. Therefore to achieve this, a more sophisticated additional code or routine has to be separately programmed and introduced to the system.
- To satisfy the convergence criteria of the exact formulation, a simulation needs to be run with a sufficiently long period of time otherwise it might easily lead to a mathematically incorrect meaning.

- Too coarse initial mesh, as used in this case for instance, may fail to establish a reasonable calculated Taylor scale field since the precise form involves gradients and hence requiring sufficiently fine mesh.

Despite all these mentioned above, it is still of great interest and worth subjecting to further investigation.

In summary, although the main task in this work was greatly influenced by the two factors; the lack of estimated form of Taylor scale and the limitation to the software access, reasonably good results can still be obtained particularly for the time-averaged flow parameters. For this particular case of circular cylinder, with an observation of the result obtained from the conventional mesh (in which higher mesh density taking place in the adjacent to the wall as well as the region where the shear layers take place and the beginning of the wake), it is then reasonable to expect better results also from the SAG application but with the same level of mesh density at those regions mentioned. This can well lead to another improvement possibly introduced to the algorithm in order to enhance the methodology which is the treatment of the region near walls.

6.2.3 The algorithm and its overall flow prediction capability

From the application of the proposed SAG algorithm to the simulations of a plane jet, it has been proven that the algorithm is capable of providing reasonably good results. Most time-averaged flow predictions are found to be in an excellent agreement with the experimental ones. Nevertheless, with the mesh changing around the mixing layer regions when changing the refinement constant, C^*, this has some effect on the onset of the small vortices triggered by the mesh. The most visible figure regarding this is the delay in the turbulent instability appearing further away from the jet orifice. This prolongs the potential core region with the increase of C^* but not by much and this gives virtually no significant influence to other flow parameter predictions.

In terms of the number of grid points generated as a result of the SAG application, it is evident that because the mesh is subject to refinement only where necessary, a maximum of approximately 90% in mesh size reduction is revealed when compared with

the conventional fixed mesh. This can be seen as a great achievement from using the SAG algorithm and it is clearly superior over the fixed mesh.

Application with the flow with separations and solid wall reveal a slight but important difference in the flow prediction quality. Even though the results obtained from all the cases are seen in fairly good agreement with the experimental ones, as far as the limitations in the 2D simplification and zero level turbulent inlet velocity are concerned, noticeable remarks in the incorrect mesh adaptation deserve closer attentions.

It is revealed from all the simulations with SAG that the relatively high discrepancy in the separation angle θ_s is mostly noticeable. While the other flow parameter predictions are acceptable, it is this parameter that is the main key in the validation of near-wall modelling. Obviously, the most relevant parameter to this one is the pressure distribution. With the results obtained in this work, the main factor that plays a crucial role is the mesh refinement along the boundary layer as well as the shear layer where high rate of strain occurs.

It is shown that in the Smagorinsky SGS model, the modelling of the small scales turbulence is a function of the strain rate and the filter width, or grid spacing in this context of finite volume discretisation. It has to be noted also that the strain rate itself is calculated from the resolved field meaning that grid spacing has once again a crucial role to play. With the existence of high velocity gradient takes place close to the surface and its conjoin with the presence of pressure adverse gradient small turbulent vortices are generated. With the insufficient fine mesh, both the mixing length scale $C_s\Delta$ and the strain rate are poorly modelled to represent the actual turbulent mechanism. In other words, small scale instabilities are poorly captured, returning inadequate results back to the resolved field. Alternatively, it could also be seen as that with coarse mesh, the model dissipates energy at too low wave number on the energy spectrum where caution still need to be taken when it comes to Smagorinsky model. This however should not be seen as a drawback of the energy equilibrium assumption as made as the principle assumption of defining the refinement variable in this work. Instead, it should be put as a result of the imprecision of the refinement variable estimation itself where for this flow case a deep analysis is clearly needed.

From the numerical point of view concerning the use of relatively coarse mesh, one might argue that the numerical error could act as an additional subgrid scale and could have positive contributions to modelling the small scale turbulent instabilities. Evidently however, the results suggest that the behaviour of the error caused by the numerical side has opposite effect trends. Judging from the poor predictions for parameter around the cylinder surface such as the separation angle and pressure distributions, it strongly suggests that no compensation is made from the numerical error effect. It can then be concluded that the coarse mesh does not take account of the complex physics in the shear layers which requires a high mesh resolution.

In terms of the total number of grid points produced from the use of SAG algorithm, it appears to be difficult to judge whether or not the algorithm is superior to the fixed mesh cases. The excessively unnecessary mesh adaptation that takes place further downstream has given the impression that the use of SAG actually results in comparatively worse outcome. As mentioned previously however, the main factor that determines the quality of the algorithm is actually to refinement estimation formulation that was actually the result of software access limitation. This is confirmed by all the positive aspects when applied with the plane jet where more precise form of refinement variable is available in the literature.

6.2.4 The Taylor scale formulation

As can be seen from the application of the proposed SAG algorithm to a plane jet as well as a circular cylinder, the key factor that determines the success of the algorithm is the local Taylor scale estimation formulation. Despite the occurrence of the unsatisfactory mesh adaptation capability near to the wall, some positive aspects of the algorithm should well be acknowledged as a success.

Referring back to the proposed form of the Taylor scale in which a time-averaged value of local velocity acts as the main parameter, $C^* \cdot \delta_x \left(\frac{\delta_x \left|\langle U_x \rangle - U_{dt}\right|}{\nu}\right)^{-\frac{1}{2}}$, below are benefits that can be obtained in general from defining refinement variable based on a mean value as well as the inclusion of the refinement constant C^*.

- **Less sensitivity to refinement frequency**

So far the proposed algorithm has been proven not to require any error indication/estimation means, refinement normalization methods, smaller mesh size bounds which it is very often the case for normal h-refinement strategy. Nevertheless, there is one aspect concerning general mesh refinement methodology which is to answer the question how often should the mesh be adapted during the calculation process. This has, so far, not been mentioned in this work.

Regarding the refinement frequency, it should ideally adapt itself at the end of every single time step. Unfortunately, one must not forget that by doing this a tremendous computational effort is unavoidably needed. This is because every time a mesh adaptation takes place it means that a process of calculating the refinement variable, storing values, modifying the mesh accordingly and interpolating value between the old and new mesh also take place as well. Therefore, having the mesh to adapt too frequently is not really desirable as such, at least from the computational CPU and time consuming point of view. On the other hand, having two mesh adaptation processes taking place too far from one another can result in missing out some important flow motions that take place in between. A compromise between these two features of mesh refinement can be made with the use of statistical mean of flow parameter as the refinement variable. This is the case in this work.

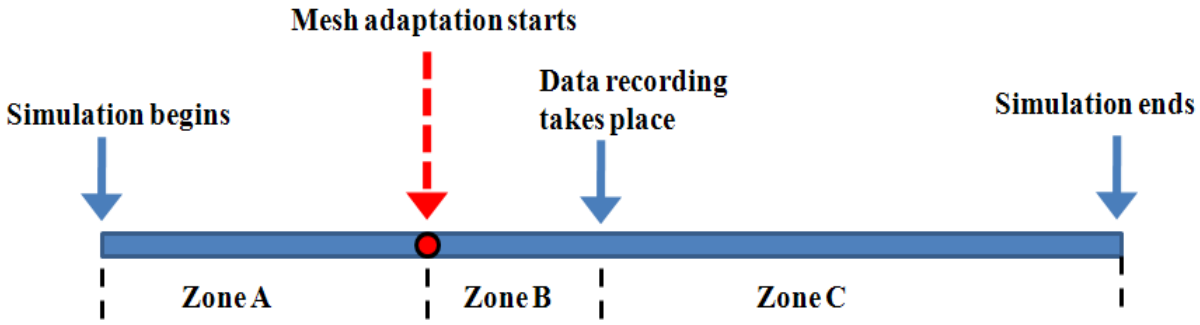

Figure 6-3 Simulation processing time when applied with mesh refinement.

The mean velocity $\langle U \rangle$ has been included in the formulation of the refinement variable not only to maintain the statistical meaning of the Taylor scale but also specifically to reduce the dependence on the refinement frequency. Figure 6-3 depicts a typical diagram of a simulation processing when used in conjunction with the solution

adaptive grid algorithm. The processing time period is divided into three zones namely **Zone A**, **Zone B** and **Zone C**. **Zone A** is the length of time needed for the simulation to establish a proper and reasonably flow field parameters to be used as an initial guess for refinement variable calculation. It is needed also for the simulation to be independent of the transient nature of the numerical scheme. **Zone B** is the length of time required between applying the mesh adaptation algorithm to the flow field and when the data collection begins to take place for statistical analysis. **Zone C** represents the total amount of simulation time required for the data collection to converge.

It can be seen then that if we allow **Zone B** to be sufficiently long, the refinement variable calculated based on a mean value will become less and less sensitive to the instantaneous change of the flow parameter as the calculation time progresses. As a result, when the data recording takes place the flow can be expected to have established a sufficiently good flow prediction and hence more accurate data can be expected. Furthermore, once the simulation progresses into **Zone C**, here is where the mean value becomes more and more stable and refinement frequency has less effect on the mesh changing behaviour. In other words, it is less sensitive and hence less effected by the refinement frequency and any small changes have negligible effect of the results as a whole. To confirm this, two extra simulations were also carried out with two different refinement frequencies; one with 20 time steps and the other one with 100 time steps. The results (not shown in this work) reveal virtually no differences in most flow parameter calculations whereas a noticeable reduction in CPU time is found. Nevertheless, it could well be worth investigating in more details since less mesh refinement frequency means less computational effort and time requirement. This promising figure can make a lot of difference particularly when it comes to industrial applications.

- **More control in mesh distribution**

Serving as one of the main concepts of this work is an attempt to close the LES system in a physical meaning by linking the filter width to a real physical turbulence scale. The Taylor scale is chosen to represent the turbulence scale and the grid spacing is used as the filter width.

Provided that the estimated formulation of the local Taylor scale is available, the presence of C^* allows one to be in more control of defining the smallest isotropic scale to be resolved by the mesh. This process is done simply by varying the constant and observe trend of the solution quality. Moreover, under the implicit LES context, the interaction between the numerical error and modelling error is nearly practically impossible for flow with complex geometry. By varying C^* and therefore the mesh size, it can be estimated that the turbulence scale can effectively be vary along the inertial subrange. This also provides an alternative way to observe the changing in magnitude of the total summation of both error types. This could lead to a more easily and effective way to improve the result accuracy of LES with implicit filtering, instead of attempting to measure the magnitude of each error separately in which mathematical complexity becomes inevitable as pointed out by Christopher (1999).

Nevertheless, by varying the refinement constant and monitoring the result may be time consuming. The choice of this parameter varies from literature to literature. Dimotakis (2005) gives a determination of this constant for a round jet of 2.3, whereas Pope (2000) gives a value of $\sqrt{10}$ for an ideal isotropic and homogeneous turbulence. At the same time Tennekes & Lumley (1972) estimate this value of $\sqrt{\left(\frac{15}{A}\right)}$, with A being a constant with an order of magnitude of one. Obviously, a number of factors will have to be taken into consideration for more precise estimations of this value that can be applied to different kinds of turbulence studies. Therefore, more work on this issue to narrow the range of its values could well be meaningful.

6.2.5 General limitations of the algorithm

- Since the algorithm is designed predominately based on the property of the Smagorinsky SGS model, any type of turbulence problem that this SGS model is still seen to have a lack of success with would also impact the success of the algorithm. Some obvious situations are flows near wall and/or with strong anisotropic phenomena, flows involving stratification and/or rotational effects, flows including strong compressibility like shock waves and so on. Nevertheless,

as long as the Smagorinsky model is acceptable to be applicable, the algorithm shall also be applicable.

- The algorithm still relies heavily on support from literature to define the local parameters involved; characteristic velocity and length scale, as long as the lack of access to the software persists.
- Due to the wide range in potential values for the refinement variable C^*, the process of finding the most appropriate value for a given application may become time consuming. This limitation hints towards the need to perform further analytical studies in order to help reduce the range in the potential values of C^*.

CHAPTER 7 CONCLUSIONS AND RECOMMENDATIONS

In this work, investigations on the use of solution adaptive grid SAG methodology for several incompressible flows were conducted. The journey began with applications on laminar flows where three of the most common studies were chosen; circular pipe flow, sudden-expansion flow and lid-driven cavity flow. The construction of the refinement variable for laminar flows study is based upon the first and second order gradient of some selected flow parameters. From these laminar cases, it has been demonstrated the general requirements for typical h-refinement strategy type.

The investigation then addressed the difficulties and issues normally encountered with simulations of turbulence under the context or large eddy simulation as well as the methodology of SAG itself. Here is where an attempt to build a new solution adaptive grid to alleviate problems from both LES fundamental and SAG methodology is made. This task, due to the combined complexity of flow structure, the core model of LES simulation, and the design of a refinement variable is not as straightforward as expected. The construction of the proposed algorithm started out with an attempt to physically close the LES system has been made with the use of solution adaptive grid. Combined with a Taylor scale, the concept is based upon the balance of energy production and dissipation which can be represented by a turbulence scale known as the Taylor scale. The SAG algorithm was tested on two two-dimensional, well documented, turbulent test cases.

From the investigations carried out in this work on both laminar and turbulent cases, several important conclusions can be drawn as follows;

- For laminar flow study, it is found that designing a proper match between an error indicator and its according refinement variable is comparatively straight-forward. The results show that the flow prediction is sensitive to both gradient and curvature of velocity and pressure.

- The use of solution adaptive grid is seen to be a very convenient and reliable tool for the selected laminar cases. With a good combination between error indicator and refinement variable, a satisfactory flow prediction can be expected with significantly less effort in computational demands.
- As the beginning of Chapter 4, literature survey has revealed that current solution adaptive grid algorithms have usually their own negative features resulting in high level of doubt and skepticism. The new h-refinement algorithm for turbulence simulation proposed in this work is proven to effectively alleviate those undesired aspects while reasonably good results can still be achieved.
- It can also be seen from the structure of the new refinement variable that the fundamental closure problem of large eddy simulation is now fulfilled. This is done by determining the choice of filter width (or grid spacing in this work) based on a physical turbulence scale.
- For the turbulent test cases, it is found that the key factor for ensuring success of the new algorithm is the accurate estimation of the local Taylor scale. The results obtained from plane jet simulations where the Taylor scale is available in the literature have shown a very promising aspect of the principal concept of the algorithm. In simulations of a circular cylinder flow on the other hand, due to the lack of analytical work on local scale estimation, some mesh mis-location is found.
- Limitations in access encountered with using commercial software is also shown to have a great influence in the access to implementing, manipulating or making modifications to the main built-in mesh refinement structure. This results in some compromises to be made including the impossibility of constructing the local Taylor scale from its exact definition when no estimated forms available i.e. for a circular cylinder flow.
- The proposed form of the refinement variable that consists of the velocity mean value, was found to provide some desirable byproduct. The presence of the mean value has caused the refinement variable to be less effected by instantaneous flow changing.

- The introduction of the refinement constant C^* has shown to allow one to be more in control in defining the smallest scale to be resolved by the mesh. This can be a very useful tool when dealing with higher Reynolds number flows where the inertial subrange is expanding proportionally to the increase of the Reynolds number and the task to define a minimum mesh size then becomes significantly difficult. Moreover, as far as the total entangled nature between the two types of error is concerned, varying C^* also provides an alternative way to observe the trend of their interaction.

Based upon the results obtained from both laminar case study as well as the turbulent, there are several aspects of solution adaptive grid methodology and large eddy simulation that deserve a closer look and are worth further investigation. Bearing in mind the restrictions caused by the software used, the following further work can be carried out.

- For laminar flows, even though it has been shown that flow parameters have a limited influence on the mesh processing activity, it is still worth testing out the effect of the initial mesh size in a wider range of flow parameters. In addition to this, more challenging laminar cases such as flow in a backward facing step, are also well worth further investigation.
- For turbulence study, a very simple coarse rectangular shape mesh was used and good results were obtained. Nevertheless, mesh with different shapes and sizes are also of great of interest. This is crucial particularly when dealing with flows with complex geometry for which rectangular mesh might no longer be suitable.
- Since it has proven that the algorithm capability is strongly determined by the Taylor scale estimation and that analytical works are available for free jets, it is then challenging to apply the same refinement criteria to other types of turbulent free jet such as round jet or rectangular jet, etc.
- Despite the 2-dimension simplification adopted in this work and all the encouraging results, full scale three dimensional simulations are still well worth further attention.

- With this SAG algorithm and its shortcoming in treating near wall region, it is then interesting to minimise this by paying attention to mesh adaptation criteria specifically for that region.
- A closer look at the Taylor scale estimation formulation is highly required for different flow phenomena.
- An extension of the SAG methodology to turbulence modelling in the RANS family is also interesting. Moreover, any commercial CFD software that provides grid adaptation feature can also be worth further investigations.

CHAPTER 8 REFERENCES

Achenbach E. (1968). "Distribution of local pressure and skin friction around a circular cylinder in crossflow up to Re = 5e+6." J. Fluid Mech. **34**(4): 625-639.

Achenbach E. (1971). "Influence of surface roughness of the cross-flow around a cicular cylinder." J. Fluid Mech. **46**: 321-335.

Ait-Ali-Yahia D., Baruzzi G., Habashi W.G., Fortin M., Dompierre J. Vallet M-G., (2002). "Anisotropic mesh adaptation: towards user independent, mesh-independent and solver-independent CFD solution: Part II: structured grids." Int. J. Numer. Meth. Fluids **39**: 657-674.

Ait-Ali-Yahia D., Habashi WG.,Tam A., Vallet M-G., Fortin M. (1996). "A directionally adaptive methodology using an edge-based error etimate on quadrilteral grids." Int. J. Numer. Meth. Fluids **23**: 673-690.

Alexander H, Michel V. (2005). "Adaptive mesh strategy applied to turbulent flows." C.R. Mecanique **333**: 103-110.

Anderson D.A. (1983). Adaptive grid methods for partial differential equations. New York, ASME Publication.

Baker T.J. (1997). "Mesh adaptation strategies for problems in fluid dynamics." Finite Elements Anal. Design **25**: 243.

Battagila F., Tavener S.J., Kulkarni A.K., Merkle C.L. (1997) "Bifurcation of low Reynolds number flows in symmetric channels" AIAA J., **35**:99-105.

Beaudan P. , Moin P. (1994). Numerical experiments on the flow ast a circular cylinder at sub-critical Reynolds number. Report No. TF-62. Department of Mechanical Engineering, Stanford University.

Bochev P., Liao G., dela Pena G., (1996). "Analysis and computation of adaptive moving grids by deformation." Numerical Methods for Partial Differential Equations **12**: 489-506.

Bogey C., Bailly C. (2006). "Large eddy simulation of transitional round jets : Influence of the Reynolds number on flow development and energy dissipation." Phys. Fluids **18**: 065101-1-14.

Boor C.d. (1974). Good approximation by splines with variable knots II. New York, Springer-Verlag.

Bouard R., Coutanceau M. (1980). "The early state of development of the wake behind and impulsively started cylinder for 40 <Re < 10^4." Journal of Fluid Mechanics **101**(3): 583-607.

Bova S.W., Carey G.F. (1992). "Mesh generation/refinement using fractal concepts and iterated function systems " Int. J. Numer. Meth. Engineering **33**: 287-305.

Brackbill J.U. (1993). "An adaptive grid with directional control." Journal of Computational Physics **108**: 38-50.

Breuer M. (1998). "Large eddy simulation of the subcritical flow past a circular cylinder: Numerical and modeling aspects." International journal for numerical methods in fluids **28**: 1281-1302.

Breuer M. (2000). "A challenging test case for large eddy simulations : high Reynolds number circular cylinder flow." International journal of heat and fluid **21**: 648-654.

Browne L.W.B., Antonia R.A., Rajagopalan S, Chambers A.J. (1983). Interaction region of a two-dimensional turbulent plane jet in still air. Structure of complex turbulent shear flows, IUTAM Symposium, Marseille.

Cantwell B., Coles D. (1983). "An experimental study of entrainment and transport in the turbulent near wake of a circular cylinder." Journal of Fluids Mechanics **139**: 321-374.

Cao W., Huang W., Russell R.D. (1999). "An r-adaptive finite element method based upon moving mesh PDEs." Journal of Computational Physics **149**: 221-244.

Cao W., Huang W., Russell R.D. (1999). "A study of monitor functions for two-dimensional adaptive mesh generation." SIAM J. Sci. Comput. **20**(6): 1978-1994.

Catherall D. (1991). "The adaption of structured grids to numerical solutions for transonic flow." Internat.J.Numer.Methods Engrg **32**: 921-937.

Celik I., Shaffer F.D. (1995). "Long time -averaged solutions of turbulent flow past a circular cylinder." Journal of wind engineeing and industrial aerodynamics **56**: 185-212.

Ceniceros H.D., Hou T.Y. (2001). "An efficient dynamically adaptive mesh for potentially singular solutions." Journal of Computational Physics **172**: 609-639.

Charles C.S.S, Mingshun Y. (1990). "Simulation of vortex shedding flow about a circular cylinder a high Reynolds numbers." Journal of Fluids Engineering **112**: 155-163.

Ghia K.N. , Shin C.T. (1982) "High-Re solutions for incompressible flow using the Navier-Stokes equations and a multi-grid method." J.Comp. Phys.**48:** 387-411.

Christopher JF. (1999). The issue of numerical uncertainty. Second international conference on CFD in the Minerals and Process industries, CSIRO, Melbourne, Australia.

Comte P., Lesieur M., Laroche H., Normannd X. (1989). Numerical simulations of turbulent plane shear layers. In Turbulent Shear Flows 6, Springer.

Sampaio P.A.B., Coutinho A.L.G.A. (2000). Simulating vortex shedding at high Reynolds numbers. the Tenth (2000) International Offshore and Polar Engineering Conference, Seattle, USA, The International Society of Offshore and Polar Engineers.

Dai Y., Kobayashi T., Taniguchi N. (1994). "Large eddy simulation of plane turbulent jet flow using a new outflow velocity boundary condition." JSME Intl J. B Fluids and Thermal Engng **37**: 242-253.

Darke R., Manoranjan V.S. (1996). "A method of dynamic mesh adaptation." Int. J. Numer. Meth. Engineering **39**: 939-949.

Delaunay B. (1934). "Sur la sphere vide." Bul. Acad. Sci. URSS, Class. Sci. Nat.: 793-800.

Demkowicz L., Oden J.T., Rachowicz W., Hardy O. (1991). "An h-p Taylor-Galerkin element method for compressible Euler equations." Comput. Methods Appl. Mech. Engrg **88**: 363-396.

Devloo P., Oden T., Tattani P., (1988). "An h-p adaptive finite element metod for the numerical simulation of comporessible flow." Comput. Methods Appl. Mech. Engrg **70**: 203-235.

Dietachmayer G.S., Droegemeier K.K. (1992). "Application of continuous dynamic grid adaptation techniques to meteorological modeling. Part I: Basic formulation and accuracy." Mon. Wea. Rev. **120**: 1675-1706.

Dimotakis P. E. (2005). "Turbulent Mixing." Ann. Rev. Fluid Mech. **37**: 329-356.

Dimotakis P.E., Miake-Lye R.C., Papantoniou D.A. (1983). "Structure and dynamics of round tubulent jets." Phy. Fluids **26**: 3185-92.

Dompierre J., Vallet M-G., Bourgault Y., Fortin M., Habashi WG. (2002). "Anisotropic mesh adaptation: towards user-independent, mesh-independent and solver-independent CFD solutions: Part III: unstructured meshes." Int. J. Numer. Meth. Fluids **39**: 675-702.

Durst F., Melling A., Whitelaw J.H. (1974) "Low Reynolds number flow over a plane symmetric sudden expansion" J.Fluid Mech.,**64**: 111-128.

Dvinsky A.S. (1991). "Adative grid generation from harmonic maps on Eiemannian manifolds." Journal of Computational Physics **95**: 221-244.

Dwer H.A., Kee R.J., Sanders B.R. (1980). "Adaptive grid method for problems in fluid mechanics and heat transfer." AIAA. **18**: 1205-1212.

Elhami A. A., Kazemzadeh S., Mashayek F. (2005). "Evaluation of a fourth-order finite-volume compact scheme for LES with explicit filtering." Numerical Heat Transfer **48**(Part B): 147-163.

Everitt K.W., Robins A.G. (1978). "The development and structure of turbulent plane jets." J. Fluid Mech. **88**: 563-583.

Fearn R.M., Mullin T., Cilffe K.A. (1990). "Nonlinear flow phenomena in a symmetric sudden expansion" Journal of Fluid Mechanics. **211**: 595-608.

Ferziger J.H., Peric M. (2002) Computational Methods for Fluid Dynamics. New York, Springer.

Fey U., Konin M., Eckelmann H. (1998). "A new Strouhal-Reynolds number relationship for the circular cylinder in the range $47 < Re < 2 \times 10^5$." Phys. Fluids **10**(7): 1547-1549.

Fiedler B. H., Trapp R.J. (1993). "A fast dynamic grid adaptation scheme for meteorological flows." Mon. Wea. Rev. **121**: 2879-2888.

Figueira S.L.F., Azevedo J.L.F., Korzenowski H (2000). "Unstructured adaptive grid flow simulations of inert and reactive gas mixtures." J. Comput. Phys. **160**: 522-540.

Fluent (2003):*Fluent 6.1 user's guide volume 3*.-Fluent Inc.

Fluent (2005):*Fluent 6.1 tutorial 1*.-Fluent Inc.

Franke J, Franke W. (2002). "Large eddy simulation of the flow past a circular cylinder at Re = 3900." Journal of wind engineeing and industrial aerodynamics **90**: 1191-1206.

Franke R., Rodi W., Schonung B. (1989). Analysis of experimental vortex shedding data with respect to turbulence modelling the 7th Turbulent Shear Flow Symposium, Stanford, USA.

Frey P., Alauzet F. (2005). "Anisotropic mesh adaptation for CFD computations." Comput. Methods Appl. Mech. Engrg **194**: 5068-5082.

Fox R. W., McDonald A.T. and Pritchard P.J. (2008) Introduction to Fluid Mechanics. Wiley.

Geurts B. J. (2004). Elements of direct and large-eddy simulation, Edwards.

Ghia K.N. and Shin C.T. (1982) "High-Re solutions for incompressible flow using the Navie-Stokes equations and a multi-grid method." J.Comp. Phys.**48**: 387-411.

Ghosal S. (1996). "An analysis of numerical errors in large -eddy simulations of turbulence." Journal of Computers and Fluids **125**: 187-206.

Gui W., Babuska I. (1986). "The h,p and hp Versions of the Finite Element Method in 1 dimension, Parts I, II, III." Numerische Mathematik **49**: 577-683.

Gutmark E., Wygnanski I. (1976). "The planar turbulent jet." J. Fluid Mech. **73**(3): 465-495.

Gerrard J.H. (1966). "The mechanics of the formation region of vortices behind bluff bodies." J. Fluid Mech. **25:** 401-413.

Habashi WG., Dompierre J., Bourgault Y., Ait-Ali-Yahia D., Fortin M., Vallet M-G. (2000). "Anisotropic mesh adaptation: towards user-independent, mesh-independent and solver-independent CFD. Part I: general principles." Int. J. Numer. Meth. Fluids **32**: 725-744.

Habashi WG., Dompierre J., Bourgault Y., Fortin M., Vallet M-G. (1998). "Certifiable computational fluid dynamics through mesh optimization." AIAA. **36**(5): 703-711.

Hawa T., Rusak Z. (2001):"The dynamics of a laminar flow in a symmetric channel with a sudden expansion". J. Fluid Mech.,**436:** 283-320.

Hetu J.F., Pelletier D.H. (1992). "Adaptive finite element scheme for viscous incompressible flows" AIAA.**30**(11): 2677.

Holdø A.E., Simpson B.A.F. (2002). "Simulations of high-aspect-ratio jets." International journal for numerical methods in fluids **39**: 343-359.

Howell L.H., Greenough J.A. (2003). "Radiation diffusion for multi-fluid Eulerian hydrodynamics with adaptive mesh refinement." Journal of Computational Physics **184**: 53-78.

Huang W., Russell R. D. (1999). "Moving mesh strategy based on a gradient flow equation for two-dimensional problems." SIAM J. Numer. Anal **20**(3): 998-1015.

Huang W., Ren Y., Russell R.D. (1994). "Moving mesh partial differential equations (MMPDES) based on the equidistribution principle." SIAM J. Numer. Anal **31**(3): 709-730.

Ilinca C., Zhang XD, Trepanier J-Y, Camarero R. (2000). "A comparison of three error estimation techniques for finite-volume solutions of compressible flows." Comput. Methods Appl. Mech. Engrg **189**: 1277-1294.

John D., Anderson J. (1995). Comuptational Fluid Dynamics The Basics with Applications. New York, McGraw-Hill, Inc.

Kaennakham S., Holdø A.E. (2008). "The use of solution adaptive grid for low Reynolds number flows." IJAME **13**(1): 21-38.

Kakuda K., Simura S., Tosaka N. (2006). "Finite element simulation of 3D flow around a circular cylinder." International journal of Computational Fluid Dynamics **20**(3-4): 193-209.

Kallinderis Y., Vijayan P. (1993). "Adaptive refinement-coarsening scheme for three-dimensional unstructured meshes." AIAA JOURNAL **31**(8): 1440-1447.

Kato C, Ikegawa M. (1991). "Large eddy simulation of unsteady turbulent wake of a circular cylinder using the finite element method." Advances in Numerical Simulation of Turbulent Flows, ASME FED 1991 **117**: 49-58.

Kim H., Hong S., Choi K., Jung H., Hahn S. (1991). "A three dimensional adaptive finite element method for magnetostatic problem." IEEE Trans. Megnetics **27**: 4981-4084.

Klein M. (2005). "An Attempt to Assess the Quality of Large Eddy Simulation in the Context of Implicit Filtering." Flow, Turbulence and Combustion **75**: 131-147.

Klein M., Sadiki A., Janicka J. (2003). "Investigation of the influence of the Reynolds number on a plane jet using direct numerical simulation." Int. J. Heat. Fluid Flow **24**: 785-794.

Khawaja A., Minyard T., Kallinderis Y. (2000). "Adaptive hybrid grid methods." Comput. Methods Appl. Mech. Engrg **189**: 1231-1245.

Kravchenko A.G., Moin P. (1997). "On the effect of numerical errors in large eddy simulation of turbulent flows." J. Comput. Phys **131**: 310.

Kravchenko A.G., Moin P. (2000). "Numerical studies of flow over a circular cylinder at Re = 3900." Phys. Fluids **12**(2): 403-417.

Larue J.C., Ly T., Rahai H., Jan P.Y. (1997). "On similarity of a plane turbulent jet in a co-flowing stream." In Proc. Eleventh Symp. on Turbulent Shear Flows **3**: 25.11-25-16.

Launder B.E., Spald D.B. (1972). Mathematical Models of Turbulence, Academic Press: London.

Li R., Tang T., Zhang P. (2001). "Moving mesh methods in multiple dimensions based on Harmonic maps." Journal of Computational Physics **180**: 562-588.

Li R., Tang T., Zhang P. (2002). "A moving mesh finite element algorithm for singular problems in wo and three space dimensions." Journal of Computational Physics **177**: 365-393.

Li S., Petzold L. (1997). "Moving mesh methods with upwinding schemes for time-dependent PDEs." J. Comput. Phys. **131**: 368-377.

Liao G., Liu F., de la Pena G.C., Peng D., Osher S. (2000). "Level-set-based deformation methods for adaptive grids." Journal of Computational Physics **159**: 103-122.

Liu F., Ji S., Liao G. (1998). "An adaptive grid method and its application to steady Euler flow calculations." SIAM J. Numer. Anal **20**(3): 811-825.

Liu Y., Tucker P.G., Kerr R.M. (2008). "Linear and nonlinear model large-eddy simulations of a plane jet." Journal of Computers and Fluids **37**: 439-449.

Lohner R. (1987). "An adaptive finite element scheme for transient problems in CFD." Comput. Methods Appl. Mech. Engrg **61**: 323-338.

Lohner R. (1988). "An adaptive finite element solver for transient problems with moving bodies." Computers and Structures **30**: 303-317.

Lohner R. (1989). "Adaptive remeshing for transient problems." Comput. Methods Appl. Mech. Engrg **75**: 195-214.

Lohner R. (1995). "Mesh adaptation in fluid mechanics." Engineering and Fracture Mechanics **50**(5/6): 819-847.

Lohner R., Baum J.D. (1992). "Adaptive h-refinement on 3D unstructured grids for transient problems." Int. J. Numer. Meth. Fluids **14**: 1407-1419.

Mavriplis C. (1990). A posterori error estimators for adaptive spectral element techniques. Proceedings of the 8th GAMM Conference on Numerical Methods and Fluid Mechanics.

MajumdarS., Rodi W. (1985). Numerical calculation of turbulent flow past circular cylinder. 3rd Symposium onPhysical Aspects of Aerodynamic Flows, Long Beach, CA.

Mansell R. S., Ma L., Ahuja L.R., Bloom, S.A. (2002). "Adaptive grid refinement in numerical models for water flows and chemical transport in soil: a review." Vadose Zone Journal **1**: 222-238.

Miller K, Miller R.N.(1981). "Moving finite element ,I." SIAM J. Numer. Anal **18**: 1019-1032.

Nambiar R.V., Valera R.S., Lawrence K.L., Morang R.B., Amil D. (1993). "An algorithm for the adaptive triangular meshes." Int. J. Numer. Meth. Engineering **36**: 499-509.

Namer I., Otugen M. (1988). "Velocity measurements in a plane turbulent air jet at moderate Reynolds numbers." Exp. Fluids **6**: 387-399.

Oden J.T., Devloo P., Strouboulis T. (1986). "Adaptive finite element methods for the analysis of inviscid compressible flows: I. Fast refinement/unrefinement and moving mesh methods for unstructured meshes." Comput. Methods Appl. Mech. Engrg **59**: 327-362.

Oliveira P.J. (2003) "Asymmetric flows of viscoelastic fluids in symmetric planar expansion geometries." J.Non-Newtonian Fluid Mech. **114**: 33-63.

Ong M.C., Utnes T., Holmedal L.E., Myhaug D., Pettersen B. (2009). "Numerical simulation of flow around a smooth circular cylinder att very high Reynolds numbers." Marine Structures **22**: 142-153.

Piomelli U., Cabot W.H., Moin P., Lee S. (1991). "Subgrid-Scale Backscatter in Turbulent Transitiolnal Flows." Phys. Fluids **3**: 1766-1771.

Pope, S. B. (2000). Turbulent flows. UK, Cambridge University Press.

Popiolek T.L., Awruch A.M. (2006). "Numerical simulation of compressible flows using adaptive unstructured meshes and the pseudo-compressibility hypothesis." Advances in Engineering Software **37**: 260-274.

Potter M.D., Wiggert (1997). Mechanics of fluids, Prentice Hall Inc.

Prusa J., Smolarkiewicz P. (2003). "An all-scale anelastic model for geophysical flows: Dynamic grid deformation." J. Comput. Phys. **190**: 601-622.

Quinn W.R., Pollard A., Marsters G.F. (1983). On 'Saddle-backed' velocity distributions in three-dimensional turbulent free jets. AIAA 16th Fluid and Plasma Dynamics Conference.

Ravinesh C. D., Jianchun M., Graham J.H. (2008). "The influence of Reynolds number on a plane jet." Phys. Fluids **20**: 075108-(1-16).

Ribault C., Sarkar S., Stanley S.A. (1999). "Large eddy simulation of a plane jet." Phys. Fluids **11**(10): 3069-3083.

Rhie C.M., Chow W.L. (1983) "Numerical study of the turbulent flow pas an airfoil with trailing edge separation." AIAA J., **21**(11): 1525-1532.

Roache P. (1998). Verification and validation in computational sicience and engineering, Hermosa Publishers, Albuquerque.

Rodi W., Ferziger J.H., Breuer M, Pourquie M. (1997). "Status of large eddy simulation: results of a workshop." Transactions of the ASME of Fluids Engineering **119**: 248-262.

Sagaut P. (1998). Large eddy simulation for incompressible flows: An Introduction, Springer.

Sobey I.J. (1985) "Observation of waves during oscillatory channel flow." J. Fluid Mech.,**151**: 395-426.

Scalabrin L., Azevedo JLF. (2004). "Adaptive mesh refinement and coarsening for aerodynamic flow simultations." Int. J. Numer. Meth. Fluids **45**: 1107-1122.

Schumann, U. (1975). "Subgrid scale model for finite difference simulations of turbulent flows in plane channels annuli." Journal of Comutational Physics **18**: 376-404.

Scott M.D. (2000). "r-Refinement grid adaptation algorithms and issues." Comput. Methods Appl. Mech. Engrg **189**: 1161-1182.

Semper B., Liao G. (1995). "A moving grid finite-element method using grid deformation." Numerical Methods for Partial Differential Equations **11**: 603-615.

Smagorinsky J. (1963). "General circulation experiment with the primitive equations I. The basic experiment." Month. Wea. Rev. **91**: 91-99.

Son J.S., Hnratty T.J. (1969). "Velocity gradients at the wall for flow around a cylinder at Reynolds numbers from 5×10^3 to 10^5" J. Fluid Mech. **35**(2): 353-368.

Soni B.K., Koomullil R., Thompson D.S., Thornburg H. (2000). "Solution adaptive grid strategies based onpoint redistribution." Comput. Methods Appl. Mech. Engrg **189**: 1183-1204.

Soni B.K., Yang J.C. (1992). General purpose adaptive grid generation system. Aerospace Sciences Meeting, Reno NV, AIAA-92-0664.

Speares W., Berzing M. (1997). "A 3D unstructured mesh adaptation algorithm for time-dependent shock-dominated problems." Int. J. Numer. Meth. Fluids **25**: 81-104.

Speziale C.G. (1978). "On non-linear k-l and k-epsilon models of turbulence." Journal of Fluids Mechanics **178**: 459-475.

Stanley S.A, Sarkar S. (2000). "Influence of nozzle conditions and discrete forcing on turbulent plannar jets." AIAA J. **38**: 1615-1623.

Stanley S., Sarkar S. (1997). "Simulations of spatially developing two-dimensional shear layers and jets." Theoret. Comput. Fluid Dynamics **9**: 121-147.

Stanley S.A., Sarkar S., Mellado J.P. (2002). "A study of the flow-field evolution and mixing in a planar turbulent jet using direct numerical simulation." J. Fluid Mech. **450**: 377-407.

Stephane M., Camille S., Michel P. (2000). Parametric analysis of the impinging plane air jet on a variable scaled-down model. ASME/JSME Fluids Engineering Division Summer Meeting, Boston, Massachusetts.

Tam A., Robichaud MP., Tremblay P., Habashi WG., Hohmeyer M., Peeters MF., Guevremont G., Germain P. (1998). A 3-D adaptive anisotropic method for external and internal flows. Proceedings of the 36th aerospace sciences meeting, Reno, NV, AIAA 98-00771.

Tang H.-Z., Tang T. Zhang P. (2003). "An adaptive mesh redistribution method for nonlinear Hamilton-Jacobi equation in two- and three-dimensions." J. Comput. Phys. **188**: 543.

Tennekes H., Lumley J.L. (1972). A first course in turbulence, The Massachusetts Institute of Technology.

Thomas F.O., Chu H.C. (1989). "An experimental investigation of the transition of a plannar jet: subharmonic suppression and upstream feedback." Phys. Fluids **A(1)**: 1566-1587.

Tutar M., Holdø A.E. (2001). "Computational modelling of flow around a circular cylinder in sub-critical flow regime with various turbulence models." International journal for numerical methods in fluids **35**: 763-784.

Goldsschmidt V.W., Bradshaw P. (1981). Effect of nozzle exit turbulence on the spreading (or widening) rate of plane free jets. Joint Engineering, fluid Engineering and Applied Mechanics Conference, ASME, Boulder, Colorado.

Vay J.-L., Colella P., Kwan J.W., McCorquodale P., Serafini D.B., Friedman A., Grote D.P., Westenskow G., Adam J.-C., Heron A., Haber I. (2004). "Application of adaptive mesh refinement to particle-in-cell simulations of plasmas and beams." Physics of Plasmas **11**(5): 2928-2934.

Vreman B., Geurts B., Kuerten H. (1996). "Comparison of numerical schemes in large-eddy simulation of the temporal mixing layer." Int. J. Numer. Methods Fluids **22**: 297-311.

Warren G.P., Anderson W.K., Thomas J.T., Krist S.L. (1991). "Grid convergence for adaptive methods." AIAA JOURNAL **91**: 1592.

Weiming C., Weizhang H., Robert D. R. (2001). "An error indicator function for an r-adaptive finite element method." Journal of Computational Physics **170**: 871-892.

Winslow A. (1967). "Numerical solution of the quasi-linear Poisson equation in a nonuniform triangular mesh." Journal of Computational Physics **1**: 149-172.

With G., Holdø A.E. (2005). "The use of turbulent inflow conditions for the modeling of a high aspect ratio jet." Fluid dynamics research **37**: 443-461.

With G., Holdo A.E., Huld T.A. (2003). "The use of dynamic grid adaptation algorithms for the modelling of flow around a circular cylinder in sub-critical flow regime." Int. J. Numer. Meth. Fluids **41**: 789-808.

With de G., Holdø A. E. (2005). "The use of solution adaptive grid for modeling small scale turbulent structures." ASME **127**: 936-944.

Yamaleev N.K. (2001). "Minimization of the truncation error by grid adaptation." Journal of Computational Physics **170**: 459-497.

Yamaleev N.K., Carpenter M.H. (2002). "On accuracy of adaptive grid methods for captured shocks." Journal of Computational Physics **181**: 280-316.

Zdravkovich M.M. (1997). Flow around circular cylinders. New York, Oxford University Press.

Zhang J, Dalton C. (1996). "Interactions of vortex induced vibrations of a circular cylinder and a steady approach flow at a Reynolds number of 13,000." Computers and Fluids **25**(3): 238-294.

Zienkiewicz O.C., Zhu J.Z., (1987). "A simple error estimator and adaptive procedure for practical engineering analysis." Int. J. Numer. Meth. Engineering **24**: 337-357.